Design and Development of Injectable Intraperitoneal Sustained Release Drug Delivery System for Ovarian Cancer

Chaudhry Zahid Nazir

Thesis submitted to the University of Nottingham

for the degree of Doctor of Philosophy

February 2020

Declaration

Unless otherwise acknowledged, the work presented in this thesis is my own. No part has been submitted for any other degree at The University of Nottingham or any other institution.

The project was a part-time doctorate programme, while I was working full time at AstraZeneca. Therefore, most of experimental work was done at AstraZeneca, Macclesfield.

This doctoral dissertation was conducted under the supervision of:

Dr Maria Marlow, Associate Professor, School of Pharmacy, the University of Nottingham, UK

Dr Stephanie Allen, Professor of Pharmaceutical Biophysics, School of Pharmacy, the University of Nottingham, UK

Dr Marianne Ashford, Senior Principal Scientist, Pharmaceutical Sciences, R&D, AstraZeneca, Macclesfield, UK

Chaudhry Zahid Nazir

February 2020

Abstract

Multiple clinical trials have shown improved survival after IP (intraperitoneal) over IV (intravenous) chemotherapy in women with optimally resected ovarian cancer and the National Cancer Institute (NCI) encourages the use of IP chemotherapy. Despite this, IP chemotherapy has still not been widely accepted due to various concerns [1,2].

In this PhD thesis, an injectable intraperitoneal sustained release drug delivery system has been developed for ovarian cancer to address some of these concerns hindering the clinical application of IP chemotherapy e.g. risk of chemical peritonitis due to high drug concentrations, catheter associated infections, bowel obstructions, and lack of dedicated products. The drug delivery system is comprised of paclitaxel and carboplatin encapsulated in PLGA microspheres to provide sustained release over a period of approximately 1 month after single injection. It was also intended to administer microspheres in a hydrogel to prevent microsphere clearance from peritoneal cavity and avoid inflammation and adhesions.

Firstly, an intraperitoneal pharmacokinetic mathematical model was developed to support the formulation design. Secondly, various PLGA microsphere manufacturing methods were evaluated to make controlled, uniform size microspheres. The selected method was then systematically optimised by using a design of experiment (DOE) approach to achieve the particle size ($D_{0.5}$) between 50 – 200 μm. Thirdly, various hydrogels were developed and/or evaluated, and their stability assessed in the simulated IP fluid at 37 °C, in the presence or absence of PLGA microspheres. Subsequently, the paclitaxel and carboplatin release rates from PLGA microspheres were optimised by using four different grades of PLGA. Finally, the preliminary IP PK mathematical model was adjusted to fit the optimised release rates and a dosage regimen for carboplatin and paclitaxel was determined.

The preliminary IP PK mathematical model predicted doses of 0.84 mg and 82 mg of paclitaxel and carboplatin loaded PLGA microspheres, respectively, assuming a drug loading of 10 % w/w and a zero- order release profile.

From the PLGA microsphere manufacturing method evaluation, a passive flow-focussing droplet microfluidics method was selected. However, none of the tested hydrogels was found to be physically stable in the simulated IP fluid at 37 °C, with or without PLGA microspheres. Therefore, it was decided to exclude the hydrogels from the drug delivery system and carry on the optimisation of PLGA micropsheres manufacturing method(s).

The results from the optimisation of the microfluidics method by using DOE approach clearly identified the PLGA concentration in the organic phase and aqueous to organic flow ratio as the most significant factors that affected the microsphere size. The optimised conditions for the manufacture of paclitaxel loaded PLGA microspheres by single emulsion (O/W) method resulted in approximately 100 % w/w encapsulation efficiency with 10 % w/w drug loading. Whereas, for carboplatin the single emulsion (O/W) method was modified and an innovative method was developed. In this method, carboplatin was first wet-milled to make carboplatin nanocrystals which were then suspended in the organic phase to make S/O/W emulsion. The remainder of the method was same as for paclitaxel. This resulted in approximately 60 % w/w encapsulation efficiency and 6 % w/w carboplatin loading.

From the release rate optimisation experiments it was found that, in general, release rates from PLGA microspheres decreased and the lag phase (i.e. no release) became longer with increasing the PLGA molecular weight (10 to 50 kDa) and/or increasing the lactide to glycolide ratio (50/50 to 75/25).

Finally, by using one formulation of carboplatin and a combination of two paclitaxel formulations, IP PK mathematical model estimated that steady state therapeutic concentrations (exposure) can be maintained in the intraperitoneal cavity for at least 23 days after a single dose of 1 mg of paclitaxel and 28 days after single dose of 330 mg of carboplatin loaded PLGA microspheres. In addition, the simulated data also predicted that the exposure can be maintained for several months by administering multiple doses of paclitaxel and carboplatin (as PLGA microsphere formulations) at a dosing interval of 23 days and 28 days, respectively.

Acknowledgments

I would like to thank my supervisors, Dr Maria Marlow and Dr Stephanie Allen from University of Nottingham and Dr Marianne Ashford from AstraZeneca, for their guidance and support throughout my PhD.

Dr Tracey Bradshaw and Francesca Citossi (PhD student) from University of Nottingham are gratefully acknowledged for providing training in the preliminary cell viability study experiments and helping in the lab work at the University of Nottingham. Eric Tang and John Vincent from AstraZeneca are thanked for their support, training and supervision of my in-vitro cell viability assay (SYTOX green assay) experimental work at AstraZeneca.

I would also like to acknowledge; Long Jiang and Julie Watts from the University of Nottingham for their help with ToF-SIMS and ESEM analysis, respectively. Robert Shaw from AstraZeneca for helping in the design of experiment (DOE) planning and data interpretation. Iain Grant from AstraZeneca for his guidance and help in the development of intraperitoneal pharmacokinetic models, implementation of model in software (Berkley Madonna) and with some equations.

Finally, I would like to extend my gratitude to AstraZeneca for allowing me the time and providing part funding for travel and materials. School of Pharmacy, the University of Nottingham for paying my tuition fees and Dr Maria Marlow for sharing travel and material costs from her grants.

Table of Contents

1 INTRODUCTION 21

1.1 OVARIAN CANCER (OC) 21

1.1.1 Patterns of ovarian cancer spread 21

1.1.2 Intraperitoneal fluid and ascites 23

1.2 CURRENT TREATMENT STRATEGIES 23

1.2.1 Surgery 24

1.2.2 Chemotherapy 24

1.2.2.1 Paclitaxel 25

1.2.2.2 Carboplatin 27

1.3 LOCALISED CONTROLLED RELEASE DELIVERY OF CHEMOTHERAPEUTICS 28

1.3.1 Controlled release drug delivery 28

1.3.2 Intraperitoneal drug delivery 30

1.3.3 Intraperitoneal chemotherapeutic delivery strategies 31

1.4 PROPOSED DRUG DELIVERY SYSTEM 33

1.5 SUMMARY AND OBJECTIVES 35

2 INTRAPERITONEAL PHARMACOKINETIC MODEL FOR DESIGNING THE IP SUSTAINED RELEASE DRUG DELIVERY SYSTEM FOR OVARIAN CANCER 37

2.1 INTRODUCTION 37

2.1.1 Pharmacodynamic properties 37

2.1.2 Pharmacokinetic mathematical model 38

2.2 MATERIALS AND METHODS 39

2.2.1 Materials 39

2.2.2 Methods 40

2.3 INTRAPERITONEAL PK MATHEMATICAL MODEL 43

2.4 RESULTS AND DISCUSSION 48

2.4.1 Monotherapy dose response and GI50 values 48

2.4.2 Combination therapy results 51

2.4.3 Intraperitoneal PK mathematical model results 53

2.5 CONCLUSION 55

3 EVALUATION OF DIFFERENT METHODS FOR THE MANUFACTURE OF PLGA MICROSPHERES 56

3.1 INTRODUCTION 56
3.1.1 Microsphere QTPP (quality target product profile) 56
3.1.2 Evaluation of PLGA microsphere manufacturing methods 57
3.2 MATERIALS AND METHODS 59
3.2.1 Materials 59
3.2.2 Methods 59
3.3 RESULTS AND DISCUSSION 65
3.3.1 Microsphere preparation by homogenisation and filter extrusion techniques 65
3.3.2 Microspheres preparation by microfluidics method 67
3.3.3 Effect of DCM extraction and evaporation rate on microsphere formation 69
3.3.4 Particles breakage due to magnetic stirring 70
3.3.5 Porosity in the PLGA microspheres 70
3.3.6 Comparison of SEM and optical microscope images for the characterisation of microsphere porosity 72
3.3.7 Preparation of carboplatin/PLGA microspheres by double emulsion method 73
3.3.8 HPLC method development for the analysis of carboplatin drug loading and encapsulation efficiency in microspheres 75
3.4 CONCLUSION 76

4 EVALUATION OF DIFFERENT METHODS FOR THE PREPARATION OF INTRAPERITONEALLY INJECTABLE HYDROGELS CONTAINING PLGA MICROSPHERES 78

4.1 INTRODUCTION 78
4.2 MATERIALS AND METHODS 81
4.2.1 Materials 81
4.2.2 Methods 81
4.3 RESULTS AND DISCUSSION 86
4.3.1 Preparation and characterisation of HA and chitosan gel 86

4.3.2 Physical stability of hybrid composite gels in simulated IP fluid (SIPF): 88
4.3.3 Preparation and characterisation of pectin hydrogels and composites with PLGA microspheres for physical stability evaluation in SIPF 89
4.3.4 Preparation and characterisation of Peptide gel 92
4.3.5 Conclusion 94

5 OPTIMISATION OF MICROFLUIDICS METHOD FOR THE MANUFACTURE OF CARBOPLATIN AND PACLITAXEL LOADED PLGA MICROSPHERES 95

5.1 INTRODUCTION 95
5.2 MATERIALS AND METHODS 97
5.2.1 Materials 97
5.2.2 Methods 97
5.3 RESULTS AND DISCUSSION 105
5.3.1 Design of experiment (DOE) results 105
5.3.2 Drug encapsulation results 112
5.3.3 Microsphere size and appearance 115
5.3.4 Solid state results (X-RPD and DSC) 117
5.4 CONCLUSION 120

6 TAILORING THE RELEASE RATES OF CARBOPLATIN AND PACLITAXEL FROM PLGA MICROSPHERES AND FINDING THE OPTIMUM DOSAGE REGIMEN WITH THE AID OF AN INTRAPERITONEAL PK MATHEMATICAL MODEL 121

6.1 INTRODUCTION 121
6.2 MATERIALS AND METHODS 123
6.2.1 Materials 123
6.2.2 Methods 123
6.3 RESULTS AND DISCUSSION 131
6.3.1 SEM 131
6.3.2 ESEM results 134
6.3.3 Drug Loading and Encapsulation Efficiency 137

6.3.4 ToF-SIMS 139
6.3.5 Drug Release from Microspheres 147
6.4 CONCLUSION 156
7 SUMMARY AND FUTURE PERSPECTIVES 157
7.1 SUMMARY 157
7.1.1 Selection of the drug delivery system design parameters 157
7.1.2 Selection of PLGA microsphere and hydrogel manufacturing methods 158
7.1.3 Optimisation of microfluidics methods for the manufacture of paclitaxel and carboplatin PLGA microspheres 159
7.1.4 A strategy to tune the release rates from PLGA microspheres and determine the dosage regimen with the help of IP PK mathematical model 161
7.2 FUTURE PERSPECTIVE 163
7.2.1 Improvements in carboplatin drug loading 163
7.2.2 In-vivo studies in rodents 164
8 REFERENCES 165
9 APPENDICES 178

Abbreviations

API	Active pharmaceutical ingredient
ALK	Anaplastic Lymphoma Kinase
BSED	Back scattered electron detector
CCLE	Cancer Cell Line Encyclopaedia
DCM	Dichloromethane
DMSO	Dimethyl Sulfoxide
DOE	Design of Experiment
DPBS	Dulbecco's Phosphate Buffered Saline
DSC	Differential scanning calorimetry
EOC	Epithelial Ovarian Cancer
EDX or EDS	Energy dispersive X-ray spectroscopy
ESEM	Environmental Scanning Electron Microscopy
FCS	Foetal Calf Serum
FDA	Food and Drug Administration
GI50	Concentration of a compound that inhibits 50% cell growth
GOG	Gynaecologic Oncology Group
HA	Hyaluronic acid
HGSC	High Grade Serous Cancer
HILIC	Hydrophilic Interaction Liquid Chromatography
IP	Intraperitoneal
IV	Intravenous
LFD	Large field detector
MDM2	Murine Double Minute 2
NCI	National Cancer Institute
OC	Ovarian Cancer
OS	Overall Survival
PARP	Poly ADP (Adenosine Diphosphate) Ribose Polymerase
PBS	Phosphate buffered saline
PFS	Progression Free Survival
PLGA	Poly-Lactide-co-Glycolic acid
PLM	Polarised Microscope
PK	Pharmacokinetics

PVA	Polyvinyl Alcohol
SBF	Simulated Body Fluid
SEM	Scanning Electron Microscopy
TCGA	The Cancer Genome Atlas
ToF-SIMS	Time-of-Flight Secondary Ion Mass Spectroscopy

Table of Figures

Figure 1-1: Patterns of spread of ovarian carcinoma [12] 22
Figure 1-2: Paclitaxel mechanism of action; Paclitaxel inhibits cellular replication in transition from G0 to G1 and pre-mitotic G2 and mitotic M phases of the cell cycle [28]. 26
Figure 1-3: Carboplatin mechanism of action, formation of carboplatin – DNA adducts and cell death [24]. 27
Figure 1-4: Examples of typical controlled release drug delivery systems including spatial release system (top) and temporal release system (bottom). Redrawn from [41] 29
Figure 1-5: Graph showing the number of publications describing the intraperitoneal chemotherapy administration per year during last 40 years (from 1978 – 2018). PubMed search dated 10 January 2020, for term “intraperitoneal chemotherapy”..... 32
Figure 2-1: Schematic flow diagram of SYTOX green nucleic acid stain assay 41
Figure 2-2: Intraperitoneal pharmacokinetic model to design the drug delivery system by estimating the required release rate from the microspheres and dose to maintain the therapeutic concentration (i.e. 3x GI50) of the API..... 44
Figure 2-3: Example of a zero order release kinetic from PLGA microsphere-based formulation. 44
Figure 2-4: A representation of steady state of API concentration in the IP cavity. The region 1 represents initial phase where the release from the formulation is greater than the rate of removal of the API from the IP cavity. It is assumed that this phase is relatively short (compared to the steady state) and considered negligible. The region 2 represents the steady state where the release (input) of the API from the formulation is equivalent to the rate of removal from the IP cavity. 46
Figure 2-5: Single agent dose response curves in IGROV1 cell line. Top left: carboplatin day 3, top right: carboplatin day 6, bottom left: paclitaxel day 3 and bottom right: paclitaxel day 6 dose response curves. Error bars are standard deviation of at least six replicates. 49

Figure 2-6: Single agent dose response curves in OVCAR4 cell line. Top left: carboplatin day 3, top right: carboplatin day 6, bottom left: paclitaxel day 3 and bottom right: paclitaxel day 6 dose response curves. Error bars are standard deviation of at least six replicates. 51
Figure 3-1: QTPP (quality target product profile) for the development of microsphere based drug product. 57
Figure 3-2: Schematic for the manufacture of PLGA microspheres by single emulsion method using the microfluidics 61
Figure 3-3: Schematic for the preparation of carboplatin PLGA microspheres by double emulsion method, using microfluidics 63
Figure 3-4: Optical microscope image of PLGA microspheres prepared by homogenisation method 65
Figure 3-5: Microspheres preparation by filter extrusion, (Top) Optical microscope pictures (Bottom) Particle size distribution by Malvern 2000 (laser light scattering). (Left) filter extrusion through 2µm filter (Right) filter extrusion through 5µm filter..... 66
Figure 3-6: Comparison of microsphere preparation by two different chips designs. Left: Micromixer chip, Right: Droplet generation chip, formulation 20% w/v PLGA 95/5, M_w 25 kDa, in DCM and 0.5% w/v PVA in water. Ratio of organic to aqueous phase flow rate 1:10 for both chip designs..... 67
Figure 3-7: Optical microscope image showing effect of organic / aqueous flow rate ratio on particle size and size distribution in droplet generation chip. Organic / aqueous phase flow rate ratio 1:5 (Left), 1:10 (Right). The formulation was 20% w/v PLGA in DCM, 0.5% PVA for both experiments 68
Figure 3-8: Optical microscope pictures showing the effect of DCM extraction/removal rate on the emulsion droplet. Formulation: 5% w/v PLGA in DCM, 0.5% PVA, organic / aqueous phase flow rate ratio 1:10, droplet collection and DCM evaporation by orbital shaking at room temperature. 69
Figure 3-9: Optical microscope picture showing the microsphere breakage due to magnetic stirring. Formulation: 5% w/v PLGA in DCM, 0.5% PVA, organic / aqueous phase flow rate ratio 1:10..... 70
Figure 3-10: Optical microscope pictures showing the effect of PLGA concentration on porosity. 71

Figure 3-11: Optical microscope pictures showing the effect of PLGA molecular weight on the porosity. Formulation, 20% w/v PLGA in DCM used in both experiments 71
Figure 3-12: Comparison of optical microscope (PLM) and SEM images to evaluate porosity in PLGA microspheres. PLM samples were analysed as suspension in 0.01% w/v PVA solution. SEM samples were taken from the same suspension as for the PLM samples but samples were dried under vacuum at ambient temperature for at least 24 hrs and gold sputter coated before analysis. 72
Figure 3-13: Optical microscope picture of carboplatin PLGA microspheres prepared by double emulsion (W/O/W) method using microfluidics. Left hand side images are for the samples suspended in aqueous media. Right hand side images are for the dried samples. Top four images are for the lower magnifcation wereas, bottom four images are for the higher magnifcation.... 74
Figure 3-14: Chromatogram of carboplatin solution by using HILIC method. 75
Figure 4-1 Hyaluronic acid and Chitosan gel preparation by using a double barrel syringe. 82
Figure 4-2 Camera pictures (A-D) of HA and Chitosan gels with different additives, made by using double barrel syringe where anionic components (solution 1) placed in one barrel and the cationic components (solution 2) in the other. 86
Figure 4-3: Camera pictures of gels B and D composites made by using double barrel syringe where anionic components (mixture 1) placed in one barrel and the cationic components (mixture 2) in the other. Both gels were prepared in the presence of simulated IP fluid (1:10 gel to SIPF ratio). Gel B composite: mixture 1 (0.5% w/v HA + 1% w/v sodium alginate + 2% w/w PLGA microspheres), mixture 2 (0.5% w/v chitosan in 1% acetic acid + 0.4% w/v $CaCl_2$). Gel D: mixture 1 (0.5% w/v HA + 1% w/v sodium alginate + 0.2% w/v $CaCO_3$ + 2% w/w PLGA microspheres), mixture 2 (0.5% w/v chitosan in 1% GDL) 90
Figure 4-4: Camera pictures of pectin – calcium gels made from three different grades of pectin (P102, P104 and P105) and two different concentration of calcium chloride. 91

Figure 4-5: Camera pictures of pectin – calcium gels in simulated IP fluid, made from pectin P105 in the absence (top) and presence (bottom) of PLGA microspheres. 92
Figure 4-6: Camera pictures of two PeptiGel® (Alpha 001 and Alpha 002) composites with PLGA microspheres with and without simulated intraperitoneal fluid. The SIPF (1:10 v/v composite to SIPF) was added to the composite and stored at room temperature and 37 °C for 24 hours. 93
Figure 5-1: Graph showing the number of publications describing the use of microfluidic for drug delivery applications per year during last 20 years. PubMed search dated 29th January 2020, for term “microfluidic drug delivery”. 95
Figure 5-2: Flow diagram for the manufacture of PLGA microspheres by using single emulsion (O/W) method in microfluidics. 98
Figure 5-3: Planetary micro mill and principle of operation 101
Figure 5-4: Box plot showing the results from DOE 1. Arrow directions indicating the increasing values. Yellow squares contain the particle size ($D_{0.5}$). Middle yellow square is an average of three replicates. *standard deviation. 105
Figure 5-5: DOE 1 Pareto chart ranking the significance of independent variables for particle size change. AC is the interaction between independent variables A (total flow rate) and C (flow rate ratio). Plot is also displaying the 5 % significance threshold (t-value limit) and an additional threshold corrected for multiple comparisons (Bonferroni limit). 107
Figure 5-6: DOE2 Pareto chart ranking the significance of the independent variables for particle size change. CD is the interaction between independent variables C (flow rate ratio) and D (polymer concentration). Plot is also displaying the 5 % significance threshold (t-value limit) and an additional threshold corrected for multiple comparisons (Bonferroni limit). 110
Figure 5-7: DOE 2 interaction plot between flow rate ratio and polymer concentration showing the effect of the independent variables on the particle size. The data is based on the 2-level factorial design, which is why only two data points are shown on this plot, as standard. 111
Figure 5-8: Contour plot showing the overall summary of the DOE 2 results. The independent variables evaluated in DOE 2 were: i) total flow rate, ii) aqueous to organic phase flow rate ratio, iii) PVA concentration in aqueous phase and iv)

PLGA concentration in the organic phase. Microspheres particle size ($D_{0.5}$) was used as the dependent variable in this DOE. 112
Figure 5-9: Laser diffraction particle size and size distribution of carboplatin nanosuspension milled in PEG 200. Ethanol is used as dispersant for particle size measurement. The particle size d(0.5) of 0.13 µm and d(0.9) of 0.29 µm. 114
Figure 5-10: Optical microscope pictures of un-milled (top) and milled (bottom) carboplatin in PEG 200 by using planetary micro mill. Left: cross-polarised light showing the crystalline nature of the particles and Right: plane-polarised light showing the shape and size of the particles. 115
Figure 5-11: SEM (a) and Optical microscope (b) images of Carboplatin and Paclitaxel microspheres. Both Microspheres were prepared with PLGA 75/25 (lactide/glycolide) polymer by using O/W emulsion and microfluidics methodology. The critical parameters included total flow rate 200 µL/min, aqueous to organic flow rate ratio 10, polymer concentration in the organic phase 20% w/w and PVA concentration in aqueous phase 0.5% w/w. Samples were dried under vacuum for at least 24 hr at ambient temperature. SEM samples were gold sputter coated with 5-10 nm coating density. PLM images were taken without any further processing. 116
Figure 5-12: XRPD data for PLGA, paclitaxel and carboplatin powders and microspheres. All Microspheres were prepared with PLGA 75/25 (lactide/glycolide) polymer by using an O/W emulsion and microfluidics methodology. Samples were dried under vacuum for at least 24 hr at ambient temperature before analysis. Samples were measured in reflection geometry in θ - 2θ configuration over the scan range 2° to 40° 2θ with a nominal 25 second exposure per 0.02° increment. 118
Figure 5-13: DSC data showing endothermic and exothermic events in the blank, carboplatin and paclitaxel loaded PLGA microspheres (top) and carboplatin and paclitaxel reference compounds (controls)(bottom). 119
Figure 6-1: Updated Intraperitoneal pharmacokinetic model to design the drug delivery system by estimating the required release rate from the microspheres and dose required to maintain the therapeutic concentration (i.e. GI50) of the API..... 128

Figure 6-2: Example release profiles showing typical zero order (A) and sigmoidal (B) release kinetics from a single dose. 128
Figure 6-3: SEM pictures of blank PLGA microspheres at three magnifications. Formulations were made with three different grades of PLGA, Top row: PLGA 50/50 50 kDa (BF2), Middle row: PLGA 75/25 50 kDa (BF4) and Bottom row: PLGA 75/25 10 kDa (BF3). 131
Figure 6-4: SEM pictures of Carboplatin-PLGA microspheres at three magnifications. Formulations were made with three different grades of PLGA, Top row: PLGA 50/50 50 kDa (CF2), Middle row: PLGA 75/25 50 kDa (CF4) and Bottom row: PLGA 75/25 10 kDa (CF3) 132
Figure 6-5: SEM pictures of Paclitaxel-PLGA microspheres at three magnifications. Formulations were made with three different grades of PLGA, Top row: PLGA 50/50 50 kDa (PF2), Middle row: PLGA 75/25 50 kDa (PF4) and Bottom row: PLGA 75/25 10 kDa (PF3) 134
Figure 6-6: ESEM results showing cross section of blank (top), paclitaxel (middle) and carboplatin (bottom) microspheres made by using PLGA 75/25 50 kDa. Left-hand side images are from the large field detector (LFD) and right-hand side images are from back scattered electron detector (BSED). All sample were analysed uncoated by using FEI Quanta650 eSEM operated at 10kV and 75pa. 135
Figure 6-7: ESEM analysis by using BSED (back scattered electron detector) (left) and EDX/EDS (Energy dispersive X-ray spectroscopy) (right) detectors. All sample were analysed uncoated by using FEI Quanta650 eSEM operated at 10kV and 75pa. 136
Figure 6-8: ESEM results showing the porous shell of freeze-fractured carboplatin microsphere made by using PLGA 75/25 50 kDa. Left-hand side images are from the large field detector (LFD) and right-hand side images are from back scattered electron detector (BSED). All sample were analysed uncoated by using FEI Quanta650 eSEM operated at 10 kV and 75 pa. 137
Figure 6-9: ToF-SIMS analysis of reference materials to select characteristic secondary ions to identify PVA, PLGA, paclitaxel and carboplatin in PLGA microsphere based formulations. 141
Figure 6-10: ToF-SIMS surface scan images, comparing the compound secondary ion intensities for the identification of paclitaxel, carboplatin and

PLGA on the microsphere surfaces. Brighter images indicate stronger signal and therefore, the presence of specified compound on the surface. 143
Figure 6-11: ToF-SIMS surface scan images of blank and carboplatin microspheres made with PLGA 50/50 50kDa comparing two secondary ions, $C_3H_3O_3^-$ (m/z 87) a specific secondary ion for PLGA and . $C_3H_3O_2^-$ (m/z 59.01) a specific secondary ion for PVA. 144
Figure 6-12: ToF-SIMS depth profiling 3D images of PLGA microspheres of carboplatin (top row) and paclitaxel (bottom row) showing spatial distribution of API and PLGA throughout the bulk microspheres. Colour coding: Blue PLGA, Red carboplatin (Sum of $C_6H_6O_4PtNH^-$, $C_6H_6O_4PtNH_2^-$ and $C_6H_6O_4PtNH_3^-$) and Golden paclitaxel ($C_{16}H_{14}NO_4$-). 145
Figure 6-13: ToF-SIMS depth profile analysis results presented as ion intensity vs sputtered depth, showing the spatial distribution of carboplatin (top picture, sum of $C_6H_6O_4PtNH^-$,$C_6H_6O_4PtNH_2^-$ and $C_6H_6O_4PtNH_3^-$ ions) and paclitaxel (bottom picture, ion $C_{16}H_{14}NO_4$-) within the bulk microspheres in all three formulations of each compound..... 146
Figure 6-14: Cumulative release of carboplatin and paclitaxel from PLGA microspheres made with three different grades of PLGA. Carboplatin microspheres were incubated in 10 mM PBS pH7.4 buffer containing 0.02% w/v sodium azide whereas, paclitaxel microspheres were suspended in 10% HPβCD in 10 mM PBS pH7.4 buffer containing 0.02% w/v sodium azide. Samples were continuously agitated at 37 °C in a shaking water bath at 150 rpm. Supernatant samples were collected at regular intervals and analysed by HPLC-UV for paclitaxel and ICP-OES for carboplatin. The results are a mean of the three replicates with the error bars representing the standard deviation. 148
Figure 6-15: Hill function (a mathematical function) fitted to the release data of carboplatin CF2 (PLGA 50/50 50kDa) microsphere formulation by using SigmaPlot (Version 13 from Systat Software)..... 151
Figure 6-16: A steady state of carboplatin concentration in IP fluid above the target concentration (C_{target}) of 5.7 mg/L after administering six doses of 14.5 mg of carboplatin (equivalent to 330 mg of microsphere formulation made from PLGA 50/50 50kDa with 4.4 % w/w drug loading) at a dosing interval of 28 days. 152

Figure 6-17 Hill function (a mathematical function) fitted to the release data of paclitaxel PLGA microsphere formulations by using SigmaPlot (Version 13 from Systat Software). 153
Figure 6-18: A predicted intraperitoneal (IP) steady-state concentration of paclitaxel above the target concentration (0.0726 mg/mL) by using a IP pharmacokinetic model implemented in Berkeley Madonna (software package). These results are after administering total 6 doses of 0.096 mg/dose paclitaxel by using a mixture of paclitaxel formulation PF3 (46% w/w) and formulation PF2 (54% w/w) at a dosing interval of 23 days. 154
Figure 9-1:Fitted model for estimating the value of carboplatin k_{ip} by using data from McClay et. al. paper. 182
Figure 9-2 Hyaluronic acid chemical structure..... 183
Figure 9-3 Chitosan chemical structures 185
Figure 9-4 Alginate chemical structure 186
Figure 9-5. Egg-box structure of Ca2-Alginate hydrogel..... 187
Figure 9-6: Dynamic viscosity (η) vs shear rate (γ) plots of two different grades of hyaluronic acid solutions, one grade of sodium alginate and one grade of chitosan solutions, at 25°C by using HAAKE MARS III rheometer (Thermo Scientific) equipped with 35mm diameter / 1-degree angle cone and plate and HAAKE RheoWin 4 software (Thermo Scientific). 195
Figure 9-7: Selection of sample holding devices evaluated for the release testing of carboplatin and paclitaxel from PLGA microspheres. A: commercially available devices, B: “homemade” device components and assembly, C: pictures showing the visual assessment of the rate of Fluorescein (dye) release from two different “homemade” devices. 201
Figure 9-8: Chromatograms showing the impurities from different components of the “homemade” sample holding devices in comparison to the neat paclitaxel solution in release media. 202
Figure 9-9: Comparison of the total peak areas of paclitaxel by HPLC at day 1 and 10 in the presence and absence of the sample holding device (assembly). This data indicates that the selected device has no significant impact on paclitaxel dissolved (released) in the release media. 203

Figure 9-10: ToF-SIMS survey spectra (negative ions) by analysing reference materials for carboplatin, paclitaxel, PVA and two PLGA 50kDa (75/25 and 50/50) 204
Figure 9-11: Pictures showing the release samples at the start and end of release testing. Left: paclitaxel-PLGA microspheres suspended in release media (replicate 1) at the start of release testing. Right: Paclitaxel-PLGA microspheres suspended in release media (replicate 1 and 2) at the end of release testing. 206
Figure 9-12: SEM images of the microspheres after 60 days of release testing. Sample preparation included the isolation of microspheres by filtration, drying under vacuum at ambient temperature for at least 24 hours and gold sputter coating before SEM analysis. 207
Figure 9-13: A “nonideal” simulated intraperitoneal (IP) steady-state concentration of paclitaxel above the target concentration (0.0726 mg/mL) by using a IP pharmacokinetic model implemented in Berkeley Madonna (software package). These results are after administering total 6 doses of 0.27 mg/dose paclitaxel by using a blend of paclitaxel formulation 1 (43% w/w) and formulation 2 (57% w/w) at a dosing interval of 28 days. The pulsatile periodic variations have different heights i.e. nonideal. 210
Figure 9-14:Optimisation of paclitaxel formulation 1 and 2 blend ratios to find the steady state at minimum dose required to consistently keep the intraperitoneal concentration of paclitaxel above the target concentration (0.0726 mg/L) after six doses with dosing interval of 23 days. Top: Profile showing all six doses, Bottom: profile showing first two doses. 211
Figure 9-15: A coparison of simulated intraperitoneal (IP) fluid steady-state concentration of paclitaxel at two different IP fluid volumes. The simulation is performed by using a IP pharmacokinetic model implemented in Berkeley Madonna (software package). These results are after administering total 6 doses of paclitaxel-PLGA micropsheres by using a blend of formulation PF2 (54% w/w) and PF3 (46% w/w) at a dosing interval of 28 days. 213

1 Introduction

1.1 Ovarian cancer (OC)

Ovarian cancer originates from ovarian tissues. It has been classified into several distinct histotypes. The main types are epithelial in origin which accounts for 90% of total OCs [3-5]. Epithelial ovarian cancers (EOCs) include high-grade serous carcinoma (HGSC), clear cell carcinoma, endometrioid carcinoma, low-grade serous carcinoma, and mucinous carcinoma. Out of all EOCs, HGSC is the most malignant form and it accounts for up to 70% of all OC cases [5,6] and it is the most responsive to the chemotherapy (Paclitaxel / Carboplatin) treatment [7].

Among all the cancers, globally, ovarian cancer is the 7th most frequent and 8th leading cause of cancer mortalities and it is the number one cause of death among gynaecological malignancies [4,6]. Even after great improvements in surgery, advanced therapeutics and chemotherapy, 5-year survival among ovarian cancer patients is still poor, ranging from 36 – 46 % across seven high income countries [8]. One of the main reasons of such low survival rate is the poor diagnosis at early stages. Majority (>70 %) of the patients are still diagnosed at an advanced stage when disease had spread to the regional tissues near ovaries, primarily the intraperitoneal tissues [3,6 9,10] and that is why, rightly or wrongly, OC is sometimes termed as the “silent killer”.

1.1.1 Patterns of ovarian cancer spread

At the earlier stages (stage IA/IB), OC is confined to the ovaries (Figure 1-1), the ovarian capsule is still intact, and there are no tumour cells on the ovarian surface or in ascites (abnormal accumulation of fluid in the abdomen) or the peritoneal washings [11].

The tumour spreads beyond the ovaries when the ovarian capsule is disrupted. The metastasis can start by direct entry of tumour cells into adjacent tissues i.e. uterus, fallopian tubes, the mesothelial lining of the pelvic cavity (peritoneum), and the broad ligament (a fold of peritoneum that supports the uterus). Tumour cells are transported by peritoneal fluid and then implant on the peritoneum and mesothelial linings of the pelvic and abdominal organs (serosa). This stage is

usually associated with ascites formation. This behaviour is particularly common in HGSC. Tumour cells can also spread through the lymphatic system that drains the ovaries to the pelvic and paraaortic lymph nodes. Unlike most of the other cancers, OC rarely spreads via the vasculature [12].

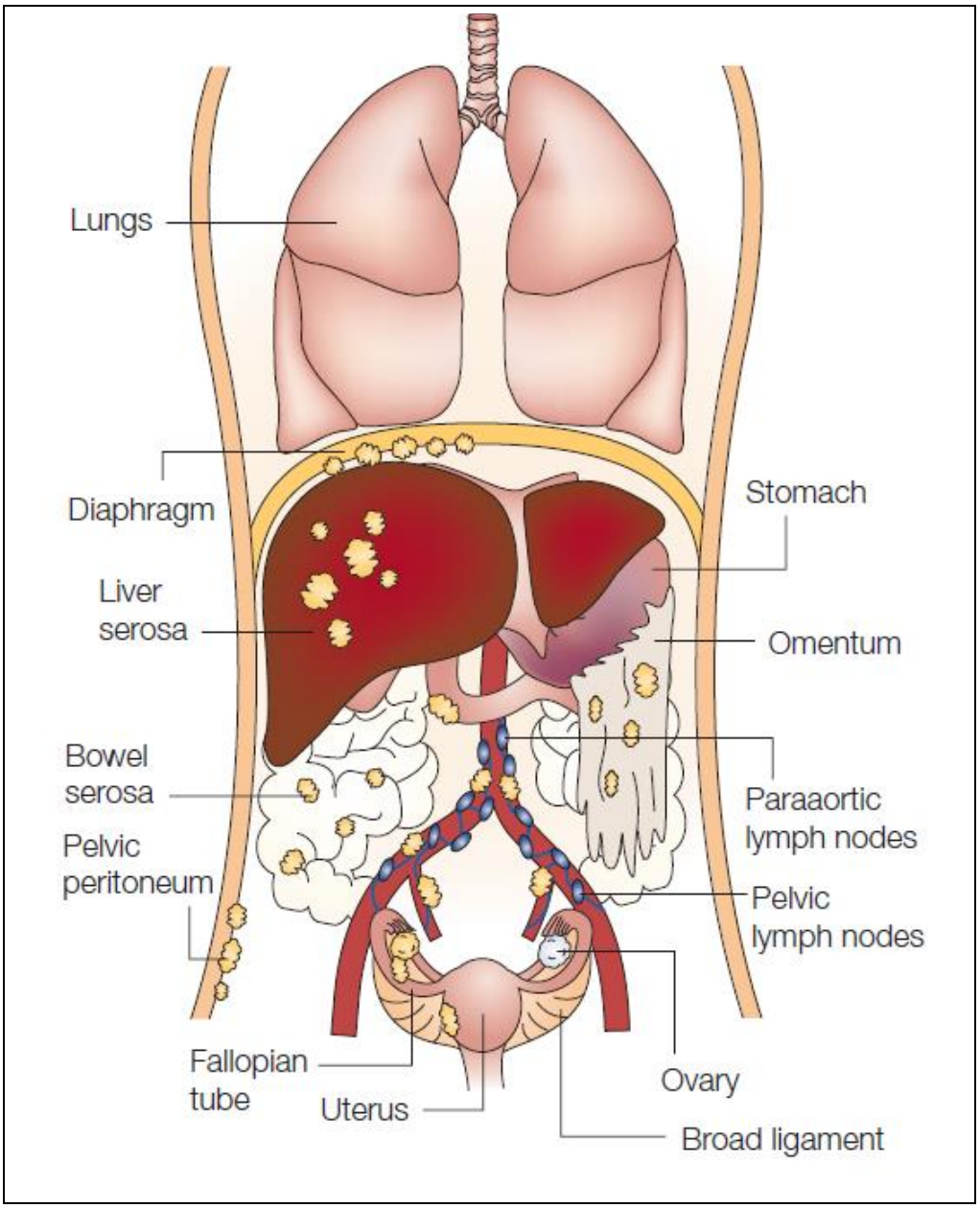


Figure 1-1: Patterns of spread of ovarian carcinoma [12]

OC is a diffuse cancer and therefore, surgery alone is rarely successful. In almost all the cases postoperative chemotherapy is certainly required, except for patients with organ-confined, low-grade disease [12].

1.1.2 Intraperitoneal fluid and ascites

In healthy individuals the intraperitoneal fluid volume is negligible. In women IP fluid volume changes at various stages of menstrual cycle, it can range from 1 to 20 ml [13], [14]. Whereas, in healthy female mice (~30g average body weight) mean IP fluid volume is 100 µL +/- 50µL [15].

Ascites is an abnormal accumulation of fluid in the peritoneal cavity (abdomen). Cancer is the second most common cause of ascites after liver cirrhosis and it accounts for 10% of all the ascites cases [16]. Out of all the cancer related ascites, 37% cases are due to ovarian cancer [16]. Up to 25 litres of ascites can accumulate in the patients. Intraperitoneal chemotherapy, after removal of ascites fluid by paracentesis, has been suggested as an attractive approach to treat ascites. Locoregional administration of chemotherapeutics can kill the cancer cells at the peritoneal surface which are the main culprit of the ascites accumulation in ovarian cancer and therefore can prevent the ascites recurrence [16].

1.2 Current treatment strategies

Current standard of care for OC involves cytoreductive surgery followed by intravenous (IV) chemotherapy (most commonly a combination of carboplatin and paclitaxel) for removal of residual microscopic tumours [17-19]. Most of the patients respond well to initial chemotherapy however, majority of these patients develop disease recurrence at some stage [20,21]. It has been reported that >67 % patients that are diagnosed at advanced stage may develop disease recurrence [18,22].

In some cases, chemotherapy is administered before surgery (neoadjuvant chemotherapy), in particular for the patients with significant medical comorbidities and non-debulkable tumours [21]. However, neoadjuvant chemotherapy has not been recommended via the intraperitoneal route [21].

Although, many newer therapies are becoming available but surgery, chemotherapy or a combination of the two is still the first choice treatment for ovarian cancer [5].

1.2.1 Surgery

Surgery is a crucial step for the successful treatment of OC. Surgical intervention is necessary for at least three main reasons including, diagnosis establishment, disease staging and tumour debulking [19,21]. Biopsy is generally not recommended in patients with large tumour masses in order to avoid the disease spreading, therefore, the histological confirmation of disease diagnosis can be made at the time of surgery. Accurate disease staging is necessary to determine extent of disease spread, plan further treatment options and provide valuable prognostic information. It has been demonstrated by multiple studies that comprehensive surgical staging can identify one third of the occult disease [21]. The primary goal of tumour debulking is to minimise the tumour size which significantly increases the treatment success rate [6,21].

1.2.2 Chemotherapy

A large number of target specific and personalised medications are becoming available due to the increasing number of innovative collaborations between global investigators and cooperative groups (comprises of 10 groups that involve more than 3100 institutions and 14000 investigators) [21,23]. However, chemotherapy remains the standard of care for ovarian cancer [6,18,19]. In addition, combination of molecularly targeted therapeutics (e.g. Bevacizumab, Olaparib, etc) with chemotherapeutics offers a powerful new approach for cancer treatment and this might also counteract drug-resistance which is one of the major challenges in the treatment of cancer [6,24].

For ovarian cancer treatment, chemotherapy typically begins two to six weeks after surgery and continues for maximum 6 cycles with three weekly dosing per cycle [7]. Typical dosing schedule is Paclitaxel (Taxol) 175 mg/m^2 (formulation composition of Taxol: 6 mg/ml Paclitaxel in 527 mg/ml Cremophore EL and 49.7% v/v dehydrated alcohol, diluted with 250 ml saline solution for infusion, Bristol-Myers Squibb) administered by IV infusion over 3 hr period followed by Carboplatin AUC (**area under** the concentration vs time **curve**) 5-6 mg/ml per min by IV infusion on the same day [25]. Carboplatin dose is calculated by the Calvert formula (Formulation composition of PARAPLATIN: 10 mg/ml

carboplatin aqueous solution diluted with 250 ml of 5% dextrose solution for infusion, Bristol-Myers Squibb).

In a recent clinical trial, an alternate dosing schedule of paclitaxel has been tested, while keeping carboplatin dosing schedule the same. Paclitaxel was administered weekly at reduced dose of 80 mg/m^2 compared to 175 mg/m^2 every three weeks. This DOSE-DENSE approach resulted in prolonged progression free survival (PFS) and overall survival (OS) [26]. In another multicentre, randomised phase 3 clinical trial, standard 3 weekly paclitaxel / carboplatin chemotherapy (as detailed above) was compared with weekly (dose-dense) schedule (Paclitaxel 60 mg/m^2 and Carboplatin AUC 2 mg/ml per min) for 18 weeks. No progression free survival benefit was observed in this study however; significant improvement in quality of life and toxicity profile has been shown [17]. Shawky et. al. has shown in a phase II clinical trial that extended dose-dense carboplatin / paclitaxel regimen is both effective and well tolerated with minimal toxicity in platinum resistant and platinum sensitive recurrent EOC patients who have been previously treated with carboplatin / paclitaxel 3 weekly regimen [27].

Moreover, as described above, ovarian cancer is primarily contained within the peritoneum [7]. Therefore, we propose that intraperitoneal sustained release chemotherapy administration could provide a step change in OC treatment because it would maintain the therapeutic drug concentrations in the vicinity of tumour for a prolonged period (i.e. dose densing) whilst reducing systemic side effects, which result in improved therapeutic index.

1.2.2.1 Paclitaxel

Paclitaxel is a member of the taxane family of chemotherapeutic agents. It induces tubulin polymerization by interfering with the late G_2 and M phases of the cell cycle (Figure 1-2) [28]. This effect is dependent on both the concentration and length of exposure of paclitaxel to the tumour cells [29]. Further research has indicated that paclitaxel induces programmed cell death (apoptosis) in cancer cells by binding to an apoptosis inhibiting protein called Bcl-2 (B-cell leukaemia 2) and thus arresting its function [30,31].

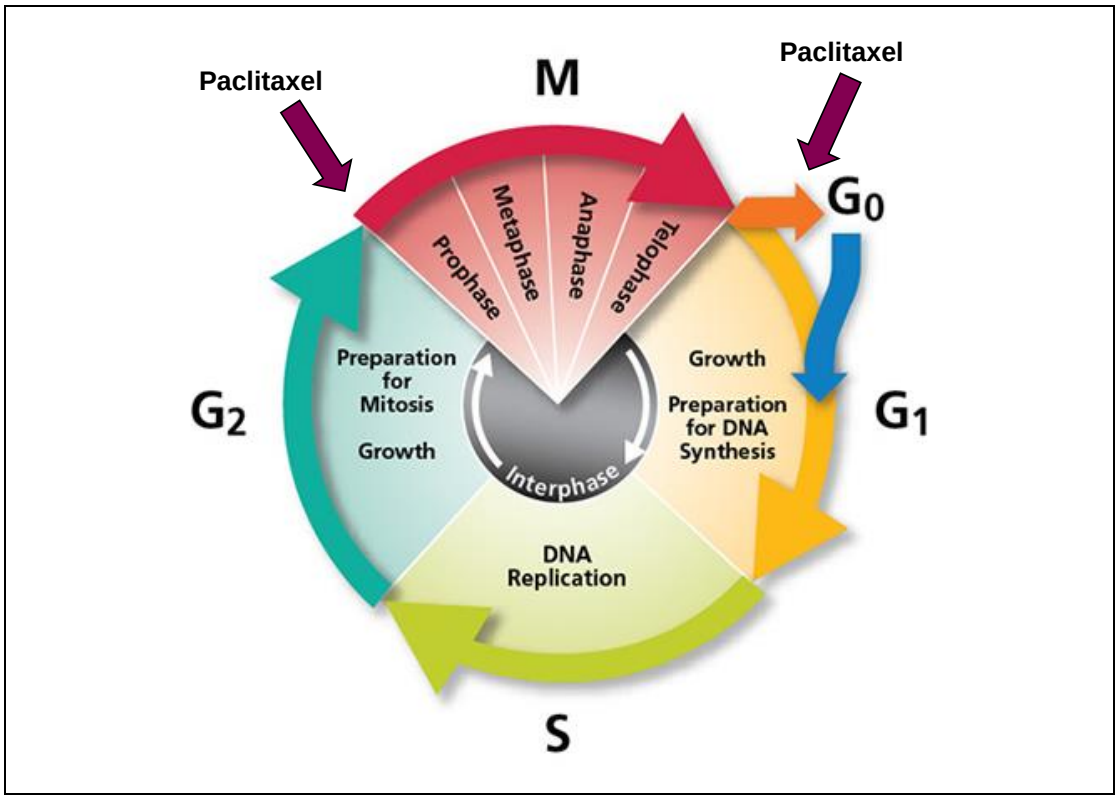


Figure 1-2: Paclitaxel mechanism of action; Paclitaxel inhibits cellular replication in transition from G0 to G1 and pre-mitotic G2 and mitotic M phases of the cell cycle [28].

Paclitaxel has various dose limiting toxicities including, leucopoenia, neurotoxicity and mucositis. The main dose limiting side effect of intraperitoneal paclitaxel is severe abdominal pain [29]. Controlled release drug delivery strategies have shown promise to reduce paclitaxel toxicities while maintaining efficacy. For example, Demetrick et. al. administered sustained release 30% w/w paclitaxel loaded PLGA microspheres (size 30-100 µm) via intraperitoneal route to the Wistar rats implanted with glioblastoma tumour cells in the peritoneal cavity. In this study they demonstrated that compared to the bolus paclitaxel (paclitaxel solution in cremophore EL) sustained release PLGA microspheres loaded with 30% paclitaxel prevented the tumour implantation and growth in all of the five animals without any mortality or significant morbidity throughout the study period (15 days). Whereas, in the paclitaxel bolus injection group four out of five animals died, primarily linked to high paclitaxel concentration resulting in systemic and localised toxic effects [29].

1.2.2.2 Carboplatin

Carboplatin, cis-diammine (cyclobutane-1,1-dicarboxylato)-platinum(II), is a second generation organoplatinum antineoplastic drug. It is classed under the alkylating agents and is used to treat various forms of cancer [32-34]. Carboplatin's cellular mechanism of action is similar to cisplatin, which involves activation of the platinum compound by "replacement of leaving group with water" inside the cell, a process called aquation [35]. Although activated platinum compounds can interact with various cellular components, DNA is the main target of action [24]. The activated platinum atoms covalently bind to the N7 positions of purine bases and results primarily in intra-strand crosslinks and some inter-strand crosslinks (Figure 1-3) [24].

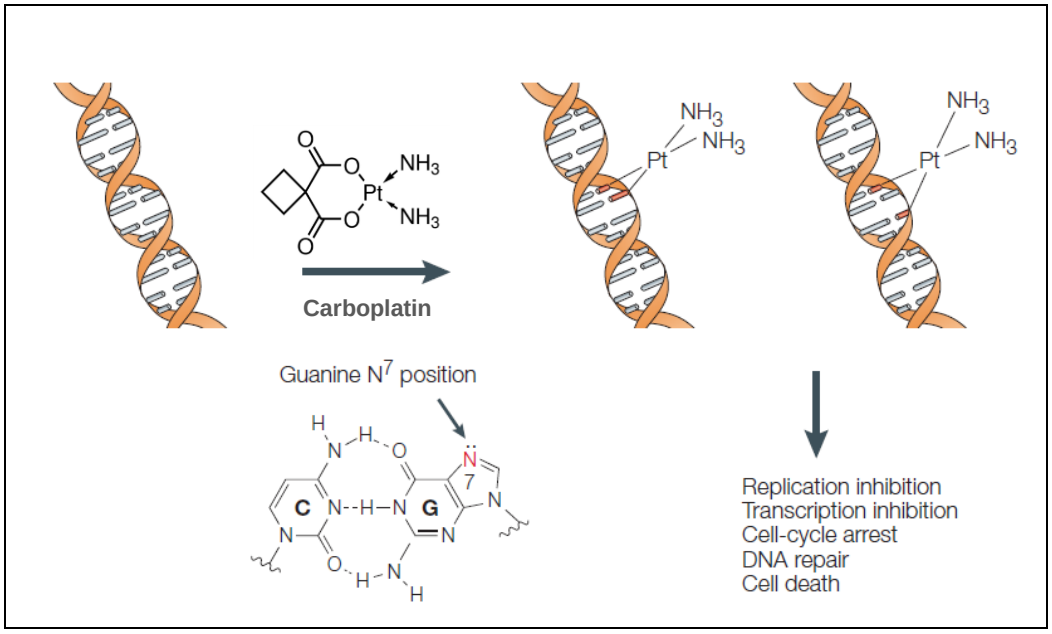


Figure 1-3: Carboplatin mechanism of action, formation of carboplatin – DNA adducts and cell death [24].

Carboplatin has good aqueous solubility (50 mM) [36] and stability [24]. Its clinical activity is comparable to the cisplatin but with significantly fewer side effects [36]. Although, carboplatin causes considerably lower nephrotoxicity than cisplatin the renal function is strictly monitored when determining the carboplatin dosage regimens to avoid acute nephrotoxicity [37].

The primary dose limiting toxicity of carboplatin is cumulative myelosuppression which is characterised by thrombocytopenia, granulocytopenia and anaemia [37].

In addition, carboplatin also carries a significant risk of neurotoxicity and hypersensitivity reactions [37]. IP administration of carboplatin has shown significantly reduced toxicity, where the toxicities after IP administration included mild-to-moderate abdominal pain, nausea and vomiting [38]

1.3 Localised Controlled Release Delivery of Chemotherapeutics

Chemotherapy is generally administered systemically even though the pharmacologic target sits in a specific tissue or single body compartment [39]. The systemic administration, inadvertently, results in the distribution of drug to the healthy tissues as well as the diseased tissues. It is therefore difficult to achieve selective chemotherapeutic actions with the use of systemic administration, hence systemic administration results in serious side effects [39]. Therefore, it seems logical to administer the chemotherapeutics via localised controlled released drug delivery systems at the site of action, especially for localised cancers e.g. ovarian cancer. This is to ensure higher locoregional drug concentration, reduced systemic exposure and therefore, improved therapeutic index [40].

1.3.1 Controlled release drug delivery

Controlled release drug delivery technology is one of the most rapidly advancing areas of science. It offers many advantages over conventional drug delivery, including improved therapeutic index, enhanced patient compliance, reduced number of drug administrations and site specific drug delivery [41,42]. It has been estimated that around 90% of the 100 best selling prescription medicines may further improve patient quality of life by switching to a controlled release drug delivery approach and reducing the frequency of administration [43]. An ideal controlled release drug delivery system matches the rate of drug release with rate of elimination and therefore, maintains therapeutic dose for longer compared to the conventional drug delivery where the drug concentration fluctuates (Figure 1-4).

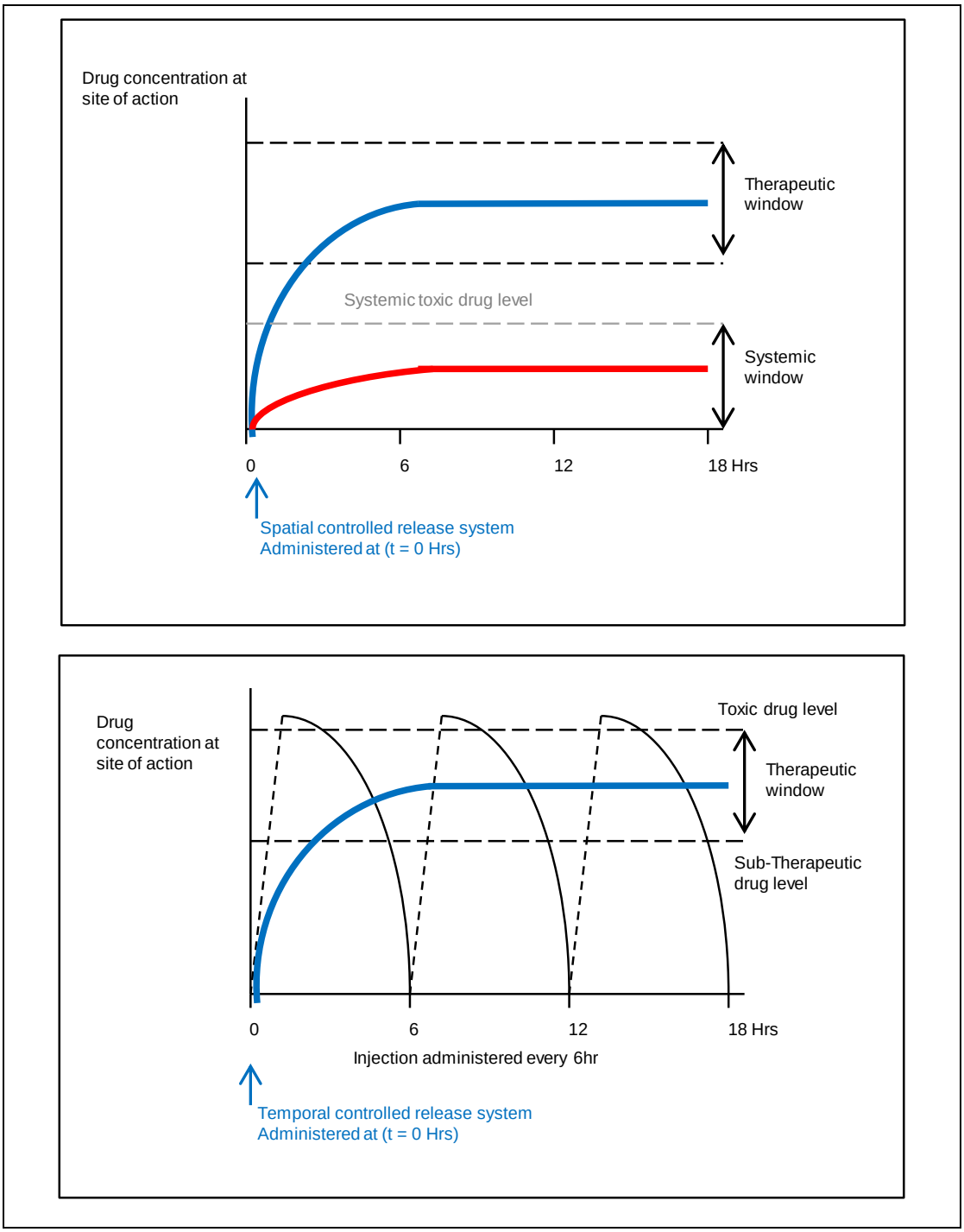


Figure 1-4: Examples of typical controlled release drug delivery systems including spatial release system (top) and temporal release system (bottom). Redrawn from [41]

Controlled release systems can be designed to provide temporal and/or spatial (localised) control over the release of active agent [41]. Spatial release systems deliver the drug to the site of action and therefore, provide higher drug concentration locally at the therapeutic site with minimal systemic exposure (Figure 1-4) and therefore reduced off target toxicity [41].

However, spatial release drug delivery systems would be most beneficial in cases where the site of drug delivery and action is accessible with minimal risk/discomfort to patient (i.e. minimal surgical intervention). In addition, such drug delivery systems would be favourable for anatomical sites (tissue or compartment) from where the free drug does not easily escape due to unique anatomical structure of tissue e.g. blood-brain barrier [41], blood-peritoneal barrier [44], Bladder, Eye and Skin [39].

For cell cycle specific drugs that target pathways involved in cell replication (e.g. paclitaxel), it has been shown that extended exposure of cancer cells to chemotherapy over multiple cell cycles is more cytotoxic compared to bolus delivery [45]. This is because at any single time only 10-15% of tumour cells are expected to be in the mitotic phase of cell division [45-47].

1.3.2 Intraperitoneal drug delivery

IP drug administration has pharmacokinetic advantages because of the peritoneal–plasma barrier, this is primarily due to interstitial capillary wall and interstitial space surrounding the capillaries [39]. IP administered drugs are mainly cleared from the peritoneal cavity via the hepatic portal circulation, however, portal circulation is quite slow which results in preferentially higher drug accumulation in the peritoneal cavity compared to systemic concentration and other parts of the body [39,48]. IP chemotherapy is therefore, an attractive option for the treatment of OC [39].

It has been reported that drug penetration into solid tumours is limited which can compromise cytotoxicity of chemotherapeutics, therefore, it is recommended that IP chemotherapy administration would be more beneficial for patients with small volume tumours or after tumour debulking surgery [49,50].

Multiple clinical studies have shown improved therapeutic index benefits therefore, the National Cancer Institute (NCI) encourages the use of IP chemotherapy for the treatment of advanced OC. However, still the clinical application of this route of chemotherapy administration is low [51,52]. This in part, is due to some practical and theoretical concerns linked with IP administration, including, the risk of chemical peritonitis due to high drug exposure [52], risk of catheter-associated subcutaneous and peritoneal cavity infections, bowel perforations and obstructions [53], inadequate drug penetration into bulky

tumours [52], and lack of dedicated and approved formulations for IP treatment [52,53].

We propose that a localised controlled release drug delivery system can address the majority of above-mentioned hurdles and will improve the application of IP drug administration and provide drugs with improved therapeutic index for the treatment of ovarian cancer in particular.

1.3.3 Intraperitoneal chemotherapeutic delivery strategies

Weissberger first introduced the concept of IP chemotherapy in 1955 [54]. Since then various IP chemotherapeutic delivery strategies has been tested for various peritoneal carcinomatoses including ovarian cancer. The major strategies include;

Hyperthermic Intraperitoneal Chemotherapy (HIPEC): this is one of the most mature IP chemotherapy administration strategy for peritoneal tumours. The PharmaCircle™ search (www.pharmacircle.com, accessed January 2020) for terms “hyperthermic intraperitoneal chemotherapy” and “ovarian cancer” found 9 US and 5 EU clinical trials. HIPEC is the administration of chemotherapy at optimum temperatures between 42 to 43 °C and it is performed immediately after cytoreductive surgery for 60 to 120 minutes [54]. HIPEC is typically followed up by early postoperative intraperitoneal chemotherapy (EPIC) which involves the administration of intraperitoneal chemotherapy from day 1 after surgery and continued daily for 5 to 7 days. This approach is based on the dose intensification principle i.e. exposing the residual tumour to very high doses of chemotherapy [55].

Pressurised Intraperitoneal Aerosol Chemotherapy (PIPAC): it is a relatively new technology which was introduced for the treatment of peritoneal metastases in 2011. This technique utilises aerosolised chemotherapy in carbon dioxide gas which is instilled into intraperitoneal cavity under pressure via laparoscopic ports [56,57]. A number of clinical trials have been reported where PIPAC is used for the treatment of various peritoneal metastases [56], indicating that this is also an attractive method for intraperitoneal chemotherapy administration.

Although various other approaches for the intraperitoneal administration of chemotherapy has been reported in the literature, none of these approaches have reached the clinical phase of development (www.pharmacircle.com, accessed January 2020) e.g.

- Nanoparticles: Including liposomes [58], micelles [59], polymeric nanoparticles [60], gelatin nanoparticles [61] and expansile nanoparticles [45].
- Microspheres / Microparticles: including polymeric microspheres [52,62] and activated charcoal microparticles [63].
- Hydrogel and Particle composites: Including implantable films [64,65] and in-situ forming composites [66,67], to name a few.

From this literature search, it is apparent that the interest in the intraperitoneal chemotherapeutic delivery has steadily grown over the years (Figure 1-5).

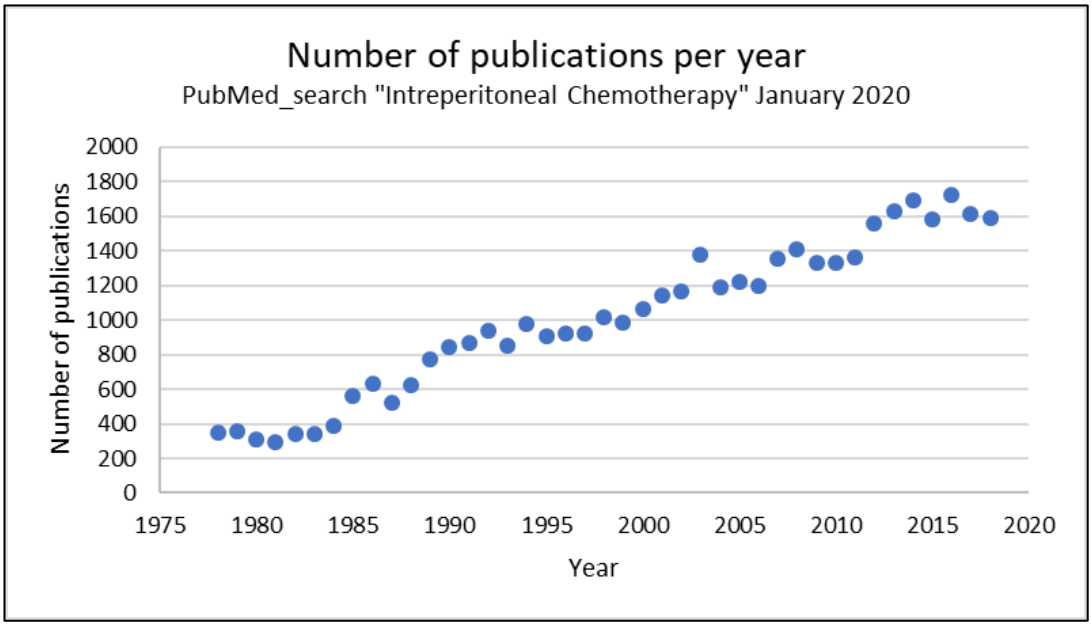


Figure 1-5: Graph showing the number of publications describing the intraperitoneal chemotherapy administration per year during last 40 years (from 1978 – 2018). PubMed search dated 10 January 2020, for term "intraperitoneal chemotherapy".

Although, HIPEC and PIPAC approaches are gaining attention but both of these methods require specialised facilities i.e. equipment, staff, etc. It is apparent that, still there are no dedicated and approved products available for the sustained release administration of IP chemotherapy, with minimal intervention,

to take the advantage of proven “dose intensification” strategy for the treatment of peritoneal carcinomatoses, in general and ovarian cancer, in particular.

1.4 Proposed Drug Delivery System

The proposal for this research project was to develop an injectable sustained release drug delivery system comprising of paclitaxel and carboplatin loaded PLGA microspheres suspended in a hydrogel, to deliver therapeutic concentrations of both APIs in the intraperitoneal cavity for a 1 month or longer duration after single injection. The proposed target patient population was “patients that have had maximal surgical cytoreduction, at least”. This drug delivery system may also be used for the sustained delivery of chemotherapeutics in support of other procedures e.g. HIPEC, PIPAC, etc.

We have selected PLGA as the primary component because it is one of the most commonly used biomaterials for medical applications. It has excellent biodegradation and biocompatibility properties and is generally regarded as safe material by international regulatory agencies e.g. US FDA, EMA, etc. [68]. In addition, number of PLGA microsphere based formulations are already approved for clinical applications by various routes of administration, see Table 1.1 [69-71]. Therefore, PLGA microspheres were selected as the back bone of this proposed drug delivery system.

Although several PLGA microsphere manufacturing technologies have been developed over the years, the “precision microsphere fabrication / manufacturing technologies” are relatively new. This includes, microfluidics which is the science and technology of systems with integrated channels on microscale allowing the systematic manipulation of small quantities of fluids to form well controlled, uniform size microspheres [72-74]. We have selected to use a microfluidics technique to make PLGA microspheres because, to the best of our knowledge, there are no studies performed on this technique to systematically evaluate the critical factors for making PLGA microspheres, encapsulate compounds with different physicochemical properties and tailor the release rates of these compounds from PLGA microspheres.

Table 1.1: Examples of commercially available pharmaceutical products containing PLGA-based microspheres

Product name	Active ingredient	Company	Application
Bydureon® Bcise™	Exenatide	AstraZeneca AB	Type 2 diabetes
Bydureon®	Exenatide	AstraZeneca AB	Type 2 diabetes
Lupron Depot®	Leuprolide acetate	TAP	Prostate cancer
Nutropin Depot®	Growth hormone	Genetech	Pediatric growth hormone deficiency
Suprecur® MP	Buserelin acetate	Aventis	Prostate cancer
Decapeptyl®	Triptorelin pamoate	Ferring	Prostate cancer
Sandostatin LAR® Depot	Octreotide acetate	Novartis	Acromegaly
Somatuline® LA	Lanreotide	Ipsen	Acromegaly
Trelstar™ Depot	Triptorelin pamoate	Pfizer	Prostate cancer
Arestin®	Minocycline	Orapharma	Periodontal disease
Risperdal® Consta™	Risperidone	Johnson & Johnson	Antipsychotic
Signifor Lar®	Pasireotide pamoate	Novartis	Acromegaly
Triptodur Kit®	Triptorelin pamoate	Arbor	Central precocious puberty

Hydrogels were primarily used to improve the PLGA microsphere biocompatibility, prevent microsphere clearance from peritoneal cavity [75] and avoid inflammation and adhesion in the peritoneal cavity due to PLGA microspheres [62,76,77]. Although, hydrogels has been extensively used to control the release of various therapeutic agents [78,79], it is not the intention in this study because the API release rates would be mainly controlled by the PLGA microspheres.

1.5 Summary and Objectives

There is an unmet need to improve the treatment of ovarian cancer. It is evident from the research so far that intraperitoneal sustained release chemotherapy administration could provide a step change in OC treatment by maintaining therapeutic drug concentrations at the tumour site for prolonged period and taking the advantage of a “dose intensification” approach. However, there are still no dedicated and approved drug products available for this purpose.

The aim of this study was to develop an injectable sustained release drug delivery system comprised of paclitaxel and carboplatin loaded PLGA microspheres suspended in hydrogel to maintain the therapeutic concentrations of both APIs in the intraperitoneal cavity for a prolonged duration (>1 month) after a single injection. The proposed target patient population is those patients that have had maximal surgical cytoreduction.

In order to achieve the aim, we set following objectives:

- Develop an intraperitoneal pharmacokinetic mathematical model to determine the key parameters e.g. drug loading, release kinetics and dosage regimen (i.e. dose, dosing frequency and duration) for the design of the drug delivery system, so that the required therapeutic concentrations of paclitaxel and carboplatin can be achieved and maintained in IP cavity for the desired duration (Chapter 2).
- Define the QTPP (quality target product profile) for the manufacture of PLGA microspheres by using the data from chapter 2. Use this QTPP to evaluate different methods to manufacture PLGA microspheres and select the most suitable method(s) (chapter 3)
- Evaluate hydrogel manufacturing and characterisation methods. Prepare microsphere-hydrogel composites and evaluate their physical stability in simulated intraperitoneal fluid and select the most appropriate hydrogel (chapter 4).
- Optimise the PLGA microsphere manufacturing method(s), selected in chapter 3, by using a DOE (design of experiment) approach to obtain the microsphere size as defined in the QTPP (50-200 μm). In addition, determine the critical process parameters to tune the microsphere size

in order to maintain the size in the desired range (50-200 μm) after loading the API, if needed. This will make the method(s) generic and may allow the application for a wide variety of APIs. Manufacture the paclitaxel and carboplatin loaded PLGA microspheres by using the optimised method (chapter 5).

- Use the manufacturing methods selected in chapter 5 to optimise the release rates of paclitaxel and carboplatin from PLGA microspheres by using four different grades of PLGA polymer. Select the final method(s) with optimum release rates for carboplatin and paclitaxel and apply the intraperitoneal PK mathematical model (chapter 2) to the final data and determine the optimum dosage regimen (chapter 6).

2 Intraperitoneal pharmacokinetic model for designing the IP sustained release drug delivery system for ovarian cancer

2.1 Introduction

In order to systematically develop a localised controlled release drug delivery system, it is essential to determine the pharmacodynamic (e.g. IC50 or GI50 values) and pharmacokinetic properties of the API in the relevant site of administration and action for the disease of interest [80].

2.1.1 Pharmacodynamic properties

Various studies have been reported in the literature where carboplatin and paclitaxel GI50 concentrations were determined in different cancer cell lines, including ovarian cancer [81-84]. However, firstly very few studies used appropriate ovarian cancer cell lines (i.e. HGSC) and secondly, the reported GI50 values are quite variable which has been shown to be due to differences in the cell lines and dosing schedule [83].

A careful selection of the cell line to ensure they closely resemble the genomic alterations of a tumour type or subtype of interest is essential for a successful outcome [85]. Domcke et. al. evaluated 47 ovarian cancer cell lines by comparing data from The Cancer Genome Atlas (TCGA) and Broad-Novartis Cancer Cell Line Encyclopaedia (CCLE). They divided these cell lines into four broad categories based on the genetic similarity to high-grade serous ovarian carcinoma (HGSC), in order to identify most suitable invitro cell models for the HGSC [85]. These categories include; likely high grade serous, possibly high grade serous, unlikely high grade serous and hyper-mutated cell lines [85]. Although the high degree of genetic similarity is necessary for the target (molecular) specific therapeutic agents e.g. inhibitors of MDM2, BCL-2, ALK, PARP, etc [86] , this is not a requirement for non-specific cytotoxic drugs. e.g. carboplatin. Here, it was considered a sensible approach to use at least one cell line that closely resembles the tumour subtype of interest i.e. HGSC and a second cell line which may not closely match the HGSC but may represent a broad range of tumour types i.e. hypermutated ovarian cancer cell line.

Therefore, based on the categorisation of Domcke et. al. two cell lines i) OVCAR4 (likely high grade serous) and ii) IGROV1 (hyper mutated ovarian cancer cell line) were selected to determine the pharmacodynamic characteristics (i.e. GI50) of carboplatin and paclitaxel by using cell viability (cytotoxicity) assays.

Cell viability assays can be broadly divided into two categories i) the assays that determine the bona fide cell death [87] and ii) the assays that determine the biochemical processes that are viewed as surrogate viability markers [88]. A wide variety of in-vitro cell viability or cytotoxicity assays have been reported in literature to determine the GI50 of therapeutic agents [88-92].The first step in the selection of a cell viability assay is to choose the end point determination criteria [93]. Most of the common cell viability assays utilises vital dyes, these are fluorescent or coloured molecules that differentiate between living and dead cells [88]. Vital dyes that are preferentially excluded by the living cells with intact plasma membrane provide more robust, artefact free information [88]. Therefore, such vital dye based assays are most reliable, selective and easy to perform in-vitro cell viability assays [91]. In addition, fluorometric assays are highly sensitive compared to traditional colorimetric and radioactivity-based assays [91]. SYTOX green nucleic acid stain assay is one of the commonly used assays in this category and therefore selected as method of choice in our study, SYTOX green was also the method of choice for the AstraZeneca.

2.1.2 Pharmacokinetic mathematical model

A pharmacokinetic mathematical model was developed to assist in the design of the drug delivery system and to estimate the dosage regimen for the selected drug delivery system to ensure the therapeutic drug concentrations are achieved and maintained in the IP cavity for the desired period. In the context of this study, the therapeutic drug concentration was defined as “three times the GI50 concentration”, which is a typical starting point for the in-vivo studies, until in-vivo data is available.

Dedrick et. al. have presented a two-compartment model to estimate the pharmacokinetic advantage of IP over IV administration [48] and Tamura et. al. has developed a two-compartment PK model to estimate the unchanged

cisplatin concentration in the peritoneal fluid by using a zero-order rate of infusion into the peritoneal fluid.

We do not intend to evaluate the pharmacokinetics of the API in plasma and other parts of the body. The focus of our work was on the factors which affect the “concentration time profile” of API in the IP fluid.

Therefore, a simplified three-compartment model involving i) API encapsulated in the microspheres, ii) free API (released and unbound) in the IP fluid and iii) API elsewhere in the body has been developed.

The first part of this chapter is comprised of the experimental work to determine GI50 values of paclitaxel and carboplatin in two ovarian cancer cell lines when administered as monotherapy and combination therapy.

This data was then used along with the intraperitoneal pharmacokinetic data of carboplatin and paclitaxel from literature [61,94], to establish the mathematical model to help design the drug delivery system by estimating the release rates from the formulation, drug loading and dosage regimen.

2.2 Materials and methods

2.2.1 Materials

Cell lines: OVCAR4 (cell bank ID 71772) and IGROV1 (cell bank ID 61588) were sourced from AstraZeneca Alderley Park Cell Bank; DPBS (Dulbecco’s phosphate buffered saline) without calcium and magnesium, TrypLE™ express enzyme with phenol red (1X), GlutaMAX™ supplement, Penicillin-Streptomycin (10,000 U/ml), RPMI-1640 Medium phenol red free, Trypan blue stain (0.4%) for use with Countess automated cell counter and SYTOX green nucleic acid stain (5 mM solution in DMSO) were obtained from Gibco Invitrogen; FCS (foetal calf serum) was purchased from PAA Labs. / GE Healthcare; 40 µM nylon cell strainers was sourced from BD Falcon; Saponin from quillaja bark (sapogenin content > 10%) was obtained from Sigma-Aldrich; CELLSTAR® 384 well microplate, polystyrene, tissue culture treated, flat bottom, black / µClear®, with Lid was purchased from Greiner Bio-One and 175 cm^2 Nunc™ cell culture treated flasks with filter caps (T175 flask) were sourced from Thermo Scientific.

2.2.2 Methods

Routine cell passage

Cells were cultured in T175 flask using 50 ml RPMI-1640 growth media supplemented with 10% v/v FCS, 1% v/v glutamax and 1% v/v penicillin-streptomycin (growth media recommended by the cell line supplier). The cell passage frequency was at least once in a week to maintain logarithmic growth when incubated at 37 °C with humidified atmosphere of 5% CO_2. After the first culture, cells were used within 30 passages to minimise phenotypic/genotypic drift [95].

SYTOX green nucleic acid stain assay

The schematic of the method is given in **Figure 2-1.**

Cell Preparation for plating

Cells were rinsed with DPBS, stripped from flasks using 3-4 ml TrypLE™ express and neutralised with 16 ml growth media. Cell suspensions were syringed twice through a 1.2 mm bore needle to break up clumps and filtered through a 40 µm cell strainer to remove large cell clumps and free DNA strands (to reduce background detection after SYTOX green staining). The total number of cells in cell suspension was determined by Trypan blue staining method using an Invitrogen™ Countess™ automated cell counter (ThermoFisher Scientific, UK). The cell suspension was diluted with the cell growth media, to achieve 1000 cells / 70 µL cell suspension. 70 µL cell suspension was therefore, transferred into each well of the 384 well plate using a Multidrop Combi liquid handler. A day 0 plate containing each cell line (top ½ plate containing IGROV1 and bottom ½ OVCAR4) was set up to determine cell number at the start of dosing. For compound dosing two plates of each cell line were prepared, one for day 3 and other one for day 6. All plates were incubated at 37 °C and 5 % CO2 in a rotating incubator with relative humidity of 99% to reduce evaporation of media.

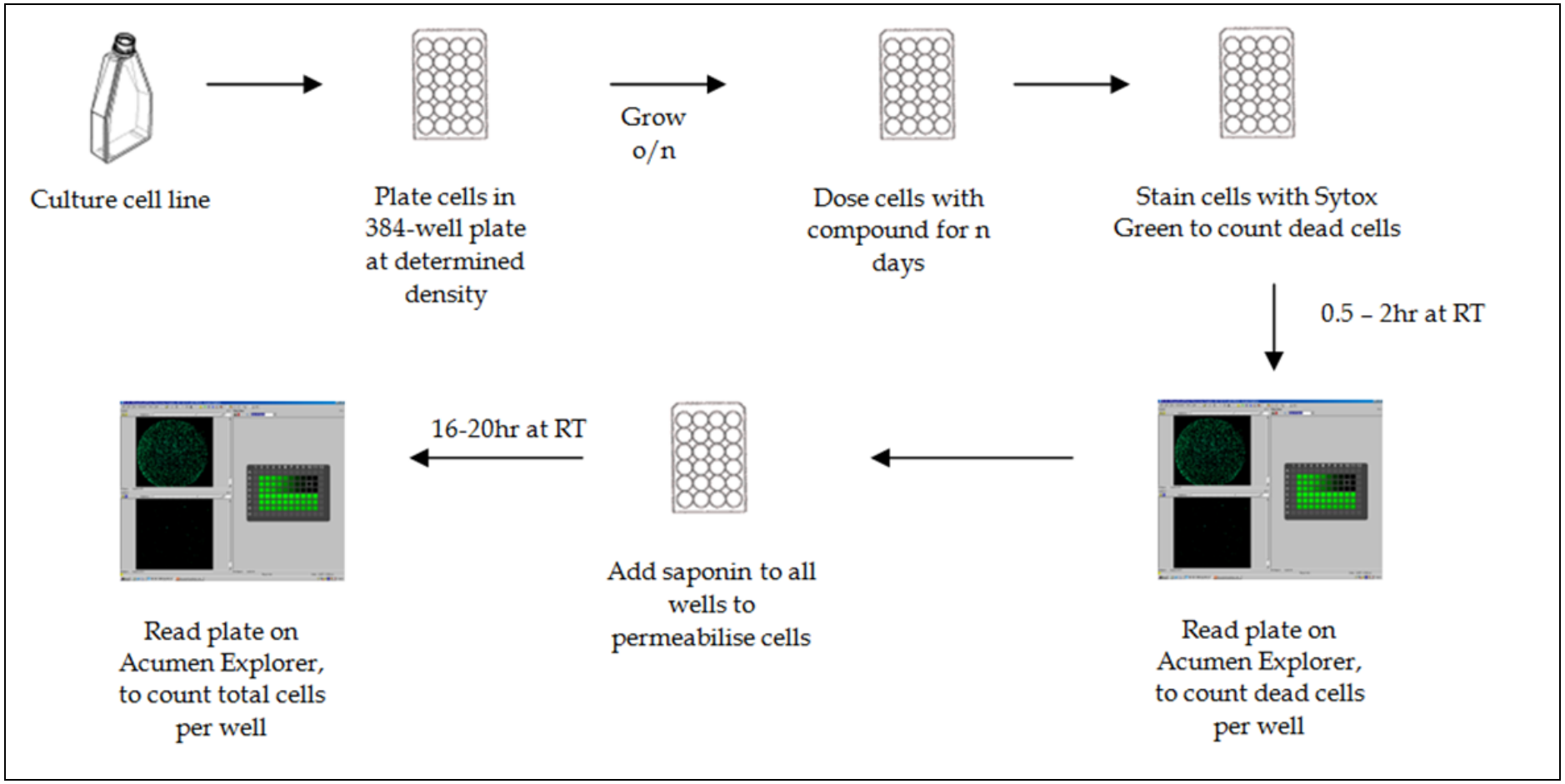


Figure 2-1: Schematic flow diagram of SYTOX green nucleic acid stain assay

API Dosing (Day 0)

After overnight (24 hr) incubation all plates, except day 0 plate, were dosed using the integrated Echo® 555 system (Labcyte Inc.), dose files were generated using the CombAT software which determines the required stock solution concentrations and volumes dispensed to achieve the desired final compound concentration in each well of the plate. Carboplatin 10 mM stock solution was prepared in DPBS. Paclitaxel 10 mM stock solution was prepared in DMSO and further diluted with DMSO to 100, 1 and 0.001 nM sub stock solutions. These solutions were loaded into the dosing source plate as per the combAT source file.

Table 2.1 Carboplatin and Paclitaxel concentrations used in this study, for duplicate experiments.

Dose label	Carboplatin (µM)		Paclitaxel (nM) (Same concentrations for both experiments.)
	Exp 1	Exp 2	
1	300	500	3
2	100	200	1
3	30	70	0.3
4	10	20	0.1
5	3	7	0.03
6	1	2	0.01
7	0.3	0.7	0.003

The above Table 2.1 is showing the compound doses administered in each of the duplicate experiment. These dose ranges were determined from a preliminary in-vitro cell viability assay (MTT assay) where carboplatin dose range 0.01 to 500 µM and paclitaxel dose range 0.01 nM to 10 µM were evaluated. Each dose was administered as a monotherapy and combination therapy, at least in duplicate, see Appendix A for the dosing matrix. In addition, each plate also had DMSO control wells containing a final concentration of 0.14% v/v DMSO and blank control wells containing only growth media. After dose administration, plates were incubated for the respective duration (3 or 6 days) at 37 ºC and 5 %CO_2 in a rotating incubator with a relative humidity of

99%. For the combination therapy, both compounds were administered sequentially, paclitaxel followed by carboplatin without any delay. This simultaneous dosing regimen is selected to mimic dose delivery from our proposed drug delivery system, where both compounds will be released simultaneously at a predefined rate and concentration.

Cell staining and counting:

After overnight (24 hr) incubation, 5 µl Sytox green working stock was added into all wells of the day 0 plate and a plate left at ambient conditions for approximately 2 hrs. These plates were then read on the acumen plate reader to count the dead cells, followed by addition of 10 µl Saponin working stock to permeabilise the cells. The plates were then incubated for further 16-24 hrs at ambient conditions before reading the plate on the acumen plate reader for total cell count, Figure 2-1. The total live cell number was then calculated by subtracting the dead cell count from the total cell count. Similarly, the assay plates were stained with sytox green, cells counted with acumen plate reader and total number of live cells determined at the day 3 and day 6 time points, Figure 2-1.

The acumen plate reader data was further processed by using the Genedata Screener software package (Genedata, Switzerland) to calculate GI50 concentrations and synergy scores. The GI50 concentration of the individual compound was calculated from the monotherapy dose response curves by fitting sigmoidal function. Three models were used in this software to determine the synergy scores (combination effects) including Loewe, Bliss and HSA (highest single agent) model. Loewe is the most commonly used and widely accepted model to determine the combination effects [96,97] and therefore, synergy scores generated by Loewe model have been reported in the results section.

2.3 Intraperitoneal PK mathematical model

A simplified PK mathematical model shown in Figure 2-2 was implemented in the Berkeley Madonna modelling software, version 8.3.14 (University of California, Berkeley). The model was based on three compartments representing drug encapsulated within the microspheres in the IP cavity, free

API (released and unbound) in the IP cavity and drug elsewhere in the body Figure 2-2. The drug is released from microspheres in the IP fluid from where it can be removed by absorption into systemic circulation and other parts of the body.

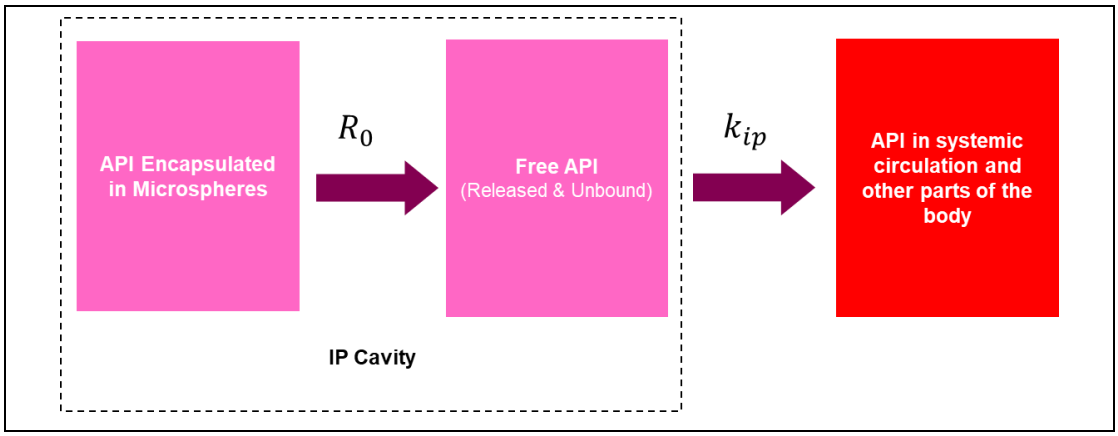


Figure 2-2: Intraperitoneal pharmacokinetic model to design the drug delivery system by estimating the required release rate from the microspheres and dose to maintain the therapeutic concentration (i.e. 3x GI50) of the API.

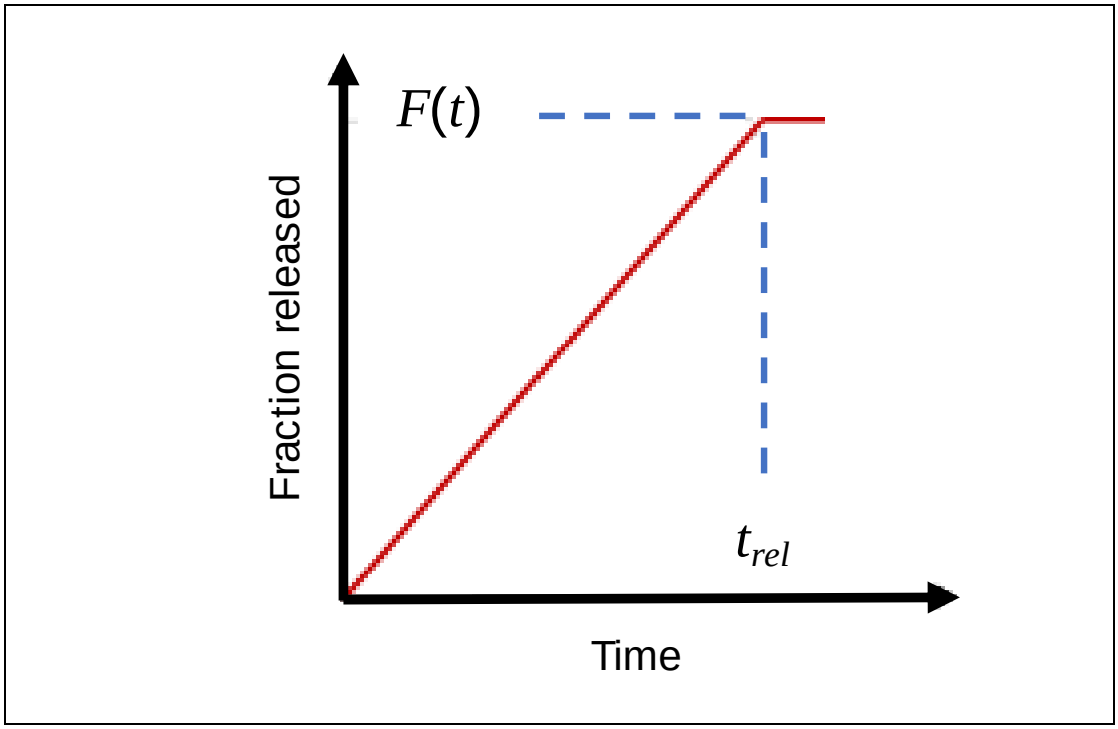


Figure 2-3: Example of a zero order release kinetic from PLGA microsphere-based formulation.

The rate of drug absorption from the IP cavity is assumed to follow first order process (relative to the amount of released drug). This could be characterised by an IP absorption rate constant (k_{ip}), analogous to absorption rate constants used to characterise absorption from the GI-tract. The paclitaxel k_{ip} value of 0.16 hr-1 was taken from Tsai et. al. paper [61], whereas, carboplatin k_{ip} value of 0.198 hr-1 was derived by using the PK data from McClay et. al. [94], see Appendix B for details. It was assumed that the microspheres (diameter >50 μm) are not cleared from the IP cavity [14] and the average IP volume in women remains constant at 10 mL [14].

An initial model was developed by using an ideal case scenario where the release from microspheres is assumed to be linear (zero order) Figure 2-3.

In this case, the fraction of API released at any particular time is represented by $F(t)$ and the release rate $F'(t)$ can simply be represented by the gradient of the slope k, where $k = 1/t_{rel}$ and the overall release rate (i.e. the drug input rate in the IP cavity) from a single dose (D) can be expressed as R_0 where, $R_0 = D \cdot k$

Initially, the constant drug input rate (R_0) would result in the increasing levels of drug in the IP cavity until a steady state is reached, where the absorption rate matches the constant release (drug input) rate from the formulation Figure 2-4. This steady state can be expressed as Equation 2-1

$$R_0 = k_{ip} X_{ip} \qquad \textbf{Equation 2-1}$$

Where R_0 is the drug input rate in the IP cavity from a formulation with zero-order release rate constant (in mass per unit time), k_{ip} is the first order API elimination (absorption) rate constant from the IP cavity and X_{ip} is the total amount (mass) of API in the IP cavity.

It is intended to maintain a minimum threshold concentration c_{min} of unbound drug in the IP cavity (i.e. three times above GI50), so the total concentration of API required in the IP cavity is simply this threshold concentration divided by the fraction unbound in IP fluid.

The minimum amount of drug, X_{min} required in the IP cavity at any time to ensure efficacy is therefore,

$$X_{min} = \frac{c_{min}}{f_u} V_{ip}$$ **Equation 2-2**

Where V_{ip} and f_u are the volume of the IP cavity and the fraction of unbound API in the IP cavity, respectively. The fraction unbound was determined from the plasma protein binding (ppb). For example, paclitaxel has a ppb of 94%, therefore, paclitaxel fraction unbound (f_u) would be 0.06. Whereas, carboplatin has no plasma protein binding i.e. f_u = 1 for carboplatin [30,33].

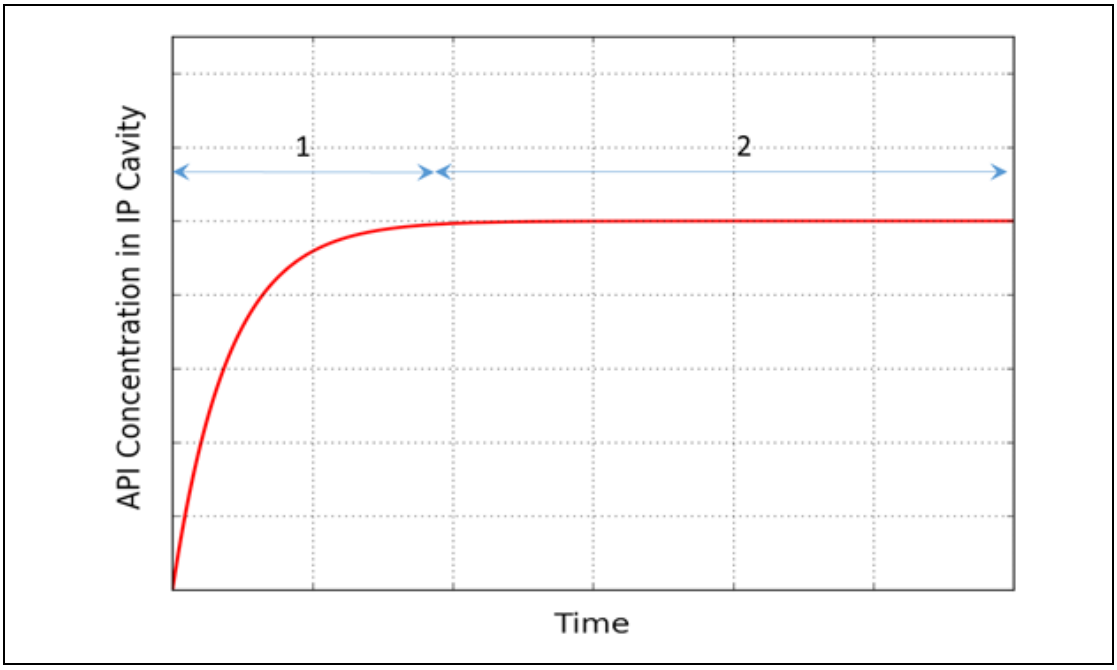


Figure 2-4: A representation of steady state of API concentration in the IP cavity. The region 1 represents initial phase where the release from the formulation is greater than the rate of removal of the API from the IP cavity. It is assumed that this phase is relatively short (compared to the steady state) and considered negligible. The region 2 represents the steady state where the release (input) of the API from the formulation is equivalent to the rate of removal from the IP cavity.

The minimum zero order release rate (in mass per unit time), required to maintain a steady state above the target therapeutic concentration in the IP cavity can therefore be represented as, Equation 2-3

$$R_{0,min} = k_{ip} \frac{c_{min}}{f_u} V_{ip}$$ **Equation 2-3**

or in terms of required dose (D), we can simply multiply above Equation 2-3 by the dosing interval (τ), as given below in Equation 2-4

$$D = k_{ip} \frac{c_{min}}{f_u} V_{ip} \tau$$ **Equation 2-4**

This Equation 2-4 was then used to determine the minimum dose required to keep the concentration of the API above target concentration $c_{target} = c_{min}/f_u$ for a specified dosing interval.

2.4 Results and Discussion

2.4.1 Monotherapy dose response and GI50 values

Monotherapy dose response curves for both compounds in both cell lines are shown in Figure 2-5 and Figure 2-6. In these plots, the activity (%) up to 100 means 100% growth inhibition (GI) whereas, activity (%) >100 indicates cell death. These figures show that the carboplatin dose response curves are typical sigmoidal in both cell lines indicating strong growth inhibition in response to the increase in the dose. Whereas, paclitaxel dose response curves do not follow the similar profile. For paclitaxel, in the IGROV1 cell line at day 3 there was no activity at 0.3 nM dose. However, when the dose was increased from 0.3 to 1 nM the activity increased but only to approximately 50% and any further increases in the dose did not increase the activity. Whereas at day 6 a moderate GI activity was observed at higher doses of paclitaxel in the IGROV1 cell line. Similarly, in the OVCAR4 cell line there was no significant activity with paclitaxel at day 3 and only moderate activity was observed at the higher doses at day 6. The clonogenic assay was also attempted to determine the cytotoxicity of paclitaxel and carboplatin for longer than 6 days duration in both cell lines (data not shown here). However, neither of the cell line formed colonies under the testing conditions. It has been reported that colony formation is highly dependent on the cell line [98]. Therefore, it was concluded that IGROV1 and OVCAR4 cell lines were most likely not suitable for clonogenic assay and no further work was conducted on clonogenic assay.

Summary of the GI50 concentrations of both compounds are given in the Table 2.2 where at day 3 the carboplatin GI50 in IGROV1 cell line was 11.7 µM and in OVCAR4 cell line it was 3.9 µM. Whereas, at day 6 carboplatin GI50 concentrations dropped slightly in both cell lines, to 5.1 µM and 1.3 µM, respectively. Similarly, the paclitaxel GI50 concentration at the day 3 time point was 3.6 nM, which reduced to 1.7 nM at day 6 in OVCAR4. However, in IGROV1 cell line GI50 concentrations were similar at both day 3 and 6 (1.1 and 0.9 nM respectively).

Table 2.2 Summary of individual compound GI50 concentrations

Compound	Cell Line	GI50 (Averages of at least 6 replicates)	
		Day 3	Day 6
Carboplatin	IGROV1	11.7 µM Std Dev 8.7 µM	5.1 µM Std Dev 3.4 µM
	OVCAR4	3.9 µM Std Dev 0.9 µM	1.3 µM Std Dev 0.1 µM
Paclitaxel	IGROV1	1.1 nM Std Dev 0.2 nM	0.9 nM Std Dev 0.3 nM
	OVCAR4	3.6 nM Std Dev 0.6 nM	1.7 nM Std Dev 0.5 nM

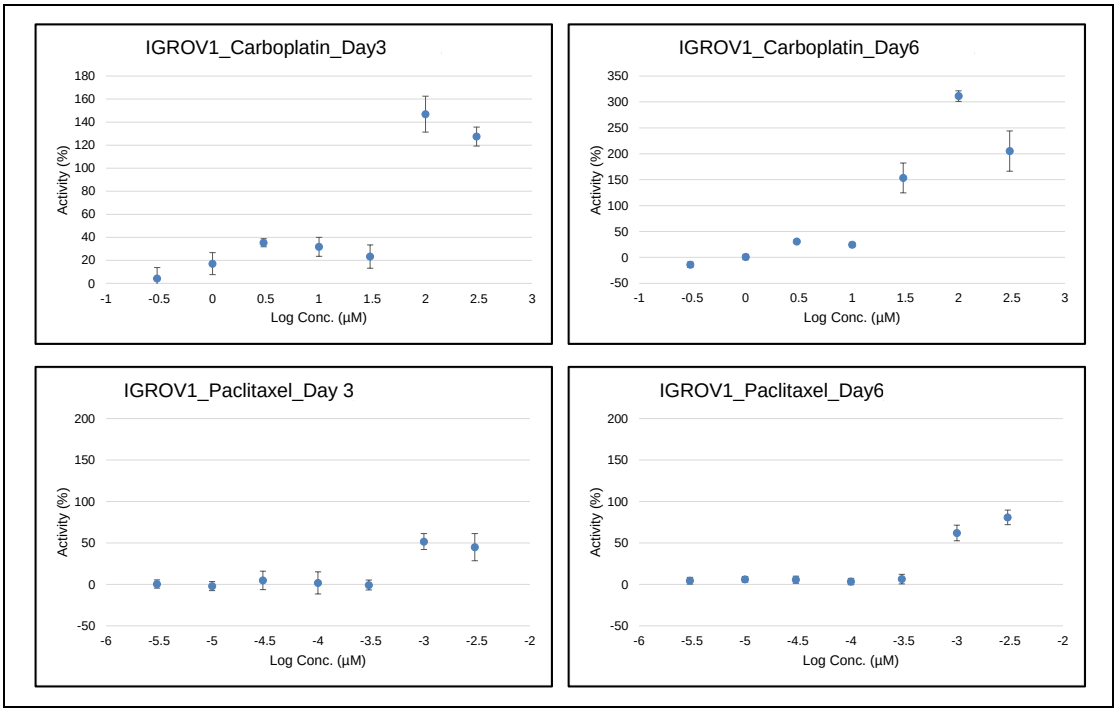


Figure 2-5: Single agent dose response curves in IGROV1 cell line. Top left: carboplatin day 3, top right: carboplatin day 6, bottom left: paclitaxel day 3 and bottom right: paclitaxel day 6 dose response curves. Error bars are standard deviation of at least six replicates.

Table 2.3 shows a comparison of paclitaxel and carboplatin GI50 values observed in this study at day 6 with the values reported by other researchers [81,82,84]. Our results are very similar to the GI50 values reported in the literature. It is also worth noting from Table 2.3 that other researchers have used different in-vitro assays and cell lines to generate these GI50 values, which indicates

that the growth inhibition activities of both of these compounds are broadly consistent with the literature, irrespective of the cell line and/or assay.

Table 2.3: Comparison of paclitaxel and carboplatin GI50 concentrations observed in this work and literature.

Cell Line	GI50		Reference	Comments
	Paclitaxel (nM)	Carboplatin (µM)		
OVCAR4	1.3	1.7	Table 2.2	Sytox green assay, 6 day
IGROV1	0.9	5.1	Table 2.2	Sytox green assay, 6 day
UTOC3	1.3	1.3	[81]	Clonogenic assay, 4 week
UTOC4	1	3	[81]	Clonogenic assay, 4 week
UTOC5	1.4	2.1	[81]	Clonogenic assay, 4 week
SKOV3	3.4	4.3	[81]	Clonogenic assay, 4 week
SKOV3	1.4	23.8	[84]	MTT assay, 72 Hrs
OVCAR3	1.4	22.2	[84]	MTT assay, 72 Hrs
ES2	0.7	25.7	[84]	MTT assay, 72 Hrs
OV90	1.8	24.9	[84]	MTT assay, 72 Hrs
TOV112D	0.7	15.1	[84]	MTT assay, 72 Hrs
TOV21G	0.9	15.1	[84]	MTT assay, 72 Hrs

It has also been reported in the literature that extended exposure of chemotherapeutics (dose densing) to tumour cells results in the increased cytotoxicity [83,99]. Hence, in our study two time points (3 day and 6 day) were used to evaluate this phenomenon. Indeed, the results (Table 2.2, Figure 2-5 and Figure 2-6) show that longer exposure (6 days compared to 3 days) for both cells lines (IGROV1 and OVCAR4) and both chemotherapeutic agents (carboplatin and paclitaxel) resulted in the increased activity.

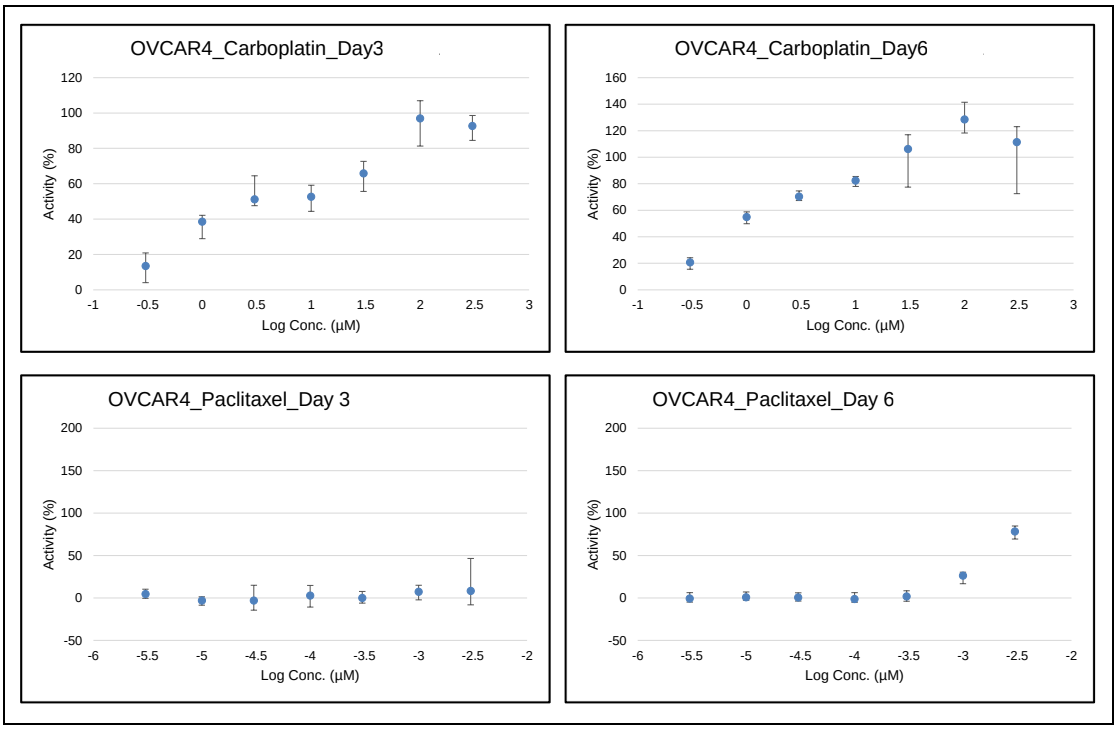


Figure 2-6: Single agent dose response curves in OVCAR4 cell line. Top left: carboplatin day 3, top right: carboplatin day 6, bottom left: paclitaxel day 3 and bottom right: paclitaxel day 6 dose response curves. Error bars are standard deviation of at least six replicates.

In addition, Liebmann et. al. has also reported that prolonged exposure of paclitaxel increased its cytotoxicity in various cell lines [100].

2.4.2 Combination therapy results

The summary of the Loewe synergy scores of the carboplatin and paclitaxel combination therapy in IGROV1 and OVCAR4 cell lines over 3 and 6 days exposure are shown in Table 2.4.

Table 2.4 Summary of Loewe synergy scores

Cell line	Loewe synergy scores	
	Day 3	Day 6
IGROV1	1 Std Dev 2	5 Std Dev 5
OVCAR4	0 Std Dev 1	1 Std Dev 2

As it can be seen from this table that synergy scores of 1.4 at day 3 and 4.6 at day 6 has been observed in IGROV1 cell line. Whereas, in OVCAR4 cell line the synergy scores were 0.1 at day 3 and 0.8 at day 6.

In combination therapy, interactions between two compounds are either synergistic (sometimes described as “1+1 >2” or supra-additive), antagonistic or additive (no interaction) [101,102]. Such general descriptions of combination therapy are ambiguous.

On the other hand, various quantitative models has been reported by some, to clearly describe the combination interactions e.g. Loewe additive model, which is one of the most commonly used and widely accepted quantitative models for synergy determination [101]. Loewe synergy scores provide information about the level of interaction between two compounds. Scores <5 are considered non-significant or noise, scores between 5-10 indicate significant synergy (growth inhibition), score between 10-20 shows substantial synergy (growth inhibition) and scores >20 indicates potency shifting (cell kill). It can be seen from Table 2.4 that three of synergy scores in this study at day 3 and at day 6 are below the noise level (<5) and therefore not considered significant. However, a score of 5 was observed in IGROV1 cell line at day 6 which indicates that there is, possibly, a borderline synergy between carboplatin and paclitaxel after longer exposures Table 2.4.

From these results, it appears that the carboplatin and paclitaxel synergy was, most likely, cell line specific. Similarly, Engblom et. al. have also reported that they didn’t find any synergy between carboplatin and paclitaxel in one of the ovarian cancer cell line (UTOC4) although in three other ovarian cancer cell lines they did observe supra-additive (synergistic) effect of the combination therapy [81].

In addition, Xiong et. al. has shown, in an in-vitro cell cytotoxicity study using a breast cancer (Bcap37) and an ovarian cancer (OV2008) cell line, that the interaction between paclitaxel and carboplatin was highly schedule dependent [103]. They reported that combination therapy actually resulted in antagonistic effect when carboplatin was administered before paclitaxel or when both compounds dosed simultaneously and the optimum schedule for this combination was paclitaxel followed by carboplatin [103]. As described above, in my study, for combination therapy both compounds were administered

simultaneously to mimic the concomitant release of paclitaxel and carboplatin from our intraperitoneal drug delivery system. It appears that with this regimen paclitaxel and carboplatin might have either weak or no synergistic effect in OVCAR4 and IGROV1 cell lines. Therefore, further work would be required to determine the optimum schedule for the administration of these two compounds (paclitaxel and carboplatin) in combination for the effective localised continuous release administration by using the drug delivery system.

In summary, GI50 concentrations determined in this study at day 6 for both compounds in both cell lines has been found comparable to the values reported in literature for various cell lines, as shown in Table 2.3. Therefore, the GI50 concentrations at day 6 will be used to design our drug delivery system.

Moreover, it can be concluded from this data that longer exposure time of both compounds (carboplatin and paclitaxel) in each of the selected cell line results in higher cytotoxicity. Therefore, a drug delivery system with continuous controlled release of paclitaxel and carboplatin over a long period of time (> 1 month) could be used to enhance the cytotoxic activity of carboplatin and paclitaxel.

2.4.3 Intraperitoneal PK mathematical model results

Table 2.5 shows the results for paclitaxel and carboplatin predicted doses for a dosing interval of 1 month, assuming the release from microspheres was linear (zero order).

For this model, carboplatin k_{ip} value was determined by using the intraperitoneal and plasma PK data from McClay et. al. [94]. A model similar to that which appears in their publication was implemented in Berkeley Madonna software to process McClay et. al. carboplatin PK data, the details of the model used and calculation of carboplatin k_{ip} can be found in Appendix B.

As it can be seen from the Table 2.5 that paclitaxel predicted dose was 0.084 mg and carboplatin dose was 8.2 mg for the duration of 1 month. The per day release rates of paclitaxel and carboplatin from the microspheres with zero order release rates can simply be determined by dividing the dose with the number of days.

Table 2.5: Results for the paclitaxel and carboplatin predicted doses and release rates, as determined by using the preliminary intraperitoneal pharmacokinetic model where the release from microspheres was assumed to be linear (zero order).

	Term description or ID	Paclitaxel	Carboplatin
Model input parameters	GI50 (µM)	1.70E-03	5.10
	Molar mass (g/mol)	853.9	371.3
	Minimum efficacious concentration (C_{min}) (mg/mL)	4.35 x 10^{-06}	5.68 x 10^{-03}
	[1]Plasma protein binding (% w/w)	94	0
	Fraction unbound (f_u)	0.06	1
	IP cavity absorption constant (k_{ip}) (day^{-1})	3.84	4.8
	IP fluid volume (V_{ip}) (mL)	10	10
	Dosing interval (τ) (days)	30	30
Results	Predicted Dose (mg)	0.084	8.2
	Predicted release rates (mg/day)	0.003	0.3

The formulation parameters shown in the following Table 2.6 were derived by using the paclitaxel and carboplatin doses determined above Table 2.5. The dose volume and the target PLGA microsphere concentration were fixed to 10 mL and up to 20 % w/w for the purpose of designing a drug delivery system.

Table 2.6: Paclitaxel and carboplatin predicted PLGA microsphere formulation concentrations, as determined from the initial intraperitoneal pharmacokinetic model where the release from microspheres is assumed to be linear (zero order).

	Paclitaxel	Carboplatin
Drug loading (% w/w) (assumed)	10	10
Microsphere amount per dose (mg/dose)	0.84	82
Dose volume (mL)	10	10
Microsphere concentration (% w/w)	0.0084	0.82

As it can be seen from this Table 2.6 that the PLGA microsphere concentration required for one dose (assuming drug loading of 10% w/w) is well within the pre-defined limits (i.e. up to 20 % w/w) therefore, these starting conditions were

[1] it is assumed that the protein concentration in the IP fluid is equivalent to plasma

found suitable to carry forward to design the paclitaxel and carboplatin-PLGA microsphere formulations.

2.5 Conclusion

In this work, firstly the activity (GI50) of carboplatin and paclitaxel were determined in two ovarian cancer cell lines. Secondly, a mathematical model was developed to estimate the concentration of both compounds in the IP cavity. Finally, this mathematical model was used to determine the critical design parameters (i.e. target release rates, drug loading and dose) for the development of PLGA microsphere-based drug delivery system which can provide sustained release of paclitaxel and carboplatin in the IP cavity to maintain therapeutic concentrations for at least 1 month or longer, for the treatment of ovarian cancer.

These parameters will be used in the work described in the following chapters to develop a PLGA microspheres-based drug delivery system.

3 Evaluation of different methods for the manufacture of PLGA microspheres

3.1 Introduction

Following on from the selection of drug delivery system design parameters in chapter 2, a quality target product profile (QTPP) was defined and various PLGA microsphere manufacturing methods were screened first to select most suitable method to make controlled, uniform size ($D_{0.5}$ of 50 – 200 μm) micropsheres.

3.1.1 Microsphere QTPP (quality target product profile)

A QTPP was defined in order to set target parameters for the development of final formulations (Figure 3-1). The target drug loading and release profile (i.e. release rate and duration) were determined by using the intraperitoneal PK mathematical model, as detailed in chapter 2. Reproducible manufacture, biocompatibility and biodegradability are basic requirements for any injectable drug delivery system.

Microsphere size is at the core of the QTPP because it is one of the most important parameters in the design of a microsphere-based drug delivery system. It has been reported that PLGA degradation rate strongly depends on the microsphere size [41,104,105]. This size dependant degradation behaviour is primarily observed in larger microspheres (>300 μm) and it is attributed to higher degradation rate in the core of the microsphere due to the accumulation of acidic degradation products which causes autocatalysis and therefore promotes faster polymer degradation. Microspheres <300 μm have shown uniform degradation behaviour [106] because small acidic degradation products can easily diffuse out of particles and therefore the degradation rate of the core is similar to the surface.

Another advantage of making, relatively, smaller microspheres is the improved syringeability with commonly used small gauge needles i.e. <22-25G for intraperitoneal injection [71,107-109].

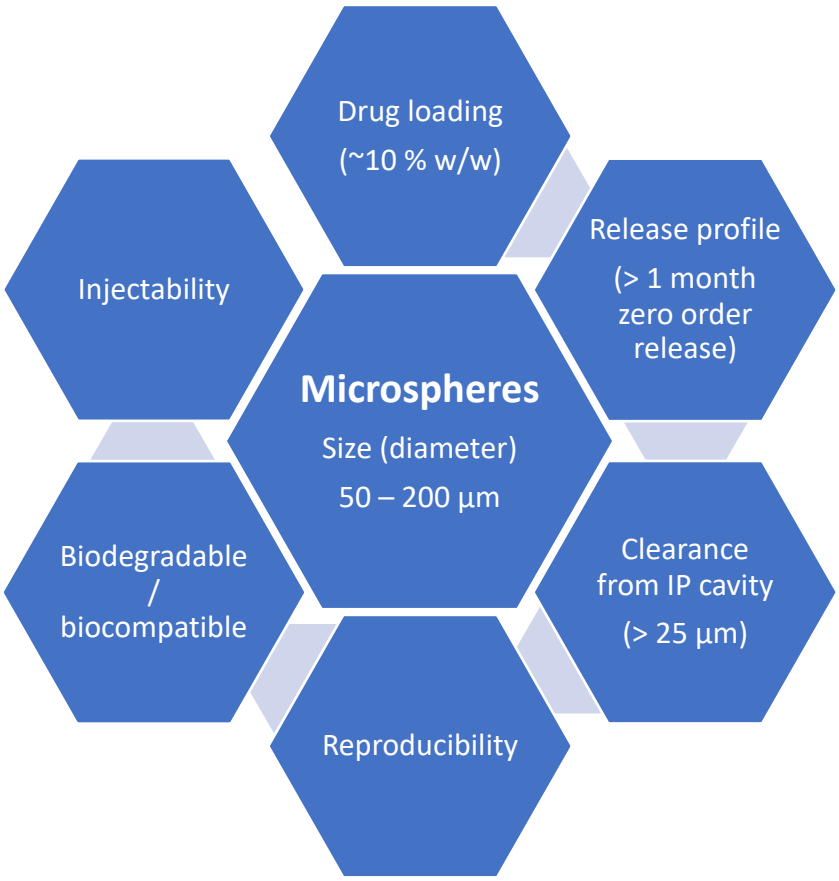


Figure 3-1: QTPP (quality target product profile) for the development of microsphere based drug product.

However, in this study, smaller than 25 µm microspheres are not preferred because it has been reported that particles up to 20 µm can be cleared from the peritoneal cavity via stomas in the diaphragmatic mesothelium [14]. In addition, relatively larger microspheres have shown longer residence and longer release duration [108].

Therefore, the aim was to make microspheres <300 µm (preferably between 50 – 200 µm, ideally 50 – 100 µm) which may have uniform degradation of polymer and uniform drug release profiles, good syringeability, longer residence time in IP cavity and longer release duration.

3.1.2 Evaluation of PLGA microsphere manufacturing methods

PLGA microspheres can be manufactured by various methods including;

- Emulsification (further subdivided into two groups)
    - Single emulsion

    - Double emulsion
- Phase separation (Coacervation)
- Spray drying
- Supercritical CO_2, etc

Various publications are available which describe the details of above microsphere manufacturing techniques and are summarised by Makadia and Siegel [109]. Readers can refer to these publications for details of each of the microsphere manufacturing method. In this study, emulsification method was selected which is by far the most commonly used and most successful method for making PLGA microspheres.

Selection of a single or multiple (double) emulsion method depends primarily on the compound physicochemical properties. Poorly water soluble (lipophilic) compounds can be very efficiently loaded into PLGA microspheres prepared by a single emulsion method, however, as the compound aqueous solubility increases the drug encapsulation efficiency of the single emulsion method reduces. Double emulsion methods, on the other hand are most suitable for hydrophilic compounds to achieve higher drug loading [110]. A comprehensive review has been recently published by Giri et. al. covering the pros and cons of the single and double emulsion methods, in particular, detailing the recent developments in the double emulsion method [110].

In both single and double emulsion methods control over emulsion droplet size is crucial in order to achieve the desired formulation characteristics. Various approaches have been described in the literature to control the emulsion droplet size, most common approaches are homogenisation [60,111], extrusion through filters [112] and microfluidics [113]. Techniques using microfluidic flow have shown great promise for making tuneable size microspheres [113].

These three techniques were evaluated, in this work, to control the emulsion droplet size, which in turn dictates the final microspheres size. In addition, various processing steps used during the manufacture of microspheres and some analytical techniques were also evaluated.

The results from this chapter were then used to inform the next stage of microsphere manufacturing method optimisation.

3.2 Materials and methods

3.2.1 Materials

PLGA 50/50 (lactide/glycolide) M_w 10 and 20 kDa purchased from Sigma Aldrich; PVA (88% hydrolysed m.wt. 20-30 kDa), sodium cholate and DCM were obtained from Sigma Aldrich, all other reagents were of pharmaceutical grade.

3.2.2 Methods

All microspheres were prepared by a single emulsion (oil in water, O/W) solvent evaporation method using DCM as oil phase and 0.5-10% PVA solution as an aqueous phase [114,115].

Microsphere preparation by homogenisation technique

A modified homogenisation method was used as described by Davies et. al. [111]. Organic phase was prepared by dissolving PLGA in DCM to make 5 % w/v solution and mixed with 5 % w/v PVA solution at 1:6 ratio. This pre-emulsion was homogenised for 5 min. at 16000 rpm using Ultra-Turrax T25 homogeniser (IKA Werke, GmbH, Germany) to make a fine emulsion. The emulsion was left stirring for ~3-4 hrs in the fume hood at ambient conditions to evaporate DCM and harden the microspheres. Finally, the microspheres were collected by centrifugation and washed three times with purified water to remove excess PVA.

Microsphere preparation by filter extrusion technique

PLGA was dissolved in DCM to make a 5% w/v solution. This organic phase was mixed with 5% w/v PVA solution at 1:6 ratio and vortexed for ~1 min to make a pre-emulsion. The pre-emulsion was passed through various nominal pore size stainless steel filters, including 2, 5, 10 and 20 µM filters. The filtrate was collected directly into a collection vessel containing purified water ~ x10 the volume of emulsion while stirring. The emulsion was then left stirring (magnetically) in the fume hood for 3 to 4 hrs to evaporate DCM and harden the microspheres. Finally, the microspheres were collected by centrifugation and washed three times with purified water to remove excess PVA.

Microsphere preparation by microfluidics technique

The Dolomite microfluidics pressure based droplet system with droplet generation or micromixer chip (The Dolomite Centre Ltd. UK) was used in this work, (see the schematic flow diagram for single and double emulsion set up below Figure 3-2 and Figure 3-3). The organic solution (oil phase) was placed in one of the pressure pump (p-pump) or a syringe pump (flow rate 25 or 50 µl/min and the aqueous solution was placed in the second p-pump (flow rate 250, 500 or 750 µl/min). Both solutions were mixed inside the flow focussing micro channel chip (either micromixer or droplet generation chip). This resulted in the formation of precisely controlled emulsion droplets which were collected in the collection vessel containing either water or dilute surfactant solution, while stirring. After collection, the emulsion was left agitating (by magnetic stirring, orbital shaking or overhead paddle stirring) at ambient conditions, in the fume hood, to evaporate DCM and harden the microspheres.

Finally, microspheres were collected either by leaving the suspension static or by centrifugation (depending on the particle size) to settle the particle, washed three times with water to remove excess surfactant (PVA or sodium cholate) and either stored as suspension or collected by vacuum filtration and dried under vacuum at ambient room temperature.

Various experimental parameters were evaluated for their effect on the particle size, size distribution and porosity. These included comparison of micromixer and droplet generation chip, aqueous and organic phase flow rate ratio, PLGA molecular weight and concentration.

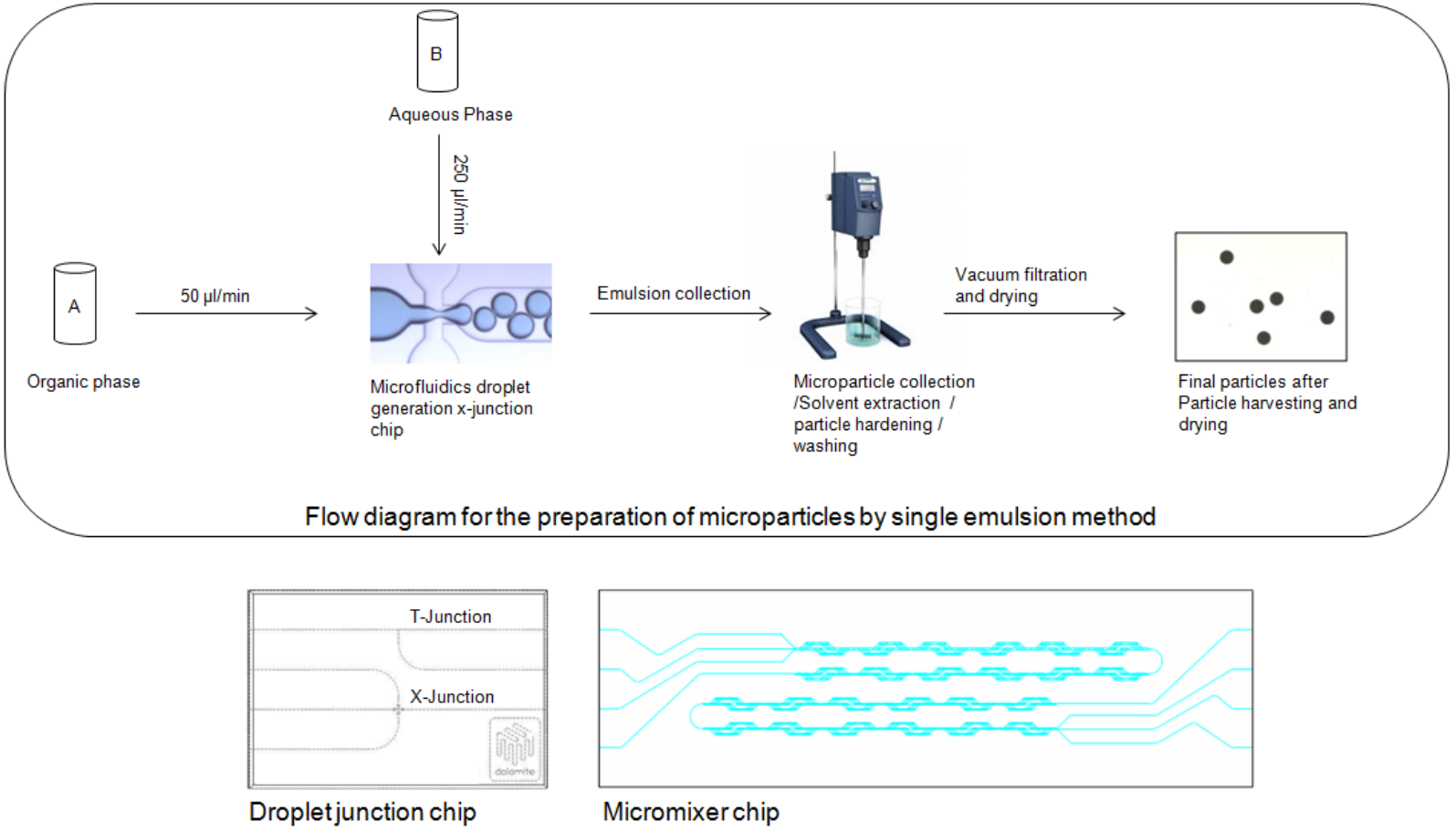


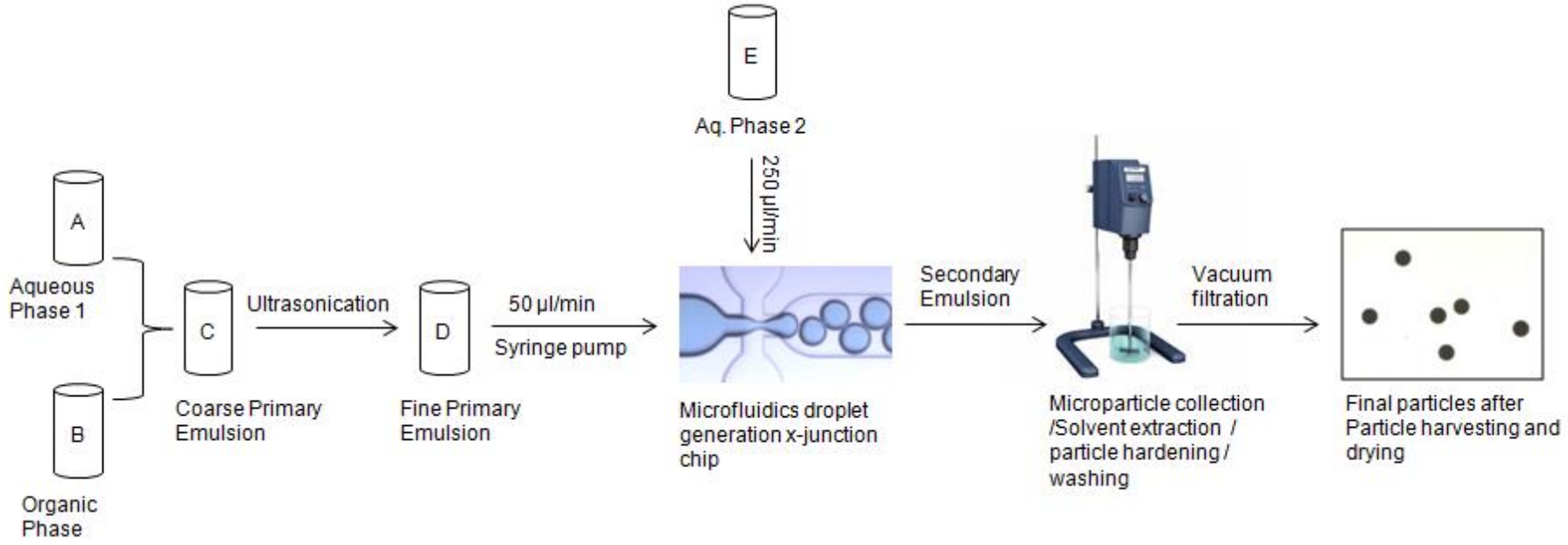
Figure 3-2: Schematic for the manufacture of PLGA microspheres by single emulsion method using the microfluidics

Double emulsion method for the preparation of carboplatin PLGA microspheres

Carboplatin is soluble in water [36] and therefore a double emulsion (water in oil in water, W/O/W) method was evaluated to make PLGA microspheres for this compound [110]. The first emulsion (W/O) was prepared by mixing 1 part of 1% w/v carboplatin in 0.1 % w/v PVA solution (aqueous phase 1) with 9 parts of 20 % w/w PLGA solution in DCM (organic phase). This was followed by ultrasonication for 5 min in Covaris S2 (Covaris Inc. USA) to reduce the internal aqueous phase droplet size. The first emulsion (W/O) was then mixed with 0.5% PVA solution (aqueous phase 2) at 1/5 ratio, to make W/O/W emulsion inside the flow focussing micro-channel chip Figure 3-3. A syringe pump was used for the first emulsion and p-pump for the second aqueous (external) phase. This resulted in the formation of micro-droplets which were collected in 0.1% PVA solution while stirring with a paddle overhead stirrer and left stirring for at least 3 to 4 hrs in the fume hood to evaporate DCM and harden the microspheres. Finally, microspheres were isolated by leaving the suspension static for 5 min, washed three times with water to remove excess PVA and carboplatin. Cleaned microspheres were either stored as suspension at 2-8 ºC or collected by vacuum filtration and dried under vacuum at ambient temperature.

Optical microscope

One drop of the microsphere suspension was placed on the glass microscope slide and a glass cover slip was placed on the drop to reduce evaporation. Slides were examined under Zeiss Microscope (Axio Scope.A1, Carl Zeiss Ltd.). Pictures were taken using the 10 and 40x times magnification with Axiocam ERc5s camera using Zen lite software (Carl Zeiss Ltd.)



Droplet junction chip channel dimension (depth x width): 100µm x 300µm for all channels and 100µm x 105µm at the x-junction.

Figure 3-3: Schematic for the preparation of carboplatin PLGA microspheres by double emulsion method, using microfluidics

Particle size and size distribution by light scattering

The microsphere suspension was analysed by using Malvern Mastersizer 2000 equipped with hydro 2000µP small volume wet dispersion accessory and Malvern 2000 software (Malvern Instruments Ltd.). Approximately, 18 ml of the dispersion medium (water) was loaded and a background measurement was taken. This was followed by adding enough sample to achieve 10-20% laser light obscuration. Three readings were taken to measure the particle size ($D_{0.5}$) and average results were reported.

HPLC method for carboplatin

The chromatographic conditions of the HPLC method given in Table 3.1 were developed to analyse the carboplatin. Agilent series 1100 HPLC system with diode array UV detector (Agilent Technologies, Canada) was used in this study.

Table 3.1: Chromatographic conditions for the HPLC method for the analysis of carboplatin

Column	SeQuant ZIC–pHILIC, 5µm polymeric, Peek 150 x 4.6 mm (Merck)		
Mobile Phase	A	Acetonitrile	
	B	Water	
Gradient	Time (min)	Mobile phase A (% v/v)	Mobile phase B (% v/v)
	0	5	95
	5	70	30
	7	70	30
	7.1	5	95
	10	5	95
Flow rate	1 mL/min		
UV detection wavelength	227 nm		
Injection volume	10 µL		
Temperature	40 °C		
Diluent	acetonitrile / water, 50/50		

3.3 Results and discussion

3.3.1 Microsphere preparation by homogenisation and filter extrusion techniques

Figure 3-4 shows an optical microscope picture of the microspheres prepared by the homogenisation method. This method resulted in very small size particles, well below the lower limit of QTPP for the microsphere size (50 - 200µm).

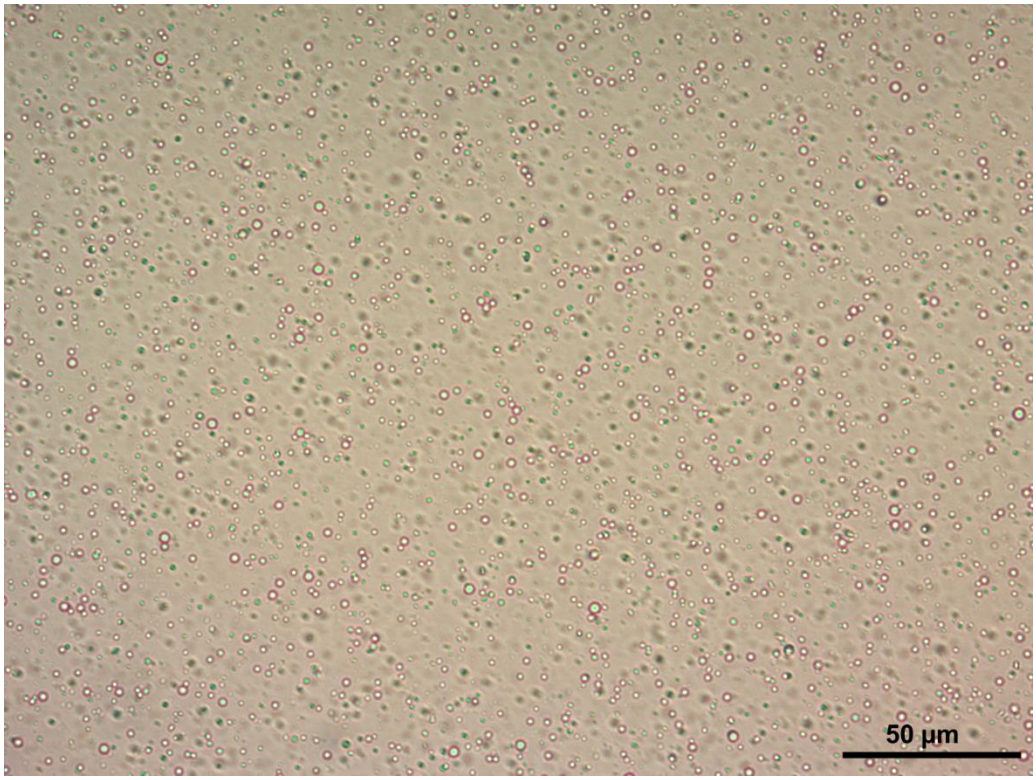


Figure 3-4: Optical microscope image of PLGA microspheres prepared by homogenisation method

After various attempts, it was not possible to make the required size microspheres with this method. Although, some control over size was possible by varying the PLGA concentration in the organic phase, PVA concentration in aqueous phase and homogenisation speed. However, in general, this method always resulted in the formation of microspheres much smaller than 50 µm. These results are consistent with the data from other researchers [112]. Another drawback noticed in this method was the formation of excessive froth (air

entrapment) which made the processing difficult. It have been reported that trapped air can dampen the turbulence intensity [116]. It was concluded that this method was not suitable for making microspheres in the desired size range of 50 - 200 µm diameter and therefore, no further work was carried out with this method.

The Figure 3-5 shows that the filter extrusion method did provide some control over the particle size and size distribution for making smaller (up to 5 µm) microspheres.

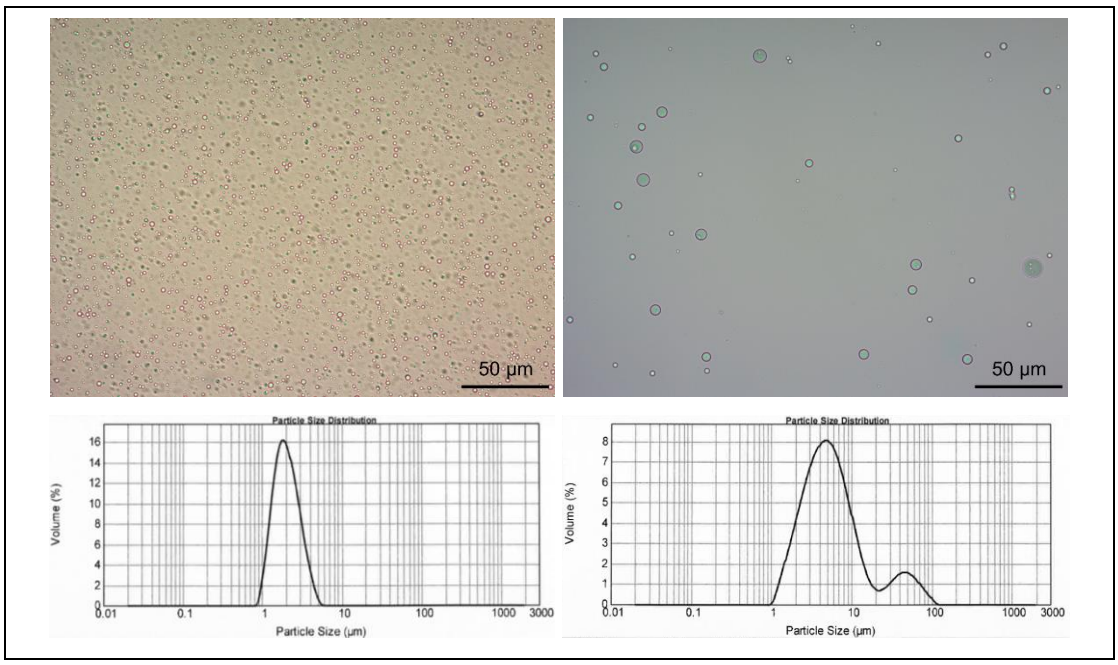


Figure 3-5: Microspheres preparation by filter extrusion, (Top) Optical microscope pictures (Bottom) Particle size distribution by Malvern 2000 (laser light scattering). (Left) filter extrusion through 2µm filter (Right) filter extrusion through 5µm filter

With this method 2 and 5 µm PLGA microspheres with narrow size distributions were successfully prepared by using 2 and 5 µm nominal pore size stainless steel filters. Similar outcomes have been reported in the literature with this method [112]. However, when it was attempted to make large microspheres with this method, it struggled to control the particle size e.g. 20 µm nominal pore size filters resulted in the formation of very large particles (precipitates and fibrous structures, data not shown here).

3.3.2 Microspheres preparation by microfluidics method

Comparison of micromixer and droplet generation chip

In this set of experiments, two types (micromixer and droplet generation) of chips were compared for the formation of the desired size microspheres with a narrow size distribution. Micromixer chip resulted in the formation of microspheres with a wide size distribution, as it can be seen from Figure 3-6.

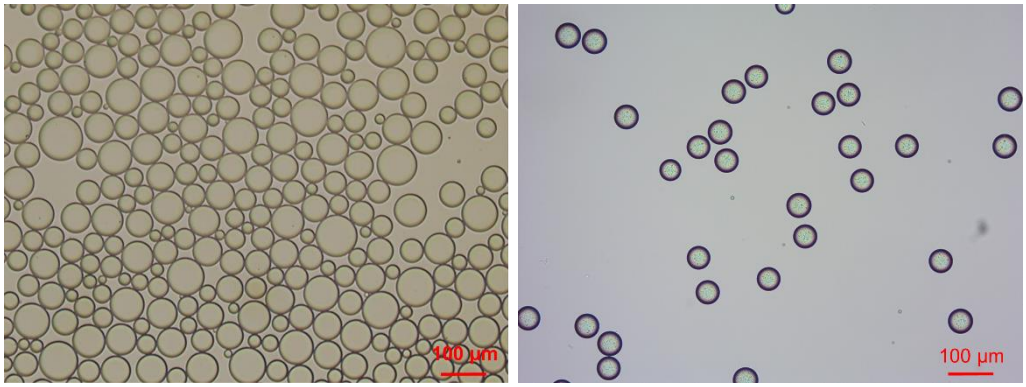


Figure 3-6: Comparison of microsphere preparation by two different chips designs. Left: Micromixer chip, Right: Droplet generation chip, formulation 20% w/v PLGA 95/5, M_w 25 kDa, in DCM and 0.5% w/v PVA in water. Ratio of organic to aqueous phase flow rate 1:10 for both chip designs.

It appears that the primary droplets formed at the x-junction by the laminar mixing of the two immiscible fluids encountered additional shearing forces downstream while passing through the chaotic mixing part of the micro channels. The micromixer chip channel dimensions reduce from 100 x 300 µm at the x-junction to 100 x 105µm (depth x width) at the mixing part Figure 3-2 (above). This reduction in the channel dimensions decreases the flow rate but shear forces increases to ensure complete mixing. These additional shearing forces and chaotic mixing has most likely further broken down the primary emulsion droplets formed at the x-junction and resulted in the wide particle size distribution Figure 3-6.

On the other hand, microspheres formed by the droplet junction chip were much more uniform and homogenous in size (Figure 3-6). One of the reason for this uniform size distribution could be the absence of additional shearing forces and

chaotic mixing as the channel dimensions stays the same throughout the micro-channels and there are no micromixer zones in the droplet generation chip compared to the micromixer chip, see Figure 3-2.

Effect of aqueous to organic phase flow rate ratio on microsphere size and size distribution when using the droplet generation chip

As the flow rate ratio was increased from 5 to 10 the overall particle size was reduced as shown in the following optical microscope picture, Figure 3-7. In addition, it was noticed that the particle size distribution was not significantly affected by increasing the flow rate ratio. Similar results has been reported by Dolomite (vendor) in the droplet generation chip user instructions [117] where they used mineral oil / water emulsion system.

Although, flow rate ratio is a simple and effective parameter to control the particle size using microfluidics system, however, there are limitations to what flow rate ratios could be achieved on this instrument. Therefore, other factors to control the particles size were also explored, (see chapter 5) including the polymer concentration, PVA concentration and total flow rate.

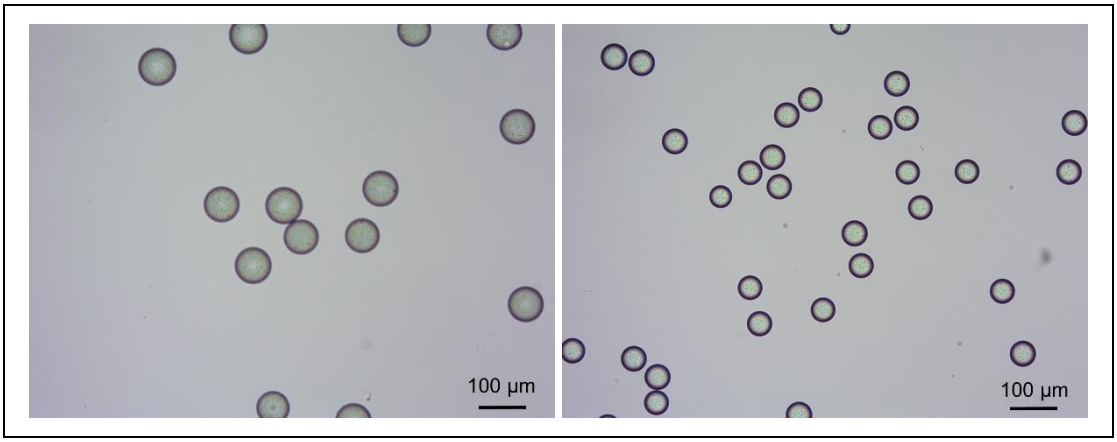


Figure 3-7: Optical microscope image showing effect of organic / aqueous flow rate ratio on particle size and size distribution in droplet generation chip. Organic / aqueous phase flow rate ratio 1:5 (Left), 1:10 (Right). The formulation was 20% w/v PLGA in DCM, 0.5% PVA for both experiments

3.3.3 Effect of DCM extraction and evaporation rate on microsphere formation

During the DCM removal process it was noticed that as the DCM was extracted from the emulsion droplets the droplet volume reduced, Figure 3-8. Similar results have been reported by Abdulkin et. al. [118]. The removal of DCM is a progressive process which is based on the diffusion of DCM. After the emulsion droplet formation DCM continuously diffuses out of the droplet into the external water phase and then evaporate to the atmosphere. This continuous removal of DCM results in the shrinkage of the remaining hydrophobic PLGA polymer.

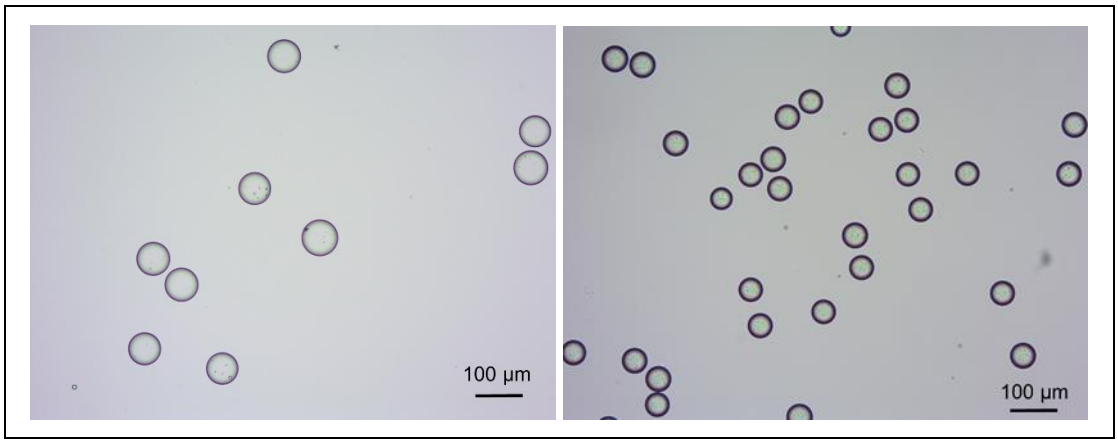


Figure 3-8: Optical microscope pictures showing the effect of DCM extraction/removal rate on the emulsion droplet. Formulation: 5% w/v PLGA in DCM, 0.5% PVA, organic / aqueous phase flow rate ratio 1:10, droplet collection and DCM evaporation by orbital shaking at room temperature.

The rate of DCM removal can also have an impact on the characteristics of the formulation. For example, slow solvent removal at the temperature just above the Tg of the polymer, the polymer remains in rubbery state and therefore polymer can anneal during this process and may result in reduced porosity and lower burst release. On the other hand, faster solvent removal can result in the lower density microspheres (higher porosity) and also a higher burst release because microspheres solidifies in a more solvent-swollen state [119].

3.3.4 Particles breakage due to magnetic stirring

In preliminary experiments DCM was evaporated while magnetically stirring the emulsion/suspension and it was noticed that as the particles hardened over time due to DCM removal, they start breaking, see Figure 3-9. This may be due to the crushing / milling action of the magnetic follower. Similar effects were observed when the stirring time was reduced from 18 hr to 1hr, see Figure 3-9. Therefore, magnetic stirring was not used from this point onward, instead an orbital shaker or overhead paddle stirrer were used for DCM removal.

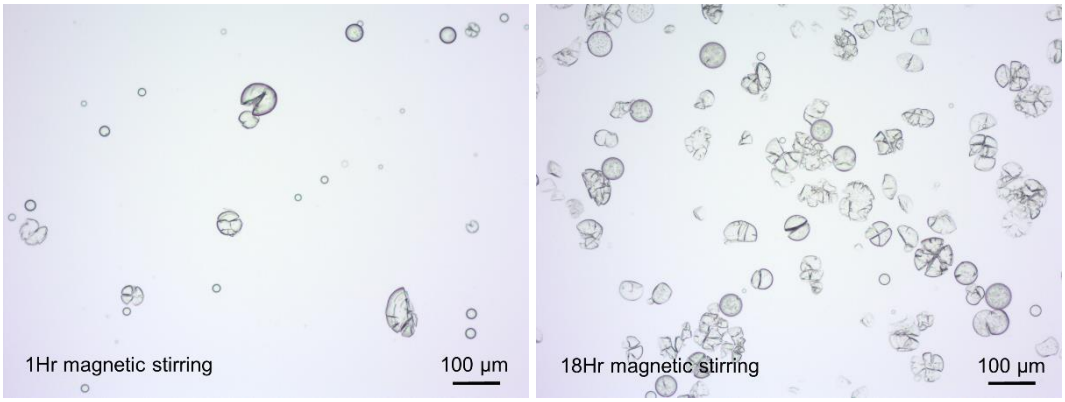


Figure 3-9: Optical microscope picture showing the microsphere breakage due to magnetic stirring. Formulation: 5% w/v PLGA in DCM, 0.5% PVA, organic / aqueous phase flow rate ratio 1:10

3.3.5 Porosity in the PLGA microspheres

Microsphere porosity has been widely studied in the literature and various strategies has been reported to reduce this phenomenon [120-122]. Porosity is generally considered a defect in the microspheres and is linked to higher burst release and faster overall release [119,123].

In this study, during our initial evaluation of the microfluidics technique, optical microscope images clearly displayed significant amount of porosity in the PLGA microspheres Figure 3-10. Therefore, to understand and control this phenomenon some of the key factors that may influence the porosity in microspheres were evaluated. The following experiments compared the effect of polymer concentration in the organic phase and polymer molecular weight on the porosity.

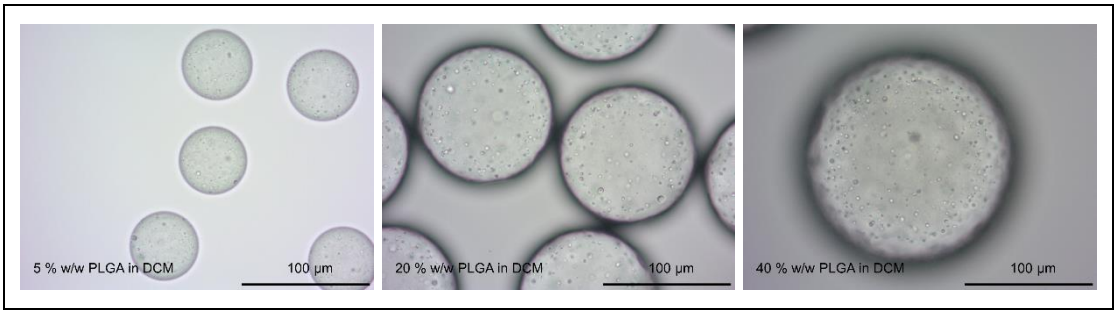


Figure 3-10: Optical microscope pictures showing the effect of PLGA concentration on porosity.

Figure 3-10 is showing the effect of three polymer concentrations on the porosity in microspheres. As shown by these optical microscope images, an increase in the polymer concentration seems to have no obvious improvement in the reduction of microsphere porosity. However, increase in the concentration had a clear increase in the microspheres size.

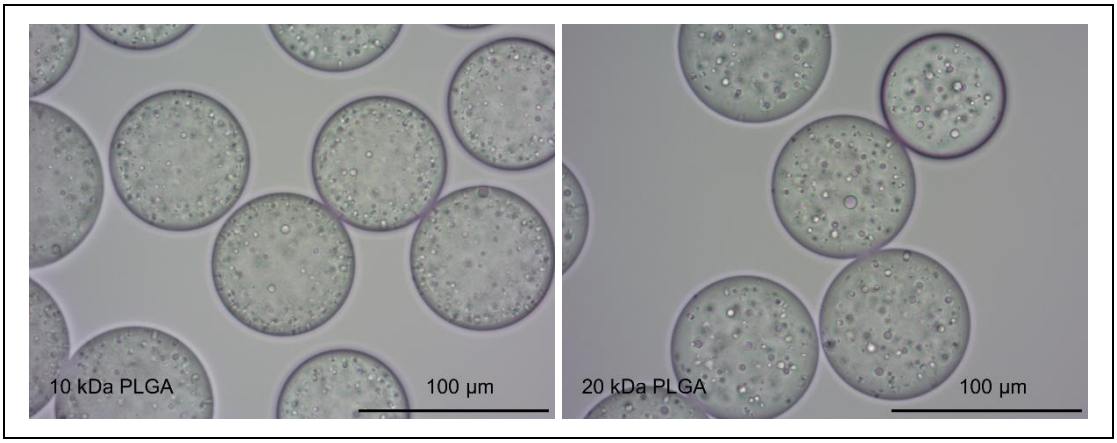


Figure 3-11: Optical microscope pictures showing the effect of PLGA molecular weight on the porosity. Formulation, 20% w/v PLGA in DCM used in both experiments

The second experiment compared the effect of polymer molecular weight on the microsphere porosity. In this experiment two molecular weights (11 kDa and 20 kDa) were used. From the optical microscope images shown in Figure 3-11 it appears that there is no obvious change in the porosity due to molecular weight as well.

3.3.6 Comparison of SEM and optical microscope images for the characterisation of microsphere porosity

As it can be seen from Figure 3-12 that the SEM images did not show any porosity in the microsphere surface, rather these pictures show smooth surface particles. Conversely, the, optical microscope images clearly displayed the presence of pores in the microspheres.

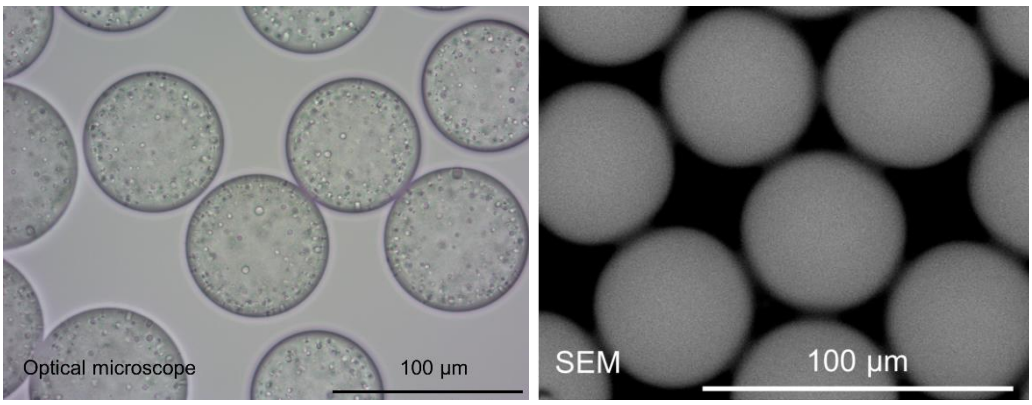


Figure 3-12: Comparison of optical microscope (PLM) and SEM images to evaluate porosity in PLGA microspheres. PLM samples were analysed as suspension in 0.01% w/v PVA solution. SEM samples were taken from the same suspension as for the PLM samples but samples were dried under vacuum at ambient temperature for at least 24 hrs and gold sputter coated before analysis.

From this data it appears that:

- The porosity observed in the PLM images is either present primarily in the core of the microspheres, as the visible light can pass through the glassy PLGA microspheres, or the surface pores are not healed while particles are still suspended in aqueous media at ambient temperature.
- The absence of surface porosity in SEM images might be due to healing of pores during SEM sample preparation i.e. drying and gold sputter coating. It has also been reported in the literature that pores or channels that exist inside the microspheres may not be observed in the SEM images [124]. In addition, it is also known that the PLGA polymer anneals under different conditions which can heal the pores in microspheres? [119,121-123] .

No further investigation has been carried out on microsphere porosity from this point onward because it was considered more logical to make drug loaded microspheres and characterise release profiles. If release profiles from drug loaded microspheres are acceptable then there might not be a need to investigate porosity further. In addition, it has also been highlighted in literature that sometimes incorporation of drug substances can result in the reduction of porosity in PLGA microspheres. Furthermore, the release profile is not only dictated by the porosity, but polymer and drug miscibility can also have a major impact on the burst release and overall release of active agents [119]. See section 6.3.5 for release data.

3.3.7 Preparation of carboplatin/PLGA microspheres by double emulsion method

In this experiment carboplatin loaded PLGA microspheres were prepared by the double emulsion method. Figure 3-13 is showing optical microscope images under plain and cross polarised light at two different magnifications. These microscope images show that firstly, carboplatin loaded PLGA microspheres could be prepared by the double emulsion method and these particles have narrow size distributions. Secondly, it appears that these particles have significantly lower porosity (plain polarised light) when compared with blank PLGA microspheres (Figure 3-10 to Figure 3-12).

Finally, these particles exhibited birefringence under cross polarised light and dried particles appeared brighter than particles in aqueous suspension. This was most likely due to the crystallisation of carboplatin in the microspheres, since we know carboplatin is soluble in water and therefore after complete removal of water by vacuum drying carboplatin might have crystallised inside the microspheres. These preliminary results were encouraging and show that carboplatin can be loaded in PLGA microspheres by a double emulsion (W/O/W) method.

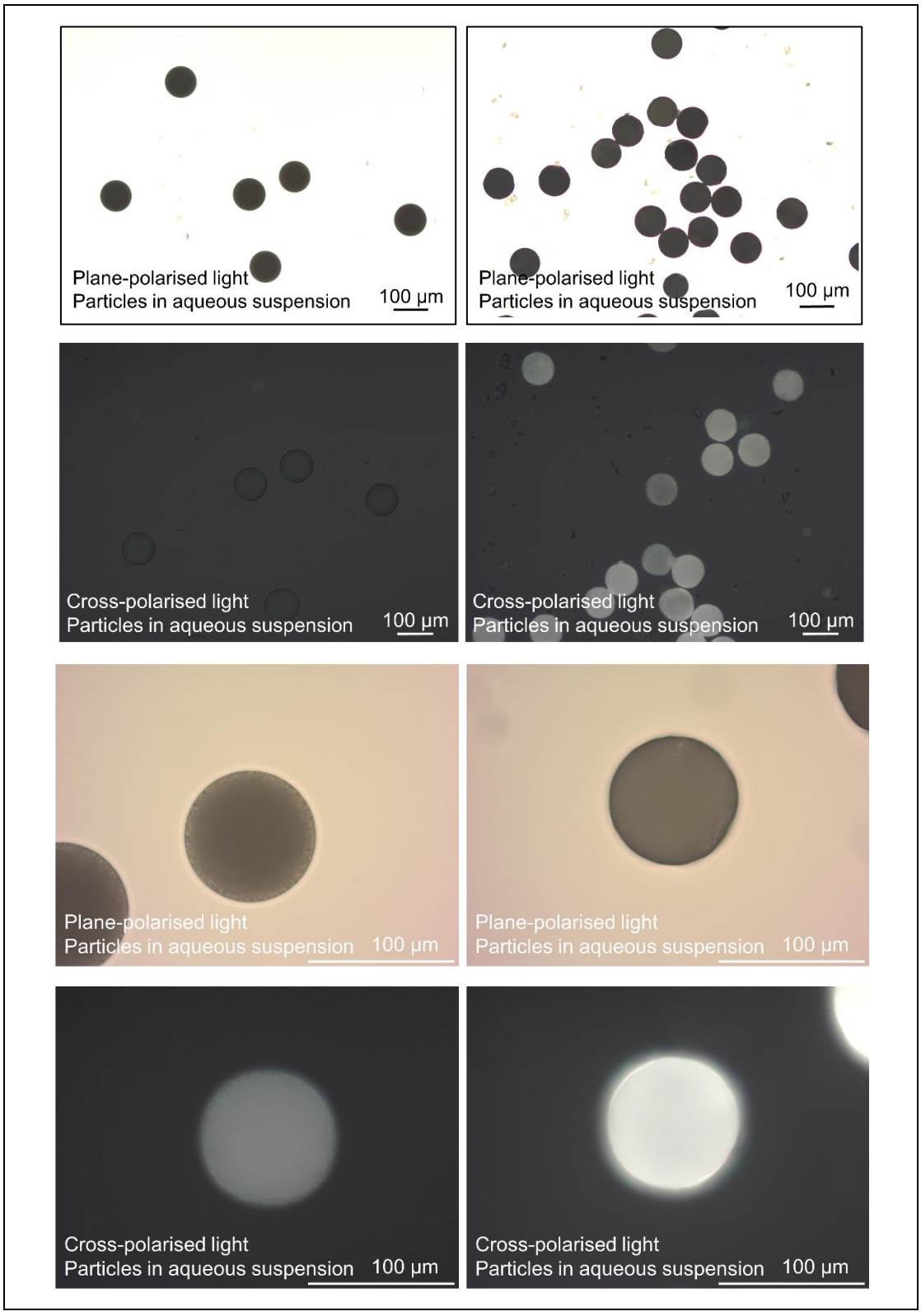


Figure 3-13: Optical microscope picture of carboplatin PLGA microspheres prepared by double emulsion (W/O/W) method using microfluidics. Left hand side images are for the samples suspended in aqueous media. Right hand side images are for the dried samples. Top four images are for the lower magnifcation wereas, bottom four images are for the higher magnifcation.

3.3.8 HPLC method development for the analysis of carboplatin drug loading and encapsulation efficiency in microspheres

Various HPLC methods are published in the literature for the analysis of carboplatin either alone or in combination of other compounds [40,125-127].

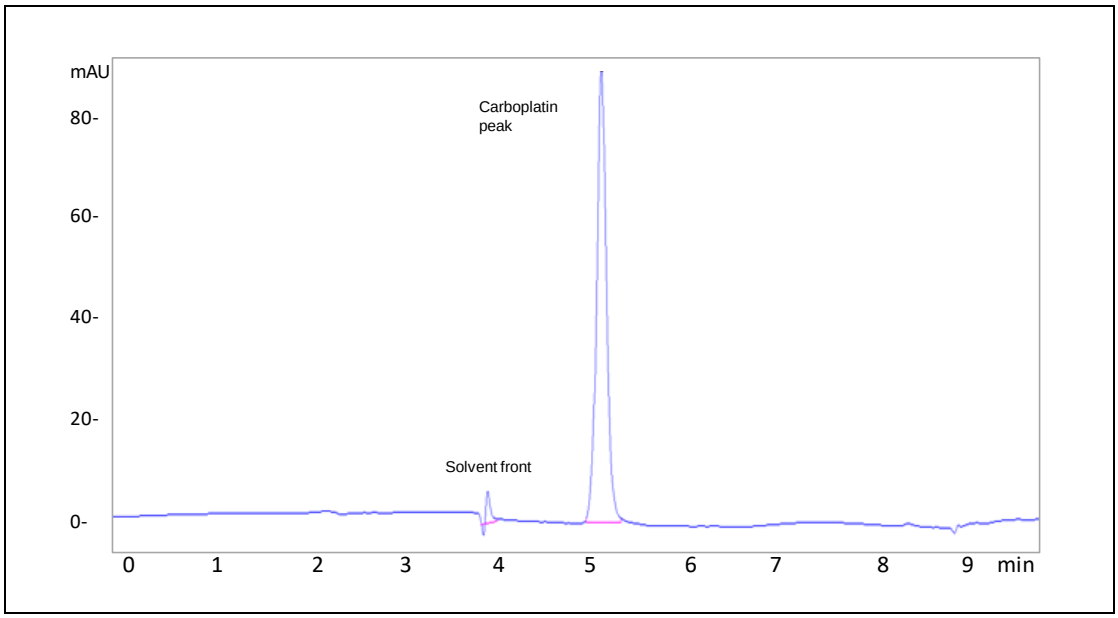


Figure 3-14: Chromatogram of carboplatin solution by using HILIC method.

A reverse phase HPLC method published by Mittal et.al [125] was selected for the preliminary analysis of carboplatin. With this method it was observed that carboplatin was eluting at the solvent front and there was not enough resolution to accurately quantify carboplatin in the samples (data not shown here). This was most likely due to hydrophilic nature of carboplatin. It was concluded that reverse phase HPLC method might not be a viable method for carboplatin analysis.

Therefore, an alternate HILIC (hydrophilic interaction liquid chromatography) method was developed for carboplatin analysis. This method resulted in a good retention and resolution of carboplatin, see Figure 3-14 for chromatogram. A similar approach has been used by others to effectively retain and separate polar (hydrophilic) compounds on polar stationary phases [128]. The final conditions of HILIC method are given in Table 3.1 and has been used to analyse carboplatin in PLGA microspheres to determine carboplatin encapsulation efficiency and drug loading.

Drug loading and encapsulation efficiency was calculated as follows

Experimental Drug Loading (D_E) = (W_C / W_M) x 100

Where, D_E is the experimental drug loading, W_C is the calculated weight of carboplatin in the dried sample determined by HPLC analysis and W_M is the total weight of dried sample analysed.

Encapsulation efficiency = (D_E / D_T) x 100

Where, D_T is the theoretical drug loading calculated by using the input weights of carboplatin and PLGA.

From this analysis, drug loading was found to be 0.22% w/w and encapsulation efficiency was calculated to be 38.1% (by using theoretical drug loading of 0.58 % w/w),
Considering these results and limited aqueous solubility (~ 14 mg/mL) of carboplatin it might not be possible to achieve high carboplatin loading with this method. For example, a primary emulsion (W/O) made of 1 part of 1.4 % w/v carboplatin solution in water mixed with 9 parts of 20 % w/w PLGA solution in DCM, will result in a maximum theoretical loading of 0.7 % w/v.

3.4 Conclusion

The microfluidics method has been found to be the most suitable technique to make well controlled, uniform size PLGA microspheres by using a single or double emulsion approach.
Various lessons were learned during this part of the study including, i) magnetic stirring should not be used at any stage after droplet formation by microfluidics, ii) PLGA concentration might have a significant effect on the microsphere size, iii) PLGA microspheres might have some internal porosity which may or may not have a significant impact on the final formulation characteristics, iv) double emulsion method is not a suitable method to achieve higher (~ 10 % w/w) carboplatin loading due to the limited aqueous solubility (~ 1.4 % w/v) of

carboplatin. Therefore, an alternate method would be required for carboplatin PLGA microsphere manufacturing.

These learnings were carried forward and implemented during further microfluidics method development and optimisation for the manufacture of PLGA microspheres, chapter 5 and 6.

4 Evaluation of different methods for the preparation of Intraperitoneally Injectable Hydrogels containing PLGA microspheres

4.1 Introduction

It has been reported that PLGA microsphere clearance from the peritoneal cavity can be size dependent, smaller than 20 μm particles clear much faster than the larger ones [75]. In addition, PLGA microspheres may also cause adhesions and inflammation response after intraperitoneal cavity administration [62,76,77].

Hydrogels can alleviate these concerns because hydrogel are composed of 3-dimensional network of hydrophilic homopolymers or copolymers which can trap the microparticles and prevent the clearance from IP cavity. Furthermore, hydrogels are capable of imbibing large amounts of water or biological fluids which gives hydrophilicity and soft (tissue like) consistency to hydrogels and result in excellent biocompatibility [78,129,130], which is why there is growing interest in the injectable “composite” hydrogels where particulate systems are co-formulated with hydrogels [75].

Injectable hydrogels are typically designed to be liquid(s) before administration which form gel either at the site of injection or in the device during administration (e.g. in the case of two precursor solutions contained in double barrel syringe systems) and allow the drug delivery with minimal surgical intervention [130-132].

Hydrogels can be made by either physically (entanglements or crystallites) or chemically cross-linking (covalent bonds) the polymer chains [75,129,133]. The polymer cross-linking makes the hydrophilic homo or copolymers water insoluble [129]. Physically cross-linked hydrogels are preferred over the chemically cross-linked gel networks for biomedical applications as the latter generally require the use of toxic initiators and cross-linking agents [133].

Detailed reviews of the gelation mechanisms of both physically and chemically cross linked hydrogel types has been published by various researchers [75,129,131,134-136]. In this study we will only focus on the physically cross-linked hydrogels because they are particularly attractive for delivery of microspheres

since these gels are made from aqueous precursor solutions and polymeric microspheres can be easily suspended in such solutions [20,75].

Although many physical cross-linking mechanisms can be used to make injectable hydrogels, as mentioned above, ionic cross-linking is one of the most commonly used mechanisms for making injectable hydrogels because ionic interactions are relatively strong and fewer cross-links are required to make a functional gel [131]. Typical, ionic cross-linked hydrogels are formed between an ionisable macromolecule and a small multivalent ion e.g. calcium-alginate gel. However, these gels are unstable and may disintegrate rapidly and unpredictably due to the extraction of small ions [130]. We hypothesise that ionically cross-linked hydrogels formed between oppositely charged high molecular weight polymers (e.g. hyaluronic acid and chitosan) may be more stable and disintegrate comparatively slowly due to the polymer chain entanglements in addition to ionic cross-links.

The primary aim of this work was to develop injectable hydrogel that would contain PLGA-microsphere composites, made from physically cross-linked hydrogels which remain stable and keep the PLGA microspheres in the intraperitoneal cavity for at least 1 month or longer.

Although, hydrogels have been extensively used to control the release of various therapeutic agents [78,79], it is not our intention in this study, rather we would prefer a hydrogel which does not significantly affect the release profile of API from PLGA microspheres.

Here we have tested the ability of various ionisable high molecular weight polymers including, hyaluronic acid, chitosan, alginate and pectin, (see Appendix C for main properties of these materials) to form hydrogels by using a double barrel syringe (with and without static mixer). The oppositely charged precursors were kept in separate barrels of the syringe before administration and mixed in a static mixer nozzle during administration. In addition, we have also tested commercially available ready-to-use hydrogels, PeptiGel®. These hydrogels were composed of self-assembling peptides that can form fibrillar structures, which in turn associate and/or entangle to form hydrogels [137]. Further details about these hydrogels are not disclosed here due to supplier confidentiality agreement. The reader is referred to Tang et. al. paper where product non-specific details of such peptide-based hydrogels has been

described [137]. One of the main reason for evaluating the PeptiGel® was that the PLGA microspheres could be easily mixed with the hydrogel at room temperature and injected by using standard syringe and needle, [138].

The most promising hydrogels were then tested for their physical stability, with and without PLGA microspheres, in the simulated intraperitoneal fluid at 37 °C.

4.2 Materials and methods

4.2.1 Materials

Hyaluronic acid sodium streptococcus equi (m.wt.1500 – 1800 kDa) was purchased from Sigma Aldrich, UK; sodium Hyaluronate-research grade HA15M (m.wt. 1.01 – 1.8 MDa) was purchased from Lifecore-Biomedical, US; Chitosan, three different grades i) high purity, 5-200 cps viscosity, ~78% deacetylation ii) low molecular weight, 20 – 300 cps viscosity, >75% deacetylation and iii) medium molecular weight, 200 – 800 cps viscosity and 75-85% deacetylated; sodium alginate (15 – 20 cps viscosity) and glucono delta-lactone (GDL) were purchased from Sigma Aldrich, UK; Pectin, four different grades of low-methoxy pectin (i.e. GENU® pectin type LM-101 AS, LM-102 AS, LM-104 AS and LM-105 AS) were purchased from CP Kelco, Germany; PeptiGel®, three different grades (Alpha1, Alpha1-001 and Alpha1-002) with different stiffness (G' - low, medium and high, respectively) were purchased from Biogel Manchester, UK. All other reagents were of analytical grade.
Double barrel syringes (5 mL, 1:1 ratio, polypropylene white) and mixer nozzles (containing 8 and 16 static mixing elements) were purchased from Adhesive Dispensing Ltd., UK.

4.2.2 Methods

Preparation of hyaluronic acid and chitosan gel by using a double barrel syringe

Range of chitosan and HA concentrations were used in the initial screening experiment. The final composition of 0.5% w/v HA and 0.5% w/v chitosan in 1% w/v acetic acid was selected based on the screening experiments (full data not shown here) and the calculated cationic and anionic functional groups (see Appendix D for calculation details). The anionic (HA) and cationic (chitosan) polymer solutions were loaded in the separate barrels of a double barrel syringe and dispensed simultaneously through the mixing nozzle, connected at the front of double barrel syringe (Figure 4-1). The nozzle with 16 static mixing elements was selected based on the preliminary results. This gel was called gel A.



Figure 4-1 Hyaluronic acid and Chitosan gel preparation by using a double barrel syringe.

The anionic and cationic solutions were placed in separate barrels and injected through a nozzle containing 16 static mixing elements.

Preparation of hybrid-gels by using double barrel syringe

Hybrid-gels were made by combining two or more different gels. Three hybrid-gels were prepared as follows, while keeping the base of the gel same as gel A above, see summary of the gel A – D compositions in Table 4.1.

Gel B: 1% w/v alginate-sodium was added in the 0.5% w/v HA solution and 0.4 % w/v $CaCl_2$ was added in the 0.5% w/v chitosan solution in 1% w/v acetic acid. The method to make alginate-Ca^{2+} gel by using $CaCl_2$ is also called an “external gelation” method [139].

Gel C: 1% w/v alginate-sodium and 0.2% w/v $CaCO_3$ added in the 0.5% w/v HA solution and 1% w/v glucono delta-lactone was added in the 0.5% w/v chitosan solution in 1% w/v acetic acid. The method to make alginate-Ca^{2+} gel by using $CaCO_3$ and GDL is also called an “internal gelation” method [139].

Gel D: 1% w/v alginate-sodium and 0.2% w/v $CaCO_3$ added in the 0.5% w/v HA solution whereas, the 0.5% w/v chitosan solution was prepared in 1% w/v

Glucono delta-lactone solution which was aged (stored) for 24 hours at room temperature) instead of 1% acetic acid. This is a modified method which we are reporting for the first time.

Table 4.1: Summary of gel A – D compositions.

Gel ID	Solution ID	Components	Concentration (all % values are as w/v)
A	Anionic	Hyaluronic Acid	0.5 %
	Cationic	Chitosan	0.5 % in 1 % acetic acid
B	Anionic	Hyaluronic Acid	0.5 %
		Alginate Sodium	1 %
	Cationic	Chitosan	0.5 % in 1 % acetic acid
		Calcium Chloride	0.4 %
C	Anionic	Hyaluronic Acid	0.5 %
		Alginate Sodium	1 %
		Calcium Carbonate	0.2 %
	Cationic	Chitosan	0.5 % in 1 % acetic acid and 1 % glucono delta-lactone
D	Anionic	Hyaluronic Acid	0.5 %
		Alginate Sodium	1 %
		Calcium Carbonate	0.2 %
	Cationic	Chitosan	0.5 % in 1 % glucono delta-lactone

The rest of the process to make the hydrogel by using a double barrel syringe and static mixing nozzle was the same as detailed above for gel A, see Figure 4-1.

Physical stability evaluation of the composites of PLGA microspheres and hybrid-gels B and D in SIPF

The aim was to develop an injectable drug delivery system for IP cavity containing hydrogel and PLGA microspheres. Therefore, in this experiment composites of blank PLGA-microspheres (made from PLGA 75/25 50 kDa) and hybrid-gels B and D were prepared. These composites were injected directly in the simulated IP fluid, at 37 °C and at 1:10 gel composite to simulated IP fluid volume ratio, to evaluate the physical stability of the composites in biorelevant conditions. The composition of the simulated IP fluid was the same as described in chapter 6.2.2, but in this case 3% w/v bovine serum albumin (as plasma protein) was included in the simulated IP fluid because proteins, being ionisable large molecules, may positively or negatively impact the stability of hydrogels.
The PLGA microspheres were dispersed in the anionic solution for both composite gels (B and D) at the concentration of 2% w/w. The rest of the process of making gels was same as given above. However, in this case gels were injected directly into a vial containing simulated IP fluid.

Syneresis

In order to quantify the amount of free fluid in each gel, syneresis was determined by weighing the gel before and after removing the free liquid.

Preparation and characterisation of PeptiGel and composites with PLGA-microspheres for physical stability evaluation in the SIPF

Three different grades of PeptiGel (Alpha1, Alpha1-001 and Alpha1-002) were evaluated first, as received from the supplier. Two hydrogels (Alpha1-001 and Alpha1-002) were selected for further evaluation with the PLGA microspheres as follows. A known quantity of (approximately 5 % w/w) blank PLGA-microspheres (made from PLGA 75/25 50 KDa) was mixed with a known quantity (e.g. 0.25 mL) of each of the gel. The composites were carefully mixed by pipetting “up and down” a few times to ensure homogeneous distribution of microspheres throughout the gel, while avoiding the entrapment of air bubbles.

The vial inversion test was performed and visual inspection (camera pictures were also taken) carried out to evaluate the impact of microsphere mixing on the gel.

A known quantity of simulated IP fluid was added on top of the composites, visual inspection was performed and then samples were placed in water bath at 37 °C and 150 rpm orbital mixing for at least 24 hours.

The vial inversion and visual inspection tests were performed at the start and end of 24-hour period, to evaluate the physical stability of composites i.e. to observe the gel integrity and presence of microspheres outside the composite.

Preparation and characterisation of pectin gels and composites with PLGA microspheres to evaluate physical stability in the SIPF

5% w/v Pectin and 10 to 0.7% w/v $CaCl_2$ solutions were prepared separately in purified water. Pectin and calcium chloride solutions were then mixed at 1:1 ratio by using either double barrel syringe.

The composites were prepared by mixing known quantity (e.g. 5% w/w) of blank PLGA-microspheres (made from PLGA 75/25 50 KDa) with a known quantity (e.g. 1 mL) of each of the Pectin gels. The composites were carefully mixed by pipetting “up and down” few times to ensure homogeneous distribution of microspheres throughout the gel, while avoiding the entrapment of air bubbles.

The hypothesis for using pectin was that certain low-methoxy grades of pectin can form gel at relatively lower (biorelevant) concentrations of Ca^{2+} compared to alginate. See Appendix F for net charge of each of the pectin grade used in this study and the impact of $CaCl_2$ on the net charge. This data was used to shortlist pectin grades for making composites.

4.3 Results and discussion

4.3.1 Preparation and characterisation of HA and chitosan gel

The Figure 4-2 is showing the camera pictures of hydrogels A – D. It can be seen from pictures that gel A contained white fibrous precipitates and it also failed the vial inversion test (bottom pictures) which indicated that HA and chitosan did not make a gel. Whereas, formulations B-D did appear to form gels. It is worth noting that gels B-D contain alginate (along with HA and chitosan), which was primarily used to provide strength to the HA and chitosan gel. It was assumed that alginate (being a high molecular weight polymer) may also enhance the physical strength and longevity of the HA-chitosan gel by providing additional physical entanglements, in addition to providing initial rigidity.



Figure 4-2 Camera pictures (A-D) of HA and Chitosan gels with different additives, made by using double barrel syringe where anionic components (solution 1) placed in one barrel and the cationic components (solution 2) in the other.

Formulation A solution 1 (0.5% w/v HA), solution 2 (0.5% w/v chitosan in 1% acetic acid). **Formulation B** solution 1 (0.5% w/v HA + 1% w/v sodium alginate), solution 2 (0.5% w/v chitosan in 1% acetic acid + 0.4% w/v $CaCl_2$). **Formulation C** solution 1 (0.5% w/v HA + 1% w/v sodium alginate + 0.2% w/v $CaCO_3$), solution 2 (0.5% w/v chitosan in 1% acetic acid + 1 % w/v GDL). **Formulation D** solution 1 (0.5% w/v HA + 1% w/v sodium alginate + 0.2% w/v $CaCO_3$), solution 2 (0.5% w/v chitosan in 1% GDL)

In formulation B, the gel appeared as an irregular compact mass with some free liquid and it passed the vial inversion test indicating that the addition of alginate in the HA solution and calcium in the chitosan solution does form a gel. However, as shown in the above camera pictures gel B did not appear as a homogenous mass. This was most likely due to the instantaneous interaction of dissolved calcium with alginate, which is a known feature of alginate-calcium gel [139], and also potentially with HA. Which has resulted in the formation of hydrogel while injecting anionic and cationic solutions via the static mixer and the hydrogel formed during this process kept it's tubular shape after injection.

In order to make a homogenous alginate-calcium gel an alternate approach has been used by some researchers [140], where water soluble $CaCl_2$ is replaced with water insoluble $CaCO_3$ along with the addition of glucono delta-lactone (GDL) to slowly dissolve $CaCO_3$. The GDL partially hydrolyses to gluconic acid in aqueous solution until an equilibrium is established between lactone and acid forms ([141]). As a result of this the pH of the GDL solution drops over time which helps to slowly dissolve $CaCO_3$. In a preliminary experiment a 1% w/v GDL solution was prepared and aged for at least 24 hours which resulted in a drop of pH from 3.5 to 2.4. This change in pH (or formation of gluconic acid) liberates Ca^{2+} from $CaCO_3$, which slowly diffuses throughout the matrix and formed a homogenous calcium-alginate gel.

This approach has been used in the formulation of hydrogels C and D. As it is can be seen from the Figure 4-2 that both formulations C and D did result in the formation of homogenous gels which passed the vial inversion test. The only difference between gels C and D was the use of acidic solution to dissolve chitosan. Gel C contained 1% v/v glacial acetic acid to dissolve chitosan and 1% GDL to liberate Ca^{2+} from $CaCO_3$. Whereas gel D contained only 1% GDL solution which was aged for at least 24hr to produce enough quantity of gluconic acid to dissolve chitosan. From the vial inversion test and visual observations, it appeared that Gel D was also a homogenous gel which verified that sufficient Ca^{2+} concentration was released from $CaCO_3$ by the gluconic acid to form the gel.

Interestingly, the method of aging the GDL for 24 hours to form gluconic acid and keeping the CaCO3 in separate vial/syringe barrel until administration resulted in a homogenous gel in a relatively quicker time (i.e. less than 30

minutes) compared to what has been described by Schmitt et. al. [139]. As far as we are aware, it is a unique method to quickly form a homogenous calcium-alginate gel (i.e. partial gel forms instantaneously and gelation completed in less than 30 minutes) and offers an advantage for making injectable hydrogel.

Syneresis:

As it can be seen from Figure 4-2 that all the gels (A-D) contained some free fluid in addition to the gel mass. In order to quantify the amount of free fluid syneresis was determined by weighing the gel before and after removing all the free fluid. The results shown in the Table 4.2 supports visual observations and the camera pictures in Figure 4-2 indicating that gels C and D were the most homogenous hydrogels with minimum syneresis and therefore are better-quality hydrogels compared to A and B in terms of holding the higher quantity of water.

Table 4.2: Results of syneresis measurement for gels A-D.

Formulation ID	Syneresis (% w/w)
A	92
B	56
C	46
D	46

4.3.2 Physical stability of hybrid composite gels in simulated IP fluid (SIPF):

From this data gel B and D looks promising in terms of physical appearances and the capacity to hold the water content. Therefore, these two gels were selected for making composites with PLGA microspheres and comparing the physical stability in SIPF. Additionally, these two gels were based on different gel formation mechanisms (i.e. “external gelation and “internal gelation”) which makes them interesting candidates for this comparison.

Figure 4-3 is showing the camera pictures of gels B and D composites (i.e. gel and PLGA microsphere mixtures) when prepared in the presence of simulated IP fluid to evaluate the physical stability.

As it can be seen from these pictures that; both gel B & D composites maintained the gel structure, as confirmed by vial inversion test, in the absence of SIPF. Visually, these gels contain aggregates or noodle-like structures which form while injecting the two mixtures through static mixer nozzle rather than being a single mass. These aggregates or noodle-like structures fuse to some extent and appear uniform single or multiple masses after injection.

Whereas, in the presence of SIPF both gels resulted in more diffuse matrix with some detached precipitates or pieces of gel. It is difficult to clearly see the microspheres from the camera pictures in Figure 4-3 due to the cloudy and frothy nature of the liquid. However, it was noticed during visual observations that the majority of the microspheres were released out of the gel composites. The camera pictures also show some white precipitates in both gel B and D composites which are most likely due to free chitosan because at neutral pH (SIPF pH 7.4) chitosan has negligible aqueous solubility [142].

One of the main reasons for the instant physical instability of these gels in simulated IP fluid was the dilution of the Ca^{2+} concentration in the presence of SIPF. As mentioned above that the main body of the hybrid-gels was due to the calcium-alginate which only persists at certain Ca^{2+} concentrations, as shown by Schmitt et. al. [139]. Therefore, once the calcium concentration dropped below critical level the hydrogel started disintegrating.

In the next phase we have evaluated pectin-calcium gels as pectin can form gels at relatively lower Ca^{2+} concentrations, see section 4.3.3.

In addition, gel B and D results indicated that the polymers used in this study did not result in the physical entanglement of the polymer chains or these entanglements were not strong enough to persist in the presence of simulated IP fluid.

4.3.3 Preparation and characterisation of pectin hydrogels and composites with PLGA microspheres for physical stability evaluation in SIPF

Three grades of low-methoxy pectin (P105, P104 and P102) were selected for the initial gel screening, based on the results from the evaluation of the net charge of each pectin grade with or without calcium (see Appendix F).

Gel ID	Without SIPF	With SIPF
Gel B		
Gel D		

Figure 4-3: Camera pictures of gels B and D composites made by using double barrel syringe where anionic components (mixture 1) placed in one barrel and the cationic components (mixture 2) in the other. Both gels were prepared in the presence of simulated IP fluid (1:10 gel to SIPF ratio). Gel B composite: mixture 1 (0.5% w/v HA + 1% w/v sodium alginate + 2% w/w PLGA microspheres), mixture 2 (0.5% w/v chitosan in 1% acetic acid + 0.4% w/v $CaCl_2$). Gel D: mixture 1 (0.5% w/v HA + 1% w/v sodium alginate + 0.2% w/v $CaCO_3$ + 2% w/w PLGA microspheres), mixture 2 (0.5% w/v chitosan in 1% GDL)

Figure 4-4 is showing the camera pictures of hydrogels made with two different concentrations of calcium chloride and all three grades of pectin. These images show that all three grades of pectin did form gels with 0.1% w/v calcium chloride, as confirmed by the vial inversion test, and these gels visually appeared homogenous. However, the gels made with 0.7% w/v calcium chloride did not

look homogenous. In particular, the gels made from P105 and P104 failed the vial inversion test. Although the gel made from P102 did pass the vial inversion test but visually it looked granular in appearance.

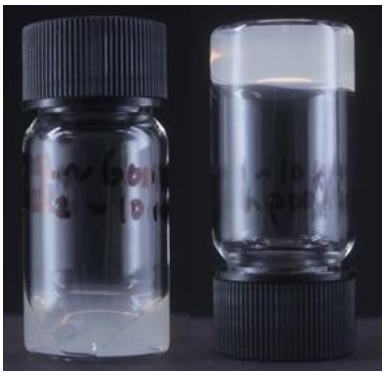
Gel ID	$CaCl_2$	
	10 mM	50 mM
P105 – 5% w/v		
P104 – 5% w/v		
P102 – 5% w/v		

Figure 4-4: Camera pictures of pectin – calcium gels made from three different grades of pectin (P102, P104 and P105) and two different concentration of calcium chloride.

Based on these initial results the gel made from grade P105 and 0.1 % w/v calcium chloride, was selected for the next step to evaluate the physical stability in simulated IP fluid in the presence and absence of PLGA micropsheres (Figure 4-5). These camera pictures show that both of the gels were also physically unstable in the SIPF, they partially dissolved and released majority of the microspheres immediately. Therefore, pectin gels were not selected for any further work.

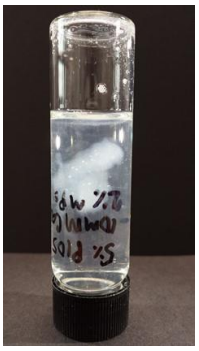
P105 5% w/v + $CaCl_2$ 0.1% w/v		
P105 5% w/v + $CaCl_2$ 0.1% w/v + 2% w/w microspheres		

Figure 4-5: Camera pictures of pectin – calcium gels in simulated IP fluid, made from pectin P105 in the absence (top) and presence (bottom) of PLGA microspheres.

4.3.4 Preparation and characterisation of Peptide gel

Two PeptiGel® composites containing PLGA microspheres were evaluated as shown in Figure 4-6. The camera pictures display that both of these composite gels were relatively more stable in the simulated IP fluid at room temperature compared to the 37 °C. However, the stability at room temperature was not more than 24 hours because free particles were observed on visual inspection in both composites after this time.

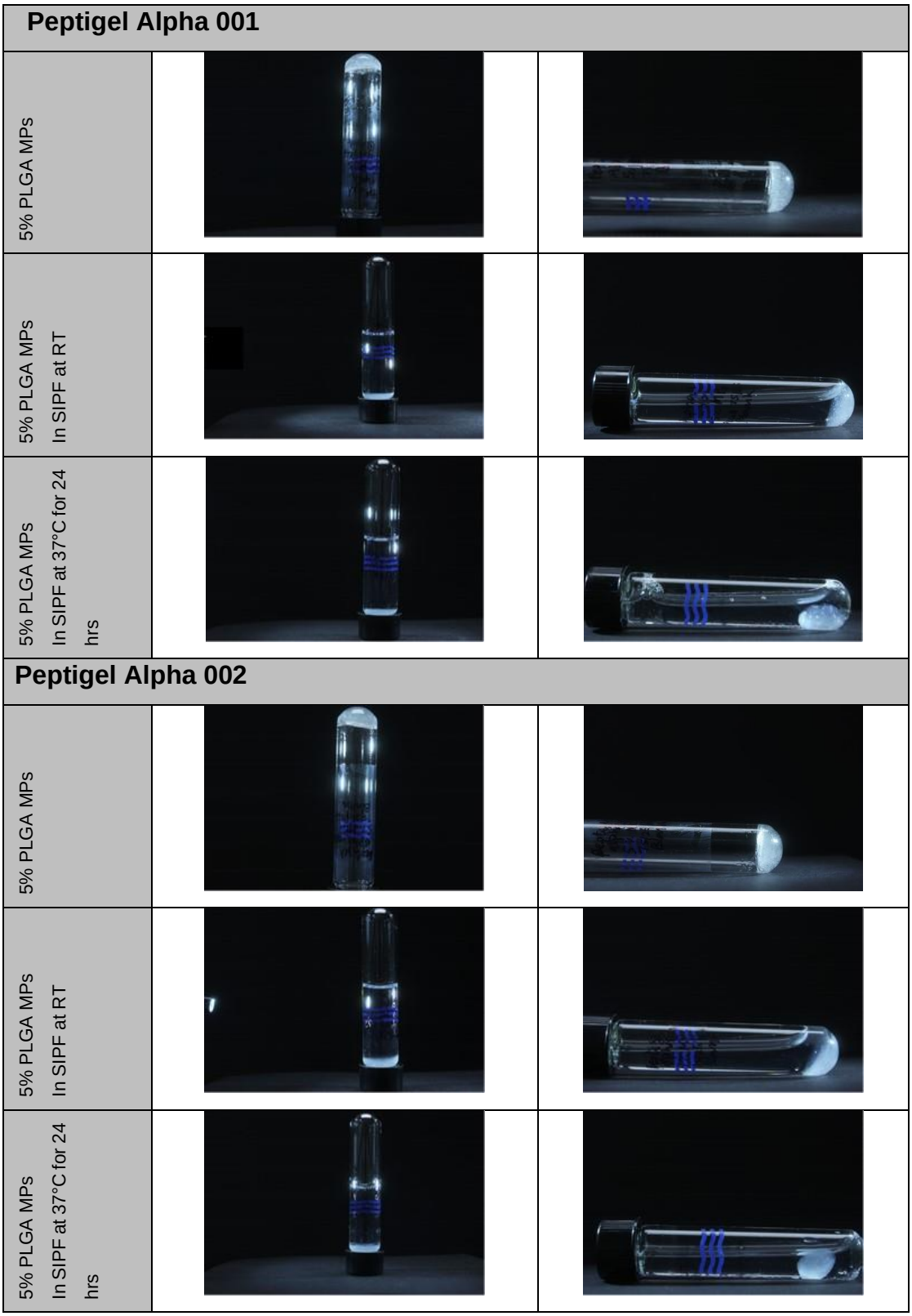


Figure 4-6: Camera pictures of two PeptiGel® (Alpha 001 and Alpha 002) composites with PLGA microspheres with and without simulated intraperitoneal fluid. The SIPF (1:10 v/v composite to SIPF) was added to the composite and stored at room temperature and 37 °C for 24 hours.

However, at 37 °C the free particles and broken gel pieces were observed immediately after the addition of SIPF, as shown in camera pictures. Therefore, PeptiGel® was also not found suitable for this application.

Two thermosensitive hydrogels were also briefly evaluated, including; i) a supramolecular nucleoside based hydrogel developed by our (Maria Marlow's) research group [143] and ii) a commercially available triblock copolymer, PLCL-PEG-PLCL (from Polyscitech division of AKINA, INC. USA) based hydrogel [79]. These gels were tested by using the same methods as detailed above and were also not found to be physically stable in SIPF, data is not shown here.

4.3.5 Conclusion

Preliminary results from HA and chitosan gel indicated that these precursors did not result in the formation of a hydrogel rather they formed a white precipitated matrix which was unstable in the simulated IP fluid. We have managed to improve this gel by developing the hybrid-hydrogels of HA and chitosan in combination with alginate-calcium hydrogel. However, these hybrid-hydrogels and their composites with PLGA microsphere were not stable in the SIPF and they released majority of the microspheres within short time (~ 24 hours). All other hydrogels tested in this study (including, pectin-calcium, PeptiGel®, supramolecular nucleoside-based hydrogel and a triblock copolymer, PLCL-PEG-PLCL, based thermogel) were also not found to be stable in SIPF upon dilution. Therefore, it was concluded that none of these gels were suitable for the desired application i.e. administration of PLGA microsphere in the IP cavity.

However, during this study a unique hybrid-hydrogel was developed to improve the formation of alginate-calcium gel by an "internal gelation" mechanism. In this method, glucono delta-lactone was aged for at least 24 hours and kept separate from $CaCO_3$ until administration by using the double barrel syringe with a static mixer nozzle. As far as we are aware, this method has not been reported by anyone and we are reporting this method for the first time.

5 Optimisation of Microfluidics Method for the Manufacture of Carboplatin and Paclitaxel loaded PLGA microspheres

5.1 Introduction

As detailed in chapter 3, after screening different methods, microfluidics was found to be the most suitable technique to make controlled size PLGA microspheres with a narrow size distribution. Although, the interest in using microfluidics technique for drug delivery applications (including microspheres, nanoparticles, etc.) has grown over the last 20 years (Figure 5-1). However, it is still a relatively new technique and there are not many comprehensive reports available where it is systematically evaluated for making PLGA microspheres of carboplatin and paclitaxel with the help of DOE.

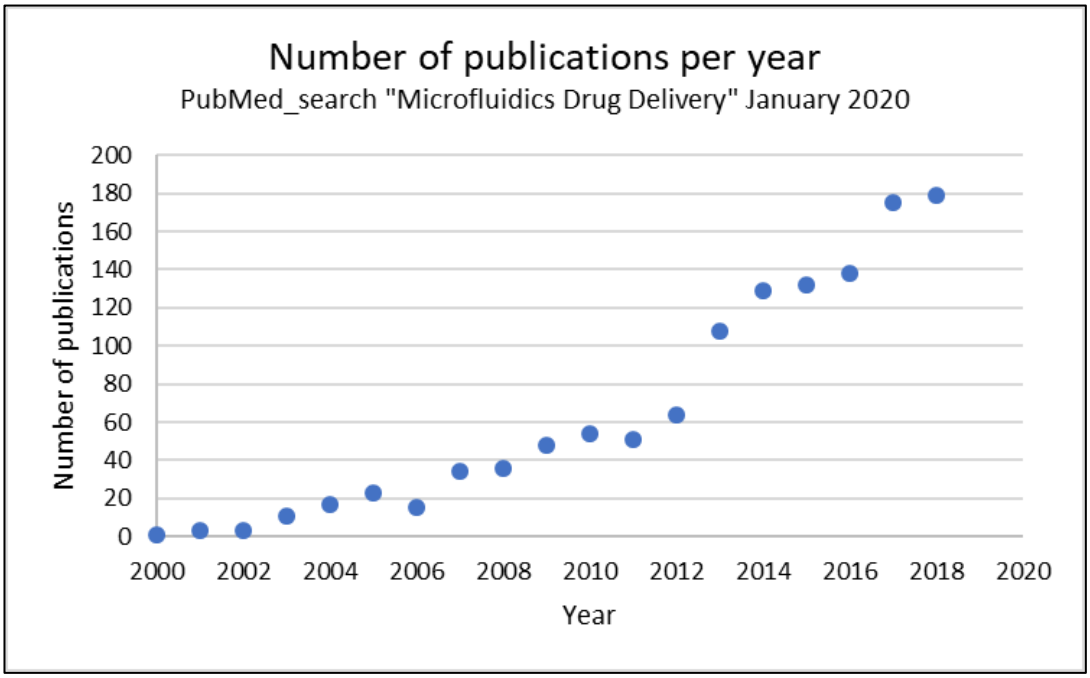


Figure 5-1: Graph showing the number of publications describing the use of microfluidic for drug delivery applications per year during last 20 years. PubMed search dated 29th January 2020, for term "microfluidic drug delivery".

A brief introduction of the technique is as follows, microfluidics is the science and technology of systems with integrated channels on the microscale (tens to hundreds of micrometres), through which small quantities of fluids (usually 10^{-9} to 10^{-18} L) can flow in designed configurations that are controlled and manipulated systematically [73,74].

Droplet microfluidics is a subcategory of microfluidics which is used to make discrete droplets by mixing immiscible fluids inside microchannels [144]. In this technique the droplets are either generated by passive (hydrodynamic pressure) or active (external actuations) methods [145,146]. Passive droplet microfluidics can be further subdivided into cross-flow, co-flow, flow-focussing or step emulsification classes. [147]. For further details about the other microfluidics techniques the reader is referred to two comprehensive reviews by Shang *et. al*. and Zhu *et. al.* [146,147].

In this study, we have focused on a passive flow-focusing droplet microfluidics technique where the dispersed and continuous phases flow coaxially through a contraction region and generates an elongation filament that ultimately breaks into uniform droplets (Figure 5-2). We have selected this method because it generally produces relatively smaller (50 – 200 μm) uniform droplets closely related to the size of the narrow contraction [147]. Other critical factors that control the droplet size in flow-focusing droplet microfluidics include; i) the flow rates (i.e. total flow and ratio of continuous / dispersed phase flow rates), ii) interfacial tension between the dispersed and continuous phase which can be modified by using suitable surfactants and iii) fluid viscosity (in particular the dispersed or organic phase viscosities, which is highly dependent on the concentration of the polymer e.g. PLGA and the API) [147].

Therefore, in this study, firstly, we have used a design of experiment (DOE) approach to determine the optimum conditions for the above-mentioned critical parameters for a microfluidics setup. The primary aim of the DOE approach was to determine the design space where 50 – 200 μm microspheres can be reproducibly prepared, as per the QTPP (section **3.1.1**).

Subsequently, we have developed method to encapsulate two compounds (carboplatin and paclitaxel) with different physicochemical properties (i.e. poorly water soluble paclitaxel and water soluble carboplatin) in the PLGA microspheres by using the optimised manufacturing method.

There are several publications describing the manufacture of paclitaxel loaded PLGA microspheres by oil in water single emulsion (O/W) methods [148-150] including precise particle fabrication methods (PPF) [151]. In-general, it has been reported that paclitaxel has good encapsulation efficiency and slow release from PLGA microspheres. However, we have not seen any reports where a holistic systematic approach has been taken to design, develop and manufacture paclitaxel loaded PLGA microspheres by combining, mathematical pharmacokinetic modelling, a DOE and microfluidics techniques.

On the other hand, encapsulation of carboplatin in PLGA microspheres is challenging [152-154]. To the best of our knowledge to date, no one has attempted to manufacture carboplatin loaded PLGA microspheres by combining mathematical PK modelling, solid-in-oil-in-water (S/O/W) emulsion method using microfluidics, DOE and carboplatin nanocrystals. In this work, we have achieved relatively high encapsulations efficiency (> 60 % w/w) of carboplatin using this holistic innovative approach.

5.2 Materials and Methods

5.2.1 Materials

RESOMER® Select 7525 DLG/PLGA (M_w 50-60 kDa, IV 0.35 – 0.45 dL/g) was purchased from Evonik Birmingham Laboratories, USA; Paclitaxel was purchased from Sigma Aldrich and Apollo Scientific Ltd. UK, and Carboplatin was purchased from Tocris Bioscience, UK. PVA (88% hydrolysed m.wt. 20-30 kDa) and DCM were purchased from Sigma Aldrich. All other reagents were of pharmaceutical grade.

5.2.2 Methods

Microfluidics

The Dolomite microfluidics pressure-based system with a flow focusing droplet junction chip, from The Dolomite Centre Ltd. UK, was used in this work. The organic solution (oil phase) was filled in a gas tight syringe which was operated by a syringe pump to control the flow rate and the aqueous solution was placed in the dolomite pressure-pump where the flow rate was controlled by nitrogen

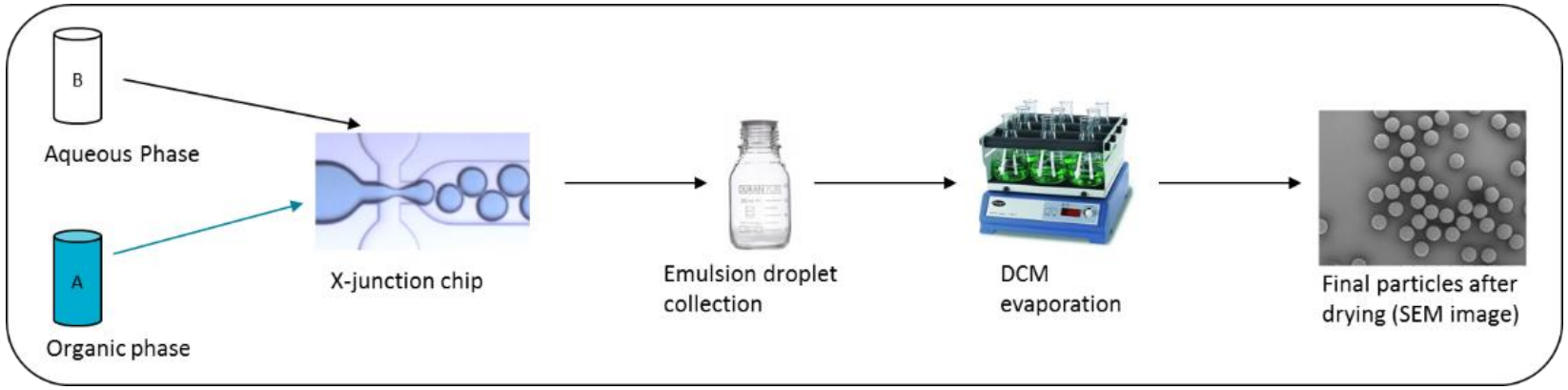


Figure 5-2: Flow diagram for the manufacture of PLGA microspheres by using single emulsion (O/W) method in microfluidics.

pressure. Both solutions were mixed inside the micro channel chip to form uniform droplets of the oil phase which were collected in a collection vessel containing dilute PVA solution (~0.02% w/v). After collection, the emulsion was left agitating uncovered on an orbital shaker at ambient conditions for at least 24 hrs to evaporate DCM and harden the microspheres (**Figure** 5-2)

Design of Experiments (DoE)

Design Expert 9.0 (State-Ease, Inc. USA) software was used for the design of experiments (DOEs). A two-step approach was taken where the first DOE was used to screen the broad ranges of three independent variables including, i) total flow rate, ii) aqueous to organic phase flow rate ratio and iii) PVA concentration. A regular two-level full factorial design (2^n) was used to determine the main effects and interactions and fully characterise the process conditions. Each factor was tested by using the levels generally reported in the literature, Table 5.1. In addition, a centre point was also tested in triplicate to evaluate curvature of the statistical model. All experiments were randomised to avoid biased variance. The dependent variables included the microsphere size and size uniformity.

Table 5.1: Independent variables for first design of experiments (DOE 1)

Independent variables	Applied levels		
	Low	Medium	High
Total flow rate (µL/min)	50	100	200
Aqueous/Organic phase flow rate ratio	3	6	12
PVA concentration (%w/w)	0.5	1.5	5

A second DOE was then used to evaluate selected tighter ranges of the three independent variables from the first DOE. In addition, polymer (PLGA) concentration was included as a fourth independent variable in the second DOE. A regular two-level fractional factorial design (2^{n-1}) was selected for the second DOE to assess the main effects and interactions with reduced number of experiments. Each factor was tested using the levels shown in Table 5.2 and a centre point was included in triplicate to evaluate curvature of the statistical model. All experiments were randomised to avoid biased variance. The dependent variables included the microsphere size and size uniformity.

The data was processed by using Design Expert 9.0 (State-Ease, Inc. USA) software and the summary of the results was presented as typical graphical representations including pareto charts, interaction plots, contour plots, etc.

Table 5.2: Independent variables used in the second design of experiments (DOE 2)

Independent variables	Applied levels		
	Low	Medium	High
Total flow rate (µl/min)	100	200	400
Aqueous/organic phase flow rate ratio	6	12	24
PVA concentration (% w/v)	0.15	0.5	1.5
PLGA concentration (% w/w)	5	10	20

Encapsulation methods for Paclitaxel and Carboplatin

Paclitaxel encapsulation method

The oil in water (O/W) emulsion and solvent evaporation method were used to manufacture paclitaxel loaded PLGA microspheres. Briefly, the oil (organic) phase was prepared by dissolving PLGA and paclitaxel in dichloromethane (DCM) and the aqueous phase was prepared by dissolving PVA in water. Both phases were mixed at predefined flow rates and flow rate ratios by using the Dolomite microfluidics (UK) system fitted with a droplet junction microchannel chip (Figure 5-2) to make controlled, uniform size microspheres. The rest of the process was the same as described in the section 3.2.2. The solidified microspheres, after DCM removal, were washed three times with 0.01 % w/v PVA solution and dried under vacuum for 24 hr at ambient temperature. The final microspheres were stored below 8° C before use.

Carboplatin encapsulation method

Carboplatin loaded PLGA microspheres were manufactured using the same method as detailed for paclitaxel with some modifications in the preparation of organic phase, as detailed below.

Carboplatin is insoluble in DCM and it has large crystalline particles (>200 µm). Therefore, it was not suitable to disperse such large crystals in the organic phase. Hence, the carboplatin crystalline particle size was reduced to less than

1µm by wet milling in PEG 200 using a Planetary Micro Mill (Fritsch PULVERISETTE 7 classic line, Fritsch GmbH, Germany), Figure 5-3.

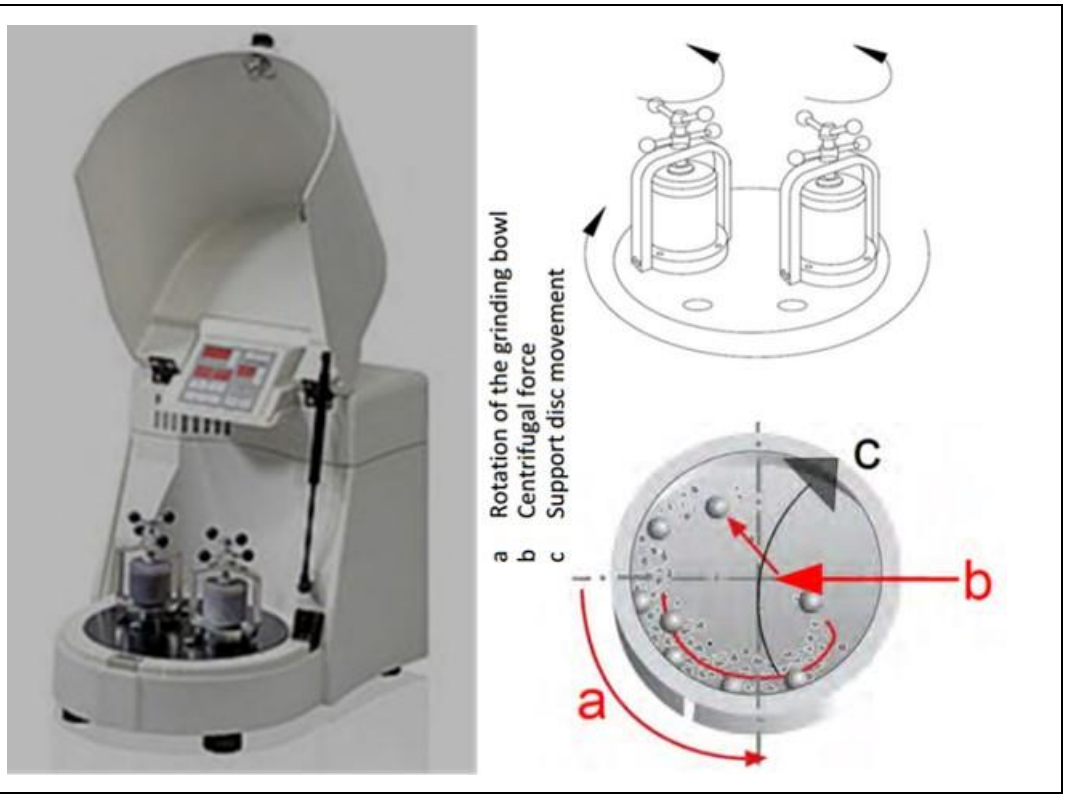


Figure 5-3: Planetary micro mill and principle of operation

The carboplatin nanocrystals were then dispersed in the organic phase. The organic phase was filtered through 5 µm stainless steel filter to remove any larger particles (which may block the microfluidic channels) and continuously stirred during the manufacture of micropsheres to ensure homogeneity of carboplatin nanocrystals inside the microspheres. The rest of the microsphere manufacturing method was same as for the paclitaxel microspheres.

The particle size of the milled carboplatin nanosuspension was analysed by dynamic light scattering (DLS) and laser diffraction using ethanol as the dispersant. Assay of the carboplatin nanosuspension was determined by HPLC-UV using the method described below.

Microsphere characterisation methods

Microsphere size by laser diffraction

The microsphere size was analysed by using a Malvern Mastersizer 2000 equipped with a hydro 2000μP small volume wet dispersion accessory and Malvern 2000 software (Malvern Instruments Ltd.). Approximately, 18 ml of the dispersion medium (0.02% PVA) was loaded and a background measurement was taken. This was followed by adding enough sample to achieve 10-20% laser light obscuration. Three readings were taken for each sample and average results for particle size ($D_{0.5}$) and uniformity were reported. Particle size ($D_{0.5}$) is the median size in microns at which 50% of the sample is smaller than this size. Particle size uniformity is the absolute deviation from median and was calculated by using following equation.

Uniformity = $\sum Xi \, |d(x, 0.5) - di| \, / \, d(x, 0.5) \sum Xi$

where, $d(x,0.5)$ is the median size of the distribution and d_i and x_i are respectively the mean diameter of, and result in, size class i.

Optical microscope (Polarised light microscopy)

All microspheres were dried for 24 hr in a vacuum oven at ambient temperature before analysis. A small quantity of dried microspheres was sprinkled over a glass microscope and examined using a Zeiss Microscope (Axio Scope.A1, Carl Zeiss Ltd.). Digital images were taken using the 10K and 40K times magnification with Axiocam ERc5s camera using Zen lite software (Carl Zeiss Ltd.)

Scanning Electron Microscopy (SEM)

A Hitachi TM-1000 table-top scanning electron microscope was used to analyse the microsphere surface characteristics (e.g. porosity, smoothness). Dried samples were mounted on the aluminium specimen stub with carbon adhesive discs (leit tabs). Samples were gold coated (5-10 nm coating density) prior to examination by using a Quorum EMS 150R gold sputter coater.

Differential Scanning Calorimetry (DSC)

A standard modulated DSC method was used with initial temperature equilibration at 5 °C for 5 min, modulations of 1 °C/min and heat ramp of 3 °C/min from 5 – 250 °C. Approximately 10 mg of each sample was prepared in standard Tzero (deep well) pans. Data was processed using TA instruments, Universal Analysis 2000, version 4.5A software.

X-ray Powder Diffraction (X-RPD)

The samples were mounted on a silicon wafer and analysed using the PANalytical CubiX PRO diffractometer (λ = 1.5418Å). Samples were measured in reflection geometry in θ - 2θ configuration over the scan range 2° to 40° 2θ with a nominal 25 second exposure per 0.02° increment. The X-rays were generated by a copper long-fine focus tube operated at 45 kV and 40 mA.

HPLC methods

Paclitaxel

A standard Agilent 1100 HPLC system equipped with a photodiode array detector was used and chromatographic separation was carried out using the Acquity UPLC BEH (C18, 1.7µm, 4.6 x 30 mm) column. The mobile phase consisted of A) 0.03% TFA in water and B) 0.03% TFA in acetonitrile. The mobile phase gradient was 5 -95% mobile phase B in 4 min. The flow rate was set at 1.5 ml/min, the detection wavelength was 229 nm, the injection volume was 10 µl and column compartment temperature was set at 40 °C. A standard solution was prepared at 0.1 mg/ml concentration and was used as the system suitability test (SST) before and after each analysis and to calculate assay for unknown samples. Method linearity was determined between 0.04 – 10 µg/ml concentrations.

Carboplatin

A standard Agilent 1100 HPLC system was equipped with a photodiode array detector was used for this analysis. The chromatographic separation was carried out using the SeQuant ZIC-pHILIC, 5 µm, polymeric PEEK 150 x 4.6 mm column. Mobile phase consisted of A) water and B) acetonitrile. The mobile phase gradient was 95 -30 % B in 7 min. The flow rate was set at 1 ml/min, the

detection wavelength was 227 nm, the injection volume was 10 µl and column compartment temperature was set at 40 °C. A standard solution was prepared at 0.1 mg/ml concentration and was used as SST before and after each analysis and to determine carboplatin concentrations in the unknown samples. Method linearity was determined between 0.1 – 100 µg/ml concentrations.

Drug loading

Microspheres were dried in a vacuum oven at ambient temperature for at least 24 hr. The appropriate quantity of the dried microspheres was weighed and dissolved in a solvent, as follows. Paclitaxel microspheres were dissolved in DMSO whereas, carboplatin microspheres were dissolved in 70 % acetonitrile. The concentration of each solution was determined by HPLC methods as described above. Drug loading was calculated as follows.

Drug loading (% w/w) = (Amount of API in microspheres / weight of microspheres) x 100.

5.3 Results and Discussion

5.3.1 Design of experiment (DOE) results

Microspheres of a wide size range were manufactured in the first full factorial randomised DOE, spanning from $D_{0.5}$ of approximately 90 – 800 µm, as shown in Figure 5-4 and
Table 5.3.

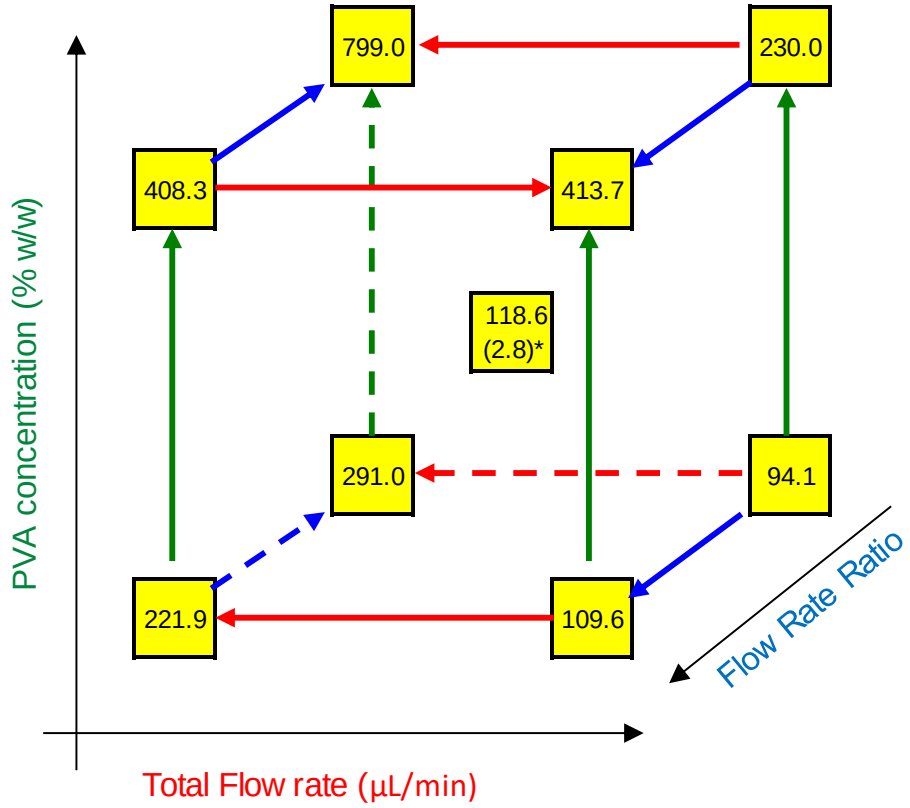


Figure 5-4: Box plot showing the results from DOE 1. Arrow directions indicating the increasing values. Yellow squares contain the particle size ($D_{0.5}$). Middle yellow square is an average of three replicates. *standard deviation.

The particle size uniformity was also quite variable ranging from approximately 0.19 – 0.6 Table 5.3. The pareto plot in Figure 5-5 show that the PVA concentration and the total flow rate were the most significant factors affecting the particle size in DOE 1 and Figure 5-4 also clearly shows that the particle size increased dramatically with increase in the PVA concentration.

Table 5.3: Results for DOE 1 showing the Independent and Dependent variables

Experiment number	Total flow rate (µL/min)	Flow rate ratio (A/O)	PVA Concentration (% w/w)	Particle size $D_{0.5}$ (µm)	Particle Size Uniformity
1	100	6	1.5	117.2	0.192
2	50	12	0.5	221.9	0.605
3	50	12	5	408.3	0.194
4	50	3	5	799	0.404
5	200	3	5	230	0.308
6	200	12	0.5	109.6	0.189
7	50	3	0.5	291	0.614
8	200	12	5	413.7	0.264
9	100	6	1.5	116.7	0.191
10	100	6	1.5	121.8	0.186
11	200	3	0.5	94.1	0.192

It appears that, higher total flow rates and flow rate ratios reduced the particle size in particular at the lower PVA concentrations (base of the box plot, Figure 5-4), which is consistent with the results reported by other researchers where flow-focusing droplet generation chip was used [155]. This phenomenon has been comprehensively explained by Fu et. al.[156]. In general, higher the flow rate ratio thinner the dispersed phase stream would be which results in the smaller size droplets whereas, higher total flow rate increases the shear forces and mixing efficiency within the channels which results in reduced particle size.

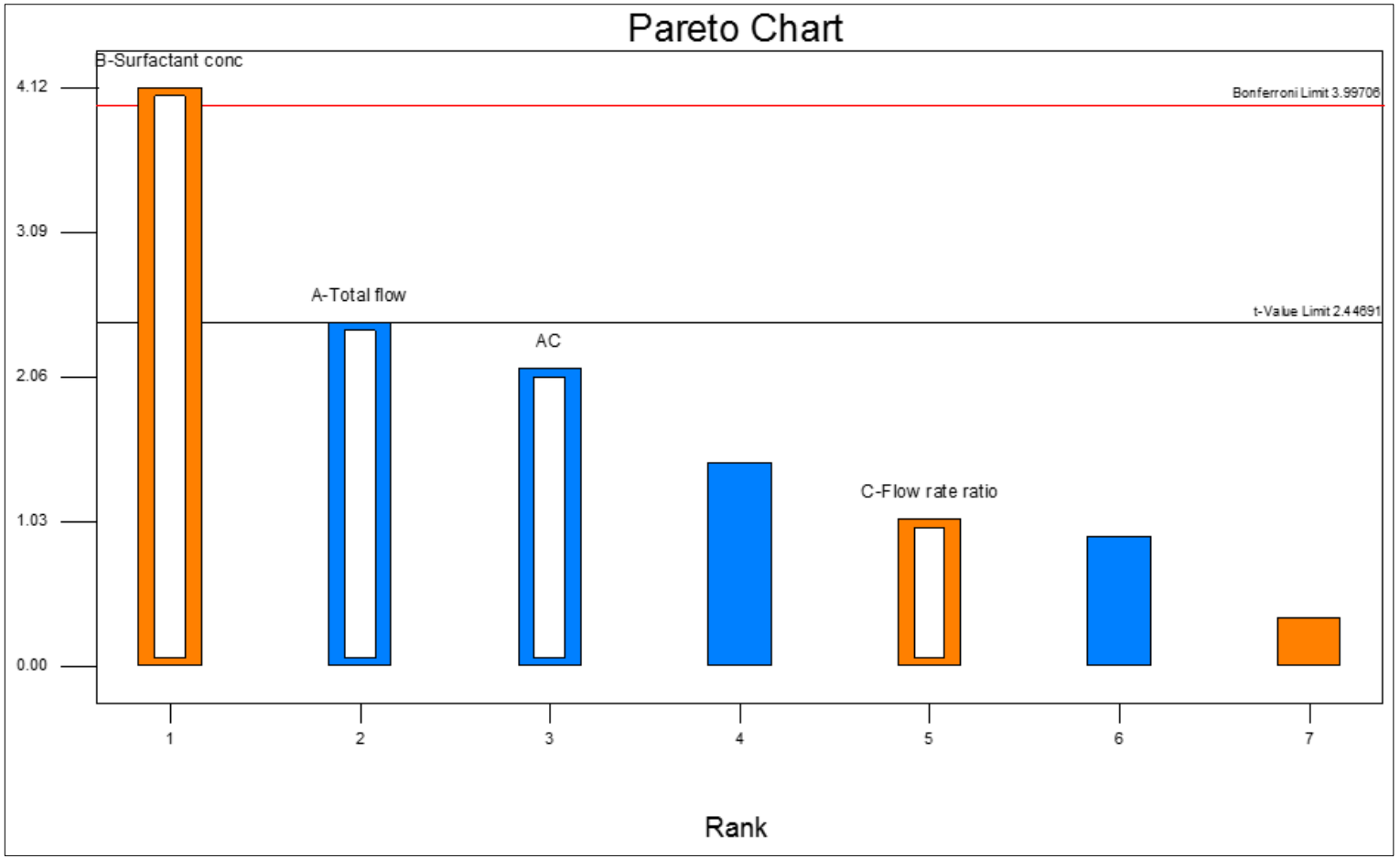


Figure 5-5: DOE 1 Pareto chart ranking the significance of independent variables for particle size change. AC is the interaction between independent variables A (total flow rate) and C (flow rate ratio). Plot is also displaying the 5 % significance threshold (t-value limit) and an additional threshold corrected for multiple comparisons (Bonferroni limit).

Figure 5-5 indicates that there is some evidence of an interaction between total flow rate (A) and flow rate ratio (C) i.e. at the lower total flow rate the increase in flow rate ratio clearly reduced the particle size whereas, at the higher total flow rate the particle size increased with increase in the flow rate ratio (Figure 5-4).

In general, majority of the microspheres made during DOE 1 experiments were larger than the desired size range of 50 – 200 μm. Therefore, based on this data, the independent variables were tuned for DOE 2 by reducing the PVA concentration, increasing the flow rate ratio and total flow rate, as shown in following Table 5.4

The second DOE resulted in a much narrow range of microsphere sizes compared to first DOE, Table 1.1. Majority of microspheres were between the desired size (D 0.5) range of 50 – 200 μm and size uniformity was also below 0.2 for almost all the experiments.

Table 5.4: Results for DOE 2 showing the Independent and Dependent variables

Experiment number	Total flow rate (μL/min)	Flow rate ratio (A/O)	PVA Conc. (% w/w)	PLGA Conc. (% w/w)	Particle size $D_{0.5}$ (μm)	Particle Size Uniformity
1	200	12	0.5	10	65	0.185
2	100	6	0.15	20	484	0.202
3	100	6	1.5	5	72	0.193
4	400	6	1.5	20	499	0.198
5	400	24	0.15	20	80	0.189
6	200	12	0.5	10	64	0.189
7	100	24	1.5	20	81	0.192
8	100	24	0.15	5	75	0.189
9	200	12	0.5	10	66	0.186
10	400	6	0.15	5	192	0.192
11	400	24	1.5	5	86	0.371

Only experiment 2 and 4 gave the microspheres >200 μm. Interestingly the size uniformity of these larger microspheres was also quite low (<0.2). The common features between experiment 2 and 4 were the highest polymer concentration

in organic phase (20 % w/w) and lowest aqueous to organic phase flow rate ratios. Therefore, these results suggest that if we want to make larger (>200 µm) size microspheres we may have to expand the DOE towards higher polymer concentration and/or lower flow rate ratios. However, going below 3 aqueous to organic flow rate ratio may be difficult because it might not be possible to make O/W single emulsion below this ratio. Therefore, from DOE 2 it appears that by simply varying the polymer concentration we might be able to tune microsphere size. This is not surprising as polymer concentration has a direct impact on the viscosity of the organic phase and it is known to have an impact on the microsphere size [155,157]

Figure 5-6 also highlights that the flow ratio and polymer concentration in the organic phase were the most significant factors affecting the particle size and size uniformity in DOE 2. In addition, there is a significant interaction between these two independent variables shown as CD in the Figure 5-6.

This interaction between polymer concentration and flow rate ratio is also shown in Figure 5-7, where it can be clearly seen that the flow rate ratio has a more pronounced effect on the particle size at the higher (20 % w/w) polymer concentration whereas, at lower (5 % w/w) polymer concentration the flow rate ratios has a minimal effect. These data suggest that the microsphere size could be tuned either by keeping the polymer concentration constant (e.g. ~20 %w/w) and simply alter the aqueous to organic flow rate ratio or alternatively the flow rate ratio constant and alter the polymer concentration to make desired size microspheres.

An overall summary of the DOE 2 data is presented as a contour plot in Figure 5-8. It shows that by increasing the polymer concentration from 5 – 20 % w/w and reducing the aqueous to organic flow rate ratio from 24 to 6 the microsphere size increases significantly. More importantly, this contour plot is also showing a large design area where microspheres between the desired size range of 50 – 200 µm (blue colour) can be reproducibly prepared.

It is worth noting here that there was no API used in these DOEs and the presence of API may influence the microsphere size and uniformity. However, by simply altering the polymer concentration or flow rate ratio any such effect should be minimised.

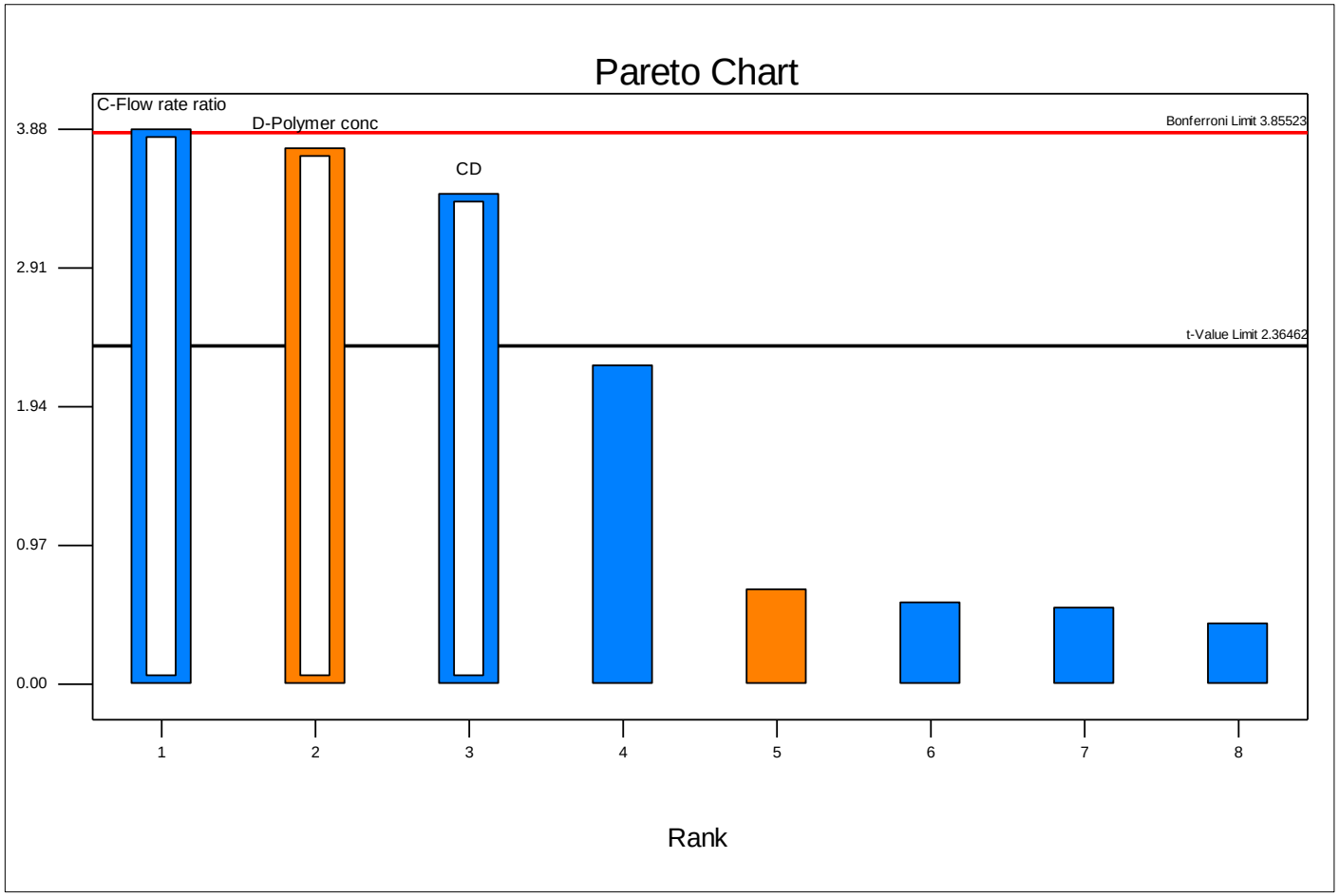


Figure 5-6: DOE2 Pareto chart ranking the significance of the independent variables for particle size change. CD is the interaction between independent variables C (flow rate ratio) and D (polymer concentration). Plot is also displaying the 5 % significance threshold (t-value limit) and an additional threshold corrected for multiple comparisons (Bonferroni limit).

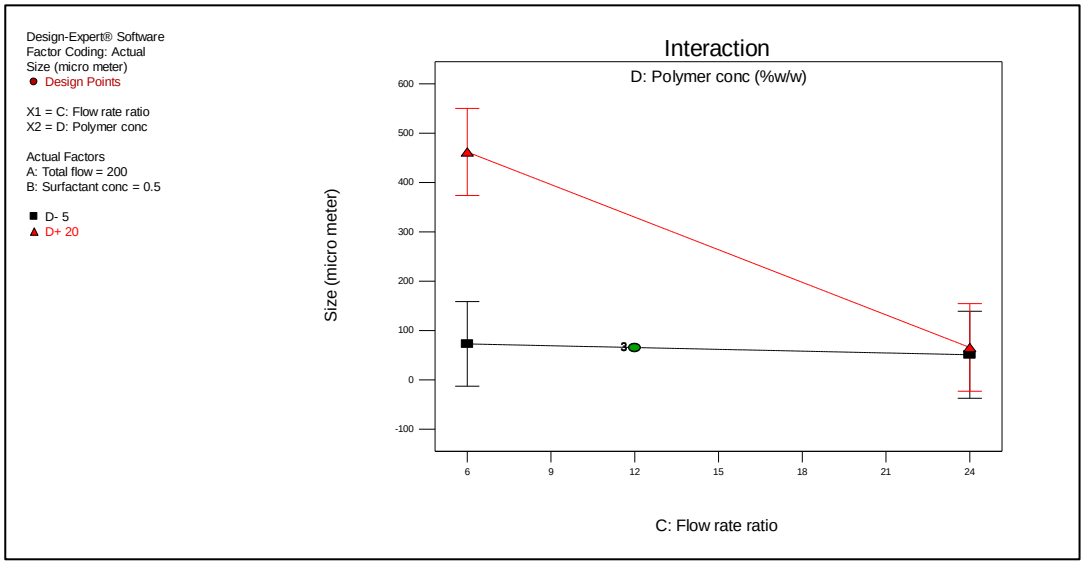


Figure 5-7: DOE 2 interaction plot between flow rate ratio and polymer concentration showing the effect of the independent variables on the particle size. The data is based on the 2-level factorial design, which is why only two data points are shown on this plot, as standard.

In a recently published article [155], Amoyav and Benny have also tested a similar microfluidics system (Micronit Microtechnology) and evaluated the critical parameters which affect the size of microspheres and nanoparticles (i.e. flow rates, PVA concentration and PLGA concentration). Although, they have used a “one factor at a time (OFAT)” approach which is inefficient compared to multifactorial DOE approach, however, their overall results are comparable to data presented here.

In my study microfluidics has been found to be a suitable technique for the manufacture of uniform and controlled size PLGA microsphere on a small scale. However, some challenges were faced during the manufacturing process including the low output rate and blockage of microchannels which resulted in partial or complete stoppage of flow and changes in the microsphere size. Similar concerns have been raised by other researchers [158,159]. Due to these issues, although, the scale up of the PLGA microsphere manufacturing method by using microfluidics might be challenging but we believe that it is still a powerful and convenient technique to make tuneable and controlled size microspheres by using minimal quantities of materials.

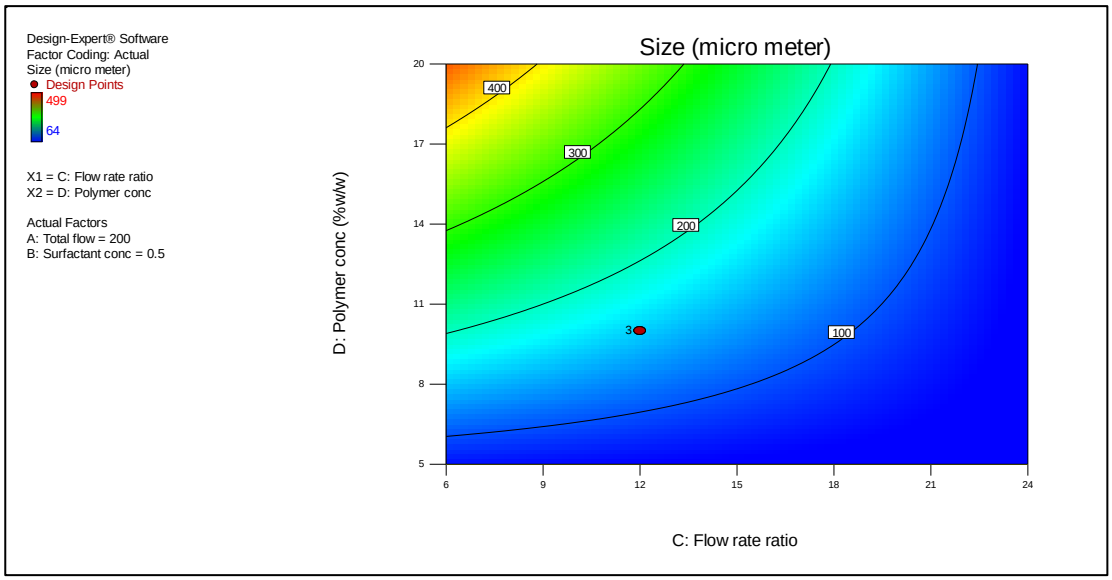


Figure 5-8: Contour plot showing the overall summary of the DOE 2 results. The independent variables evaluated in DOE 2 were: i) total flow rate, ii) aqueous to organic phase flow rate ratio, iii) PVA concentration in aqueous phase and iv) PLGA concentration in the organic phase. Microspheres particle size ($D_{0.5}$) was used as the dependent variable in this DOE.

5.3.2 Drug encapsulation results

Following on from both DOE results the final selected method; 20 % PLGA in the organic phase, 0.5 % PVA in the aqueous phase, a total flow rate of 200 µL/min and aqueous to organic flow rate ratio of 10, was used to make the paclitaxel and carboplatin loaded PLGA microspheres. The summary of results for drug loaded microspheres is shown in Table 5.5.

Paclitaxel microspheres had nearly 100 % w/w encapsulation efficiency, which is consistent with the values reported in the literature [148,160,161], and microsphere size of 110 µm with a narrow size distribution indicated by the uniformity <0.2. The carboplatin microspheres on the other hand had a slightly lower encapsulation efficiency of 64 % w/w. However, the microsphere size and uniformity were comparable to paclitaxel microspheres. Carboplatin is a hydrophilic compound which can diffuse into aqueous phase during emulsification and microsphere hardening process, therefore, slightly lower encapsulation is not unexpected.

Table 5.5: Results for the paclitaxel and carboplatin loaded PLGA micropsheres

Test ID	Paclitaxel microspheres	Carboplatin microspheres
Drug loading (% w/w)	10	6.4
Encapsulation efficiency (% w/w)	100	64
Particle size D (0.5) (µm)	111	100
Particle size uniformity	0.194	0.189

The results show that the experimental conditions selected from the DOE approach were reproducible and a robust and generic approach to make drug loaded microspheres in the injectable size range of 50-200 µm has been developed. In addition, this data also clearly demonstrates that microfluidics method can produce controlled, uniform size microspheres of compounds with very different physicochemical properties by using different encapsulation approaches.

The innovative S/O/W emulsion method used to encapsulate carboplatin was developed because the double emulsion method tested in chapter **3** was not found suitable to achieve high drug loading due to the limited solubility of carboplatin in the aqueous phase (~ 14 mg/mL). Additionally, carboplatin is not soluble in the organic phase (DCM) which does not allow to use a single emulsion method. The non-aqueous milling method was developed after evaluating various aqueous and non-aqueous continuous phases. Milling of carboplatin in PEG 200 was found to be suitable to make a physically and chemically stable nanosuspension with particles size not more than 1 µm as shown in Figure 5-9. This nanosuspension was then dispersed in the organic phase before making the microspheres.

The following optical microscope pictures in Figure 5-10 are showing the un-milled and milled carboplatin suspension in PEG 200. It can be clearly seen that after milling a very fine homogenous suspension was produced which maintained its crystallinity, as evident by the birefringence observed with cross polarised light.

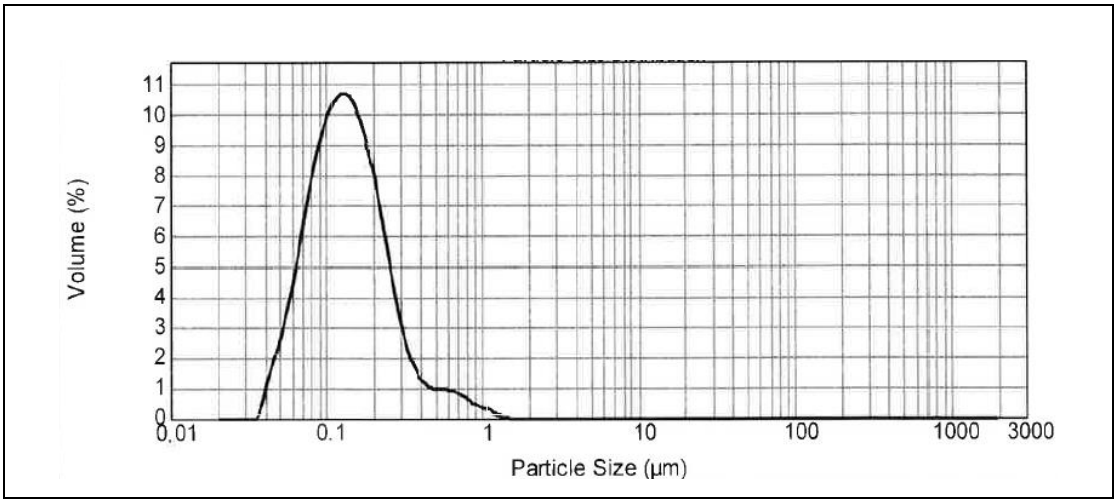


Figure 5-9: Laser diffraction particle size and size distribution of carboplatin nanosuspension milled in PEG 200. Ethanol is used as dispersant for particle size measurement. The particle size d(0.5) of 0.13 µm and d(0.9) of 0.29 µm.

There are not many methods reported in literature for encapsulating carboplatin into PLGA microspheres. Chen et. al.(1999) has described an interesting method for the preparation of carboplatin-PLGA microspheres, involving acetone and mineral oil with apparently good drug loading ranging from 5 to 9 % w/w and release duration of up to 22 days, with similar release profile (i.e. a lag phase followed by zero order release) as found in my work section 6.3.5 [162,163]. However, this method has some drawbacks e.g. the encapsulation efficiency is less than 50 % w/w, it requires large quantities of non-aqueous solvents (acetone and mineral oil) and it involves a complex and lengthy microsphere isolation and cleaning process.

Paclitaxel was soluble in the organic phase and therefore was dissolved in the organic phase to make the microspheres.

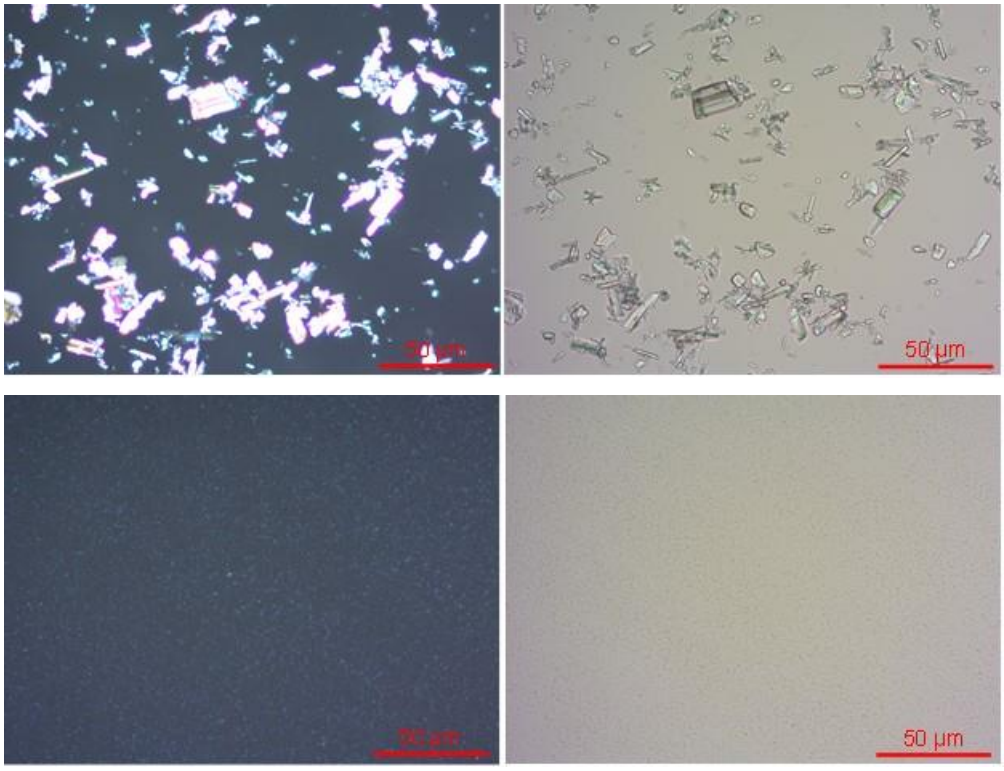


Figure 5-10: Optical microscope pictures of un-milled (top) and milled (bottom) carboplatin in PEG 200 by using planetary micro mill. Left: cross-polarised light showing the crystalline nature of the particles and Right: plane-polarised light showing the shape and size of the particles.

5.3.3 Microsphere size and appearance

It can be observed from Table 5.5 and Figure 5-11(a) that both carboplatin and paclitaxel microspheres had very uniform sizes and spherical shapes with predominantly smooth surfaces. The carboplatin microspheres, however, have some spots on the surface whereas, the paclitaxel microspheres had no such spots.

Figure 5-11(b) is showing the optical microscope images of the carboplatin and paclitaxel microspheres. The carboplatin microspheres appear dense particles as no light passed through the microspheres when plane polarised light was used. Whereas, the cross-polarised light gave a distinct uniform glow (birefringence) throughout the microsphere which most likely is due to the presence of carboplatin nanocrystals inside the microspheres. This observation is also supported by the XRPD results given in section 5.3.4 . The paclitaxel microspheres appear less dense under plane polarised light because light passed through the microspheres which most likely is due to the glassy nature

(and single-phase matrix) of the microsphere that allows the plain polarised light to pass through the microspheres. In addition, numerous spots or pores were also visible in the paclitaxel microspheres under plain polarised light which we believe are most likely the pores inside the microspheres rather than on the surface because no spots or pores were observed in paclitaxel microspheres in the SEM analysis (Figure 5-11a, left). The cross-polarised light gave a relatively faint glow in the paclitaxel microspheres (birefringence) which we trust is due to the inside pores or microsphere shape rather than the presence of crystallinity

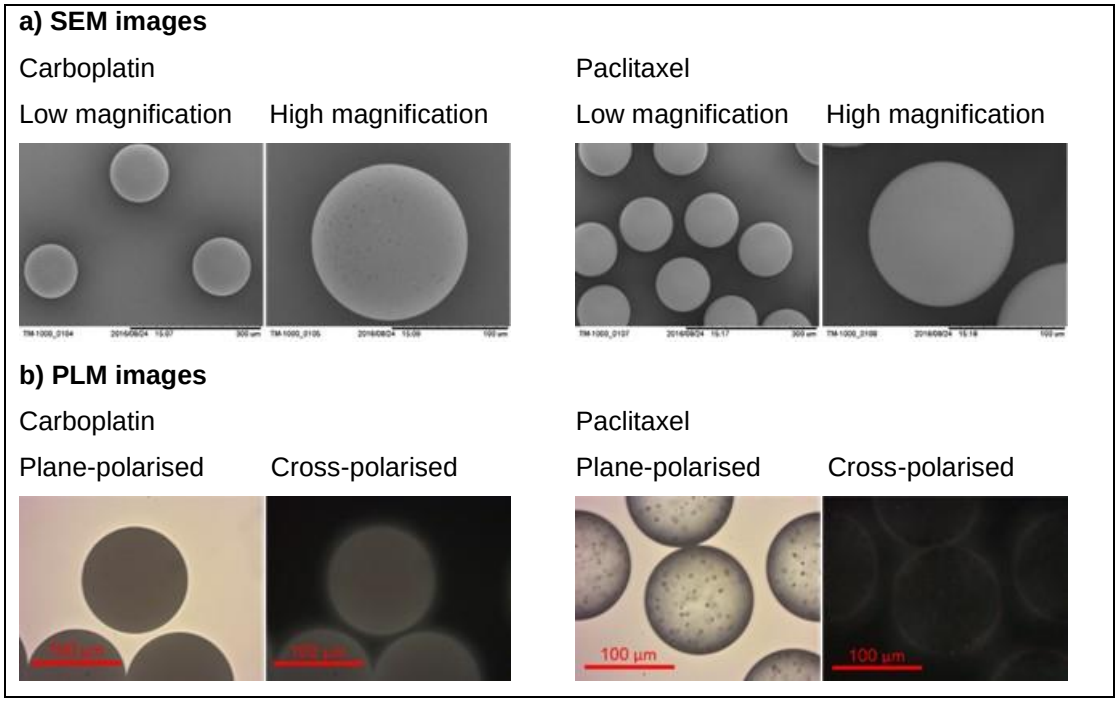


Figure 5-11: SEM (a) and Optical microscope (b) images of Carboplatin and Paclitaxel microspheres. Both Microspheres were prepared with PLGA 75/25 (lactide/glycolide) polymer by using O/W emulsion and microfluidics methodology. The critical parameters included total flow rate 200 µL/min, aqueous to organic flow rate ratio 10, polymer concentration in the organic phase 20% w/w and PVA concentration in aqueous phase 0.5% w/w. Samples were dried under vacuum for at least 24 hr at ambient temperature. SEM samples were gold sputter coated with 5-10 nm coating density. PLM images were taken without any further processing.

5.3.4 Solid state results (X-RPD and DSC)

The XRPD results also support previous observations (Figure 5-12) that the paclitaxel and blank PLGA microspheres appear amorphous. The lack of peaks in the diffraction pattern indicates that paclitaxel is predominately amorphous. In contrast, the carboplatin microsphere diffraction pattern clearly shows sharp peaks indicating the presence of crystalline material in the microspheres. DSC data in Figure 5-13 shows that there is only single glass transition (Tg) temperature at 36 °C in the blank PLGA microsphere which indicates that this sample is composed of single amorphous phase. Paclitaxel loaded PLGA microspheres have more than one weak endothermic (downward) and exothermic (upward) peaks. The endothermic peak at 41 °C is the glass transition temperature which is slightly higher than the blank PLGA microsphere Tg. We have also found additional peaks in the paclitaxel microsphere sample as reported by other researchers [164]. Carboplatin microspheres also have more than one endothermic peak. The first signal at 42 °C is most likely the Tg which is slightly higher than the blank microspheres but very similar to the paclitaxel microspheres. Such a shift towards a higher Tg is usually due to some interaction (miscibility) between polymer and the compound [165]. In addition, the carboplatin microsphere DSC results show an exotherm at the higher temperature (230 °C) which is most likely due to the melting of the carboplatin nanocrystals inside the microspheres followed by degradation [166]. A similar effect was observed in the carboplatin reference sample (control) DSC Figure 5-13.

This DSC data also indicates that both blank and paclitaxel loaded PLGA microspheres were predominantly amorphous in nature whereas, carboplatin loaded microspheres have some crystallinity which is consistent with the PLM, XRD data and DSC (Figure 5-11 to Figure 5-13).

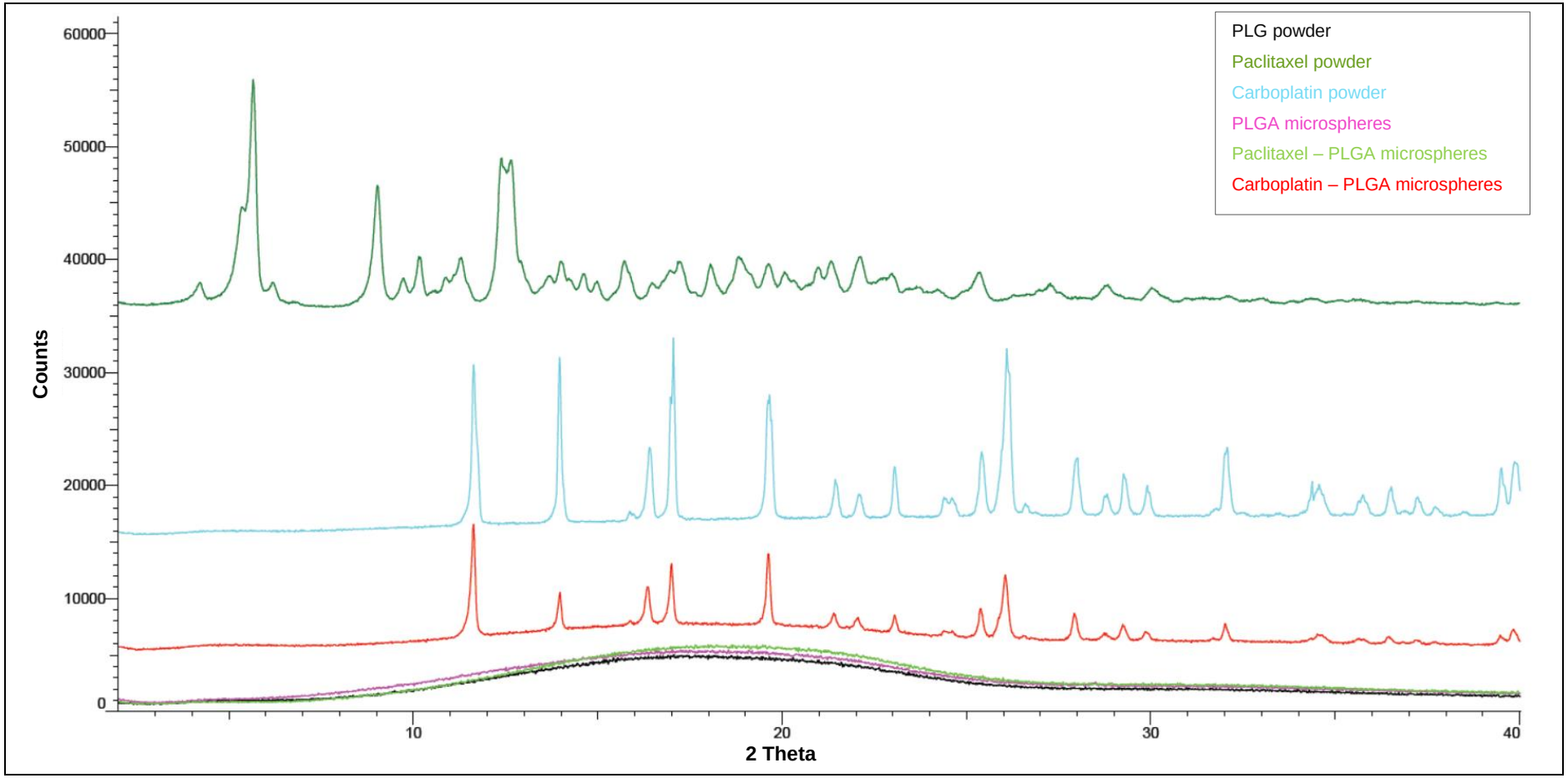


Figure 5-12: XRPD data for PLGA, paclitaxel and carboplatin powders and microspheres. All Microspheres were prepared with PLGA 75/25 (lactide/glycolide) polymer by using an O/W emulsion and microfluidics methodology. Samples were dried under vacuum for at least 24 hr at ambient temperature before analysis. Samples were measured in reflection geometry in θ - 2θ configuration over the scan range 2° to 40° 2θ with a nominal 25 second exposure per 0.02° increment.

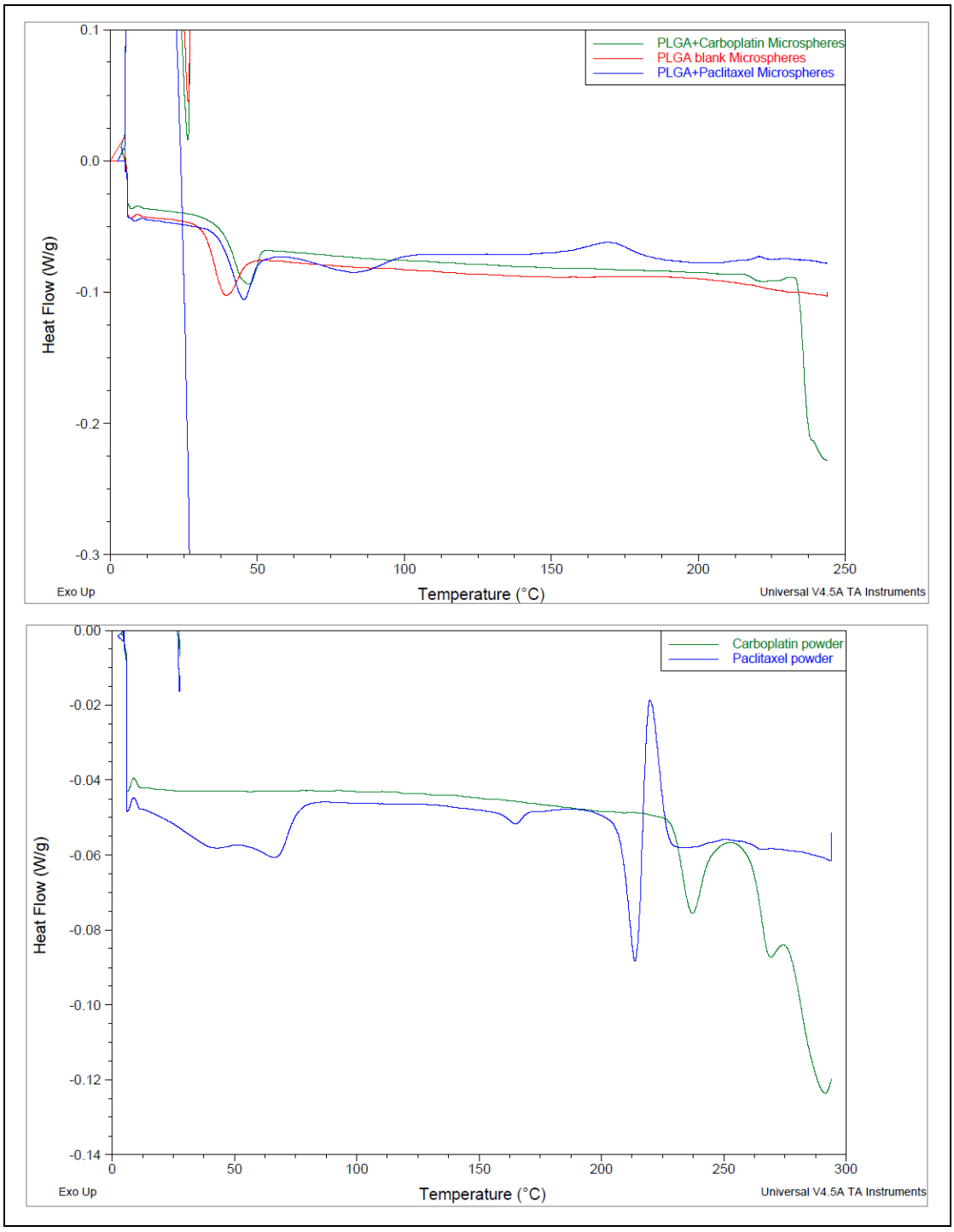


Figure 5-13: DSC data showing endothermic and exothermic events in the blank, carboplatin and paclitaxel loaded PLGA microspheres (top) and carboplatin and paclitaxel reference compounds (controls)(bottom).

5.4 Conclusion

We have successfully evaluated the microfluidics technology by using a DOE approach and determined optimum conditions to make uniform PLGA microspheres in the injectable size range of 50-200 µm. In addition, we have also demonstrated that compounds with very different physicochemical chemical properties can be efficiently loaded into PLGA microspheres without significantly affecting the overall characteristics of the microspheres. The microfluidics technology has been found a simple, reproducible and versatile technique to make PLGA microspheres with a range of properties and high encapsulation efficiency.

The DOE results have identified the key factors which dictate the microsphere properties (in-particular size) in microfluidics and have clearly shown that a range of different sized microspheres can be conveniently manufactured by simply altering polymer concentration in the organic phase and/or aqueous to organic flow ratio.

Finally, for the first time we are reporting an innovative method to load high concentrations of carboplatin by encapsulating carboplatin crystalline nanoparticles in PLGA microspheres by using microfluidics approach.

6 Tailoring the release rates of carboplatin and paclitaxel from PLGA microspheres and finding the optimum dosage regimen with the aid of an intraperitoneal PK mathematical model

6.1 Introduction

Various strategies have been reported in the literature to tailor the release rates of diverse active pharmaceutical ingredients (APIs) from PLGA microspheres including, microsphere size [167-172], microsphere porosity [170], addition of excipients [173,174], drug loading [172] and PLGA grade (polymer chemistry) [109].

Changing the PLGA grade is by far the most commonly and successfully used strategy to alter the release rates from PLGA microspheres. PLGA is a copolymer composed of different ratios of lactide and glycolide monomers. The ratio of monomers is represented by two numbers e.g. 75/25, where first number represent the lactide content and second number represent the glycolide content in the polymer. The monomers are linked together by ester linkage resulting in a linear polyester [175]. The ester linkages hydrolyse when the copolymer comes in contact with water, resulting in the polymer degradation. The PLGA degradation kinetics has been extensively reported in the literature [104,105,176,177].

Anderson and Shive has given a comprehensive summary of the factors affecting the hydrolytic degradation behaviour of PLGA [105] including, the lactide/glycolide ratio and molecular weight. In general, increase in the lactide content results in longer degradation half-life e.g. PLGA 65/35, 75/25, 80/20 and 95/5 have longer *in-vivo* life-times, respectively [69]. The most commonly used PLGA composition of 50/50 (lactide/glycolide) has the fastest biodegradation rate compared to compositions with higher proportion of either of the two monomers [175].

Whereas, the degradation and erosion rate of PLGA decreases with increasing molecular weight [174,178]. Furthermore, the PLGA polymer end group also plays a significant role in determining the degradation rate of the polymer. A hydrophilic end group (e.g. carboxyl) has relatively faster degradation rate compared to the hydrophobic end group (e.g. alkyl ester) [174].

This flexibility to alter the degradation rates of PLGA by varying the chemical composition provides a convenient tool to tailor the release rates from PLGA based drug delivery systems and this approach has been extensively summarised by Pavot et. al. [179].

With the advent of precision microsphere fabrication techniques, it has been shown that the release from a mixture of different size microspheres matches with the weighted average release from the individually microsphere size [168]. This has been attributed to the negligible interaction (interference) between particles, resulting in independent release profiles from each population. Therefore, uniform size microspheres allow the simplicity and ability to “pick and choose” different sizes and/or different release profile microspheres to mix and achieve desired release profiles and doses [120].

In this study, we have used the optimised microfluidics methods (chapter 5) to manufacture controlled, uniform size PLGA microsphere of paclitaxel and carboplatin. In order to tailor the release rates, we have used four different grades of PLGA, composed of two different molecular weights (10 kDa and 50 kDa) and two different lactide to glycolide ratios (50/50 and 75/25). Samples were characterised by various advanced analytical techniques including ToF-SIMS, SEM, ESEM and EDS/EDX; in addition to standard analytical methods for drug loading and release testing.

Finally, the preliminary intraperitoneal pharmacokinetic mathematical model (chapter 2), which was based on the zero order release rates, was modified to fit the experimental data from the release optimisation work in this part of the study and then used to select dosage regimen of paclitaxel and carboplatin for intraperitoneal administration for ovarian cancer treatment.

6.2 Materials and Methods

6.2.1 Materials

Four different grades of PLGA RESOMER® including 7525 DLG (M_w 50-60 kDa, IV 0.35 – 0.45 dL/g), 7525 DLG (M_w 5-15kDa, IV 0.05 – 0.15 dL/g), 5050 DGL (M_w 50-60kDa, IV 0.35 – 0.45 dL/g) and DGL 5050 (M_w 5-15kDa, IV 0.05 – 0.15 dL/g) were purchased from Evonik Birmingham Laboratories, USA. Carboplatin was purchased from Tocris Bioscience, UK and paclitaxel was purchased from Apollo Scientific, UK. PVA (88% hydrolysed m.wt. 20-30 kDa) and DCM were purchased from Sigma Aldrich. All other reagents were of pharmaceutical grade.

6.2.2 Methods

The carboplatin, paclitaxel and blank formulations were manufactured with four different grades of PLGA polymer by using the optimised microfluidics methods as described in chapter 5. The identification codes for these formulations are given in Table 6.1.

Table 6.1: Identification codes for carboplatin and paclitaxel formulations made with four different grades of PLGA

Compound	PLGA grade	Identification code
None (Blank)	50/50 10kDa	BF1
	50/50 50kDa	BF2
	75/25 10kDa	BF3
	75/25 50kDa	BF4
Carboplatin	50/50 10kDa	CF1
	50/50 50kDa	CF2
	75/25 10kDa	CF3
	75/25 50kDa	CF4
Paclitaxel	50/50 10kDa	PF1
	50/50 50kDa	PF2
	75/25 10kDa	PF3
	75/25 50kDa	PF4

Other methods including, HPLC for drug loading and encapsulation efficiency for both compounds and SEM were the same as described in section 5.2.2. The HPLC method used to analyse the free paclitaxel during release testing was also the same as used for the drug loading and encapsulation efficiency of paclitaxel.

Environmental Scanning Electron Microscope (ESEM) and Energy Dispersive X-ray Spectroscopy (EDX/EDS) Analysis

ESEM analysis was performed by using FEI Quanta650 eSEM, operated at 10 kV and 75 pa, equipped with large field detector (LFD) and back scattered electron detector (BSED). ESEM was selected because it allows the sample analysis in its natural state i.e. without any sample preparation or deposition of electrically conducting coat (e.g. gold) [180,181], therefore, it offers some advantages compared to conventional SEM to characterise the surface properties (e.g. porosity, smoothness, etc).

Energy dispersive X-ray spectroscopy (EDX or EDS) analysis was performed simultaneously, to determine the elemental composition of selected areas in samples by using oxford instruments X-max 150 detector with INCA 350 software.

All samples were placed on SEM stubs, freeze-fractured before analysis and analysed without any coating.

ToF-SIMS

ToF-SIMS data was acquired using a ToF-SIMS IV instrument (ION-TOF GmbH, Munster, Germany). Samples were prepared by sprinkling on double sided tape attached to aluminium blocks affixed into the ToF-SIMS stage. For imaging studies a bismuth liquid metal primary ion gun (Bi^{3+}, 25 keV) was used. Data was acquired over regions of 500 µm x 500µm at 256 x 256 pixel resolution. For depth profiling, an argon gas cluser (Ar_{1900}, 20 keV) was used with target current around 20 nA. Depth profiling was performed over an area of 400 × 400 µm with analysis of the central 200 × 200 µm area at 256 × 256 pixel resolution. Data were collected in the negative secondary ion polarity, acquisition and analysis were performed using SurfaceLab 6 software (ION-TOF GmbH).

Reference materials were analysed to select characteristic ions for paclitaxel, carboplatin, PLGA, PVA and tape before sample analysis.

The measured secondary ion intensity values of each characteristic ion peak were normalised to the total intensity count to allow semi quantitative comparison of different samples.

ICP-OES method for carboplatin release

ICP-OES method detailed below was used to analyse the carboplatin in the release testing samples.

A Thermo iCAP 6500 Duo fitted with a Cyclonic Spray Chamber, Concentric Nebuliser, 1 mm Injector Tube, EMT Duo Torch and Silicone Peristaltic Pump Tubing with Internal Diameter 0.762 mm for sample introduction was used for this analysis.

Yttrium was used as an internal standard. Both standard and sample solutions were prepared in 90% v/v DMSO. The instrument operating conditions were: a sample flush time of 60 sec, 6 sample repeats , an axial plasma view, an auxiliary gas flow of 1 L/min, a nebuliser gas flow of 0.5 L/min, an additional gas flow (20% O_2 in air) of 0.075 L/min and a coolant flow of 14 L/min. Wavelength of detection was set at 371.029 nm for yttrium and for platinum two wavelengths were used i.e. 214.423 and 265.945 nm.

At least three calibration standard solutions were prepared between ~10 – 1000 ppm (µg/ml), a quality control standard solution was prepared at 100 ppm, and the sample solutions were prepared to ensure the metal content of the sample lies between the calibration standard solutions (10 – 1000 ppm). All carboplatin microsphere sample solutions were prepared at ~ 1 mg/ml microspheres (equivalent to a maximum concentration of 100 ppm carboplatin and 50 ppm of platinum, assuming 10% drug loading).

A carboplatin control solution was also prepared in the release media at ~0.1 mg/ml carboplatin concentration and placed in the same shaking water bath as samples. These control solutions were analysed alongside the microsphere samples at each time point to evaluate the stability of both compounds under the test conditions and the results were corrected for the loss of assay due to degradation.

In addition, a series of standard solutions were prepared in release media to cover ~0.2 – 100 ppm concentration range (equivalent to ~ 0.1 – 50 ppm platinum) to determine the linearity and limit of quantification for the release samples.

In-vitro release testing

Selection of release media

The composition of simulated IP fluid was determined by consulting multiple literature sources [182-188].

In general, it has been found that the chemical composition of the IP fluid is very similar to plasma with the exceptions of protein and calcium concentration. IP fluid contains 3 % w/v protein [182,183] whereas, plasma contains 6-8 % w/v [189]. The calcium concentration in the IP fluid is ~ 0.002% [184] whereas, plasma contains ~ 0.01 % w/v calcium [186].

However, for release testing a simplified simulated IP fluid was used, see composition in Table 6.2.

Table 6.2: The composition of simulated intraperitoneal fluid for release testing of paclitaxel and carboplatin from PLGA microspheres

Component	**Concentration (g/L)**
Sodium Chloride	8.00
Potassium Chloride	0.20
Disodium Phosphate (anhydrous)	1.44
Monopotassium Phosphate	0.24
Hydrochloric Acid	q.s. to pH 7.4
Sodium Azide	0.2
*Hydroxy-propyl-β-cyclodextrin	100

*For paclitaxel, 10% w/v hydroxyl-propyl-beta-cyclodextrin was added as a solubiliser to increase the paclitaxel solubility and ensure a sink condition of more than three times the saturation solubility throughout the release experiment

Sample preparation for release testing

Carboplatin release testing was performed by adding ~10 mg microspheres in the sample holding device (see Appendix G and Appendix I for the details of why and how sample holding device was selected) which was then placed in 10 ml release media (maximum API concentration was less than 0.1 mg/ml and sink condition was greater than 10 times the saturation solubility). For paclitaxel, 5 mg microsphere sample was added in the sample holding device and placed in 35 ml release media (maximum API concentration was less than 0.014 mg/ml and sink was greater than 3 times the maximum solubility).

All samples were prepared in triplicate and continuously agitated at 37 °C in a shaking water bath (Stuart SBS40) at 150 rpm. At regular intervals the samples were taken out of the water bath and 2 ml supernatant was carefully removed from each sample. Fresh, 2 ml release media (pre-warmed at 37°C) was added into the remaining samples before transferring back into the water bath. All individual results were corrected for dilution and cumulative release was calculated as normal.

In addition, a control solution of each compound was also prepared at ~0.1 mg/ml in the relevant release media and placed in the same shaking water bath as samples. These control solutions were analysed alongside the microsphere samples at each time point to evaluate the stability of both compounds under the test conditions and the results were corrected for the loss of assay due to degradation.

Modified Intraperitoneal PK model

The PK model described in chapter 2 was modified by replacing the zero-order release function (R_0) with a mathematical function $R(t)$ to represent the non-linear rate of API release from the dosage form (in amount per time), Figure 6-1.

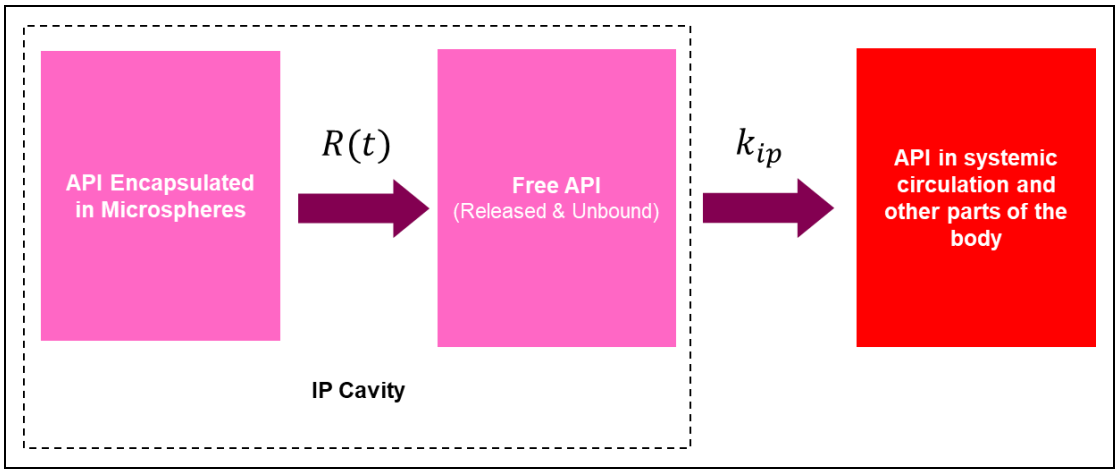


Figure 6-1: Updated Intraperitoneal pharmacokinetic model to design the drug delivery system by estimating the required release rate from the microspheres and dose required to maintain the therapeutic concentration (i.e. GI50) of the API.

For example, in the case of a formulation with linear release (Figure 6-2A) the fraction of API released as a function of time $F(t)$ can simply be represented by the gradient of the slope $k = 1/t_{rel}$ (where t_{rel} is the time of release) and the overall release rate from a single dose (*D*) can therefore be expressed as $R_0 = D \cdot k$.

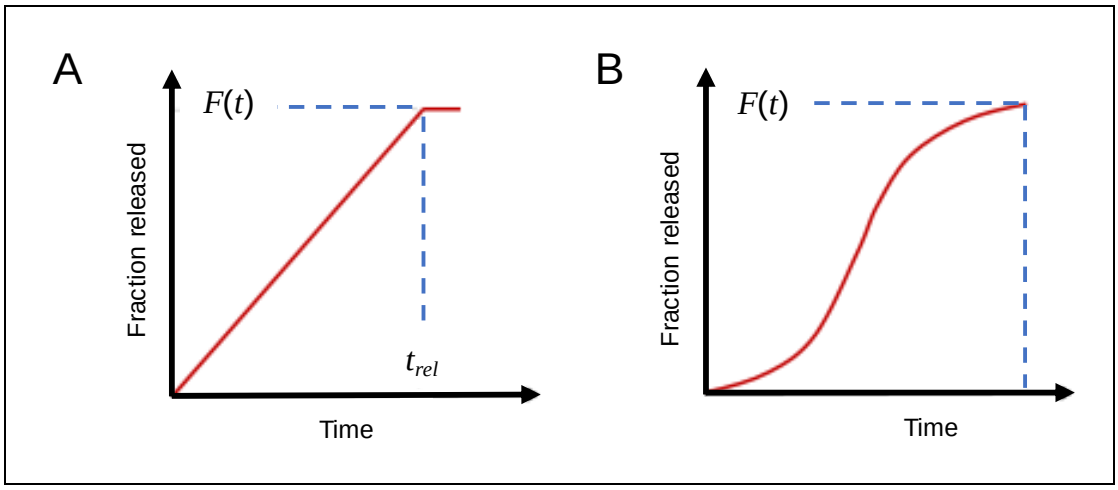


Figure 6-2: Example release profiles showing typical zero order (A) and sigmoidal (B) release kinetics from a single dose.

Whereas, for a non-linear or sigmoidal release (Figure 6-2B), as with formulations PF2, PF4 and CF2 it was required to find an appropriate mathematical function by fitting experimental data which can represent the actual release at any particular time $F(t)$.

Then the rate of the API release, $R(t)$, from a formulation at any particular time was determined by the product of the dose and the slope of the release curve at that time i.e. the derivative with respect to time $F'(t)$, Equation 6-1.

$$R(t) = D \cdot F'(t) \qquad \text{Equation 6-1}$$

If we give n number of doses, then the contribution from all the individual doses towards total release can be generalised as follows:

$$R_i(t) = \begin{cases} D \cdot F'(t-(i-1)\cdot\tau) & \text{if } t > (i-1)\cdot\tau \\ 0 & \text{otherwise} \end{cases} \qquad \text{Equation 6-2}$$

Where, i is the dosing number starting with 1 and τ is the dosing interval. This equation allows the calculation of the release rate at any given time from a single dose of formulation. However, with multiple dosing, the first dose might still be releasing the API at the time of subsequent dose. Therefore, the contribution from each dose can be accounted for by adding the input rates from all the doses, as expressed by Equation 6-3,

$$R_{tot}(t) = \sum_{i=1}^{n} R_i(t) \qquad \text{Equation 6-3}$$

The amount of API in the IP cavity can, therefore, be represented as,

$$\frac{dX_{ip}}{dt} = R_{tot}(t) - k_{ip}X_{ip} \qquad \text{Equation 6-4}$$

Where dX_{ip}/dt is the rate of change of API amount (mass) with respect to time in the IP cavity; k_{ip} is the first order API elimination (absorption) rate constant from the IP cavity and X_{ip} is the total amount (mass) of API in the IP cavity (unbound and protein bound).

Subsequently, the model implemented in Berkeley Madonna (modelling software) to solve the above Equation 6-4 across a relevant time period, specifying initial conditions of no released API in the IP cavity i.e. at time = 0, X_{ip} = 0.

Once the total amount (mass) of API (X_{ip}) as a function of time has been determined then the concentration of released (unbound and protein bound) API as a function of time can be determined by Equation 6-5

$$c_{ip}(\mathrm{t}) = \frac{X_{ip}(t)}{V_{ip}} \qquad \text{Equation 6-5}$$

Finally, the optimum dose was determined by systematically altering the dose in Berkeley Madonna, at a set dosing regimen (dosing frequency and total dosing period), to find the minimum dose where the API concentration in the IP fluid stays above the target concentration (C_{target})[2] during the entire dosing period, once the steady state was achieved.

[2] The target concentration (C_{target}) is the minimum efficacious concentration *(C_{min}) divided by the fraction unbound to the protein (f_u)*.

6.3 Results and Discussion

6.3.1 SEM

Figure 6-3 to Figure 6-5 are showing the SEM pictures of blank, carboplatin and paclitaxel loaded microspheres respectively, made with three different grades of PLGA (i.e. PLGA 50/50 50 kDa, 75/25 10kDa and 75/25 50kDa). A fourth grade PLGA (i.e. 50/50 10kDa) was also used to make similar microspheres (i.e. blank, carboplatin and paclitaxel loaded) but after drying the samples made with PLGA 50/50 10 kDa fused together and got adhered to the vial and hence it was not possible to isolate these microspheres for analysis.

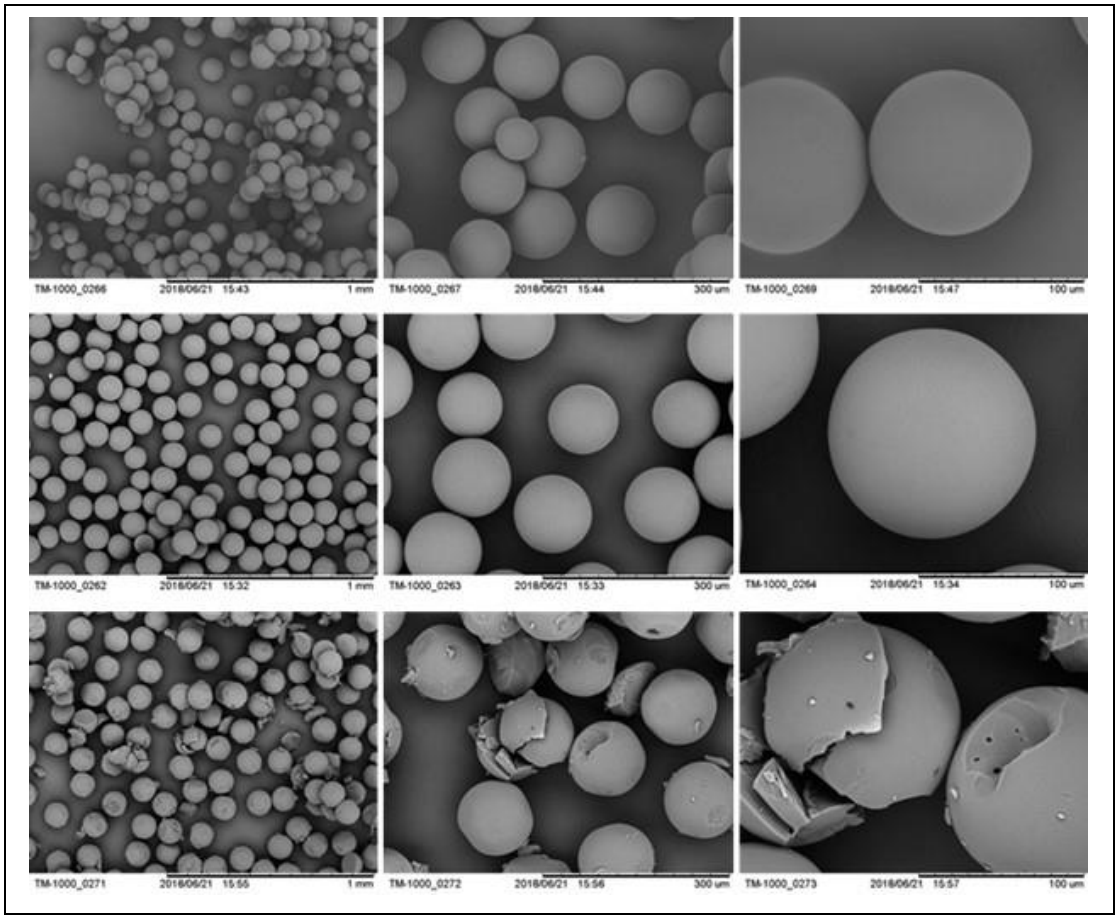


Figure 6-3: SEM pictures of blank PLGA microspheres at three magnifications. Formulations were made with three different grades of PLGA, Top row: PLGA 50/50 50 kDa (BF2), Middle row: PLGA 75/25 50 kDa (BF4) and Bottom row: PLGA 75/25 10 kDa (BF3).

Qualitatively, all the microspheres had similar size (~ 100 μm) and shape (Figure 6-3 to Figure 6-5), which indicates that by maintaining the optimised microfluidics method conditions (i.e. flow channel dimensions/design, flow rate, flow rate ratio, organic solvent, PVA) and downstream processing method (i.e. microsphere collection, removal of organic solvent and drying) the effect of PLGA grade, API characteristics and the API loading on the size and shape can be minimised

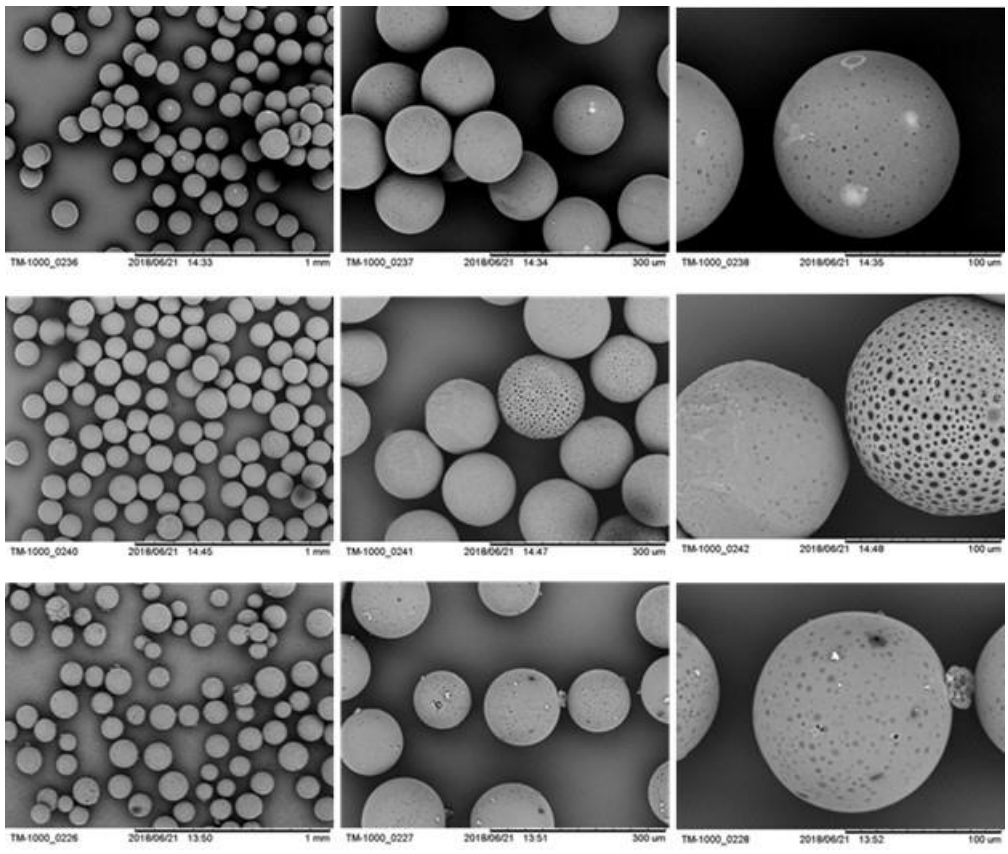


Figure 6-4: SEM pictures of Carboplatin-PLGA microspheres at three magnifications. Formulations were made with three different grades of PLGA, Top row: PLGA 50/50 50 kDa (CF2), Middle row: PLGA 75/25 50 kDa (CF4) and Bottom row: PLGA 75/25 10 kDa (CF3)

As it can be seen from the Figure 6-3 that all the blank PLGA microspheres made with high molecular weight PLGA polymers (i.e. BF2, PLGA 50/50 50 kDa and BF4, PLGA 75/25 50 kDa) had smooth surfaces and there were no broken particles whereas, the lower molecular weight formulation (i.e. BF3, PLGA 75/25 10 kDa) contained numerous broken particles. This is because BF3 sample adhered to the vial after drying and it required gentle scrapping to isolate

free microspheres, which was likely due to the relatively lower glass transition temperature of small molecular weight (~ 10 kDa) polymer.

As shown in Figure 6-4, although carboplatin microspheres had similar size and shape to the blank and paclitaxel microspheres (Figure 6-3 and Figure 6-5) but they had different surface appearance. The carboplatin formulations (CF2, CF3 and CF4) had some dark spots on the surface and some random (very few) microspheres in these formulations had porous surface, see middle right hand side picture in Figure 6-4.

It has been reported that the slow extraction of solvent (e.g. DCM) results in annealing of the polymer and form microspheres with higher density, whereas faster removal of DCM may result in higher porosity in the microspheres [119]. Therefore, during the primary removal of DCM from the microspheres (droplets), all the samples were agitated on the orbital shaker while the microspheres were still suspended in the 0.01 % w/v PVA solution, to ensure slow removal of DCM. The slow removal of DCM was governed by the low solubility of DCM in water (~ 2 % w/v), since during the DCM removal process DCM has to dissolve in the external aqueous phase first before evaporating in to the atmosphere. However, it was noticed that some microspheres adhered to the vessel just above the fluid level, these microspheres might have undergone DCM removal at relatively faster rate. This faster rate of DCM removal might have not allowed the polymer to anneal, especially near the surface and may have resulted in high surface porosity in some microspheres.

Paclitaxel microspheres appear to have smooth surfaces as shown in Figure 6-5. There is small number of broken microspheres in the formulation PF3 (bottom pictures in Figure 6-5) which was made with the lower molecular weight polymer (PLGA 75/25 10 kDa). As mentioned above for the blank formulation, this was due to the adherence of the sample to the glass vial after drying and scraping to remove sample out of the vial.

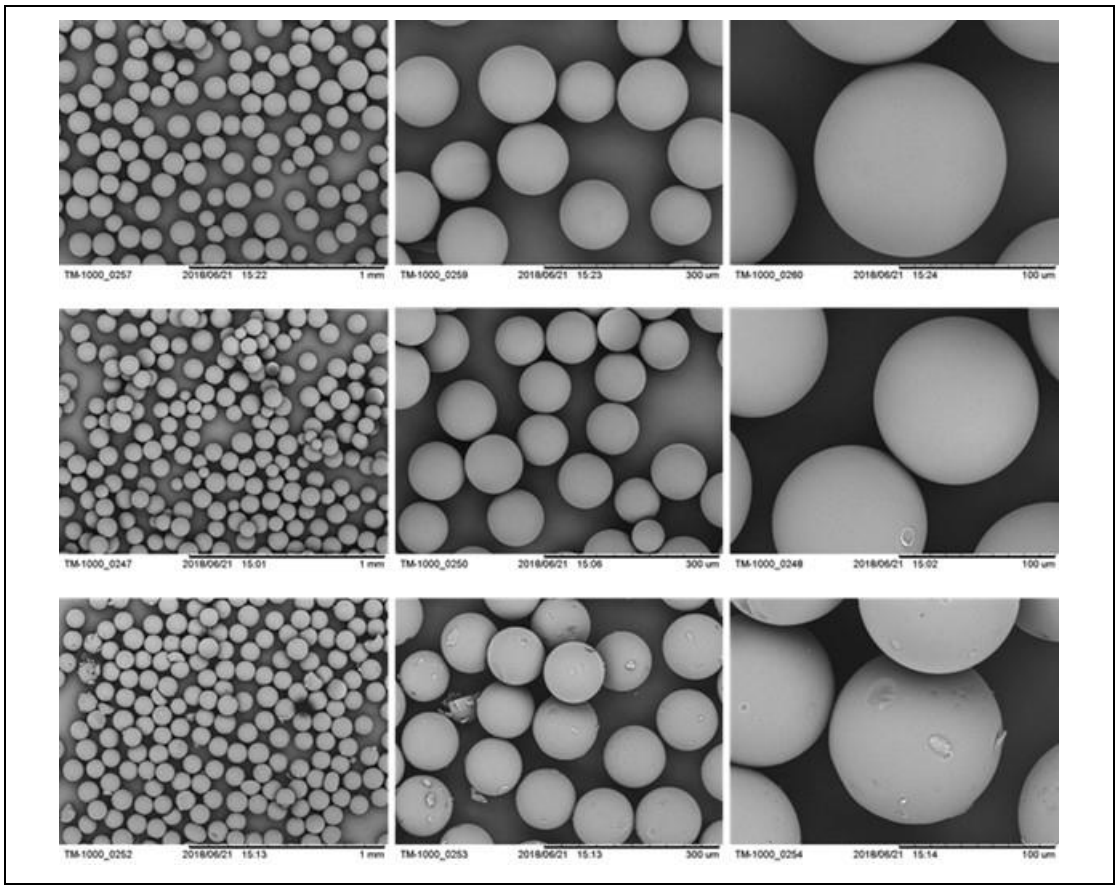


Figure 6-5: SEM pictures of Paclitaxel-PLGA microspheres at three magnifications. Formulations were made with three different grades of PLGA, Top row: PLGA 50/50 50 kDa (PF2), Middle row: PLGA 75/25 50 kDa (PF4) and Bottom row: PLGA 75/25 10 kDa (PF3)

6.3.2 ESEM results

The Figure 6-6 is showing the images of microsphere cross sections from the ESEM analysis of three formulations, blank, paclitaxel and carboplatin, all manufactured with PLGA 75/25 50 kDa. The blank and paclitaxel microspheres appear very similar by both LFD (large field detector) and BSED (back scattered electron detector). The microsphere in these samples appear homogeneous with a dense core and surface without significant number of pores. There are some minor irregular features (wrinkles) present in both of these samples which are attributed to the sample preparation technique.

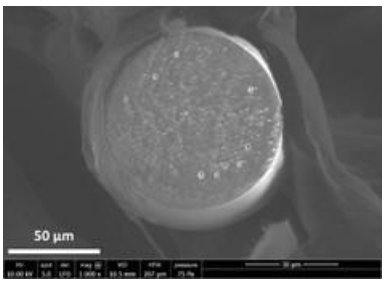
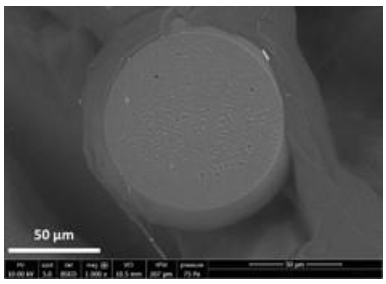
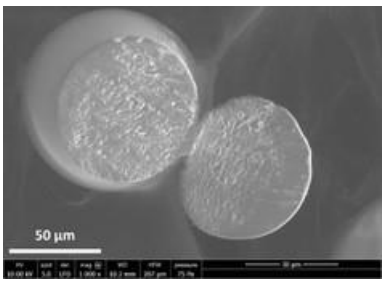
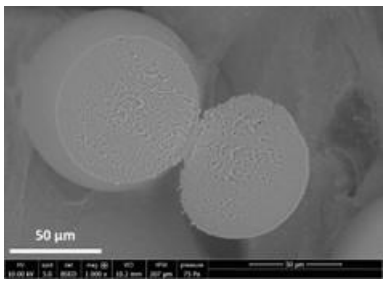
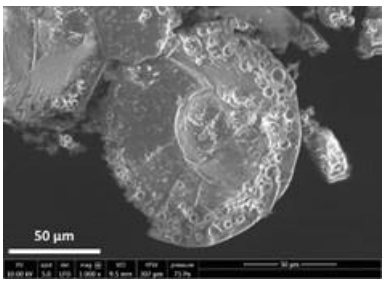
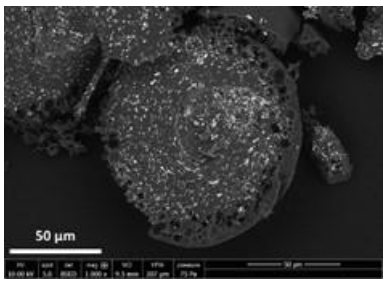
	LFD	BSED
Blank PLGA 75/25 50kDa		
Paclitaxel PLGA 75/25 50kDa		
Carboplatin PLGA 75/25 50kDa		

Figure 6-6: ESEM results showing cross section of blank (top), paclitaxel (middle) and carboplatin (bottom) microspheres made by using PLGA 75/25 50 kDa. Left-hand side images are from the large field detector (LFD) and right-hand side images are from back scattered electron detector (BSED). All sample were analysed uncoated by using FEI Quanta650 eSEM operated at 10kV and 75pa.

Whereas, the cross-section of all the carboplatin microspheres are clearly showing various features which are distinctly from the blank and paclitaxel microspheres. The LFD images are showing a relatively dense core and porous shell. While, the BSED images are showing very distinct bright spots, mainly in the core of the micropsheres. It was confirmed by EDX/EDS data (as described below) that these bright spots were due to the presence of platinum in the carboplatin (Figure 6-7).

EDS/EDX is a standard method for the determination of elemental composition in variety of materials e.g. PLGA-based microspheres [190,191,192], scaffolds [193],

craniofacial plates [194], just to name a few. It can be used to obtain the chemical information of individual points, as it have spatial resolution of about 1 μm for SEM and 1 to 20 nm for TEM [195].

In this study, EDX/EDS (energy dispersive X-ray spectroscopy) was primarily used to qualitatively determine the spatial distribution of carboplatin in the cross section of the PLGA microspheres. Selected points in the microspheres were analysed which confirmed the presence of carboplatin, Figure 6-7.

This data shows that carboplatin was homogenously distributed throughout the core of the micropsheres, whereas, there was relatively lower amount of carboplatin in the shell and near the surface of the microspheres.

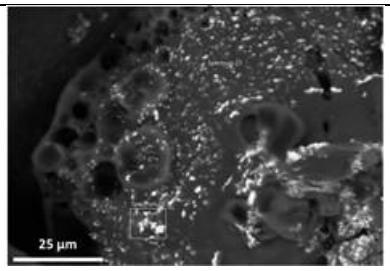
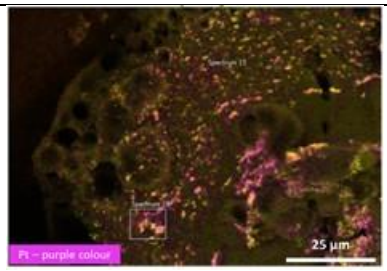
	ESEM	EDX/EDS
Carboplatin PLGA 75/25 50kDa		

Figure 6-7: ESEM analysis by using BSED (back scattered electron detector) (left) and EDX/EDS (Energy dispersive X-ray spectroscopy) (right) detectors. All sample were analysed uncoated by using FEI Quanta650 eSEM operated at 10kV and 75pa.

It was interesting to see from ESEM data Figure 6-8 that all the carboplatin formulations had a highly porous shell (beneath the surface). As mentioned in the SEM results section that some carboplatin microspheres did show highly porous surfaces (Figure 6-4) but vast majority of the carboplatin microsphere surfaces did not show any porosity by SEM analysis. This could be due to the polymer annealing [123] or gold coating [181] during SEM sample preparation. Whereas, for the ESEM analysis no coating was involved.

ESEM and EDX/EDX results were further verified by the ToF-SIMS depth profiling data (Figure 6-12 and Figure 6-13) which showed that there was negligible amount of carboplatin near the surface (shell) of the microspheres and as we move towards the core, the amount of carboplatin gradually increased and reached to a plateau after ~ 15 μm in depth.

One of the major differences between the carboplatin and other (blank and paclitaxel) formulations was the use of PEG 200, which was used to make crystalline nanosuspension of carboplatin by wet milling method, as mentioned in the methods section. It is possible that PEG 200 might have a played a role in the high porosity near the surface of the carboplatin PLGA microspheres because PEG 200 has been reported as a pore former in the literature [196-198]. This is attributed to the miscibility of PEG 200 with PLGA and higher water solubility of PEG 200 which results in faster leaching out of PEG 200 from the microspheres during microsphere hardening (DCM removal) and drying process.

The presence of high porosity in the shell of the microsphere may or may not affect the other QTPP attributes (e.g. release behaviour, drug loading, dose etc) therefore, at this stage no further work was conducted to reduce or to avoid this porosity in carboplatin microspheres. It can be considered as an option only if the carboplatin formulation failed any QTPP criteria or if no reasonable dosage regimen could be found for carboplatin by using any of carboplatin microsphere formulations.

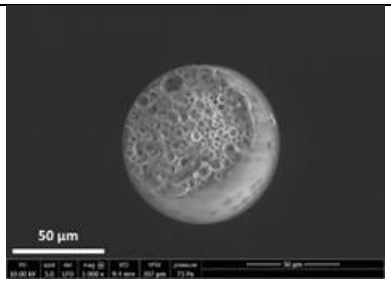
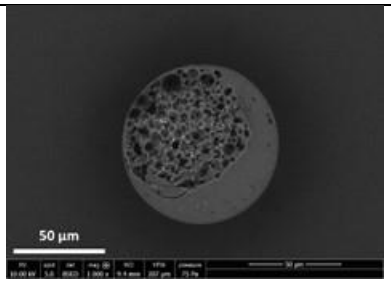
	LFD	BSED
Carboplatin		

Figure 6-8: ESEM results showing the porous shell of freeze-fractured carboplatin microsphere made by using PLGA 75/25 50 kDa. Left-hand side images are from the large field detector (LFD) and right-hand side images are from back scattered electron detector (BSED). All sample were analysed uncoated by using FEI Quanta650 eSEM operated at 10 kV and 75 pa.

6.3.3 Drug Loading and Encapsulation Efficiency

Drug loading analysis was performed on all the samples, data given in Table 6.3 shows that all paclitaxel formulations, except PF1, achieved high drug loading (~ 10% w/w) with close to 100% w/w encapsulation efficiency, which is

consistent with generally reported results for paclitaxel PLGA microspheres manufactured by different methods [148,160,161,199]. The formulation PF1 resulted in slightly lower drug loading (7.47% w/w) and encapsulation efficiency (74.7 % w/w). This was most likely due to the lower molecular weight (10 kDa) and lower Tg (i.e. greater polymer chain flexibility) compared to the higher molecular weight PLGA (e.g. 50 kDa). In addition, PLGA with lower lactide to glycolide ratio (50/50 vs 75/25) is relatively more hydrophilic, which may have also contributed towards the lower EE for PF1. These results are consistent with the data presented by Tsai et.al. (2013), showing relatively lower drug loading for the lower inherent viscosity (lower molecular weight) PLGA [161].

Table 6.3: Drug loading (DL) and encapsulation efficiency (EE) data for both paclitaxel and carboplatin microspheres made with four different grades of PLGA by using a microfluidics method.

Compound	Formulation ID	DL (% w/w)	EE (% w/w)	Comments
Paclitaxel	PF1	7.47	74.7	Dry cake (fused/stuck to the vial)
	PF2	9.84	98.4	Dry, free flowing powder
	PF3	9.54	95.4	Dry, free flowing powder
	PF4	9.89	98.9	Dry, free flowing powder (10% solids)*
Carboplatin	CF1	4.61	46.1	Slightly wet looking cake (it was possible to break it)
	CF2	4.39	43.9	Wet looking granular material
	CF3	4.94	49.4	Dry, free flowing powder, slightly stuck to the vial and needed scraping off
	CF4	6.24	62.4	Dry, free flowing powder

Carboplatin formulation CF4 achieved the highest drug loading of ~ 6 % w/w and encapsulation efficiency of around 60 % w/w (target drug loading was 10 % w/w) out of all four carboplatin formulations. Other carboplatin formulations had slightly lower drug loading and encapsulation efficiencies which ranged from 4.4 – 4.9 % w/w and 44 - 49 % w/w respectively Table 6.3. As described in section 5.3.2, it has not been possible to find any methods for encapsulating carboplatin into PLGA microspheres in literature. Although, Chen et. al.(1999) has described an interesting method for the manufacture of carboplatin-PLGA microspheres, with similar drug loading (5 to 9 % w/w), encapsulation efficiency (~ 50 % w/w) and release duration (up to 22 days) as found in my work, Table 6.3 and section 6.3.5 [162,163]. However, there method has some drawbacks e.g. it requires large quantities of non-aqueous solvents (acetone and mineral oil) and it involves a complex and lengthy microsphere isolation and cleaning process.

Drug loading and encapsulation efficiencies of both paclitaxel and carboplatin formulations made with the PLGA 75/25 50kDa in this part of study were very similar to the values reported in section 5.3.2 for the same formulations, which is reassuring and shows that this microfluidics method is reproducible.

As mentioned above, PF1 and CF1 formulations for both compounds (paclitaxel and carboplatin) were not found suitable for any other analysis, therefore, these formulations are highlighted as red in the following Table 6.2. The carboplatin formulations CF2 is highlighted in amber because it appeared to retain some moisture after same drying cycle as other formulations. The additional moisture may have an impact on the critical quality attributes e.g. release kinetics, burst release, etc.

6.3.4 ToF-SIMS

Spatial distribution of API in the PLGA microspheres is one of the critical parameters which can have decisive effect on the release characteristics of the formulation [200]. The application of ToF-SIMS analysis to determine the spatial distribution of API in pharmaceutical systems in general and microspheres in particular has grown over the past two decades. This is credited to the high specificity, good depth resolution (~ 1 to 2 nm) and availability of instruments [201-204]. In this study, ToF-SIMS analysis was primarily used to determine the

spatial distribution of carboplatin and paclitaxel on the surface and core of the microspheres (depth profiling) to support the interpretation of release data for the PLGA microsphere formulations.

Firstly, the characteristic secondary ions for the PVA, PLGA, paclitaxel and carboplatin shown in Figure 6-9 were selected after screening of the reference materials, full screening spectra can be found in Appendix H. As it can be seen from Figure 6-9 that PVA has a strong signal at m/z 59.01 corresponding to acetate ($C_2H_3O_2^-$) [201]. However, there was an interfering secondary ion peak from paclitaxel at this mass. Therefore, this ion could not be used to identify PVA in paclitaxel samples, nevertheless, this ion can be considered a PVA specific secondary ion for carboplatin and blank PLGA microsphere samples. Hence, in this study, $C_2H_3O_2^-$ (m/z 59.01) was selected as a selective marker for PVA. For PLGA $C_3H_3O_3^-$ (m/z 87) was selected as ion marker because there was negligible interference from any other component at this mass. Similarly, for paclitaxel $C_{16}H_{14}NO_4^-$ (m/z 284) was used as selective markers during surface scan and depth profiling of the microspheres due to no interference from any other components of the formulation.

It can be noticed from the Figure 6-9 that carboplatin has three secondary ions $C_6H_6O_4PtNH^-$, $C_6H_6O_4PtNH_2^-$,$C_6H_6O_4PtNH_3^-$ (m/z 352.1, 353.1 and 354.1) and there were no other interfering secondary ions from any other components in this region therefore, the total intensity from these three peaks was added together for carboplatin identification in order to improve the sensitivity (signal to noise ratio).

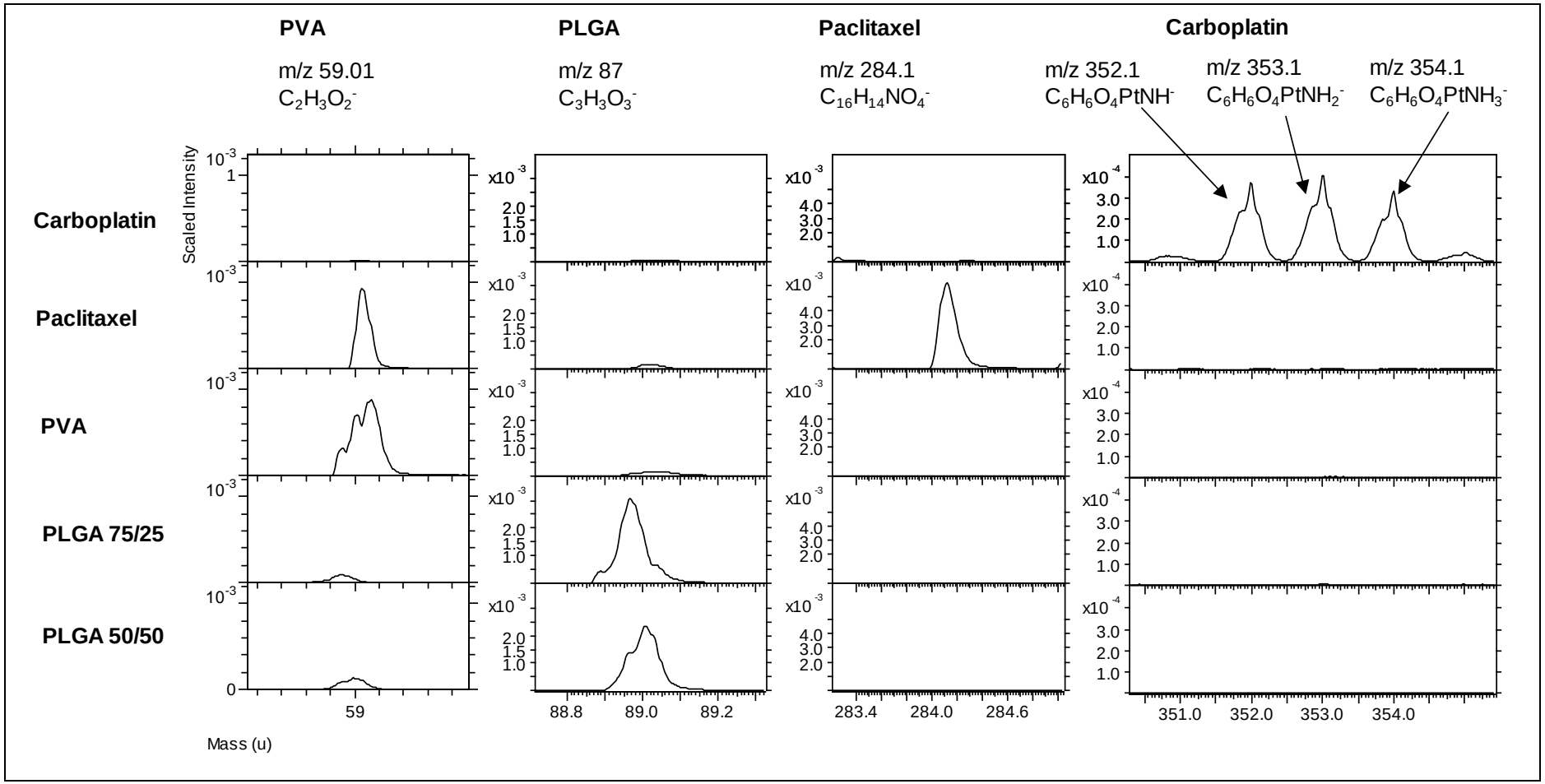


Figure 6-9: ToF-SIMS analysis of reference materials to select characteristic secondary ions to identify PVA, PLGA, paclitaxel and carboplatin in PLGA microsphere based formulations.

Surface scanning profile

The secondary ions identified as selective markers for all the components of the formulation during the screening experiment, as discussed above, (Figure 6-9) were used for the surface analysis of microspheres to determine the presence of both APIs (i.e. carboplatin and paclitaxel) on the surface of drug loaded microspheres, in addition to PLGA and PVA. For comparison the blank microspheres were also analysed. Figure 6-10 shows the results from the surface scans of all the samples. As it can be seen from this figure that there was no detectable amount of either molecule (carboplatin or paclitaxel) present on the surface of drug loaded microspheres. However, as expected, the secondary ion for PLGA ($C_3H_3O_3^-$) was clearly observed on the surface of all microspheres. As mentioned above, PVA has a common secondary ion $C_2H_3O_2^-$ (m/z 59.01) with paclitaxel therefore, PVA identification is not possible for paclitaxel samples. However, Figure 6-11 shows that the signal from the PVA secondary ion $C_2H_3O_2^-$ (m/z 59.01) was much stronger in the blank and carboplatin samples compared to the PLGA specific secondary ion $C_3H_3O_3^-$ (m/z 87) in the blank sample of PLGA 50/50 50kDa. This clearly indicates that PVA was present on the surface of the microspheres.

This was not unexpected, as PVA was used as a surfactant in the aqueous phase to stabilise the organic phase droplets during the microsphere formation. In addition, we have also used a dilute solution of PVA to clean the microspheres at the end of DCM removal process (to wash off the unencapsulated API) . Rafati et. al. have also reported the presence of PVA on the surface of PLGA microspheres [201].

The characterisation of microsphere surface for the presence of the PVA and active ingredient (drug) is an important part of the development of microspheres. This data helps to answer the question about the physical stability of the microspheres (e.g. suspendability, aggregation, etc) and more importantly to understand the release behaviour (e.g. burst release or lag phase). In general, the presence of significant amount of drug on the surface results in high burst release and vice versa. High burst release, commonly, is an undesired characteristic of microspheres [71].

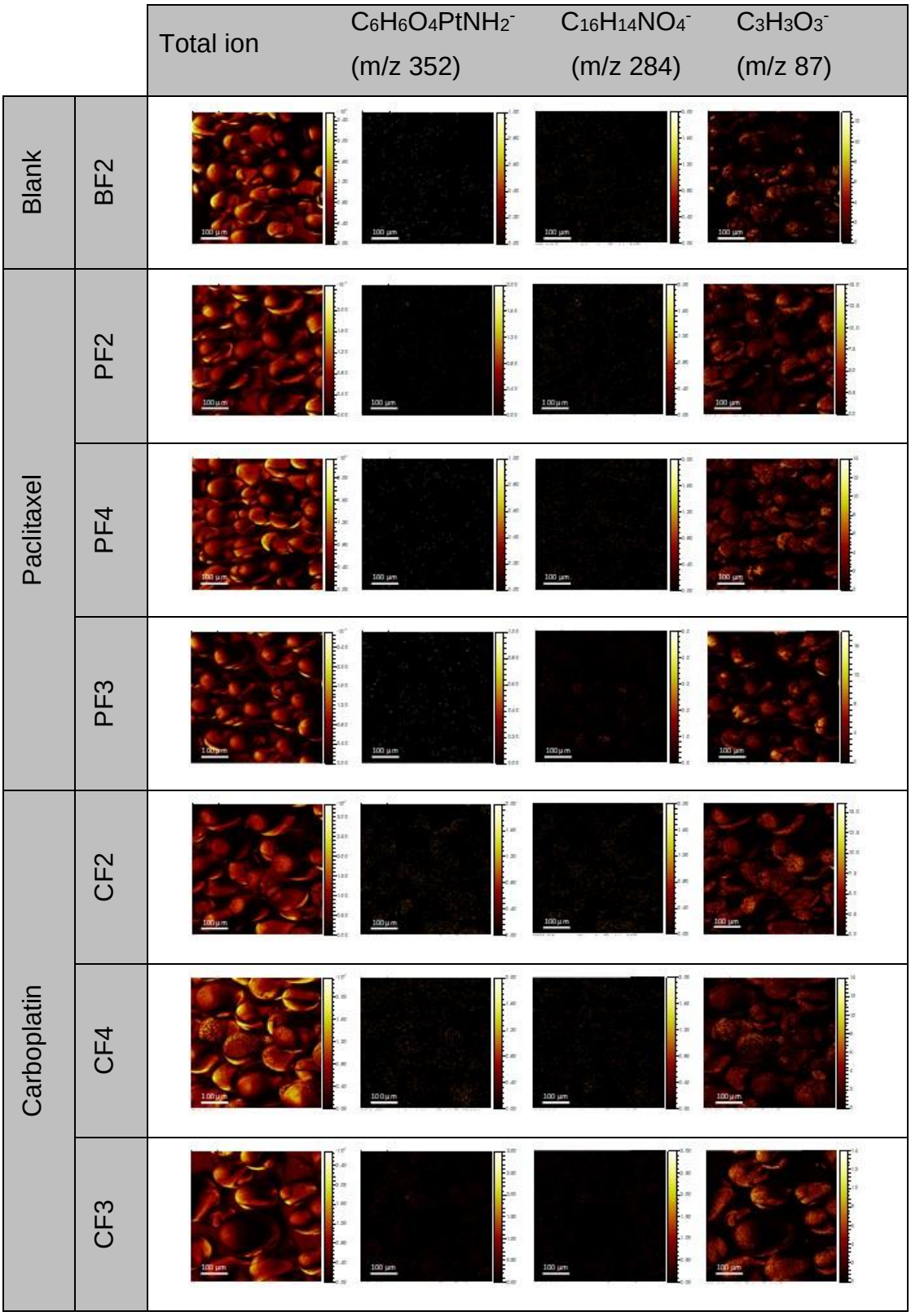


Figure 6-10: ToF-SIMS surface scan images, comparing the compound secondary ion intensities for the identification of paclitaxel, carboplatin and PLGA on the microsphere surfaces. Brighter images indicate stronger signal and therefore, the presence of specified compound on the surface.

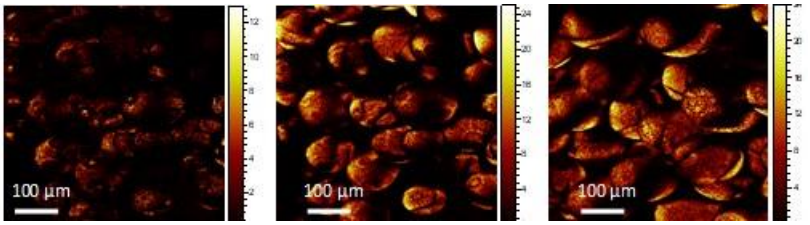
	Blank $C_3H_3O_3^-$ (m/z 87)	Blank $C_2H_3O_2^-$ (m/z 59.01)	Carboplatin $C_2H_3O_2^-$ (m/z 59.01)
PLGA 50/50 50kDa			

Figure 6-11: ToF-SIMS surface scan images of blank and carboplatin microspheres made with PLGA 50/50 50kDa comparing two secondary ions, $C_3H_3O_3^-$ (m/z 87) a specific secondary ion for PLGA and . $C_3H_3O_2^-$ (m/z 59.01) a specific secondary ion for PVA.

Depth profile analysis

ToF-SIMS depth profiling data given in Figure 6-12 is showing the distribution of the active ingredients (carboplatin and paclitaxel) and PLGA throughout the bulk of the microspheres for all the drug loaded samples. It is worth noting that these are the results from bulk sample analysis, as standard, i.e. this is not an image of single microspheres.

In general, the spatial distribution of carboplatin (Sum of $C_6H_6O_4PtNH^-$, $C_6H_6O_4PtNH_2^-$ and $C_6H_6O_4PtNH_3^-$) appears similar in all the samples where there is minimal quantity of carboplatin present near the surface and as we move towards the core of the particles the concentration of carboplatin increases (Figure 6-12). This behaviour is also clearly shown in the intensity plot against the sputtered depth in Figure 6-13. This figure shows that as we move towards the core of the microspheres the carboplatin intensity increases and from approximately 15 µm onwards the distribution becomes homogenous. This data agrees with physicochemical properties of the compound (i.e. carboplatin is soluble in water), ESEM and EDX/EDS results (Figure 6-6 to Figure 6-8) which showed that carboplatin microspheres have significantly higher level of porosity near the microsphere surface (shell) compared to the paclitaxel and blank microspheres. The higher solubility and increased porosity has most likely resulted in the depletion of carboplatin from the shell during the downstream manufacturing processes (i.e. organic solvent removal, microsphere washing and drying). Kim et. al. has also reported significantly

lower drug loading of a water soluble compound (recombinant human growth hormone, rhGH) in porous compared to pore free PLGA microspheres.

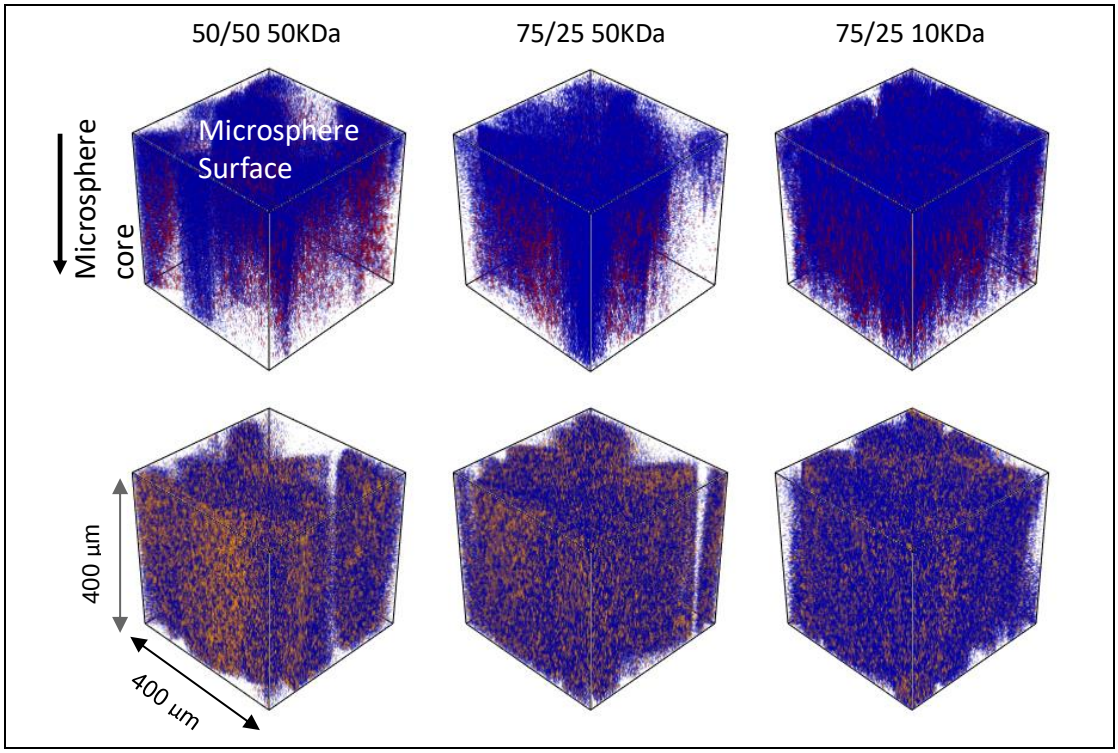


Figure 6-12: ToF-SIMS depth profiling 3D images of PLGA microspheres of carboplatin (top row) and paclitaxel (bottom row) showing spatial distribution of API and PLGA throughout the bulk microspheres. Colour coding: Blue PLGA, Red carboplatin (Sum of $C_6H_6O_4PtNH^-$, $C_6H_6O_4PtNH_2^-$ and $C_6H_6O_4PtNH_3^-$) and Golden paclitaxel ($C_{16}H_{14}NO_4$-).

On the other hand, 3D images of paclitaxel bulk microspheres demonstrated that the paclitaxel was homogenously distributed throughout the microspheres (Figure 6-12). The paclitaxel intensity plot against the sputtered depth in Figure 6-13 also supports the 3D images, which shows that paclitaxel microspheres made with all three grades of polymers appear to have similar homogenous spatial distribution throughout the microsphere. These results were as expected owing to the physicochemical properties of the paclitaxel (i.e. poor/negligible solubility in water) and dense/pore free nature of the microspheres, Figure 6-6.

The single ion intensity plots given in Figure 6-13 also, semi-quantitively, shows that all the paclitaxel samples have slightly higher ion intensity compared to the carboplatin microspheres, this is highly likely due to the higher drug loading of paclitaxel as shown in Table 6.3.

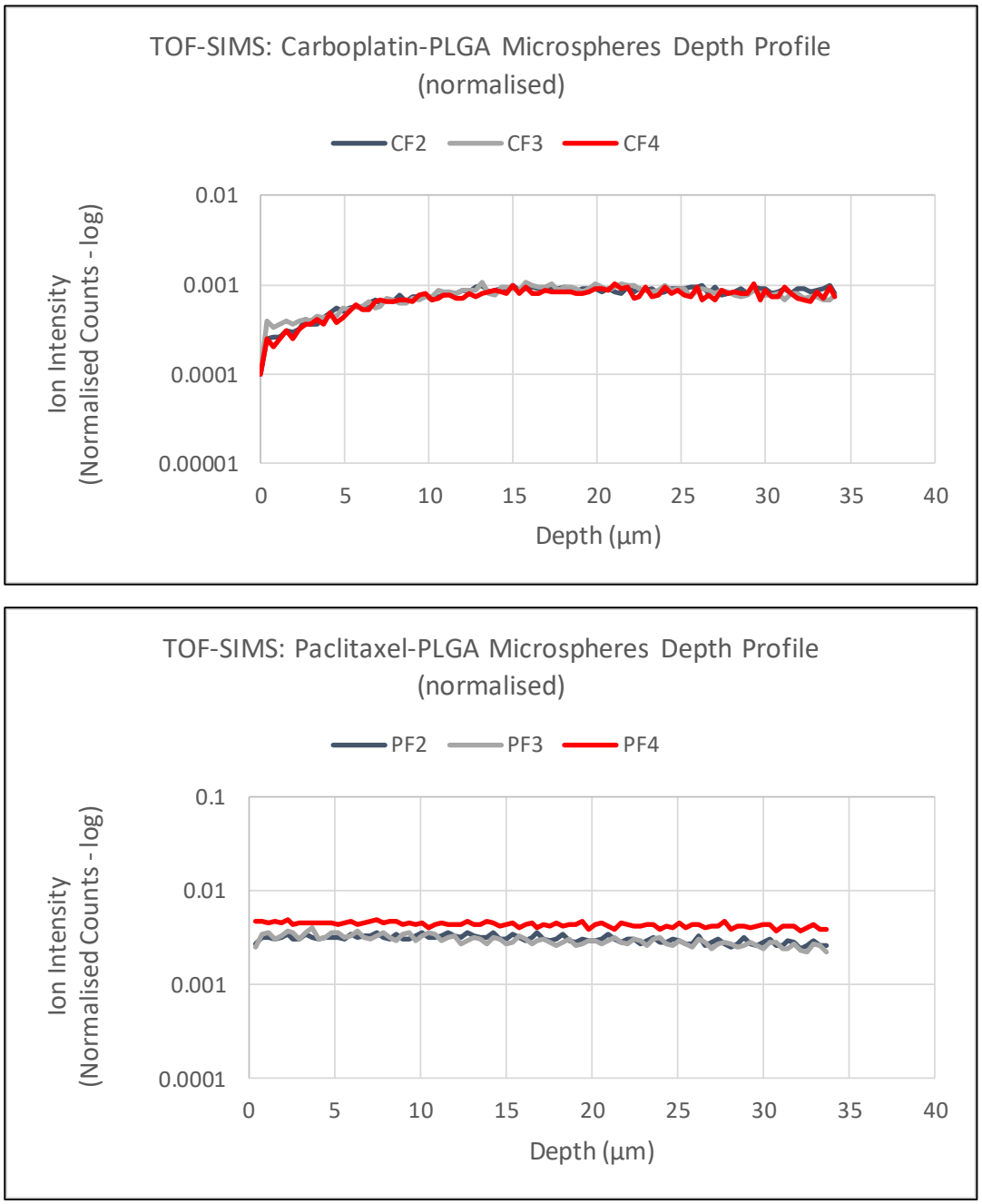


Figure 6-13: ToF-SIMS depth profile analysis results presented as ion intensity vs sputtered depth, showing the spatial distribution of carboplatin (top picture, sum of $C_6H_6O_4PtNH^-$,$C_6H_6O_4PtNH_2^-$ and $C_6H_6O_4PtNH_3^-$ ions) and paclitaxel (bottom picture, ion $C_{16}H_{14}NO_4$-) within the bulk microspheres in all three formulations of each compound.

6.3.5 Drug Release from Microspheres

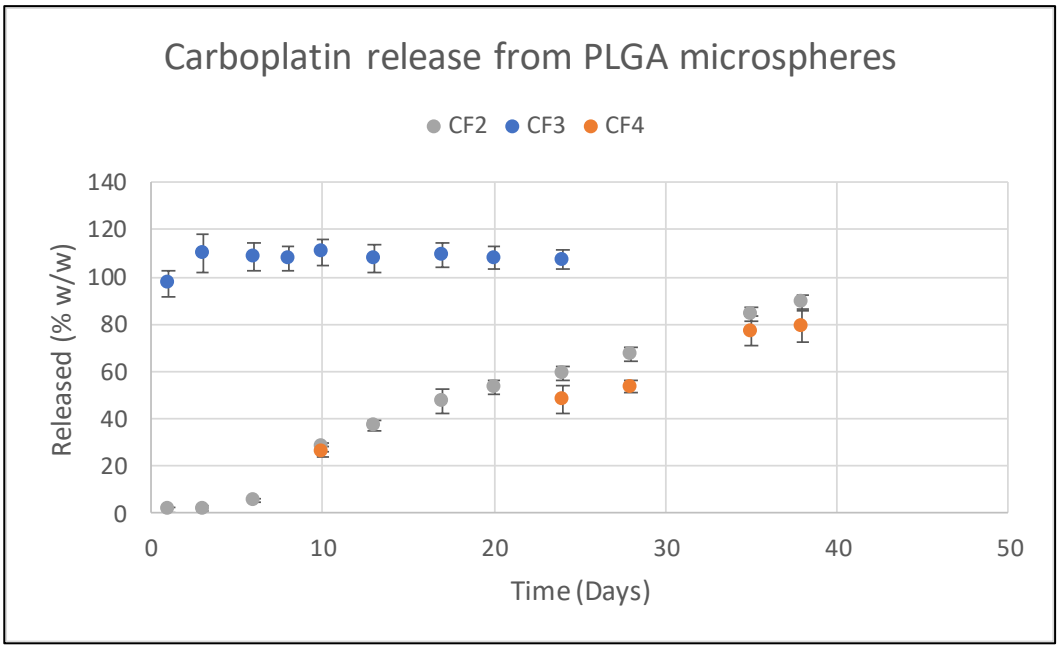
Figure 6-14 shows the release profiles of carboplatin and paclitaxel from PLGA microspheres made by using three different grades of PLGA.

For carboplatin, formulation CF3 released all the payload rapidly whereas other two formulations, CF2 and CF4 showed a sigmoidal release, involving a lag (no release) phase, bulk release phase and plateau phase. Both of these carboplatin microsphere formulations had a lag phase of six days followed by bulk release phase for 38 days before plateauing.

For paclitaxel, release profiles from all three formulations (PF2, PF3 and PF4) were also sigmoidal Figure 6-14. Paclitaxel formulation PF3 released the payload in 20 days with a lag phase of just 1 day and formulation PF2 released payload in 28 days with a lag phase of around 13 days before reaching to the plateau phase. Formulation PF4 had the longest lag phase of around 43 days and released the payload in 67 days.

The release of payload from PLGA microspheres is dictated by the diffusion and/or homogeneous bulk erosion of the polymer. This is dependent on number of factors, as detailed in section 6.1, including the PLGA m.wt. and lactide to glycolide ratios.

The results presented here are consistent with the literature, owing to the physicochemical properties of the PLGA i.e. in general, the smaller molecular weight (e.g. PF3 10 kDa vs PF4 50 kDa) and lower lactide to glycolide ratio (e.g. PF2 50/50 vs PF4 75/25) has resulted in faster release and vice versa, for both compounds.



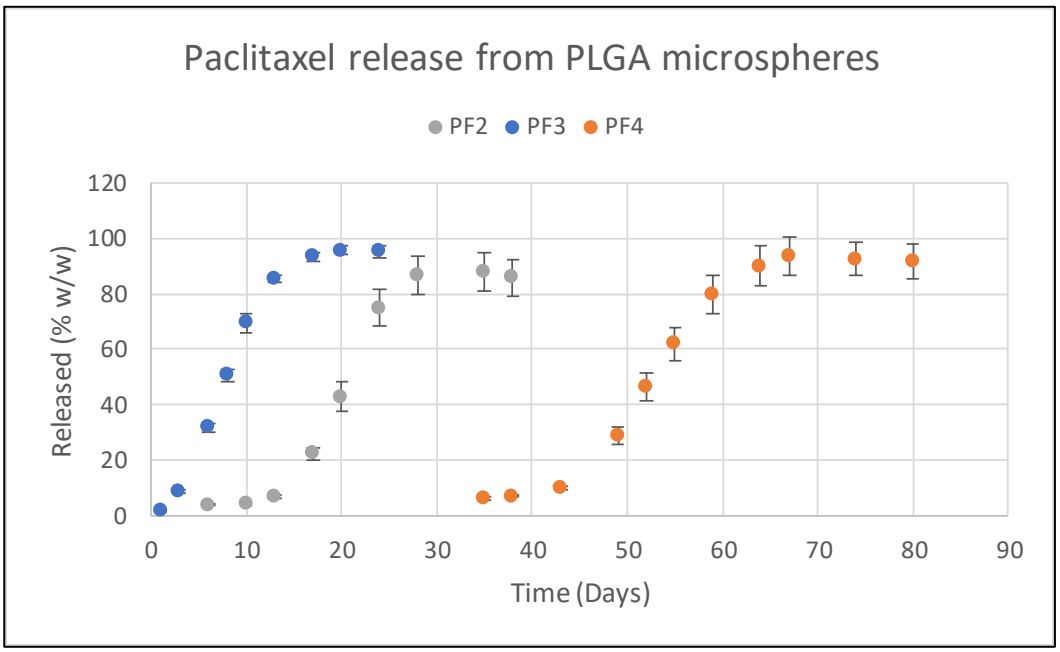


Figure 6-14: Cumulative release of carboplatin and paclitaxel from PLGA microspheres made with three different grades of PLGA. Carboplatin microspheres were incubated in 10 mM PBS pH7.4 buffer containing 0.02% w/v sodium azide whereas, paclitaxel microspheres were suspended in 10% HPβCD in 10 mM PBS pH7.4 buffer containing 0.02% w/v sodium azide. Samples were continuously agitated at 37 °C in a shaking water bath at 150 rpm. Supernatant samples were collected at regular intervals and analysed by HPLC-UV for paclitaxel and ICP-OES for carboplatin. The results are a mean of the three replicates with the error bars representing the standard deviation.

Both CF2 and CF4 carboplatin formulation has shown similar release rate. In these formulations the PLGA molecular weight was same (50 kDa) but the lactide to glycolide ratios were different (50/50 vs 75/25, respectively). This data indicates that API may also have an impact on the release rate, since based solely on the PLGA characteristics, these two formulations should have had different release rates. The similar results have also been described in the literature, where it has been shown that the physicochemical properties of API had significant effect on the release rates from PLGA microspheres [205].

It is commonly reported in the literature that the release from PLGA (bulk eroding polymer) microspheres typically involves an initial rapid (burst) release phase attributed to the release of API near the surface, which is then followed by a relatively slow and constant release due to the degradation of polymer and diffusion of API out of the microspheres. This is followed by a final burst phase due to extensive polymer degradation resulting in excessive solubilisation and erosion of polymer matrix [206-208]. Sigmoidal release profiles, similar to the one observed in this study, have also been reported by some researchers in particular for relatively small microspheres (50-100 µm) containing small hydrophobic (lipophilic) compounds [208,209]. It has also been reported that the small molecule drugs encapsulated in the monodispersed microspheres (between 50-100 µm diameter) prepared by “precision particle fabrication” (PPF) techniques (e.g. microfluidics) do not show the burst release phase rather they exhibit a sigmoidal release profile [120,169].

Some possible explanations proposed for this phenomenon in the monodispersed microspheres made by PPF techniques are; i) absence of small particles with a large surface area to volume ratio [169] and ii) a relatively gentle process in microfluidics compared to strong shearing used in the conventional bulk preparation methods which may not allow majority of the encapsulated compound to access the surface [169].

Based on this data we have selected one formulation of carboplatin (CF2) and two formulations of paclitaxel (PF2 and PF3) for further work to implement the intraperitoneal PK model and determine the dosage regimen for ovarian cancer. These formulations were selected because one of the aim for this study was to develop a drug delivery system which can maintain therapeutic concentrations of paclitaxel and carboplatin in the IP cavity for 1 month or longer after a single

dose. As described above, carboplatin formulation CF2 and a combination of two paclitaxel formulations (PF2 and PF3) has bulk release phases over a period of approximately 1 month (Figure 6-14). Although, for carboplatin CF4 formulation also has similar release profile as compared to CF2 formulation but the latter was preferred for further work because it contained same polymer as one of the paclitaxel selected formulation i.e. PF2.

Results from intraperitoneal PK model to determine the doses and dosage regimen for both carboplatin and paclitaxel by using the selected microsphere formulations

For carboplatin, experimental release data from formulation CF2 (PLGA 50/50 50kDa) Figure 6-14 was fitted to mathematical function by using SigmaPlot (Version 13 from Systat Software) and it was found to fit well (Figure 6-15) to a Hill function (or Hill equation) of the form, Equation 6-6,

$$F(t) = \frac{a.t^b}{(c^b + t^b)}$$ Equation 6-6

Where *F(t)* denotes the fraction of API released from the microspheres as a function of time and *a, b, c* are constants, which are optimised to find the best fit. The constant *a* is fixed at value of 1 to ensure that 100% release is the maximum value of the fitted function as the time tends towards infinity.
Therefore, Equation 6-6 was reduced to,

$$F(t) = \frac{t^b}{(c^b + t^b)}$$ Equation 6-7

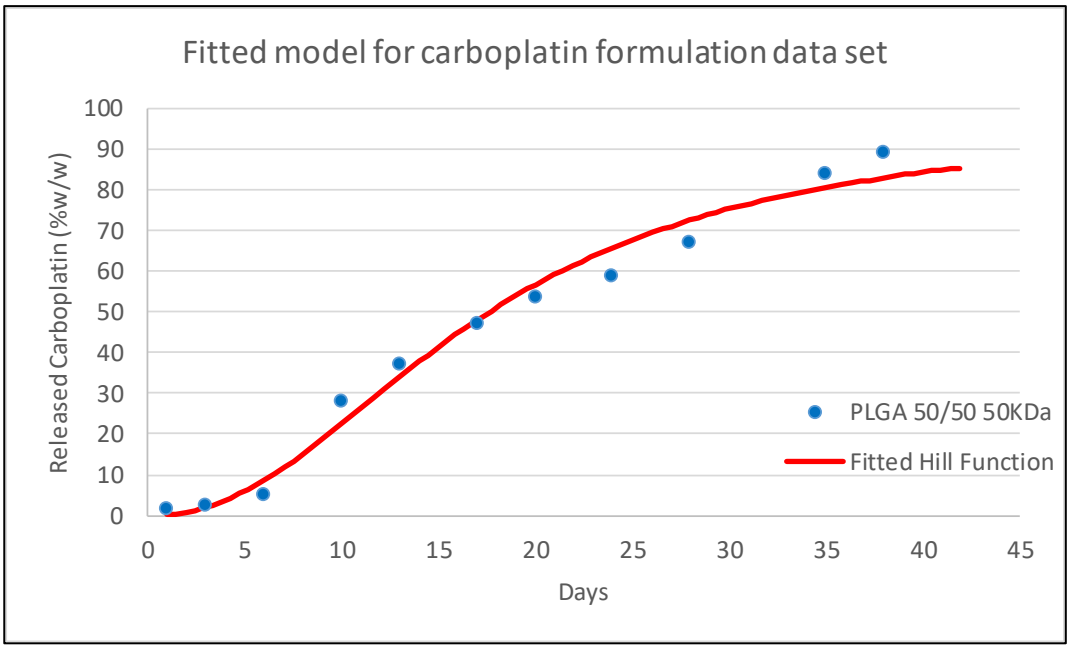


Figure 6-15: Hill function (a mathematical function) fitted to the release data of carboplatin CF2 (PLGA 50/50 50kDa) microsphere formulation by using SigmaPlot (Version 13 from Systat Software).

However, in order to make use of this in the numerical model, we needed an expression for the derivative of $F(t)$ with respect to time (i.e. slope) which lead to Equation 6-8,

$$F'(t) = \frac{b.c^b.t^{b-1}}{(c^b + t^b)^2} \qquad \text{Equation 6-8}$$

The remainder of the process to determine the concentration of carboplatin in the IP cavity and dosage regimen was same as given in methods section.

Figure 6-16 is showing the carboplatin simulated concentration change in the IP fluid as a function of time after six doses of 14.5 mg of carboplatin (equivalent to 330 mg microsphere formulation, with 4.4% w/w drug loading, Table 6.4) by using the model implemented in Berkeley Madonna (details of the code used are given in Appendix K).

It can be seen from these results that the target concentration (C_{target}) of carboplatin (5.7 mg/L) can be maintained for 28 days after a single dose and for nearly 6 months by administering 6 doses at a dosing interval of 28 days. This pulsatile-type concentration profile of released API in the IP cavity on

multiple doses is a typical feature for microsphere based sustained release drug delivery systems [172]. It is generally accepted as long as the concentration at any particular time stays above the pre-defined target concentration. The carboplatin data shows that a pulsatile steady-state concentration of released carboplatin can be maintained between 5.7 to 15 mg/L, ensuring that the IP concentration stayed above the target value at all times, with multiple doses.

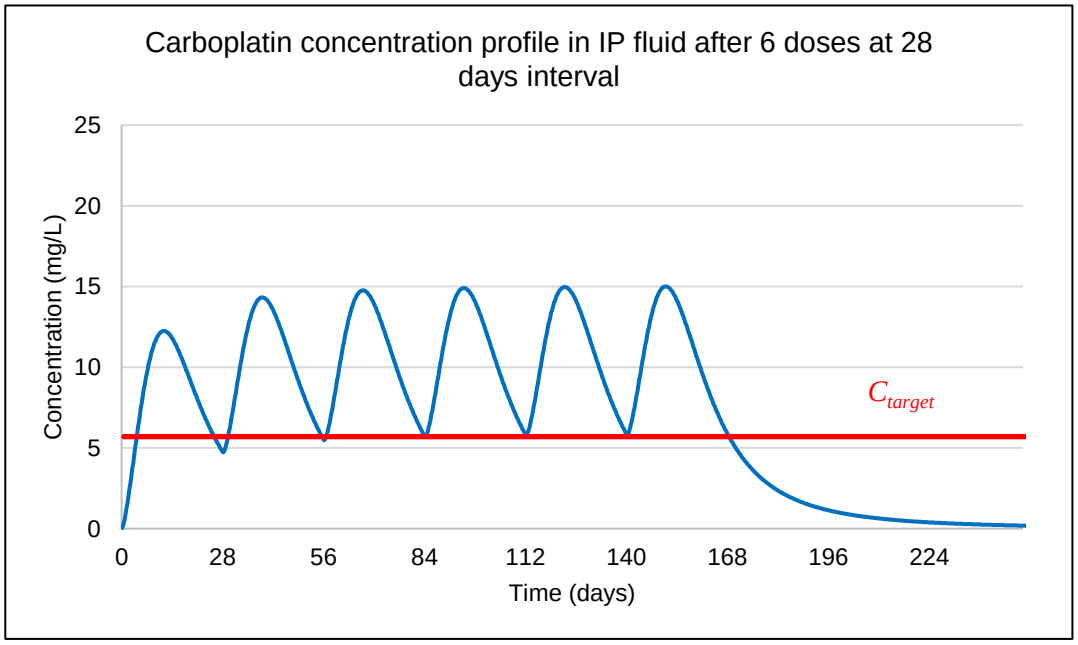


Figure 6-16: A steady state of carboplatin concentration in IP fluid above the target concentration (C_{target}) of 5.7 mg/L after administering six doses of 14.5 mg of carboplatin (equivalent to 330 mg of microsphere formulation made from PLGA 50/50 50kDa with 4.4 % w/w drug loading) at a dosing interval of 28 days.

Similarly, paclitaxel optimum dose and dosage regimen was determined by using the same approach as above. However, for paclitaxel none of the formulation had long enough release duration to achieve a steady state for one month or longer (Figure 6-14).

It has been reported by Kim et. al. and Berchane et. al. that physical mixture of two or more microsphere-based formulations results in a mass weighted average of release profiles of the individual microspheres ([171,210]).

Therefore, for paclitaxel we have used two formulations (PF2, PLGA 50/50 50kDa and PF 3, PLGA 75/25 10kDa). Similar to carboplatin, first a mathematical function was fitted to the data and it was found that same Hill

function (Equation 6-6), that fitted to the carboplatin data was also a good fit for both paclitaxel formulations Figure 6-18.

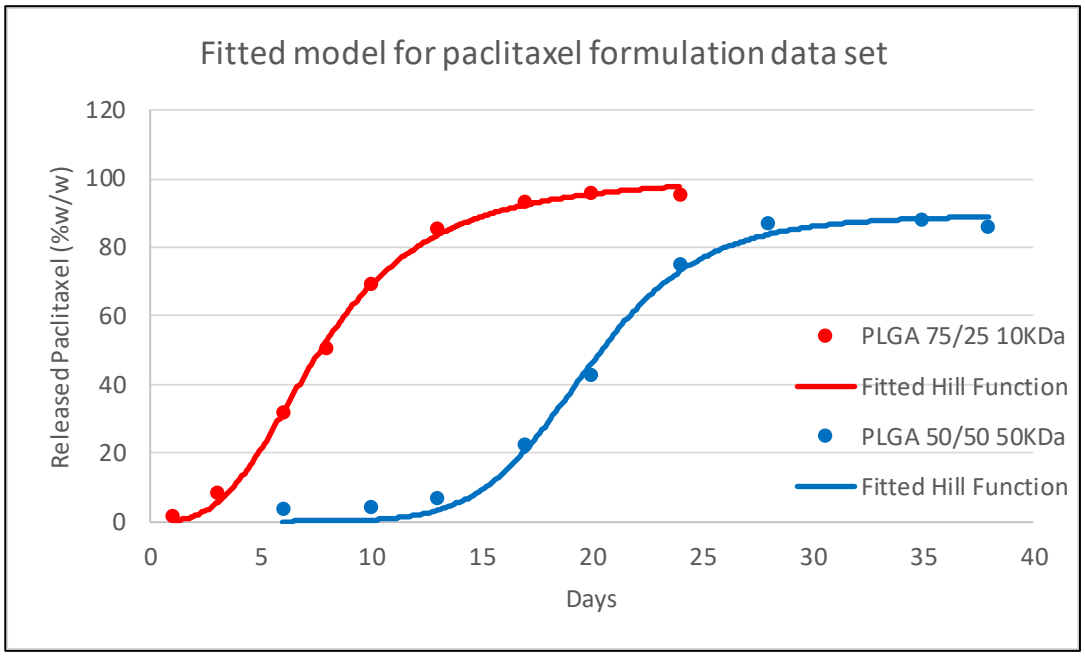


Figure 6-17 Hill function (a mathematical function) fitted to the release data of paclitaxel PLGA microsphere formulations by using SigmaPlot (Version 13 from Systat Software).

The overall release function was then determined by adding the contribution from each of the paclitaxel formulation as,

$$F(t) = f_1 \cdot \left(\frac{t^{b_1}}{(c^{b_1} + t^{b_1})}\right) + (1 - f_1) \cdot \left(\frac{t^{b_2}}{(c^{b_2} + t^{b_2})}\right) \qquad \text{Equation 6-9}$$

Which was then differentiated with respect to time to determine the $F'(t)$,

$$F'(t) = f_1 \frac{b_1 . c^{b_1} . t^{b_1 - 1}}{(c^{b_1} + t^{b_1})^2} + (1 - f_1) \frac{b_1 . c^{b_1} . t^{b_1 - 1}}{(c^{b_1} + t^{b_1})^2} \qquad \text{Equation 6-10}$$

Where f_1 is the fraction of the formulation 1 (i.e. in this case two paclitaxel formulations were mixed with 46:54 ratio of formulation PF3 to formulation PF2).

Other than the release function, all equations were same as given in the methods section. The paclitaxel model was then implemented in Berkeley Madonna (see model code in Appendix K) to, first, find an optimum blend ratio of the two formulations by systematically altering the amount of formulation 1 to achieve a steady state at a fixed dose (see Figure 9-14 in Appendix K).

This was followed by adjusting the dose (of optimum blend) by trial and error approach to bring the concentration in the IP fluid above the target concentration (C_{target}) for the total dosing period until the steady state was achieved. See Figure 6-18 for simulated IP fluid steady-state concentration of paclitaxel above the target concentration (0.0726 mg/mL) after total 6 doses of 0.096 mg/dose paclitaxel by using a blend of paclitaxel formulation PF3 (46% w/w) and formulation PF2 (54% w/w) at a dosing interval of 23 days.

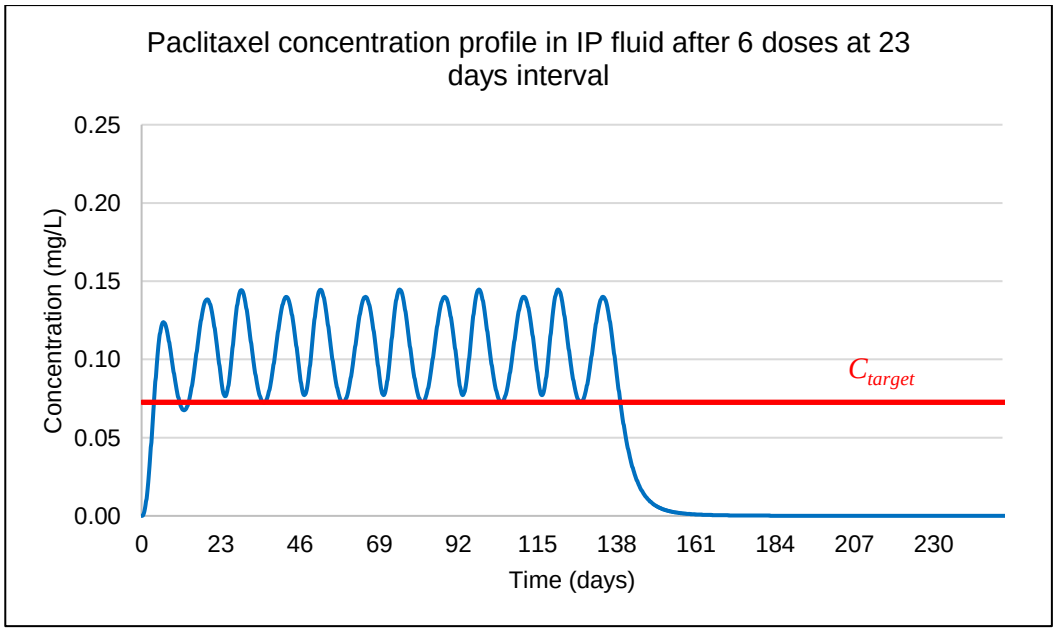


Figure 6-18: A predicted intraperitoneal (IP) steady-state concentration of paclitaxel above the target concentration (0.0726 mg/mL) by using a IP pharmacokinetic model implemented in Berkeley Madonna (software package). These results are after administering total 6 doses of 0.096 mg/dose paclitaxel by using a mixture of paclitaxel formulation PF3 (46% w/w) and formulation PF2 (54% w/w) at a dosing interval of 23 days.

It can be seen from these simulated results Figure 6-18 that the target concentration (C_{target}) of paclitaxel in the IP fluid can be maintained for 23 days after a single dose and for nearly 5 months after administering 6 doses (one dose every 23 days) of optimum blend (46:54) of paclitaxel formulations PF3 and PF2.

Current treatment for the ovarian involves chemotherapy, which typically begins two to six weeks after surgery and continues for maximum 6 cycles, with three weekly dosing per cycle [18,19]. The dosing schedule starts with paclitaxel solution formulation administered by IV infusion over 3 hr period followed by carboplatin solution formulation via IV infusion on the same day [25].

The following Table 6.4 summarises the predicted dosing scheme for the intraperitoneal administration of paclitaxel and carboplatin by using the formulations developed in this study, to maintain the therapeutic concentrations in the IP fluid.

Table 6.4: Summary of the predicted dosing scheme for the intraperitoneal administration of paclitaxel and carboplatin, by using the PLGA microsphere based controlled release formulations, for the treatment of ovarian cancer.

	Paclitaxel	Carboplatin
Total Dose (as API) (mg)	0.096	14.5
Microsphere drug loading (% w/w) *Reference Table 6.3*	10 *(average of two formulations PF2 and PF3 at blend-ratio of 54:46)*	4.4
Dose (as microsphere) (mg)	0.96	330
Dosing interval (days)	23	28
Comments	Multiple doses can be used to attain longer than 1-month continuous exposure.	

In addition to the formulation and the compound properties (e.g. drug loading, release rate, GI50, k_{ip}, etc), the IP fluid volume is also an important parameter to determine the dose. The IP fluid volume in women can vary with menstrual cycle[13], [14] and under certain disease conditions[16] which makes it difficult to accurately estimate the exact doses. The estimated doses given in Table 6.4 are based on the assumption that all the IP fluid is removed from the IP cavity

before drug product administration and the dose volume is 10 mL. Although, the final doses and dosage regimen of paclitaxel and carboplatin, by using the formulations developed in this study, can only be fine adjusted after in-vivo studies. However, I believe the simulated data presented here provides a rational starting point for the in-vivo studies. It is worth noting that the optimised dosing interval and the ideal blend ratio of formulations are not affected by IP fluid volume, see Figure 9-15 in 9Appendix K.

6.4 Conclusion

Data presented in this chapter shows that we have successfully developed PLGA microsphere-based formulations of paclitaxel and carboplatin to maintain a sustained release of these compounds for approximately 1 month in the intraperitoneal cavity. The intraperitoneal PK mathematical model developed during this study predicted that a steady state concentration at the target therapeutic levels in the intraperitoneal fluid (exposure) can be maintained for at least 23 days for paclitaxel and 28 days for carboplatin after a single dose of these formulations. In addition, the simulated data also shows that the exposure can be maintained for several months by administering multiple doses at a dosing interval of 23 days for paclitaxel and 28 days for carboplatin.

We believe that data presented here provides a rational starting point for the in-vivo studies using paclitaxel and carboplatin PLGA microsphere-based drug delivery system developed in this study.

7 Summary and Future Perspectives

7.1 Summary

An injectable intraperitoneal sustained release drug delivery system comprised of paclitaxel and carboplatin loaded PLGA microspheres has been developed. The in-vitro data and in-silico modelling presented in this thesis suggests that with this drug delivery system therapeutic concentrations can be maintained in the intraperitoneal cavity for at least 23 days for paclitaxel and 28 days for carboplatin after a single injection and for several months after multiple doses at corresponding dosing intervals.

7.1.1 Selection of the drug delivery system design parameters

Firstly, an intraperitoneal pharmacokinetic mathematical model was developed to determine the target parameters e.g. drug loading, release kinetics and dosage regimen (i.e. dose, dosing frequency and duration) for the drug delivery system. The PK model was built on some input parameters from literature including absorption constants from the IP cavity and plasma protein binding for carboplatin and paclitaxel. The IP fluid volume and the dosing interval was fixed at 10 mL and 30 days, respectively. The target minimum efficacious concentrations in the IP cavity were calculated from the GI50 values for paclitaxel and carboplatin, which were determined in two cell lines (OVCAR4 and IGROV1) by using cytotoxicity assays.

The preliminary PK model was based on three compartments, i) API encapsulated in the microspheres, ii) free API (released and unbound) in the IP fluid and iii) API elsewhere in the body. For simplicity, as a starting point, it was assumed that both compounds have zero-order release rates from the PLGA micropsheres. The model was implemented in the Berkeley Madonna modelling software. The results from this model predicted that a PLGA microspheres-based formulation with approximately 10 % w/w drug loading and zero-order release rate would be able to maintain the minimum efficacious concentration in the IP cavity for 1 month after single dose of 0.84 mg of paclitaxel and 82 mg of carboplatin microspheres.

This data was then used to set the quality target product profile (QTPP) for the drug delivery system.

7.1.2 Selection of PLGA microsphere and hydrogel manufacturing methods

Following on from the identification of the QTPP, various methods were evaluated for the manufacture of carboplatin and paclitaxel loaded PLGA micropsheres and the hydrogel. PLGA microspheres were selected as the back bone of the drug delivery system to control drug release rates, whereas, hydrogels were planned to be used to prevent microsphere clearance from peritoneal cavity and improve the PLGA microsphere biocompatibility i.e. avoid inflammation and adhesion in the peritoneal cavity due to PLGA microspheres. For PLGA microsphere manufacturing, as a starting point, a single emulsion (O/W) method was assessed for paclitaxel and a double emulsion (W/O/W) method was evaluated for carboplatin, based on the physicochemical properties of these compounds. Furthermore, three PLGA microsphere manufacturing techniques were assessed for controlling the microsphere size by using a single emulsion (O/W) method, including i) homogenisation b) filter extrusion and c) microfluidics.

In general, homogenisation and filter extrusion techniques resulted in very small microspheres (<10 μm), whereas, microfluidics gave uniform size micropsheres between 50 - 200 μm. The microfluidics technique was also used to evaluate the carboplatin loading and encapsulation efficiency (EE) by using a double emulsion method in this part of the study (chapter 3). This was because carboplatin envisaged to be a challenging compound for making PLGA microspheres due to lack of methods reported in the literature. From this carboplatin method evaluation, only 0.22 % w/w drug loading was achieved which was well below the target loading of 10 % w/w as per QTPP. Later, a modified single emulsion method was developed for carboplatin to achieve higher drug loading, see chapter 5 and section 7.1.3.

At this stage, microfluidics and single emulsion method was found suitable for further optimisation by using the design of experiment (DOE) approach.

For the hydrogel, various physical interaction hydrogels were developed and/or evaluated for physical stability in simulated IP fluid, with and without PLGA microspheres (chapter 4). In the first instance, hydrogels composed of ionisable high molecular weight polymers, including hyaluronic acid, chitosan, alginate, and pectin, were evaluated. The high molecular weight ionisable polymers were selected based on the hypothesis that the polymer chain entanglements in addition to ionic cross-links would result in more stable hydrogels and may disintegrate comparatively slowly in the IP cavity. In addition, hyaluronic is known to prevent adhesions in the IP cavity[211]. These hydrogels were made by using a double barrel syringe for injectability, where oppositely charged polymers were kept in separate barrels and mixed through a static mixer nozzle during administration. Furthermore, a self-assembling-peptide based (PeptiGel®) and two thermosensitive (supramolecular nucleoside and triblock copolymer, PLCL-PEG-PLCL, based) hydrogels were also evaluated.

None of the tested hydrogels were found to be stable in the IP fluid (with or without PLGA microspheres). They started disintegrating soon after coming in contact with the simulated IP fluid at 37 °C. Therefore, at this stage, it was decided to exclude hydrogels from the drug delivery system and carry on optimisation of the PLGA microspheres. However, during the hydrogel method evaluation work a unique approach was developed to improve the formation of alginate-calcium gel by an “internal gelation” mechanism. In this method, glucono delta-lactone was aged for at least 24 hours and kept separate from $CaCO_3$ until administration by using the double barrel syringe and static mixer nozzle. To our knowledge, we are reporting this method for the first time.

7.1.3 Optimisation of microfluidics methods for the manufacture of paclitaxel and carboplatin PLGA microspheres

The microfluidics single emulsion (O/W) method was further optimised by using a DOE (design of experiment) approach to obtain the microsphere size ($D_{0.5}$) as defined in the QTPP (50-200 μm). A two-step approach was adopted, in the first step, a DOE (regular two level full factorial design, 2^n) included total flow rate, aqueous to organic (A/O) flow rate ratio and PVA concentration as the independent variables at levels commonly reported in literature. The second DOE (a regular two-level fractional factorial design, 2^{n-1}) was then used to

evaluate tighter ranges of the above mentioned three independent variables based on the first DOE results. In addition, the PLGA concentration in the organic phase was also included in the second DOE because it is known to have an impact on the microsphere size.

Majority of the microspheres made during first DOE were much larger (90 – 800 μm) than the desired size range of 50 – 200 μm. In general, an increase in PVA concentration and decrease in the total flow rates resulted in a larger size, whereas, A/O flow rate ratio had minimal effect on the microsphere size. After tuning the independent variables in the second DOE, microspheres with the desired size range were successfully made. The PLGA concentration in organic phase and A/O flow rate ratio were found to be the most significant factors in second DOE. Their impact on size was dependent on each other i.e. at lower PLGA concentrations the A/O flow rate ratio had minimal impact whereas at higher PLGA concentrations an increase in the A/O flow ratio resulted in significant decrease in size.

Finally, the optimised conditions of 20 % w/w PLGA in organic phase, 0.5 % w/v PVA in aqueous phase, total flow rate of 200 μL/min and A/O flow rate ratio of 10 were selected to manufacture the paclitaxel and carboplatin PLGA microspheres.

For paclitaxel, the organic phase contained PLGA and paclitaxel dissolved in DCM and the aqueous phase contained 0.5 % PVA. Whereas, for carboplatin, an innovative modified single emulsion method was developed. To the best of our knowledge this carboplatin method has not been reported by anyone else. In this method, carboplatin was first wet-milled in non-aqueous media (PEG 200) to reduce the particle size to less than 1 μm, which was then dispersed in the organic phase to make a nanosuspension (solid in oil, S/O). This nanosuspension was then used as the modified organic phase. All other method conditions were the same as stated above.

The optimised methods resulted in 10 % w/w loading with 100 % w/w EE for paclitaxel and 6.4 % w/w loading with 64 % w/w EE for carboplatin. For both compounds, the microspheres size was ~100 μm.

This data demonstrated that we have successfully developed manufacturing methods for paclitaxel and carboplatin to achieve the target microsphere size

and drug loading as per the QTPP. In the next part of study, the release rates were optimised (section 7.1.4).

7.1.4 A strategy to tune the release rates from PLGA microspheres and determine the dosage regimen with the help of IP PK mathematical model

Following on from the successful development of manufacturing methods for paclitaxel and carboplatin PLGA microspheres by using microfluidics, a comprehensive strategy to tune the release rates and determine the dosage regimen was assessed in the final part of thesis.

In order to alter release rates, paclitaxel and carboplatin PLGA microspheres were manufactured by using four different grades of PLGA, two molecular weights (10 kDa and 50 kDa) and two lactide/glycolide ratios (50/50 and 75/25). In addition to standard methods for analysis of drug loading and release testing, selected samples were characterised by various advanced analytical techniques to fully understand the release behaviours e.g. ToF-SIMS to determine the presence of API on the surface and spatial distribution inside the microspheres, SEM to analyse the microsphere surface characteristics (i.e. porosity and smoothness), ESEM and EDS/EDX to determine the internal structure of the microsphere and determine the elemental composition by analysing the cross sections of microspheres.

The ToF-SIMS surface scanning data clearly shown that no API (carboplatin or paclitaxel) was present on the microspheres surface for any sample. While, the depth profile data of the bulk microspheres indicated that paclitaxel was homogenously distributed throughout the microsphere, whereas, carboplatin microspheres had negligible amount of drug near the surface and homogenous distribution towards the core of the microspheres.

ESEM images of the microsphere cross sections exposed high porosity near the surface of the carboplatin microspheres, whereas, no porosity was observed in the paclitaxel microspheres. Similar to ToF-SIMS data, the EDS/EDX also displayed homogenous distribution of carboplatin in the core of the microspheres and relatively less concentration near the surface. This data along with the physicochemical properties of the compounds i.e. paclitaxel poorly soluble and carboplatin soluble in water, explains the differences

between paclitaxel and carboplatin drug loading, indicating that carboplatin might have been lost from near the surface during the manufacturing and down-stream processes (microsphere cleaning and drying). In general, all the paclitaxel microspheres had close to 10 % w/w drug loading with approximately 100 % w/w EE, whereas, the best drug loading achieved for carboplatin was ~6 % w/w with approximately 60 % w/w EE.

For both compounds, the formulations made from three grades of PLGA (50/50 50 kDa, 75/25 10 kDa and 75/25 50 kDa) were found to be suitable for release testing. However, samples made from the PLGA grade 50/50 10 kDa (CF1 and PF1) could not be recovered after drying as they adhered together and to the vial, most likely due to the relatively low Tg of the polymer, therefore, release testing was not carried out for these samples.

For carboplatin, one formulation (CF3, PLGA 75/25 10 kDa) released all the payload rapidly, whereas, the other two formulations (CF2, PLGA 50/50 50 kDa and CF4, PLGA 75/25 50 kDa) showed a very similar sigmoidal release involving a lag (~ 6 days), bulk release (~ 32 days) and a plateau phase. For paclitaxel, all three formulations (PF2, PLGA 50/50 50 kDa; PF3, PLGA 75/25 10 kDa and PF4, PLGA 75/25 50 kDa) displayed sigmoidal release but with different durations of each phase. The lag phases for PF2 to PF4 were 13, 1 and 43 days and the bulk release phases were, 15, 19 and 24 days, respectively, see Figure 6-14.

The aim of this study was to develop a drug delivery system which can maintain therapeutic concentrations of paclitaxel and carboplatin in the IP cavity for 1 month or longer after a single dose. Therefore, carboplatin formulation CF2 and a combination of two paclitaxel formulations (PF2 and PF3) were selected for progression to the next steps based on the lag and bulk release phase durations. However, paclitaxel PF4 formulation was not selected due to a very long (43 days) lag phase. Although, the carboplatin CF4 formulation also had a similar release profile as CF2, the latter was preferred for progression because it contained the same polymer as one of the selected paclitaxel formulation (i.e. PF2). This allowed us to compare the release rates of both compounds to better understand the release mechanisms.

As described above (section 7.1.1), the initial IP PK mathematical model was based on the zero-order release kinetics from PLGA microspheres, whereas,

the experimental data for carboplatin and paclitaxel exhibited a non-linear (sigmoidal) release kinetics. Therefore, the model was adjusted to fit the experimental data and then used to select a dosage regimen of paclitaxel and carboplatin. The final model estimated a single dose of 330 mg of carboplatin PLGA microsphere formulation CF2 (with drug lading of 4.4 % w/w) for 28 days. Whereas, a dose of 0.96 mg was predicted for a blend of two paclitaxel formulations, PF2 and PF3 at a ratio of 46:54, respectively (both had a drug loading of ~ 10 % w/w), for a period of 23 days. The simulated data also showed that the intraperitoneal exposure of paclitaxel and carboplatin can also be maintained for several months by administering multiple doses at dosing intervals of 23 and 28 days, respectively.

7.2 Future Perspective

7.2.1 Improvements in carboplatin drug loading

The current drug delivery system fulfils the majority of the QTPP criteria and is considered suitable for in-vivo studies. However, carboplatin drug loading is still lower (4 to 6 % w/w) than the target value of 10 % w/w. Therefore, here we propose some improvement ideas.

The ESEM analysis revealed that the carboplatin PLGA microspheres had high porosity near the surface of the microspheres, whereas, ToF-SIMS and EDS/EDX data verified that the carboplatin concentration near the surface of the microspheres was lower compared to the core. These data sets indicate that the high porosity near the surface of microspheres could be one of the main causes for the lower carboplatin loading.

In addition, it is worth noting that the carboplatin formulation contained PEG 200, this was used to wet-mill the carboplatin to reduce the particle size to less than 1 μm. It is possible that PEG 200 might have a played a role in the high porosity near the surface of the carboplatin PLGA microspheres because PEG 200 has been reported as a pore former in the literature [196-198]. This is attributed to the miscibility of PEG 200 with PLGA and higher water solubility of PEG 200 which results in faster leaching out of PEG 200 from the microspheres during microsphere hardening (DCM removal) and drying process.

From these findings it would be worth considering the manufacture of carboplatin PLGA microspheres without PEG 200. This could be accomplished by washing out the PEG 200 with DCM after milling carboplatin in PEG 200 to reduce the particle size, since carboplatin is insoluble, whereas, PEG 200 is soluble in DCM. The “clean” carboplatin nanocrystals can then be suspended in the organic phase in same way as before.

7.2.2 In-vivo studies in rodents

A well designed in-vivo study in intraperitoneal rodent model (ideally, rats) can be performed next to evaluate the pharmacokinetic and pharmacodynamic behaviour of the final drug delivery system presented in this study. It has been reported [60,77,211] that PLGA microspheres may cause adhesions after intraperitoneal administration, however, some in-vivo data with the current PLGA microsphere based formulations developed in this study would be useful to determine; i) the IVIVC, ii) verify the biocompatibility of PLGA microspheres and iii) test the IP PK mathematical model. The in-vivo study results may suggest improvements in the drug delivery system and the IP PK model.
Meanwhile, other approaches to improve the biocompatibility of PLGA microspheres can be evaluated, for example;

- Implantable or in-situ forming, chemically cross linked hydrogels containing PLGA microspheres (e.g. cross-linked hyaluronic acid hydrogels[212], cross linked PEG hydrogels[213], etc)
- Surface modification of the PLGA microspheres with PEG e.g. by using small quantity (5 – 10 % w/w) of PEG-PLGA in the current formulations to provide the hydrophilic stealth[214,215] layer on the surface of microspheres, etc.

8 References

1 Wright, A. A. *et al.* Use and effectiveness of intraperitoneal chemotherapy for treatment of ovarian cancer. *J Journal of Clinical Oncology* **33**, 2841 (2015).

2 Monk, B. & Chan, J. Is intraperitoneal chemotherapy still an acceptable option in primary adjuvant chemotherapy for advanced ovarian cancer? *J Annals of Oncology* **28**, viii40-viii45 (2017).

3 Torre, L. A. *et al.* Ovarian cancer statistics, 2018. *J CA: a cancer journal for clinicians* **68**, 284-296 (2018).

4 Coburn, S., Bray, F., Sherman, M. E. & Trabert, B. International patterns and trends in ovarian cancer incidence, overall and by histologic subtype. *J International journal of cancer* **140**, 2451-2460 (2017).

5 Lugani, Y., Asthana, S. & Labani, S. Ovarian carcinoma: An overview of current status. *J Advances in Modern Oncology Research* **2**, 261-270 (2016).

6 Colombo, N. *et al.* ESMO–ESGO consensus conference recommendations on ovarian cancer: pathology and molecular biology, early and advanced stages, borderline tumours and recurrent disease. *J Annals of Oncology* **30**, 672-705 (2019).

7 Anon. *About ovarian cancer*, <http://www.ovcare.ca/about_ovarian_cancer/types_of_ovarian_cancer/> (Accessed January 2020).

8 Arnold, M. *et al.* Progress in cancer survival, mortality, and incidence in seven high-income countries 1995–2014 (ICBP SURVMARK-2): a population-based study. *J The Lancet Oncology* **20**, 1493-1505 (2019).

9 Siegel, R., Ma, J., Zou, Z. & Jemal, A. Cancer statistics, 2014. *CA: a cancer journal for clinicians* **64**, 9-29, doi:10.3322/caac.21208 (2014).

10 Landen, C. N., Birrer, M. J. & Sood, A. K. Early events in the pathogenesis of epithelial ovarian cancer. *Journal of Clinical Oncology* **26**, 995-1005, doi:10.1200/jco.2006.07.9970 (2008).

11 Prat, J., Gynecology & Obstetrics. Staging classification for cancer of the ovary, fallopian tube, and peritoneum. **124**, 1-5 (2014).

12 Naora, H. & Montell, D. J. Ovarian cancer metastasis: integrating insights from disparate model organisms. *Nature reviews. Cancer* **5**, 355-366, doi:10.1038/nrc1611 (2005).

13 Maathuis, J. B., Vanlook, P. F. A. & Michie, E. A. Changes in volume, total protein and ovarian steroid concentrations of peritoneal fluid throughout human menstrual-cycle. *Journal of Endocrinology* **76**, 123-133, doi:10.1677/joe.0.0760123 (1978).

14 Doherty, G. M. *Current Diagnosis and Treatment Surgery 14/E*. (McGraw Hill Professional, 2014).

15 Hartveit, F. & Thunold, S. Peritoneal fluid volume and oestrus cycle in mice. *Nature* **210**, 1123-1125 (1966).

16 Barni, S., Cabiddu, M., Ghilardi, M. & Petrelli, F. A novel perspective for an orphan problem: old and new drugs for the medical management of malignant ascites. *Critical Reviews in Oncology Hematology* **79**, 144-153, doi:10.1016/j.critrevonc.2010.07.016 (2011).

17 Lee, M. X. & Tan, D. S. Weekly versus 3-weekly paclitaxel in combination with carboplatin in advanced ovarian cancer: which is the optimal adjuvant chemotherapy regimen? *Journal of gynecologic oncology* **29** (2018).

18 American-Cancer-Society. *Treating Ovarian Cancer*, <https://www.cancer.org/cancer/ovarian-cancer/treating/by-stage.html> (Accessed January 2020).

19 Cancer-Research-UK. *Ovarian Cancer Treatment* <https://www.cancerresearchuk.org/about-cancer/ovarian-cancer/treatment/treatment-decisions> (Accessed January 2020).

20 Bajaj, G., Kim, M. R., Mohammed, S. I. & Yeo, Y. Hyaluronic acid-based hydrogel for regional delivery of paclitaxel to intraperitoneal tumors. *Journal of Controlled Release* **158**, 386-392 (2012).

21 Coleman, R. L., Monk, B. J., Sood, A. K. & Herzog, T. J. Latest research and treatment of advanced-stage epithelial ovarian cancer. *Nature Reviews Clinical Oncology* **10**, 211-224 (2013).

22 Herzog, T. J. & Pothuri, B. Ovarian cancer: a focus on management of recurrent disease. *Nature Clinical Practice Oncology* **3**, 604-611 (2006).

23 Mendelsohn, J., Moses, H. L. & Nass, S. J. *A national cancer clinical trials system for the 21st century: Reinvigorating the NCI Cooperative Group Program*. (National Academies Press, 2010).

24 Wang, D. & Lippard, S. J. Cellular processing of platinum anticancer drugs. *Nature Reviews Drug Discovery* **4**, 307-320 (2005).

25 Pignata, S. *et al.* Carboplatin plus paclitaxel once a week versus every 3 weeks in patients with advanced ovarian cancer (MITO-7): a randomised, multicentre, open-label, phase 3 trial. *The lancet oncology* **15**, 396-405 (2014).

26 Katsumata, N. *et al.* Dose-dense paclitaxel once a week in combination with carboplatin every 3 weeks for advanced ovarian cancer: a phase 3, open-label, randomised controlled trial. *The Lancet* **374**, 1331-1338 (2009).

27 Shawky, H., Tawfik, H. & Hewidy, M. Weekly dose-dense paclitaxel and carboplatin in recurrent ovarian carcinoma: A phase II trial. *Journal of the Egyptian National Cancer Institute* **26**, 139-145 (2014).

28 Sonoda, S. *et al.* Taxol-based eluting stents-from theory to human validation: clinical and intravascular ultrasound observations. *Journal Of Invasive Cardiology* **15**, 109-114 (2003).

29 Demetrick, J. S. *et al.* The development of a novel intraperitoneal tumor-seeding prophylactic. *Am. J. Surg.* **173**, 403-406 (1997).

30 Drugbank. *Paclitaxel (DB01229)*, <http://www.drugbank.ca/drugs/DB01229> (2014).

31 Whitaker, R. H. & Placzek, W. J. J. C. Regulating the BCL2 Family to Improve Sensitivity to Microtubule Targeting Agents. **8**, 346 (2019).

32 Di Pasqua, A. J., Goodisman, J. & Dabrowiak, J. C. Understanding how the platinum anticancer drug carboplatin works: From the bottle to the cell. *Inorganica Chimica Acta* **389**, 29-35 (2012).

33 Drugbank. *Carboplatin (DB00958)*, <http://www.drugbank.ca/drugs/DB00958> (2014).

34 Klein, A. V. & Hambley, T. W. Platinum-based anticancer agents. *Ligand Design in Medicinal Inorganic Chemistry*, 9-45 (2014).

35 Hall, M. D. *et al.* Say no to DMSO: Dimethylsulfoxide inactivates cisplatin, carboplatin and other platinum complexes. *Cancer Research* **74**, 3913-3922 (2014).

36 Harrap, K. Preclinical studies identifying carboplatin as a viable cisplatin alternative. *Cancer Treatment Reviews* **12**, 21-33 (1985).

37 Dunton, C. J. Management of treatment-related toxicity in advanced ovarian cancer. *J The oncologist* **7**, 11-19 (2002).

38 Mousavi, A. *et al.* The Role of Intraperitoneal Carboplatin as Consalidation Chemotherapy in Women with Ovarian Carcinoma: Report of Our Experience and Systematic Review. *J International journal of biomedical science* **12**, 120 (2016).

39 Cima, M. J. *et al.* Single compartment drug delivery. *Journal of Controlled Release* (2014).

40 Zhidkov, N., De Souza, R., Ghassemi, A. H., Allen, C. & Piquette-Miller, M. Continuous intraperitoneal carboplatin delivery for the treatment of late-stage ovarian cancer. *Molecular Pharmaceutics* **10**, 3315-3322 (2013).

41 Uhrich, K. E., Cannizzaro, S. M., Langer, R. S. & Shakesheff, K. M. Polymeric systems for controlled drug release. *Chemical reviews* **99**, 3181-3198 (1999).

42 Berchane, N. S. *Experimental and computational investigations of therapeutic drug release from biodegradable poly (lactide-co-glycolide)(plg) microspheres*, Texas A&M University, (2007).

43 Rothstein, S. N. & Little, S. R. A “tool box” for rational design of degradable controlled release formulations. *Journal of Materials Chemistry* **21**, 29-39 (2011).

44 Rippe, B. & Stelin, G. Simulations of peritoneal solute transport during CAPD. Application of two-pore formalism. *Kidney Int* **35**, 1234-1244 (1989).

45 Wolinsky, J. B., Colson, Y. L. & Grinstaff, M. W. Local drug delivery strategies for cancer treatment: gels, nanoparticles, polymeric films, rods, and wafers. *Journal of Controlled Release* **159**, 14-26 (2012).

46 Shackney, S. E., Mccormack, G. W. & Cuchural, G. J. Growth rate patterns of solid tumors and their relation to responsiveness to therapyan analytical review. *Annals of Internal Medicine* **89**, 107-121 (1978).

47 Meyer, J. S. Growth and cell kinetic measurements in human tumors. *Pathology Annual* **16**, 53 (1981).

48 Dedrick, R., Myers, C., Bungay, P. & DeVita Jr, V. Pharmacokinetic rationale for peritoneal drug administration in the treatment of ovarian cancer. *Cancer Treatment Reports* **62**, 1-11 (1978).

49 Markman, M. Intraperitoneal antineoplastic drug delivery: rationale and results. *The Lancet Oncology* **4**, 277-283 (2003).

50 Raja, F., Chopra, N. & Ledermann, J. Optimal first-line treatment in ovarian cancer. *Annals of Oncology* **23**, x118-x127 (2012).

51 Bajaj, G. & Yeo, Y. Drug delivery systems for intraperitoneal therapy. *Pharmaceutical Research* **27**, 735-738 (2010).

52 Lu, Z., Wang, J., Wientjes, M. G. & Au, J. L. Intraperitoneal therapy for peritoneal cancer. *Future Oncology* **6**, 1625-1641 (2010).

53 Markman, M. Intraperitoneal therapy of ovarian cancer. *The Oncologist* **1**, 18-21 (1996).

54 Goodman, M. D., McPartland, S., Detelich, D. & Saif, M. W. Chemotherapy for intraperitoneal use: a review of hyperthermic intraperitoneal chemotherapy and early post-operative intraperitoneal chemotherapy. *J Journal of gastrointestinal oncology* **7**, 45 (2016).

55 Van der Speeten, K., Stuart, O. A. & Sugarbaker, P. H. Pharmacology of perioperative intraperitoneal and intravenous chemotherapy in patients with peritoneal surface malignancy. *J Surgical Oncology Clinics* **21**, 577-597 (2012).

56 Alyami, M. *et al.* Pressurised intraperitoneal aerosol chemotherapy: rationale, evidence, and potential indications. *J The Lancet Oncology* **20**, 368-377 (2019).

57 Winkler, C. S. *et al.* Pressurized Intraperitoneal Aerosol Chemotherapy, a Palliative Treatment Approach for Patients With Peritoneal Carcinomatosis: Description of Method and Systematic Review of Literature. *Diseases of the Colon & Rectum* **63**, 242-255 (2020).

58 Sharma, A., Sharma, U. S. & Straubinger, R. M. Paclitaxel-liposomes for intracavitary therapy of intraperitoneal P388 leukemia. *J Cancer letters* **107**, 265-272 (1996).

59 Gelderblom, H. *et al.* Influence of Cremophor El on the bioavailability of intraperitoneal paclitaxel. *J Clinical Cancer Research* **8**, 1237-1241 (2002).

60 Kohane, D. S. *et al.* Biodegradable polymeric microspheres and nanospheres for drug delivery in the peritoneum. *Journal of Biomedical Materials Research Part A* **77**, 351-361 (2006).

61 Tsai, M. *et al.* Effects of carrier on disposition and antitumor activity of intraperitoneal paclitaxel. *Pharmaceutical Research* **24**, 1691-1701 (2007).

62 Lu, Z. *et al.* Tumor-penetrating microparticles for intraperitoneal therapy of ovarian cancer. *Journal of Pharmacology and Experimental Therapeutics* **327**, 673-682 (2008).

63 Hagiwara, A. *et al.* Prophylaxis with carbon-adsorbed mitomycin against peritoneal recurrence of gastric cancer. *J The Lancet Oncology* **339**, 629-631 (1992).

64 Ho, E. A., Soo, P. L., Allen, C. & Piquette-Miller, M. Impact of intraperitoneal, sustained delivery of paclitaxel on the expression of P-glycoprotein in ovarian tumors. *J Journal of controlled release* **117**, 20-27 (2007).

65 Grant, J., Blicker, M., Piquette-Miller, M. & Allen, C. Hybrid films from blends of chitosan and egg phosphatidylcholine for localized delivery of paclitaxel. *J Journal of pharmaceutical sciences* **94**, 1512-1527 (2005).

66 Zahedi, P., De Souza, R., Piquette-Miller, M. & Allen, C. Chitosan–phospholipid blend for sustained and localized delivery of docetaxel to the peritoneal cavity. *J International journal of pharmaceutics* **377**, 76-84 (2009).

67 Zentner, G. M. *et al.* Biodegradable block copolymers for delivery of proteins and water-insoluble drugs. *J Journal of controlled release* **72**, 203-215 (2001).

68 Han, F. Y., Thurecht, K. J., Whittaker, A. K. & Smith, M. T. Bioerodable PLGA-based microparticles for producing sustained-release drug formulations and strategies for improving drug loading. *J Frontiers in pharmacology* **7**, 185 (2016).

69 Mundargi, R. C., Babu, V. R., Rangaswamy, V., Patel, P. & Aminabhavi, T. M. Nano/micro technologies for delivering macromolecular therapeutics using poly (D, L-lactide-co-glycolide) and its derivatives. *Journal of Controlled Release* **125**, 193-209 (2008).

70 Zhong, H., Chan, G., Hu, Y., Hu, H. & Ouyang, D. A comprehensive map of FDA-approved pharmaceutical products. *J Pharmaceutics* **10**, 263 (2018).

71 Park, K. *et al.* Injectable, long-acting PLGA formulations: Analyzing PLGA and understanding microparticle formation. *J Journal of Controlled Release* **304**, 125-134 (2019).

72 Swider, E. *et al.* Customizing poly (lactic-co-glycolic acid) particles for biomedical applications. *J Acta biomaterialia* **73**, 38-51 (2018).

73 Whitesides, G. M. The origins and the future of microfluidics. *Nature* **442**, 368 (2006).

74 Nge, P. N., Rogers, C. I. & Woolley, A. T. Advances in microfluidic materials, functions, integration, and applications. *Chemical reviews* **113**, 2550-2583 (2013).

75 Hoare, T. R. & Kohane, D. S. Hydrogels in drug delivery: progress and challenges. *Polymer* **49**, 1993-2007 (2008).

76 Yeo, Y. & Kohane, D. S. Polymers in the prevention of peritoneal adhesions. *European Journal of Pharmaceutics and Biopharmaceutics* **68**, 57-66 (2008).

77 Zahedi, P. *Sustained intraperitoneal chemotherapy via an injectable depot delivery system for the treatment of ovarian cancer*, University of Toronto, (2012).

78 Kopecek, J. Hydrogels: From soft contact lenses and implants to self-assembled nanomaterials. *Journal of Polymer Science Part A: Polymer Chemistry* **47**, 5929-5946 (2009).

79 Mohammadi, M. *et al.* Injectable drug depot engineered to release multiple ophthalmic therapeutic agents with precise time profiles for postoperative treatment following ocular surgery. *J Acta biomaterialia* **73**, 90-102 (2018).

80 Steuperaert, M. *et al.* Mathematical modeling of intraperitoneal drug delivery: simulation of drug distribution in a single tumor nodule. *J Drug delivery* **24**, 491-501 (2017).

81 Engblom, P., Rantanen, V., Kulmala, J. & Grenman, S. Carboplatin-paclitaxel- and carboplatin-docetaxel-induced cytotoxic effect in epithelial ovarian carcinoma in vitro. *Cancer* **86**, 2066-2073 (1999).

82 Singh, P. P., Joshi, S., Russell, P. J., Nair, S. & Khatri, A. Purine Nucleoside Phosphorylase mediated molecular chemotherapy and conventional chemotherapy: A tangible union against chemoresistant cancer. *BMC Cancer* **11** (2011).

83 Cordes, N. & Plasswilm, L. Cell line and schedule-dependent cytotoxicity of paclitaxel (Taxol (R)): Role of the solvent cremophor EL/ethanol. *Anticancer Research* **18**, 1851-1857 (1998).

84 Smith, J. A., Ngo, H., Martin, M. C. & Wolf, J. K. An evaluation of cytotoxicity of the taxane and platinum agents combination treatment in a panel of human ovarian carcinoma cell lines. *Gynecologic Oncology* **98**, 141-145 (2005).

85 Domcke, S., Sinha, R., Levine, D. A., Sander, C. & Schultz, N. Evaluating cell lines as tumour models by comparison of genomic profiles. *Nature Communications* **4** (2013).

86 Yuan, Y., Liao, Y.-M., Hsueh, C.-T. & Mirshahidi, H. R. Novel targeted therapeutics: inhibitors of MDM2, ALK and PARP. *J Hematol Oncol* **4**, 16 (2011).

87 Kroemer, G. *et al.* Classification of cell death: recommendations of the nomenclature committee on cell death. *Cell Death & Differentiation* **12**, 1463-1467 (2005).

88 Kepp, O., Galluzzi, L., Lipinski, M., Yuan, J. & Kroemer, G. Cell death assays for drug discovery. *Nature Reviews Drug Discovery* **10**, 221-237 (2011).

89 Riss, T. *et al.* Eli Lilly & Company and the National Center for Advancing Translational Sciences, (2013).

90 Roth, B. L., Poot, M., Yue, S. T. & Millard, P. J. Bacterial viability and antibiotic susceptibility testing with SYTOX green nucleic acid stain. *Applied and Environmental Microbiology* **63**, 2421-2431 (1997).

91 Anon. *Chapter 15_Assays for cell viability, proliferation and function*, <http://www.lifetechnologies.com/uk/en/home/references/molecular-probes-the-handbook.html> (Accessed December 2014).

92 Galluzzi, L. *et al.* Guidelines for the use and interpretation of assays for monitoring cell death in higher eukaryotes. *Cell Death & Differentiation* **16**, 1093-1107 (2009).

93 Riss, T., Moravec, R. & Niles, A. Selecting cell-based assays for drug discovery screening. *Cell Notes* **13**, 16-21 (2005).

94 McClay, E. *et al.* A phase I and pharmacokinetic study of intraperitoneal carboplatin and etoposide. *J British journal of cancer* **68**, 783 (1993).

95 Raja, V. J., Lim, K.-H., Leong, C.-O., Kam, T.-S. & Bradshaw, T. D. Novel antitumour indole alkaloid, Jerantinine A, evokes potent G2/M cell cycle arrest targeting microtubules. *Investigational New Drugs* **32**, 838-850 (2014).

96 Tallarida, R. J. Quantitative methods for assessing drug synergism. *Genes & Cancer* **2**, 1003-1008 (2011).

97 Straetemans, R. *et al.* Design and analysis of drug combination experiments. *Biometrical Journal* **47**, 299-308 (2005).

98 Chan, R. W. S., Ng, E. H. Y. & Yeung, W. S. B. Identification of cells with colony-forming activity, self-renewal capacity, and multipotency in ovarian endometriosis. *J The American journal of pathology* **178**, 2832-2844 (2011).

99 Witham, J., Vidot, S., Agarwal, R., Kaye, S. B. & Richardson, A. Transient ectopic expression as a method to detect genes conferring drug resistance. *International Journal of Cancer* **122**, 2641-2645 (2008).

100 Liebmann, J. *et al.* Cytotoxic studies of paclitaxel (Taxol) in human tumour cell lines. *British journal of cancer* **68**, 1104 (1993).

101 Berenbaum, M. C. What is synergy? *Pharmacological reviews* **41**, 93-141 (1989).

102 Geary, N. Understanding synergy. *American Journal of Physiology-Endocrinology and Metabolism* **304**, E237-E253 (2013).

103 Xiong, X., Sui, M., Fan, W. & Kraft, A. S. Cell-cycle dependent antagonistic interactions between paclitaxel and carboplatin in combination therapy. *Cancer biology & therapy* **6**, 1067-1073 (2007).

104 Grizzi, I., Garreau, H., Li, S. & Vert, M. Hydrolytic degradation of devices based on poly (DL-lactic acid) size-dependence. *Biomaterials* **16**, 305-311 (1995).

105 Anderson, J. M. & Shive, M. S. Biodegradation and biocompatibility of PLA and PLGA microspheres. *Advanced Drug Delivery Reviews* **64**, 72-82 (2012).

106 Spenlehauer, G., Vert, M., Benoit, J. & Boddaert, A. In vitro and in vivo degradation of poly (D, L lactide/glycolide) type microspheres made by solvent evaporation method. *Biomaterials* **10**, 557-563 (1989).

107 Hawk, C. T. *Administration of drugs and experimental compounds in mice and rats*, <http://www.bu.edu/orccommittees/iacuc/policies-and-guidelines/administration-of-drugs-and-experimental-compounds-in-mice-and-rats/> (Accessed June 2014).

108 Schwendeman, S. P., Shah, R. B., Bailey, B. A. & Schwendeman, A. S. Injectable controlled release depots for large molecules. *Journal of Controlled Release* **190**, 240-253 (2014).

109 Makadia, H. K. & Siegel, S. J. Poly lactic-co-glycolic acid (PLGA) as biodegradable controlled drug delivery carrier. *Polymers* **3**, 1377-1397 (2011).

110 Giri, T. K., Choudhary, C., Alexander, A., Badwaik, H. & Tripathi, D. K. Prospects of pharmaceuticals and biopharmaceuticals loaded microparticles prepared by double emulsion technique for controlled delivery. *Saudi Pharmaceutical Journal* **21**, 125-141 (2013).

111 Davies, O. R. *et al.* Surface modification of microspheres with steric stabilizing and cationic polymers for gene delivery. *Langmuir* **24**, 7138-7146 (2008).

112 Qi, F. *et al.* Preparation of uniform-sized exenatide-loaded PLGA microspheres as long-effective release system with high encapsulation efficiency and bio-stability. *Colloids and Surfaces B: Biointerfaces* **112**, 492-498 (2013).

113 Xu, Q. *et al.* Preparation of monodisperse biodegradable polymer microparticles using a microfluidic flow-focusing device for controlled drug delivery. *Small* **5**, 1575-1581 (2009).

114 Liggins, R. T., D'Amours, S., Demetrick, J. S., Machan, L. S. & Burt, H. M. Paclitaxel loaded poly(L-lactic acid) microspheres for the prevention of intraperitoneal carcinomatosis after a surgical repair and tumor cell spill. *Biomaterials* **21**, 1959-1969 (2000).

115 Jalil, R. & Nixon, J. Microencapsulation using poly (L-lactic acid) I: microcapsule properties affected by the preparative technique. *Journal of Microencapsulation* **6**, 473-484 (1989).

116 Zhou, G. & Kresta, S. M. Correlation of mean drop size and minimum drop size with the turbulence energy dissipation and the flow in an agitated tank. *Chemical Engineering Science* **53**, 2063-2079 (1998).

117 The-Dolomite-Microfluidics. *Droplet chips user instructions*, <http://www.dolomitemicrofluidics.com/images/stories/PDFs/user_guides_and_manuals/droplet_chips_user_instructions_doc.pdf> (Accessed January 2020).

118 Abdulkin, P., Drobot, M. & Nappo, V. *Continuous Microfluidic Synthesis of PLGA Microparticles by Droplet Method*, <file:///C:/Users/mpb274q/Downloads/AppNote_Continuous_Microfluidic_Synthesis_of_PLGA_Microparticles_by_Droplet_Method_%20(1).pdf> (Accessed Hanuary 2020).

119 Allison, S. D. Analysis of initial burst in PLGA microparticles. *Expert Opinion on Drug Delivery* **5**, 615-628 (2008).

120 Kim, H. K., Chung, H. J. & Park, T. G. Biodegradable polymeric microspheres with “open/closed” pores for sustained release of human growth hormone. *Journal of Controlled Release* **112**, 167-174 (2006).

121 Kim, H. K., Lee, K. H., Oh, J.-G. & Lee, B.-Y. Method for preparing microparticles with reduced initial burst and microparticles prepared thereby. United States patent US 2014/0072531 A1 (2013).

122 Bouissou, C., Rouse, J., Price, R. & Van der Walle, C. The influence of surfactant on PLGA microsphere glass transition and water sorption: remodeling the surface morphology to attenuate the burst release. *Pharmaceutical Research* **23**, 1295-1305 (2006).

123 Allison, S. D. Effect of structural relaxation on the preparation and drug release behavior of poly (lactic-co-glycolic) acid microparticle drug delivery systems. *Journal of Pharmaceutical Sciences* **97**, 2022-2035 (2008).

124 Petrov, O. *et al.* Pore size distributions of biodegradable polymer microparticles in aqueous environments measured by NMR cryoporometry. *International journal of pharmaceutics* **309**, 157-162 (2006).

125 Mittal, A., Chitkara, D. & Kumar, N. HPLC method for the determination of carboplatin and paclitaxel with cremophorEL in an amphiphilic polymer matrix. *Journal of Chromatography B* **855**, 211-219 (2007).

126 Gust, R. & Schnurr, B. Investigations on the stability of carboplatin infusion solutions. *Monatshefte für Chemie/Chemical Monthly* **130**, 637-644 (1999).

127 Villarino, N., Cox, S., Yarbrough, J. & Martín-Jiménez, T. Determination of carboplatin in canine plasma by high-performance liquid chromatography. *Biomedical Chromatography* **24**, 908-913 (2010).

128 Buszewski, B. & Noga, S. Hydrophilic interaction liquid chromatography (HILIC)—a powerful separation technique. *Analytical and Bioanalytical Chemistry* **402**, 231-247 (2012).

129 Peppas, N., Bures, P., Leobandung, W. & Ichikawa, H. Hydrogels in pharmaceutical formulations. *European Journal of Pharmaceutics and Biopharmaceutics* **50**, 27-46 (2000).

130 Lin, C.-C. & Metters, A. T. Hydrogels in controlled release formulations: network design and mathematical modeling. *Advanced Drug Delivery Reviews* **58**, 1379-1408 (2006).

131 Roberts, M. C. *New in situ crosslinking chemistries for hydrogelation*. (ProQuest, 2008).

132 Yeo, Y., Bellas, E., Highley, C. B., Langer, R. & Kohane, D. S. Peritoneal adhesion prevention with an in situ cross-linkable hyaluronan gel containing tissue-type plasminogen activator in a rabbit repeated-injury model. *Biomaterials* **28**, 3704-3713 (2007).

133 Lowman, A. M. & Peppas, N. A. Hydrogels. *Encyclopedia of Controlled Drug Delivery* **1**, 397-418 (1999).

134 Narayanaswamy, R. & Torchilin, V. P. Hydrogels and their applications in targeted drug delivery. *J Molecules* **24**, 603 (2019).

135 Buwalda, S. J. *et al.* Hydrogels in a historical perspective: From simple networks to smart materials. *J Journal of controlled release* **190**, 254-273 (2014).

136 Shinde, U. P., Yeon, B. & Jeong, B. Recent progress of in situ formed gels for biomedical applications. *J Progress in polymer science* **38**, 672-701 (2013).

137 Tang, C., Miller, A. F. & Saiani, A. Peptide hydrogels as mucoadhesives for local drug delivery. *J International journal of pharmaceutics* **465**, 427-435 (2014).

138 Manchester-BIOGEL. *PeptiGels*, <https://manchesterbiogel.com/> (Accessed January 2020).

139 Schmitt, A. *et al.* Calcium alginate gels as stem cell matrix–making paracrine stem cell activity available for enhanced healing after surgery. *J PloS one* **10**, e0118937 (2015).

140 Draget, K. I., Østgaard, K. & Smidsrød, O. Homogeneous alginate gels: A technical approach. *J Carbohydrate polymers* **14**, 159-178 (1990).

141 Ellervik, U., Sterner, O., Strevens, H. & Manner, S. (Google Patents, 2019).

142 Filion, D., Lavertu, M. & Buschmann, M. D. Ionization and solubility of chitosan solutions related to thermosensitive chitosan/glycerol-phosphate systems. *J Biomacromolecules* **8**, 3224-3234 (2007).

143 Štaka, I. *Novel gel-associated drug loaded nanocarriers for intratumoural delivery*, University of Nottingham, (2018).

144 Teh, S.-Y., Lin, R., Hung, L.-H. & Lee, A. P. Droplet microfluidics. *Lab on a Chip* **8**, 198-220 (2008).

145 Shah, R. K. *et al.* Designer emulsions using microfluidics. *Materials Today* **11**, 18-27 (2008).

146 Zhu, P. & Wang, L. Passive and active droplet generation with microfluidics: a review. *Lab on a Chip* **17**, 34-75 (2017).

147 Shang, L., Cheng, Y. & Zhao, Y. Emerging Droplet Microfluidics. *Chemical Reviews* (2017).

148 Wang, Y. M., Sato, H., Adachi, I. & Horikoshi, I. Preparation and characterization of poly (lactic-co-glycolic acid) microspheres for targeted delivery of a novel anticancer agent, taxol. *Chemical and pharmaceutical bulletin* **44**, 1935-1940 (1996).

149 Dordunoo, S. K. *et al.* (ACS Publications, 2006).

150 Jackson, J. K., Hung, T., Letchford, K. & Burt, H. M. The characterization of paclitaxel-loaded microspheres manufactured from blends of poly (lactic-co-glycolic acid)(PLGA) and low molecular weight diblock copolymers. *International journal of pharmaceutics* **342**, 6-17 (2007).

151 Acharya, G. *et al.* A study of drug release from homogeneous PLGA microstructures. *Journal of Controlled Release* **146**, 201-206 (2010).

152 Mittal, A., Kurapati, P., Chitkara, D. & Kumar, N. In vitro release behavior of paclitaxel and carboplatin from poly (l-lactide) microspheres dispersed in thermosensitive biodegradable gel for combination therapy. *International Journal of Drug Delivery* **3**, 245 (2011).

153 Lu, B., Zhang, J. & Yang, H. Lung-targeting microspheres of carboplatin. *International journal of pharmaceutics* **265**, 1-11 (2003).

154 Gavini, E., Manunta, L., Giua, S., Achenza, G. & Giunchedi, P. Spray-dried poly (D, L-lactide) microspheres containing carboplatin for veterinary use: in vitro and in vivo studies. *AAPS PharmSciTech* **6**, E108-E114 (2005).

155 Amoyav, B. & Benny, O. Controlled and tunable polymer particles' production using a single microfluidic device. *J Applied Nanoscience* **8**, 905-914 (2018).

156 Fu, T., Wu, Y., Ma, Y. & Li, H. Z. Droplet formation and breakup dynamics in microfluidic flow-focusing devices: from dripping to jetting. *J Chemical engineering science* **84**, 207-217 (2012).

157 Rezvantalab, S. & Moraveji, M. K. Microfluidic assisted synthesis of PLGA drug delivery systems. *J RSC advances* **9**, 2055-2072 (2019).

158 Carugo, D., Bottaro, E., Owen, J., Stride, E. & Nastruzzi, C. Liposome production by microfluidics: potential and limiting factors. *J Scientific reports* **6**, 25876 (2016).

159 Correia, M. G. S., Briuglia, M. L., Niosi, F. & Lamprou, D. A. Microfluidic manufacturing of phospholipid nanoparticles: Stability, encapsulation efficacy, and drug release. *J International journal of pharmaceutics* **516**, 91-99 (2017).

160 Hussain, M. *et al.* Regulation of drug release by tuning surface textures of biodegradable polymer microparticles. *J ACS applied materials* **9**, 14391-14400 (2017).

161 Tsai, M., Lu, Z., Wientjes, M. G. & Au, J. L.-S. Paclitaxel-loaded polymeric microparticles: quantitative relationships between in vitro drug release rate and in vivo pharmacodynamics. *Journal of controlled release* **172**, 737-744 (2013).

162 Chen, W. & Lu, D. Carboplatin-loaded PLGA microspheres for intracerebral injection: formulation and characterization. *J Journal of microencapsulation* **16**, 551-563 (1999).

163 Chen, W., He, J., Olson, J. J. & Lu, D. R. Carboplatin-loaded PLGA microspheres for intracerebral implantation: in vivo characterization. *J Drug delivery* **4**, 301-311 (1997).

164 Martins, K. F., Messias, A. D., Leite, F. L. & Duek, E. A. Preparation and characterization of paclitaxel-loaded PLDLA microspheres. *Materials Research* **17**, 650-656 (2014).

165 Brostow, W., Chiu, R., Kalogeras, I. M. & Vassilikou-Dova, A. Prediction of glass transition temperatures: binary blends and copolymers. *Materials Letters* **62**, 3152-3155 (2008).

166 Santa-Cruz-Biotechnology. *Carboplatin (CAS 41575-94-4)*, <https://www.scbt.com/p/carboplatin-41575-94-4?requestFrom=search> (Accessed January 2020).

167 Berkland, C., Kim, K. K. & Pack, D. W. PLG microsphere size controls drug release rate through several competing factors. *Pharmaceutical research* **20**, 1055-1062 (2003).

168 Berkland, C., King, M., Cox, A., Kim, K. K. & Pack, D. W. Precise control of PLG microsphere size provides enhanced control of drug release rate. *Journal of controlled release* **82**, 137-147 (2002).

169 Berkland, C. *et al.* Macromolecule release from monodisperse PLG microspheres: control of release rates and investigation of release mechanism. *Journal of pharmaceutical sciences* **96**, 1176-1191 (2007).

170 Klose, D., Siepmann, F., Elkharraz, K., Krenzlin, S. & Siepmann, J. How porosity and size affect the drug release mechanisms from PLGA-based microparticles. *J International journal of pharmaceutics* **314**, 198-206 (2006).

171 Berchane, N., Jebrail, F. & Andrews, M. Optimization of PLG microspheres for tailored drug release. *J International journal of pharmaceutics* **383**, 81-88 (2010).

172 D'Souza, S., Faraj, J. & DeLuca, P. Microsphere delivery of Risperidone as an alternative to combination therapy. *European J of Pharmaceutics and Biopharmaceutics,* **85**, 631-639 (2013).

173 Jain, R. A., Rhodes, C. T., Railkar, A. M., Malick, A. W. & Shah, N. Controlled release of drugs from injectable in situ formed biodegradable PLGA microspheres: effect of various formulation variables. *J European Journal of Pharmaceutics and Biopharmaceutics* **50**, 257-262 (2000).

174 Tracy, M. *et al.* Factors affecting the degradation rate of poly (lactide-co-glycolide) microspheres in vivo and in vitro. *J Biomaterials* **20**, 1057-1062 (1999).

175 Gadad, A., Vannuruswamy, G., Sharath Chandra, P., Dandagi, P. & Mastiholimath, V. Study of different properties and applications of poly lactic-coglycolic acid (PLGA) nanotechnology: an overview. *J Indian drugs* **49**, 5-22 (2012).

176 Li, S. Hydrolytic degradation characteristics of aliphatic polyesters derived from lactic and glycolic acids. *Journal of Biomedical Materials Research* **48**, 342-353 (1999).

177 Vert, M., Mauduit, J. & Li, S. Biodegradation of PLA/GA polymers: increasing complexity. *Biomaterials* **15**, 1209-1213 (1994).

178 Kamei, S. *et al.* New method for analysis of biodegradable polyesters by high-performance liquid chromatography after alkali hydrolysis. *J Biomaterials* **13**, 953-958 (1992).

179 Pavot, V. *et al.* Poly (lactic acid) and poly (lactic-co-glycolic acid) particles as versatile carrier platforms for vaccine delivery. *J Nanomedicine* **9**, 2703-2718 (2014).

180 Mohammed, A., Weston, N., Coombes, A., Fitzgerald, M. & Perrie, Y. Liposome formulation of poorly water soluble drugs: optimisation of drug loading and ESEM analysis of stability. *J International journal of pharmaceutics* **285**, 23-34 (2004).

181 D'Emanuele, A. & Dinarvand, R. Preparation, characterisation, and drug release from thermoresponsive microspheres. *J International journal of pharmaceutics* **118**, 237-242 (1995).

182 Balfe, A. *et al.* (2013).

183 diZerega, G. S. & Rodgers, K. E. in *The Peritoneum* 26-56 (Springer New York, 1992).

184 Kelton, J., Ulan, R., Stiller, C. & Holmes, E. Comparison of chemical composition of peritoneal fluid and serum: a method for monitoring dialysis patients and a tool for assessing binding to serum proteins in vivo. *J Annals of internal medicine* **89**, 67-70 (1978).

185 Posiseeva, L., Gerasimov, A., Shokhina, M. & Kuz'menko, G. Magnesium and calcium ion levels in peritoneal fluid of healthy fertile women. *J Klinicheskaia laboratornaia diagnostika*, 21-23 (2001).

186 Anon. *Normal Blood Calcium Levels*, <https://www.parathyroid.com/Normal-Blood-Calcium-Levels.htm> (2018).

187 Anon. *Serum total protein*, <https://en.wikipedia.org/wiki/Serum_total_protein> (Accessed October 2019).

188 Food-and-Drug-Administration. *Investigations Operations Manual 2019. Appendix C*, <https://www.fda.gov/media/113432/download> (Accessed January 2020).

189 Guidelines-In-Practice-UK. *Plasma protein tests: how to interpret abnormal results*, <https://www.guidelinesinpractice.co.uk/liver-disease/plasma-protein-tests-how-to-interpret-abnormal-results/454286.article> (Accessed January 2020).

190 Navaei, A., Rasoolian, M., Momeni, A., Emami, S. & Rafienia, M. Double-walled microspheres loaded with meglumine antimoniate: preparation, characterization and in vitro release study. *J Drug Dev and Ind Pharmacy,* **40**, 701-710 (2014).

191 Mohan, S. *et al.* Incorporation of Human-Platelet-Derived Growth Factor-BB Encapsulated Poly (lactic-co-glycolic acid) Microspheres into 3D CORAGRAF Enhances Osteogenic Differentiation of Mesenchymal Stromal Cells. *J ACS App Mat and Interfaces,* **9**, 9291-9303 (2017).

192 Xu, Q., Crossley, A. & Czernuszka, J. Preparation and characterization of negatively charged poly (lactic-co-glycolic acid) microspheres. *J Journal of pharmaceutical sciences* **98**, 2377-2389 (2009).

193 Encarnação, I. C. *et al.* Release of simvastatin from scaffolds of poly (lactic-co-glycolic) acid and biphasic ceramic designed for bone tissue regeneration. *J Journal of Biomedical Materials Research Part B: Applied Biomaterials* **107**, 2152-2164 (2019).

194 Pimenta de Melo, L. *et al.* Thermomechanical and in vitro biological characterization of injection-molded PLGA craniofacial plates. *J of App Biomaterials and Functional Materials,* **17**, 2280800019831599 (2019).

195 Liao, Y. *Practical Electron Microscopy and Database - An Online Book*. (Accessed Januray 2020).

196 Krok, M. *et al.* Manufacturing and characterization of resorbable PLGA membranes for biomedical applications. *J Engineering of Biomaterials* **14**, 8--13 (2011).

197 Du, H., Bandara, S., Carson, L. E. & Kommalapati, R. R. in *Polyethylene Glycol* (IntechOpen, 2019).

198 Lee, S. Y. *et al.* in *Key Engineering Materials.* 485-488 (Trans Tech Publ).

199 Zhang, Z. *et al.* Paclitaxel-loaded PLGA microspheres with a novel morphology to facilitate drug delivery and antitumor efficiency. *J RSC advances* **8**, 3274-3285 (2018).

200 Meeus, J. *et al.* The influence of spray-drying parameters on phase behavior, drug distribution, and in vitro release of injectable microspheres for sustained release. *J Journal of pharmaceutical sciences* **104**, 1451-1460 (2015).

201 Rafati, A. *et al.* Chemical and spatial analysis of protein loaded PLGA microspheres for drug delivery applications. *J Journal of controlled release* **162**, 321-329 (2012).

202 Fisher, G. L., Belu, A. M., Mahoney, C. M., Wormuth, K. & Sanada, N. Three-dimensional time-of-flight secondary ion mass spectrometry imaging of a pharmaceutical in a coronary stent coating as a function of elution time. *J Analytical chemistry* **81**, 9930-9940 (2009).

203 van Hove, E. R. A., Smith, D. F. & Heeren, R. M. A concise review of mass spectrometry imaging. *J Journal of chromatography A* **1217**, 3946-3954 (2010).

204 Chan, C. M. & Weng, L.-T. Surface characterization of polymer blends by XPS and ToF-SIMS. *J Materials* **9**, 655 (2016).

205 Siegel, S. J. *et al.* Effect of drug type on the degradation rate of PLGA matrices. *J European Journal of Pharmaceutics and Biopharmaceutics* **64**, 287-293 (2006).

206 Gasmi, H., Danede, F., Siepmann, J. & Siepmann, F. Does PLGA microparticle swelling control drug release? New insight based on single particle swelling studies. *Journal of Controlled Release* **213**, 120-127 (2015).

207 O'Donnell, P. B. & McGinity, J. W. Preparation of microspheres by the solvent evaporation technique. *Advanced drug delivery reviews* **28**, 25-42 (1997).

208 Fredenberg, S., Wahlgren, M., Reslow, M. & Axelsson, A. The mechanisms of drug release in poly (lactic-co-glycolic acid)-based drug delivery systems—a review. *International journal of pharmaceutics* **415**, 34-52 (2011).

209 Sansdrap, P. & Moes, A. In vitro evaluation of the hydrolytic degradation of dispersed and aggregated poly (DL-lactide-co-glycolide) microspheres. *Journal of controlled release* **43**, 47-58 (1997).

210 Kim, K. K. & Pack, D. W. in *BioMEMS and biomedical nanotechnology* 19-50 (Springer, 2006).

211 Kohane, D. S. & Langer, R. Biocompatibility and drug delivery systems. *J Chemical Science* **1**, 441-446 (2010).

212 Yeo, Y. *et al.* In situ cross-linkable hyaluronic acid hydrogels prevent post-operative abdominal adhesions in a rabbit model. *J Biomaterials* **27**, 4698-4705 (2006).

213 Liu, S. *et al.* Effects of the proportion of two different cross-linkers on the material and biological properties of enzymatically degradable PEG hydrogels. *J Polymer Degradation and Stability*, 109067 (2020).

214 Butcher, N. J., Mortimer, G. M. & Minchin, R. F. Drug delivery: Unravelling the stealth effect. *J Nature nanotechnology* **11**, 310 (2016).

215 Shalgunov, V. *et al.* Comprehensive study of the drug delivery properties of poly (l-lactide)-poly (ethylene glycol) nanoparticles in rats and tumor-bearing mice. *J Journal of Controlled Release* **261**, 31-42 (2017).

216 Prestwich, G. D. & Vercruysse, K. P. Profiles therapeutic applications of hyaluronic acid and hyaluronan derivatives. *Pharmaceutical Science & Technology Today* **1**, 42-43 (1998).

217 Necas, J., Bartosikova, L., Brauner, P. & Kolar, J. Hyaluronic acid (hyaluronan): a review. *Veterinarni Medicina* **53**, 397-411 (2008).

218 Garg, H. G. & Hales, C. A. *Chemistry and biology of hyaluronan*. (Elsevier, 2004).

219 Cowman, M. K. & Matsuoka, S. Experimental approaches to hyaluronan structure. *Carbohydrate Research* **340**, 791-809 (2005).

220 Chao, K. L., Muthukumar, L. & Herzberg, O. Structure of human hyaluronidase-1, a hyaluronan hydrolyzing enzyme involved in tumor growth and angiogenesis. *Biochemistry* **46**, 6911-6920 (2007).

221 Sigma-Aldrich. *What is Hyaluronan ?*, <http://www.sigmaaldrich.com/life-science/stem-cell-biology/3d-stem-cell-culture/learning-center/what-is-hyaluronan.printerview.html> (Accessed March 2015).

222 Hejazi, R. & Amiji, M. Chitosan-based gastrointestinal delivery systems. *Journal of Controlled Release* **89**, 151-165 (2003).

223 Rinaudo, M. Chitin and chitosan: properties and applications. *Progress in Polymer Science* **31**, 603-632 (2006).

224 Rusu-Balaita, L., Desbrieres, J. & Rinaudo, M. Formation of a biocompatible polyelectrolyte complex: chitosan-hyaluronan complex stability. *Polymer Bulletin* **50**, 91-98 (2003).

225 Vasiliu, S., Popa, M. & Rinaudo, M. Polyelectrolyte capsules made of two biocompatible natural polymers. *European Polymer Journal* **41**, 923-932 (2005).

226 Tønnesen, H. H. & Karlsen, J. Alginate in drug delivery systems. *Drug Development and Industrial Pharmacy* **28**, 621-630 (2002).

227 George, M. & Abraham, T. E. Polyionic hydrocolloids for the intestinal delivery of protein drugs: Alginate and chitosan - a review. *Journal of Controlled Release* **114**, 1-14 (2006).

228 Cole, D. R., Waterfall, M., McIntyre, M. & Baird, J. D. Microencapsulated islet grafts in the bb/e rat - a possible role for cytokines in graft failure. *Diabetologia* **35**, 231-237 (1992).

229 DeVos, P., DeHaan, B., Pater, J. & VanSchilfgaarde, R. Association between capsule diameter, adequacy of encapsulation, and survival of microencapsulated rat islet allografts. *Transplantation* **62**, 893-899 (1996).

230 Zimmermann, U. *et al.* Production of mitogen-contamination free alginates with variable ratios of mannuronic acid to guluronic acid by free-flow electrophoresis. *Electrophoresis* **13**, 269-274 (1992).

231 Grant, G. T., Morris, E. R., Rees, D. A., Smith, P. J. & Thom, D. Biological interactions between polysaccharides and divalent cations: the egg-box model. *FEBS letters* **32**, 195-198 (1973).

232 McHugh, D. J. Production and utilization of products from commercial seaweeds. 189 (1987).

233 Munarin, F., Tanzi, M. C. & Petrini, P. Advances in biomedical applications of pectin gels. *J International journal of biological macromolecules* **51**, 681-689 (2012).

234 Müller-Maatsch, J. *et al.* Pectin content and composition from different food waste streams. *J Food chemistry* **201**, 37-45 (2016).

235 Joshi, N., Rawat, K. & Bohidar, H. Influence of Structure, Charge, and Concentration on the Pectin–Calcium–Surfactant Complexes. *J The Journal of Physical Chemistry B* **120**, 4249-4257 (2016).

236 Sundar Raj, A., Rubila, S., Jayabalan, R. & Ranganathan, T. A Review on Pectin: Chemistry due to General Properties of Pectin and its Pharmaceutical Uses. . *Open Access Scientific Reports* **1**, 1-4 (2012).

237 May, C. D. Industrial pectins: sources, production and applications. *J Carbohydrate polymers* **12**, 79-99 (1990).

238 Lootens, D. *et al.* Influence of pH, Ca concentration, temperature and amidation on the gelation of low methoxyl pectin. *J Food hydrocolloids* **17**, 237-244 (2003).

239 Dordunoo, S. K. & Burt, H. M. Solubility and stability of taxol: effects of buffers and cyclodextrins. *J International Journal of Pharmaceutics* **133**, 191-201 (1996).

240 Hutchinson, F. & Furr, B. Biodegradable polymer systems for the sustained release of polypeptides. *J Journal of Controlled Release* **13**, 279-294 (1990).

9 Appendices

Appendix A Monotherapy and combination therapy dosing matrix

Monotherapy matrix (duplicate)

Paclitaxel		Carboplatin	
1-A1	1-A1	1-B1	1-B1
1-A2	1-A2	1-B2	1-B2
1-A3	1-A3	1-B3	1-B3
1-A4	1-A4	1-B4	1-B4
1-A5	1-A5	1-B5	1-B5
1-A6	1-A6	1-B6	1-B6
1-A7	1-A7	1-B7	1-B7

Combination therapy matrix (duplicate)

Paclitxel →

Carboplatin ↓

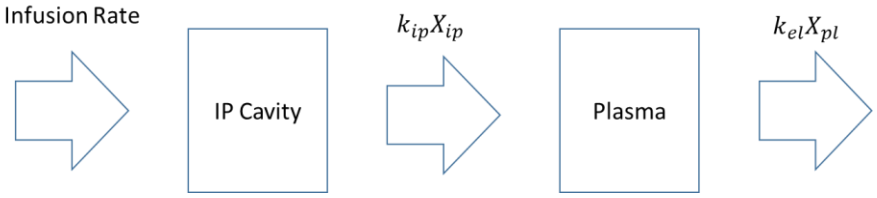
1-A1-B1	1-A1-B1	1-A2-B1	1-A2-B1	1-A3-B1	1-A3-B1	1-A4-B1	1-A4-B1	1-A5-B1	1-A5-B1	1-A6-B1	1-A6-B1	1-A7-B1	1-A7-B1
1-A1-B2	1-A1-B2	1-A2-B2	1-A2-B2	1-A3-B2	1-A3-B2	1-A4-B2	1-A4-B2	1-A5-B2	1-A5-B2	1-A6-B2	1-A6-B2	1-A7-B2	1-A7-B2
1-A1-B3	1-A1-B3	1-A2-B3	1-A2-B3	1-A3-B3	1-A3-B3	1-A4-B3	1-A4-B3	1-A5-B3	1-A5-B3	1-A6-B3	1-A6-B3	1-A7-B3	1-A7-B3
1-A1-B4	1-A1-B4	1-A2-B4	1-A2-B4	1-A3-B4	1-A3-B4	1-A4-B4	1-A4-B4	1-A5-B4	1-A5-B4	1-A6-B4	1-A6-B4	1-A7-B4	1-A7-B4
1-A1-B5	1-A1-B5	1-A2-B5	1-A2-B5	1-A3-B5	1-A3-B5	1-A4-B5	1-A4-B5	1-A5-B5	1-A5-B5	1-A6-B5	1-A6-B5	1-A7-B5	1-A7-B5
1-A1-B6	1-A1-B6	1-A2-B6	1-A2-B6	1-A3-B6	1-A3-B6	1-A4-B6	1-A4-B6	1-A5-B6	1-A5-B6	1-A6-B6	1-A6-B6	1-A7-B6	1-A7-B6
1-A1-B7	1-A1-B7	1-A2-B7	1-A2-B7	1-A3-B7	1-A3-B7	1-A4-B7	1-A4-B7	1-A5-B7	1-A5-B7	1-A6-B7	1-A6-B7	1-A7-B7	1-A7-B7

Compound A is Paclitaxel and compound B is Carboplatin, concentrations represented by the highest dose ‘1’ to the lowest dose ‘7’ and arrows represent direction of decreasing dose.

Appendix B Determination of carboplatin absorption rate constant (k_{ip}) from intraperitoneal cavity.

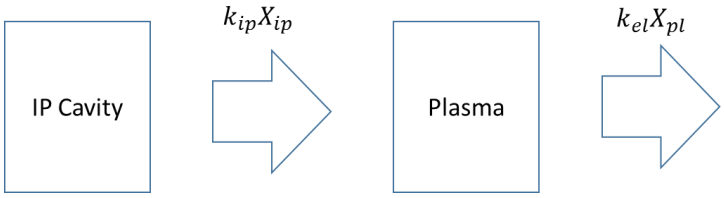
We used data from McClay et. al ([94]) and constructed a model similar to that described in the publication, to find a value of k_{ip}, which explains both the plasma and IP concentration profiles described in this paper.

During the infusion time:



k_{ip} can be thought of as an absorption constant from the IP cavity. It should not be confused with the clearance.

At the end of the dosing period:



Rate of change of mass of API with respect to time in IP cavity

$$\frac{dX_{ip}}{dt} = \begin{cases} R_{in} - k_{ip}X_{ip} & t < t_{inf} \\ -k_{ip}X_{ip} & t > t_{inf} \end{cases}$$

Rate of change of mass of API with respect to time in plasma.

$$\frac{dX_{pl}}{dt} = k_{ip}X_{ip} - k_{el}X_{pl}$$

This model is then implemented in Berkley Madonna to find the value of k_{ip} which explain the experimental data from McClay et. al., taking the plasma and IP concentration into account.

Berkeley Madonna model codes are as follows:

```
METHOD RK4

STARTTIME = 0
STOPTIME = 24
DT = 0.02

Init X_ip = 0.0
Init X_pl = 0.0

{Approximate Dosing Time}
t_inf = 1.2

{Total Dose}
dose = 300.0 * 1.7

{Infusion Rate}
R_in = dose  / t_inf
k_ip = 0.2

{Molecular Weight of API in g/mol}
mw = 373.3

{Plasma PK}
CL_pl = 8.8
V_d = 9.6
k_el = CL_pl / V_d

{IP Volume}
V_ip = 1.0

{Differential Equations for mass of API as X_ip wrt time and X_pl wrt time}
d/dt(X_ip) = IF TIME < t_inf THEN
                R_in - k_ip * X_ip  {During infusion}
                ELSE
                - k_ip * X_ip       {After infusion is complete}

                d/dt(X_pl) = k_ip * X_ip - k_el * X_pl


{Convert to concentration in µM}
c_pl = 1.0e3 * X_pl / (V_d * mw)
c_ip = 1.0e3 * X_ip / (V_ip * mw)
```

We use this model to estimate a value for k_{ip} of 0.198 hr-1, see Figure 9-1 for the fitted model.

Note: it is assumed that the IP fluid volume have no significant effect on the k_{ip}

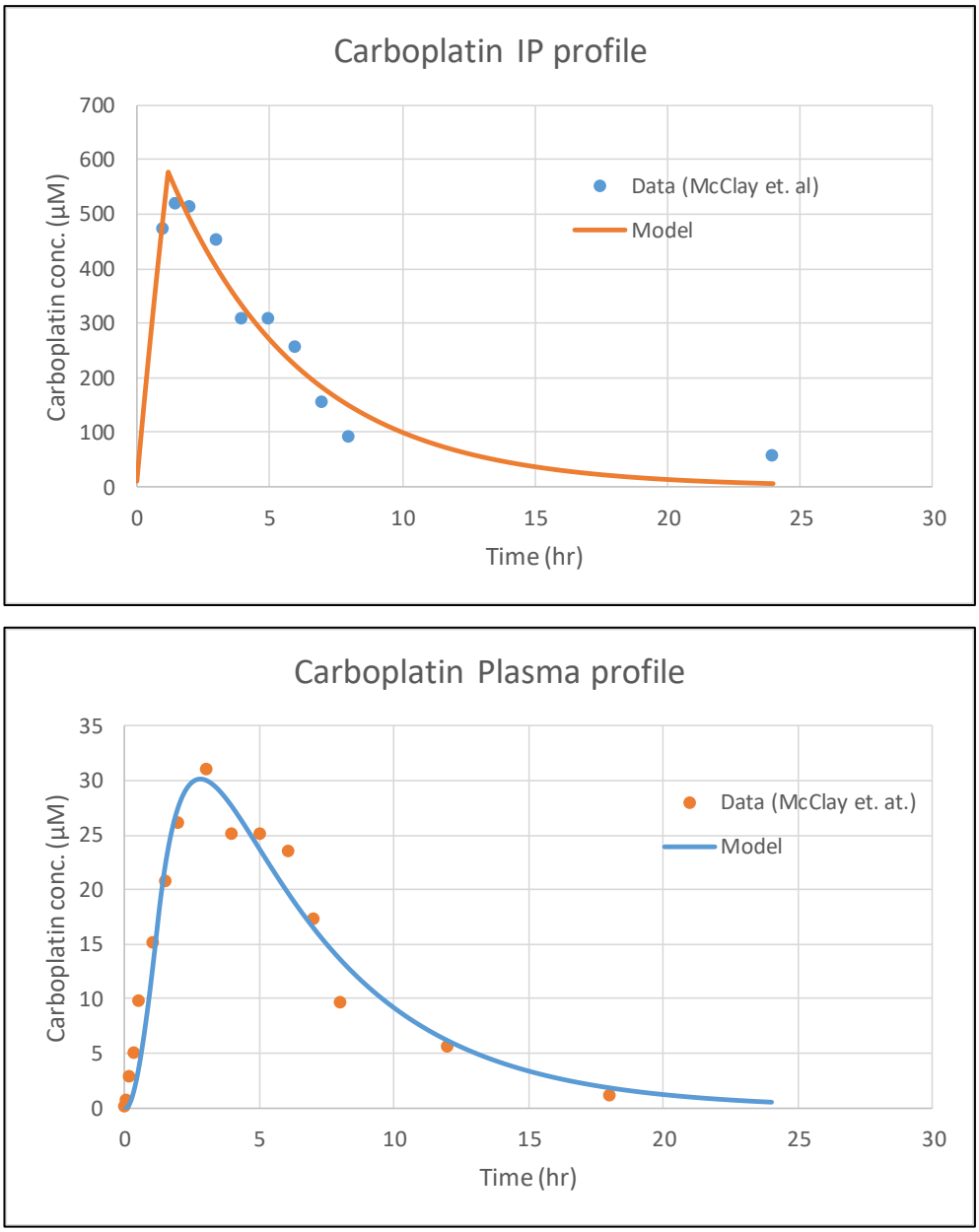


Figure 9-1:Fitted model for estimating the value of carboplatin k_{ip} by using data from McClay et. al. paper.

Appendix C Hydrogel Material details

Hyaluronic acid (HA)

HA is a high molecular weight linear polyanionic glycosaminoglycan composed of repeating disaccharide units of D-Glucuronic acid and N-acetylglucosamine [216-218].

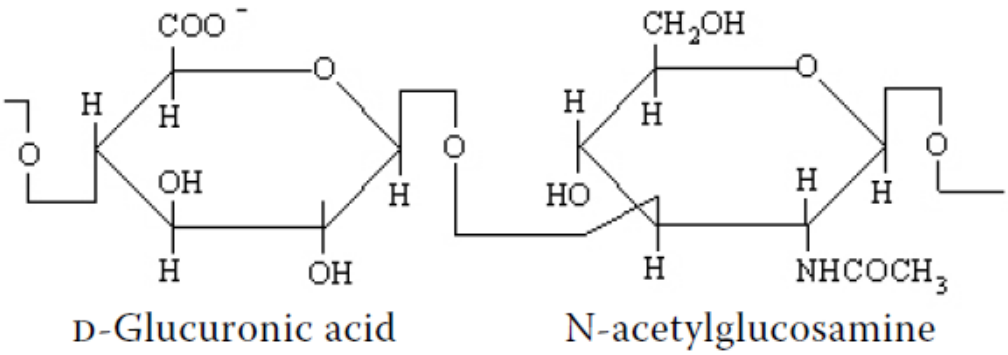


Figure 9-2 Hyaluronic acid chemical structure

HA occurs naturally in all livings organisms and is mainly found in the extracellular and pericellular matrix, it has also shown to be present intracellular [217]. In the body HA exists as salt form “hyaluronate” at high concentrations in various body parts including skin, umbilical cord, synovial fluid, vitreous humour, lungs, kidney, brain and muscles [217]. It is one of the most hydrophilic molecules in nature and in addition to number of other functions, the main function of HA is to bind water and to lubricate movable parts of the body such as joints and muscles [217]. HA has been shown to reduce postoperative adhesion formation after abdominal and orthopaedic surgery, which has been attributed to its exceptional lubrication properties [217].

The HA backbone is stiffened in physiological solution due to the combination of chemical structure of the disaccharide, hydrogen bonds and interactions with solvents. The axial hydrogen atoms forms a relatively hydrophobic face whereas, the equatorial side chains form hydrophilic faces which results in the formation of twisting ribbon like structure [217]. This coil structure traps ~ 1000 times its weight in water [219].

The number of repeated disaccharide units in a HA molecule can range between 200 to 20,000, therefore molecular weight of this polymer can range from approximately 80 to 8000 kDa (single disaccharide unit is ~ 400 Da) and as it can be seen from the above chemical structure, each disaccharide unit contains single carboxylic group which means a single HA molecule can have 200 to 20,000 anionic sites [217,218].

The role of HA in cancer is still being elucidated, at least fourteen different types of cancer have been shown to have high levels of HA in the tumour cells or surrounding stroma. In the case of ovarian cancer, the correlation between accumulation of HA and cancer is so strong that it is being considered as a prognostic marker [218].

HA is removed from the body by two routes: a) internalisation and degradation by the cells and destruction in lysozyme and b) release from the extracellular matrix and drainage into the vasculature, followed by removal via the lymph nodes, liver and kidney. Both of these routes of elimination require enzymes, in mammals three types of enzymes can cause HA degradation these are hyaluronidase (hyase), b-D-glucuronidase and β-N-acety-hexosaminidase [217,218,220]. Hyaluronidases function best at acidic pH [221]. HA complexation with other polymers also inhibits the HA clearance and degradation in vivo.

Chitosan

Chitosan is a pseudo-natural polycationic polysaccharide, which consists of copolymers of D-glucosamine and N-acetyl-D-glucosamine, and is obtained by alkaline deacetylation of chitin, Figure 9-3 [222,223]. Chitin is a natural biopolymer and is produced by large number of living organisms, it is the most abundantly produced polymer worldwide after cellulose [223].

Highly deacetylated chitosan is soluble in acidic aqueous media [223]. Chitosan can form electrostatic polyelectrolyte complexes with large numbers of natural or synthetic polymers e.g. hyaluronan, alginate, pectin, heparin, xanthan, carrageenan, etc [224,225]. It has been shown that the electrostatic polyelectrolyte complexes of chitosan, in particular, with HA and alginate are strongly dependant on the pH and ionic strength [223,224]. It has been shown that chitosan – HA complex is stable at any basic pH (note: chitosan is insoluble at pH >7,

therefore, care must be taken to differentiate the precipitate from complex), whereas it dissociates in acidic medium because the HA carboxylic group becomes unionised while the chitosan is fully ionised [224]. It has also been shown that chitosan-HA complex destabilises in excess of NaCl (completely dissolves in 0.66M NaCl) and the degree of chitosan acetylation can also affect the complex stability, the higher the charge density the stronger the complex [224].

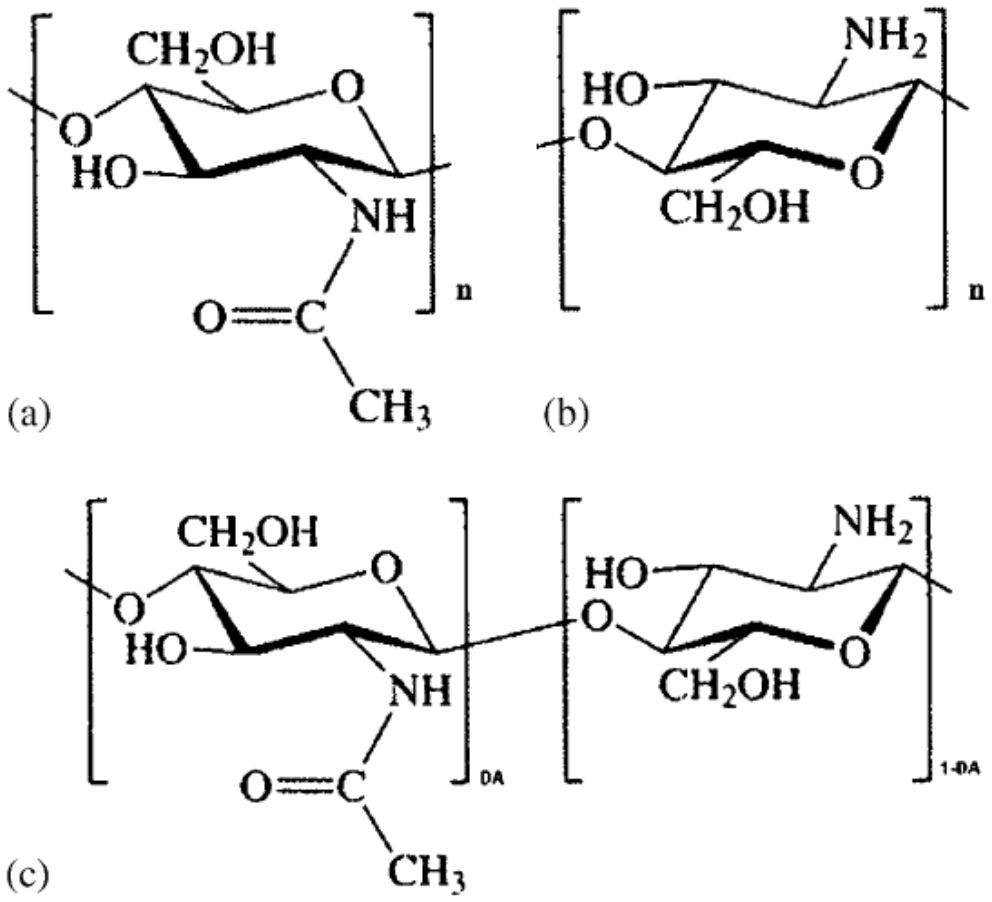


Figure 9-3 Chitosan chemical structures

(a) chitin poly(N-acetyl-β-D-glucosamine) and (b) chitosan (poly(D-glucosamine) repeat units. (c) Structure of partially acetylated chitosan, a copolymer characterized by its average degree of acetylation DA

Alginic acid (Alginate)

Alginate is isolated from brown algae (seaweed) in which alginate comprises up to 40% of the dry weight [226,227].

It is a water soluble, linear copolymer consisting of D-mannuronic acid and L-guluronic acid monomer units arranged in blocks. The monomer blocks

(homopolymeric regions M and G blocks) are separated by blocks of random or alternating units of mannuronic and guluronic acids, see Figure 9-4 [226]. Composition and sequence of the blocks and molecular weight vary depending on the source of alginates which determine the physical properties of alginates [227].

Alginates are extensively used in food industry and have been included in the GRAS (generally regarded as safe) list by FDA. There are contrasting views in the literature about the biocompatibility of alginate when administered via parenteral routes[227].

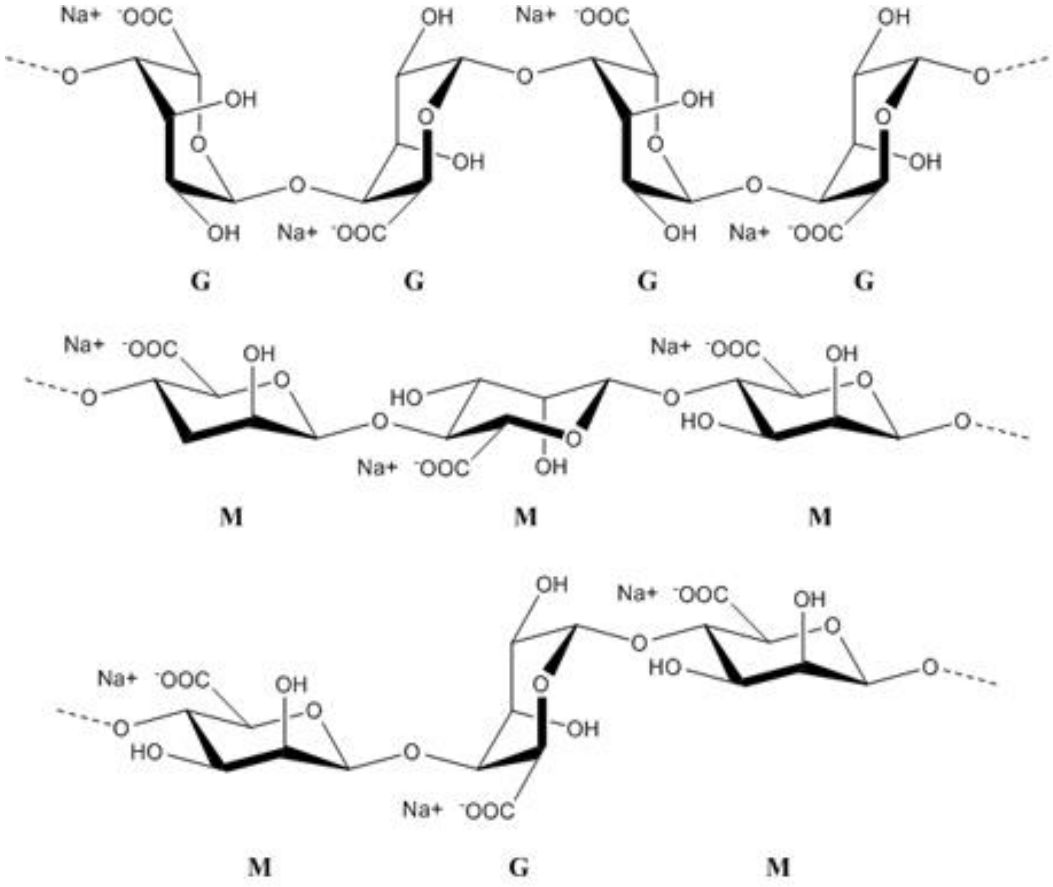


Figure 9-4 Alginate chemical structure

G = Guluronic acid, M = Mannuronic acid

Foreign body reaction and fibrosis has been reported by some researchers after intravenous administration [228,229]. It has be shown that commercial uncharacterised alginate can cause an immune response due to the presence of contaminants e.g. mitogens, phonolic and other toxins [230]. It has been

demonstrated that no immune response was induced when alginate beads prepared from electrophoretically purified alginate (various commercially available alginates) were implanted in the intraperitoneal cavity of mice or rats [230].

The most commonly used alginate gel is formed by reaction with divalent cations such as Ca^{2+} which replaces sodium ions form the guluronic acid resulting in the stacking of the guluronic acid groups to form the characteristic egg-box structure as shown in Figure 9-5 [227,231]. Ca^{+2} – Alginate gel behaves like solid in retaining its shape and resisting stress, even though 99 -99.5% mass of the gel is water [227].

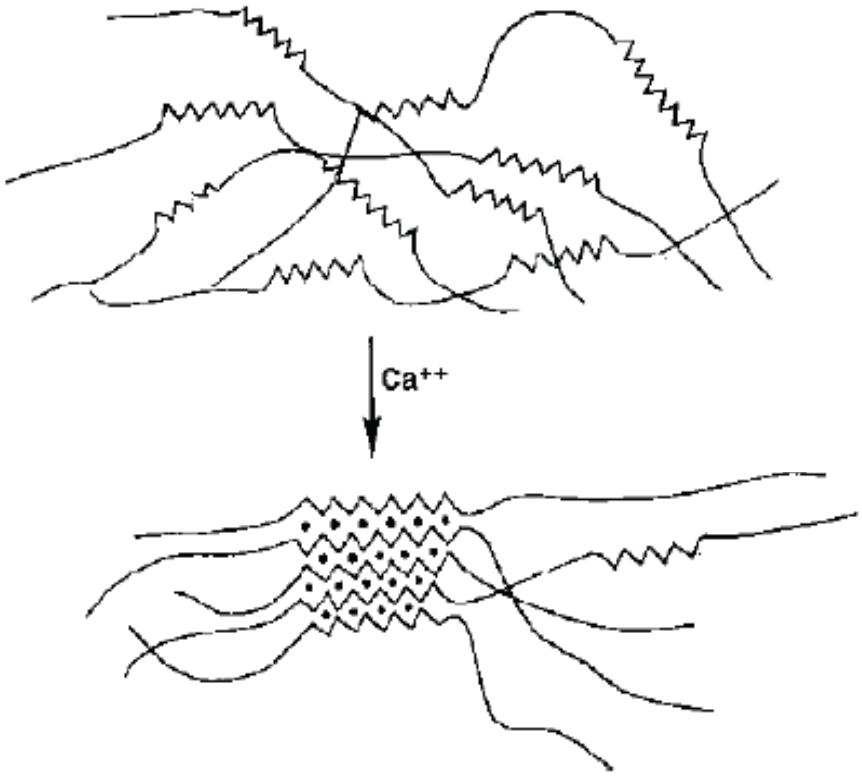


Figure 9-5. Egg-box structure of Ca2-Alginate hydrogel

(re-drawn after [232])

Pectin:

Pectin is a biocompatible and biodegradable natural anionic polysaccharide and used in various biomedical applications [233]. It is found in the cell walls of all plant tissues where it acts as an intercellular cement, giving the plant rigidity. Lemon

and orange rinds are among the richest sources of pectin, containing up to 30% of this polysaccharide.

The chemical structure of pectin varies depending on the origin, source plant, location in the plant and extraction method. The primary structure is composed of uronic acid residues linked through α-1-4-glycosidic linkages. In addition, various side chains containing sugars e.g. glucose, mannose, galactose, etc are also linked to the backbone. The galacturonic acid in the backbone can also have varying degree of esterification on the carboxylic acid which gives pectin some unique properties [234]. Pectin is commonly categorised as high methoxy (>74 % methylation) and low methoxy (<34 % methylation) based on the degree of esterification [235].

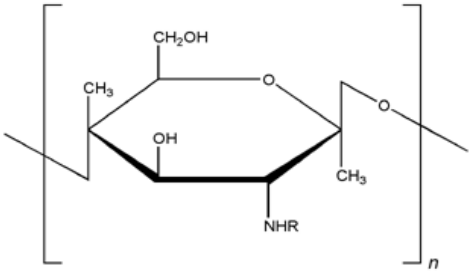
Low methoxy (LM) pectin gel in the presence of calcium and it has been reported that all LM pectin form junction zones with calcium similar to the ones proposed for the alginate-calcium in the famous “egg-box” mechanism [236,237]. The gel strength of the LM pectin gels increases with increase in the calcium concentration and decrease in the temperature [238]. Moreover, amidation of pectin can further improve the gelling ability of LM pectin i.e. gel formation at lower concentration of calcium and make gels to tolerate different levels of calcium [237] which make it attractive for pharmaceutical applications.

Appendix D Calculation of number of functional groups in hyaluronic acid and chitosan polymers to determine the mixing ratio of both polymers (by weight) and functional groups (by number).

Chitosan:

calculation of number of amine groups per molecule in a polymer bought from sigma Aldrich (product code 740063) with molecular weight 60 – 120KDa.

Monomer chemical structure



R = H or $COCH_3$

Calculation of atomic weight of monomer

Atoms	Number per monomer	Atomic wt.	Total atomic wt.
C	10	12	120
H	19	1	19
N	1	14	14
O	4	16	64
			217

Assuming 100% deacetylation,

Number of monomer units in polymer: = 60,000 / 217 = 276

= 120,000 / 217 = 553

Each monomer contains 1 amine functional group, therefore,

Corrected for 90% deacetylation (example of typical chitosan),

Number of amines in polymer = 276 x 0.9 = 249

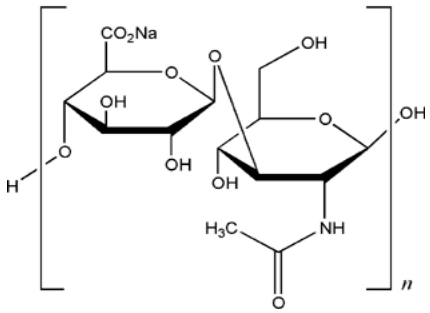
= 553 x 0.9 = 498

Average = 374

Hyaluronic acid:

calculation of number of carboxylic groups per molecule in a polymer bought from sigma Aldrich (product code 53747) with molecular weight 1500 – 1800KDa.

Monomer chemical structure



Calculation of monomer molecular weight

Atoms	Number per monomer	Atomic wt.	Total atomic wt.
C	14	12	168
H	20	1	20
N	1	14	14
O	11	16	176
Na	1	23	23
			401

Number of monomer units in polymer = 1,500,000 / 401 = 3741

= 1,800,000 / 401 = 4489

Each monomer contains 1 carboxyl functional group, therefore,

Average = 4115

As, 1 M of any compound contains same number of molecules

Therefore, ratio of carboxyl/amine functional groups at equimolar concentrations of hyaluronic acid and chitosan can be calculated as,

Functional group ratio = 4115 / 374 = 11

If we take an example of the higher end molecular weight of both polymers (i.e. chitosan 120KDa and HA 1800 kDa) and make 1 M solution of chitosan and 1/11 M solution of HA, then, we can calculate a factor that can be used to determine the mass (in grams or mgs) of each polymer required to make hydrogel with known functional group (i.e. carboxyl / amine) ratios.

e.g.

1 M solution of chitosan		= 120, 000 g/L
1/11 M solution of hyaluronic acid	= 1800, 000 / 11	= 163, 636 g/L

Factor (carboxyl / amine ration) = 163, 636 / 120, 000 = 1.36

Conclusion:

A hydrogel with 1:1 ratio of Carboxyl to Amine can be prepared by mixing 1.36 parts of HA to 1 part of chitosan by weight e.g. 5 mg/mL HA solution can be mixed with 3.7 mg/mL chitosan solution.

Appendix E Hydrogel polymers- solution viscosity behaviour

Method: Hyaluronic acid, alginate-sodium and chitosan solution viscosity determination by rheology

The solutions of two different grades of HA were prepared at 5 mg/ml in purified water. One grade of sodium alginate solution was prepared at 5 mg/mL in purified water and one grade of chitosan solution at 10 mg/ml was prepared in 1% acetic acid solution. Viscosity was determined using HAAKE MARS III rheometer (Thermo Scientific) equipped with 35mm diameter / 1-degree angle cone and plate and HAAKE RheoWin 4 software (Thermo Scientific). The viscosity of each polymer solution was determined as a function of shear rate. Approximately, 1ml of the polymer solution was placed on the lower plate. The shear rate was swept from 1 to 500 s^{-1}.

Results: Figure 9-6 shows graphs of dynamic viscosity of different polymer solutions used in this study. As it can be seen from these plots (A and B) that both HA solutions show a similar shear thinning behaviour i.e. their viscosity decreases from ~1800 cP to ~ 50 cP as the shear rate is increased from 1 to 500 s^{-1}. HA solutions are therefore called "pseudo-plastic" [217].

Conversely, sodium alginate (C) and chitosan (D) solutions have relatively low starting viscosity of ~ 50 cP. However, both solutions also appear to behave as shear thinning materials. The sodium-alginate solution viscosity changes from ~50 cP to ~ 10 cP, whereas, chitosan solution viscosity changes from ~50 cP to ~ 25 cP as the shear rate is increased from 1 to 500 $s^{-1.}$

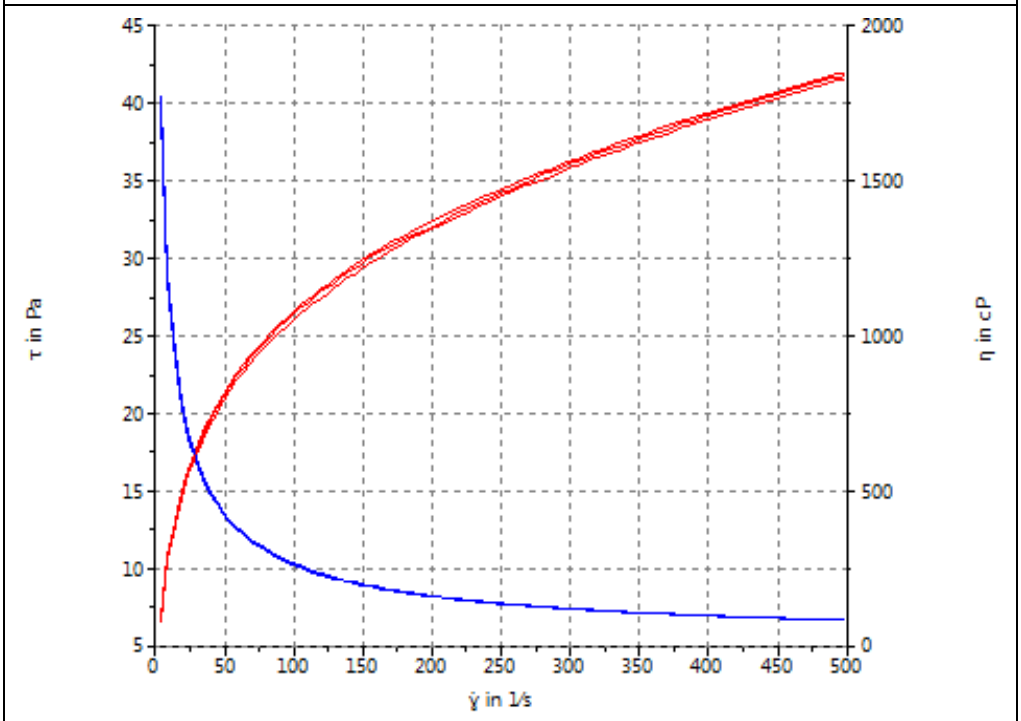
These rheology results and observations indicate that we should be able to administer all of these solutions through a narrow bore needle due to their relatively low viscosities and shear thinning behaviour.

Viscosity of a polymer solution depends on the number of factors including polymer concentration and molecular weight. It is common practice to use viscosity measurement of polymer solutions as a simple (quick) test to compare different grades and/or batches of the polymers in order to determine any

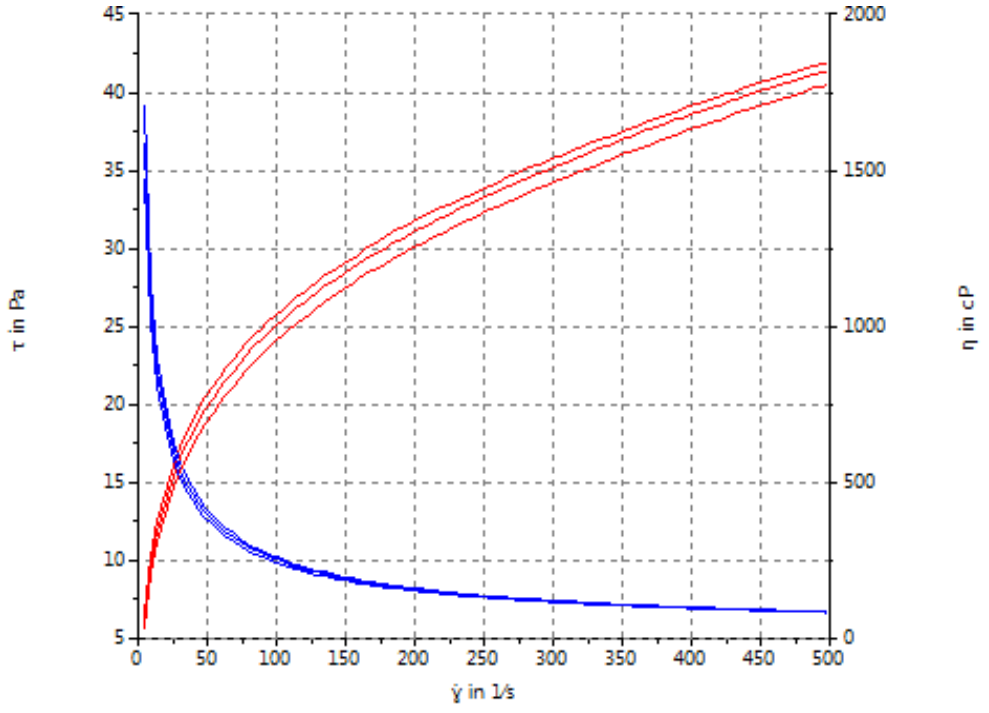
significant differences in m.wt. Therefore, we would be using this approach to characterise any new batches of our polymers.

Pseudo-elastic materials are ideal suspending agents for making microsphere suspensions, because, in the static state such suspending agents will remain viscous and thereby minimise or stop microsphere sedimentation. Whereas, when shear force is applied they flow freely and allow the dispensing or administration. HA solutions are particularly interesting for suspending PLGA microspheres (25-150 µM), because, firstly, HA is an anion and PLGA microspheres have strong negative zeta potential (typically around -40mV) therefore, similar electrostatic charge can provide additional charge stabilisation and therefore keep microspheres freely suspended. Secondly, as we are intending to use large microspheres (25-150 µm) which will require high viscosity suspending agent to avoid particle settling, therefore, higher concentration HA solution could be an ideal suspending agent for such large microspheres.

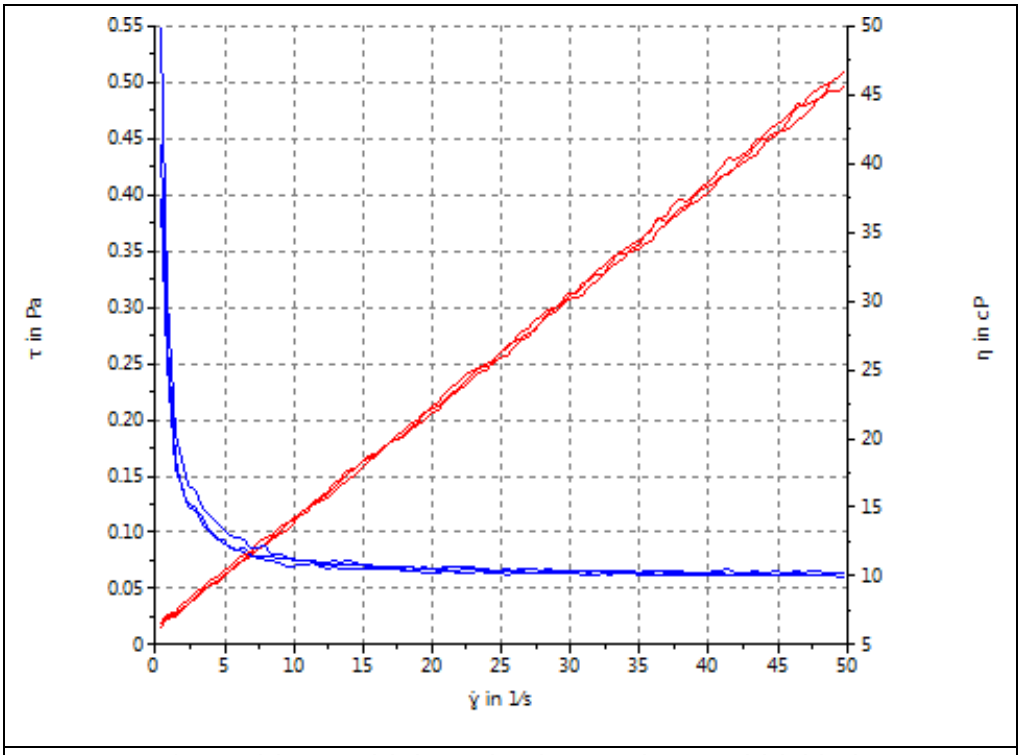
A: 5 mg/mL Hyaluronic acid (from lifecore biomedical) in purified water



B: 5 mg/mL Hyaluronic acid (from Sigma Aldrich) in purified water



C: 5 mg/mL sodium alginate-(from Sigma Aldrich) in purified water



D: 10 mg/mL Chitosan-high-purity (from Sigma Aldrich), in 1% w/w acetic acid

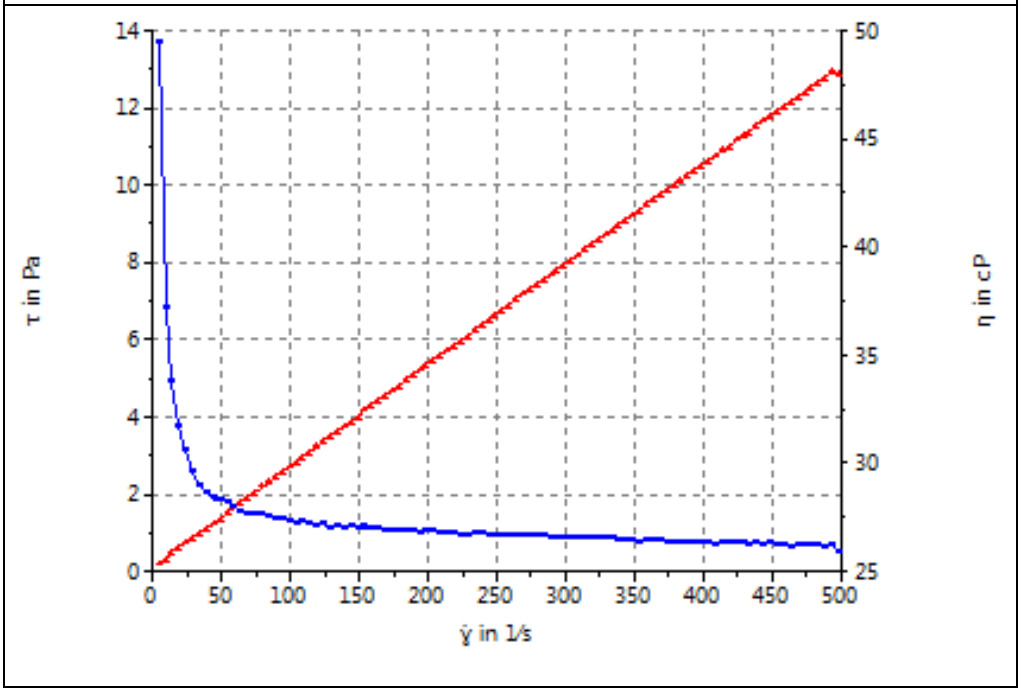


Figure 9-6: Dynamic viscosity (η) vs shear rate (γ) plots of two different grades of hyaluronic acid solutions, one grade of sodium alginate and one grade of chitosan solutions, at 25°C by using HAAKE MARS III rheometer (Thermo Scientific) equipped with 35mm diameter / 1-degree angle cone and plate and HAAKE RheoWin 4 software (Thermo Scientific).

Appendix F Evaluation of pectin net charge by dynamic light scattering and the effect of calcium concentrations on net charge.

Method: Pectin solutions were prepared at 1% w/v concentration in relevant media (i.e. purified water or dilution solutions of calcium chloride 1 – 5 mM) and analysed for zeta potential by dynamic light scattering using Zetasizer ZS, Malvern instruments ltd., UK.

Results:

Table 9.1: Zetapotential results of four low-methoxy grades of pectin in purified water, determined by dynamic light scattering method, using Zetasizer.

Sample ID	Zeta potential (mV)	Std. Deviation (mV)
P101	-49	5
P102	-49	5
P104	-48	6
P105	-46	7

All the pectin grades appear similar in terms of net surface charge in purified water. Based on this data only pectin grade P102 was selected to evaluate the impact of calcium on the surface net charge, as an indicator of gelation propensity.

Table 9.2: Zetapotential results for pectin P102 as a function of $CaCl_2$ concentration change from 1 – 5 mM.

Sample ID	Zeta potential (mV)	Std. Deviation (mV)
P102 + 1mM $CaCl_2$	-18	4
P102 + 2mM $CaCl_2$	-14	4
P102 + 3mM $CaCl_2$	-13	2
P102 + 4mM $CaCl_2$	-11	3
P102 + 5mM $CaCl_2$	-8	3

These results indicate that the pectin net charge neutralises (decreases) significantly (i.e. from -49 to -18) with only 1 mM $CaCl_2$ (0.36 mM Ca^{2+}) indicating the pectin can potentially form a gel at the biologically relevant concentration of calcium in the IP fluid (0.5 – 2.5 mM) [184,186].

Based on this data pectin P102, P104 and P105 were selected for the formation of gels with two different concentration of calcium chloride (10 and 50 mM

Appendix G Selection of sample holding device for release testing

Various devices and options were evaluated to encase the microspheres and keep them submerged in the release media but allow the free movement of released payload, throughout the release testing period. A summary is shown in the following table.

Device	Mechanism of operation	Comments
USP dissolution apparatus (accessories)	USP apparatus 2 sinkers and USP apparatus 4 flow through cells which can retain the sample submerged in the release media and allow the free movement of released payload across the membrane.	The average particle size of my samples is ~ 100 µm. The small pore size (made of >20 mesh, <841 µm pore size) USP apparatus 4 sinkers were not commercially available. Although, custom made sinkers with mesh size of 20 or 40 (~420 µm) were available but these were very expensive (~£400/sinker quoted by Cole-Parmer Ltd. via email) and they had a long lead time for delivery. In addition, the flow through cells with smaller pore size membranes can also be used with the UPS apparatus 4 but this facility was not available (at AstraZeneca or University of Nottingham) during my work, therefore, it was not selected as a preferred option. Conclusion: not suitable
Dialysis bags/cassettes	Dialysis membrane-based devises can retain the sample submerged in the release media and the released payload can partition across the membrane.	It is well known in the literature that the rate of equilibrium of the released compound across the dialysis membrane is dependent on the compound physicochemical properties and the membrane pore size. From our personal experience the equilibrium of poorly soluble compounds (e.g. paclitaxel) across the membrane can be extremely slow (i.e. from days to weeks) therefore, this approach was not used for my work. Conclusion: not suitable

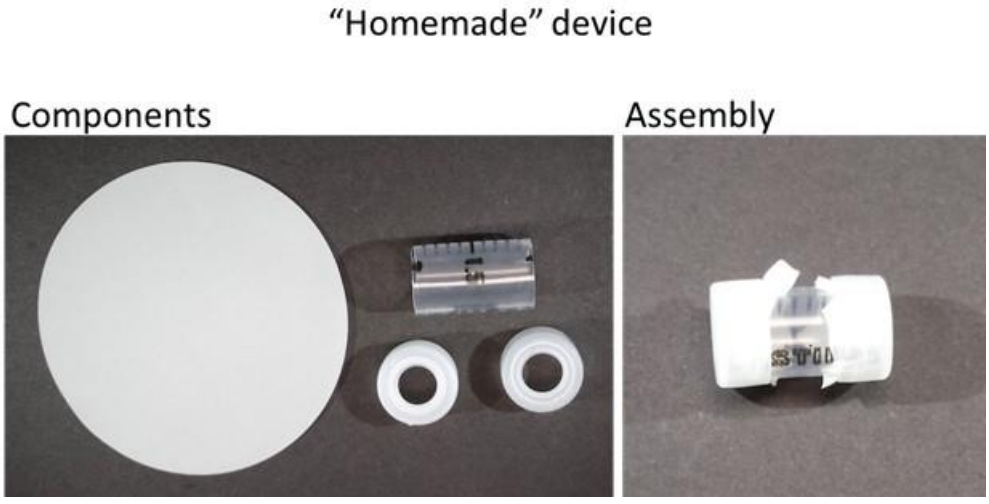
Other stand-alone devices	1) Filter holders: commonly used in various settings e.g. syringes, HPLC equipments, environmental monitoring equipments (NILU filter holder system), etc. Potentially these filter holders could be used to retain the sample between two filters. 2) Cannula filter tips: They have a cavity where, potentially, sample can be loaded and retained during release testing.	Both of these options were tested by using, 1) syringe filter holder (e.g. Cole-Parmer Advantec 43303010 filter holder and 5 micron filter). It was found difficult to determine whether the fluid will pass through the filers due to the narrow openings on each side, as it's designed to be used with syringe where the fluid is physically pushed through. 2) Canula filter tips (35 micron) were tested by attaching one filter on each side of a small silicon placing a blue dye in the cavity, although some dye passed across the filter but even after leaving overnight the majority of the dye stayed in the cavity indicating that the equilibrium across the membrane might be slow
"Home-made" device	A simple device comprising of 10 micron nylon filter membrane fitted at each end of ~ 20mm x 10mm (length x diameter) tube, sample placed inside the tube. Device was submerged in the released media to ensure whole sample stays in the release media (Figure 9-7)	Two types of materials were evaluated to make the body of the tube and the ring to hold the filter membrane in place. a) silicon tube with nitrile rubber O-ring to hold the membrane in place and b) polypropylene tube (made by cutting appropriate size piece from BD Plastipak 3mL syringe) with a polypropylene ring (HPLC vial cap without the septum) to hold the membrane in place (see Figure 9-7). Firstly, both devices were fully tested for the compatibility of API (including, API degradation, API adsorption, extractables and leachables by using API specific assay and impurities HPLC method).

		Secondly, the release of neat API (paclitaxel and carboplatin) from the device was performed, by placing a known amount of API inside the device, to determine the rate of release and ensure the suitability of these devices for release testing i.e. no significant delay in the partitioning of released/dissolved API from inside to the outside of the tube (Figure 9-8, Figure 9-9) Conclusion: Polypropylene device was found suitable for release testing.

A



B



C

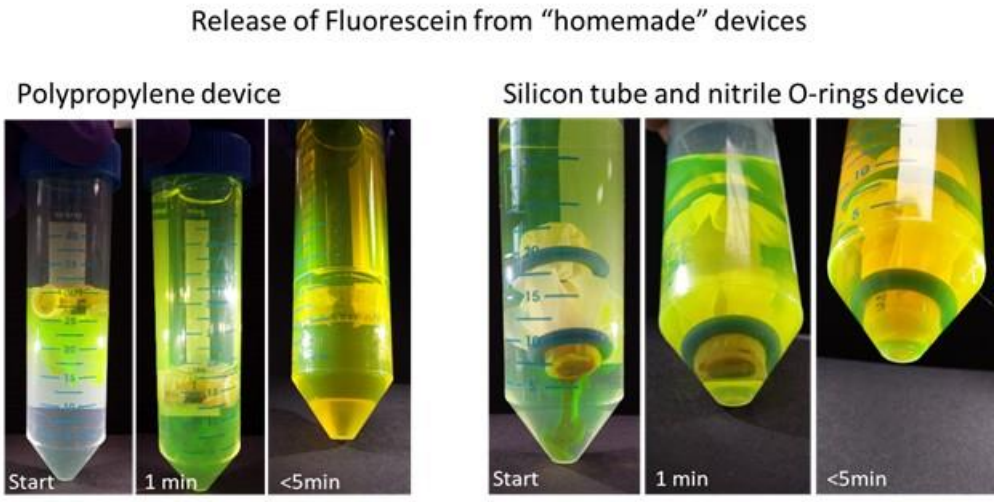


Figure 9-7: Selection of sample holding devices evaluated for the release testing of carboplatin and paclitaxel from PLGA microspheres. A: commercially available devices, B: “homemade” device components and assembly, C: pictures showing the visual assessment of the rate of Fluorescein (dye) release from two different “homemade” devices.

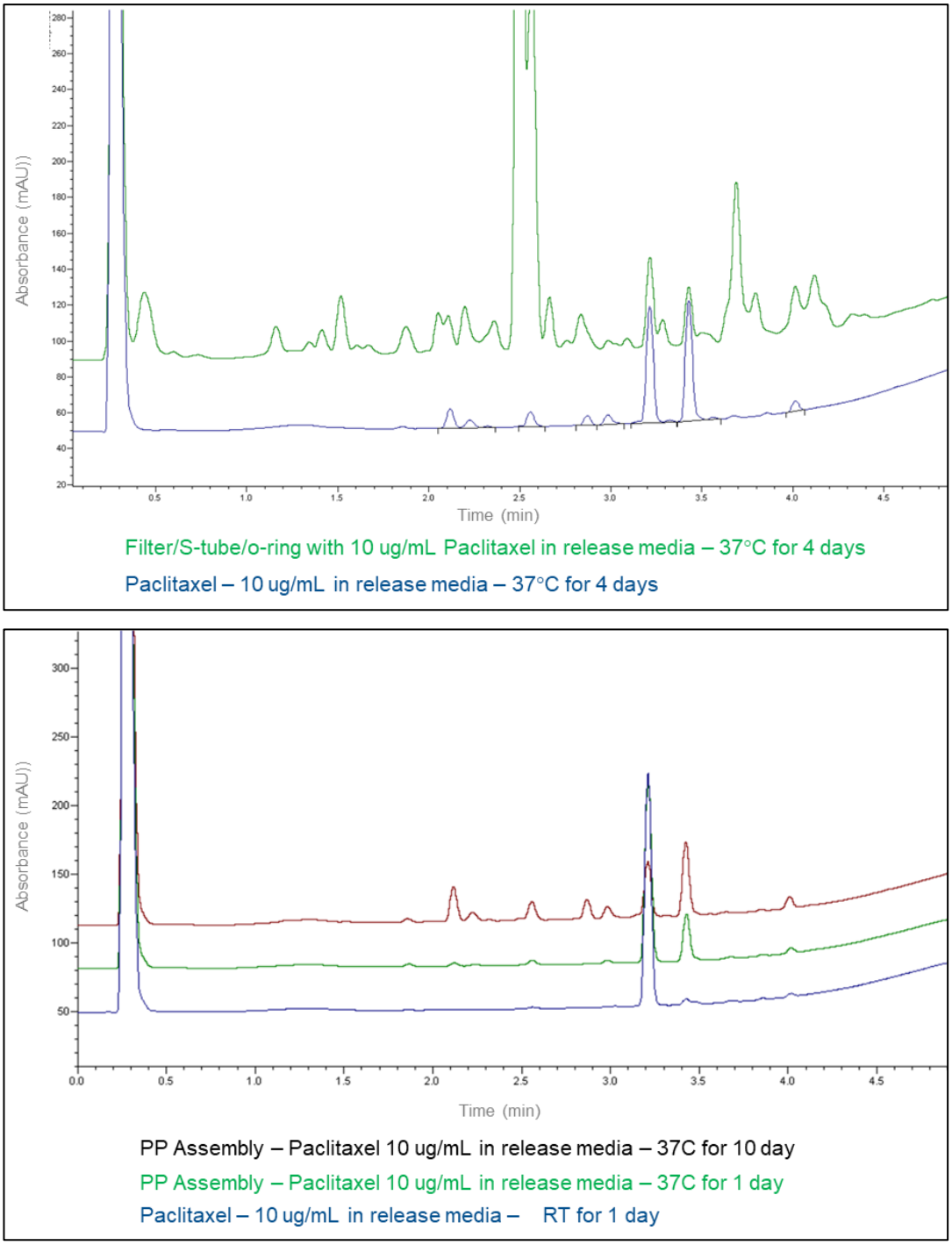


Figure 9-8: Chromatograms showing the impurities from different components of the "homemade" sample holding devices in comparison to the neat paclitaxel solution in release media.

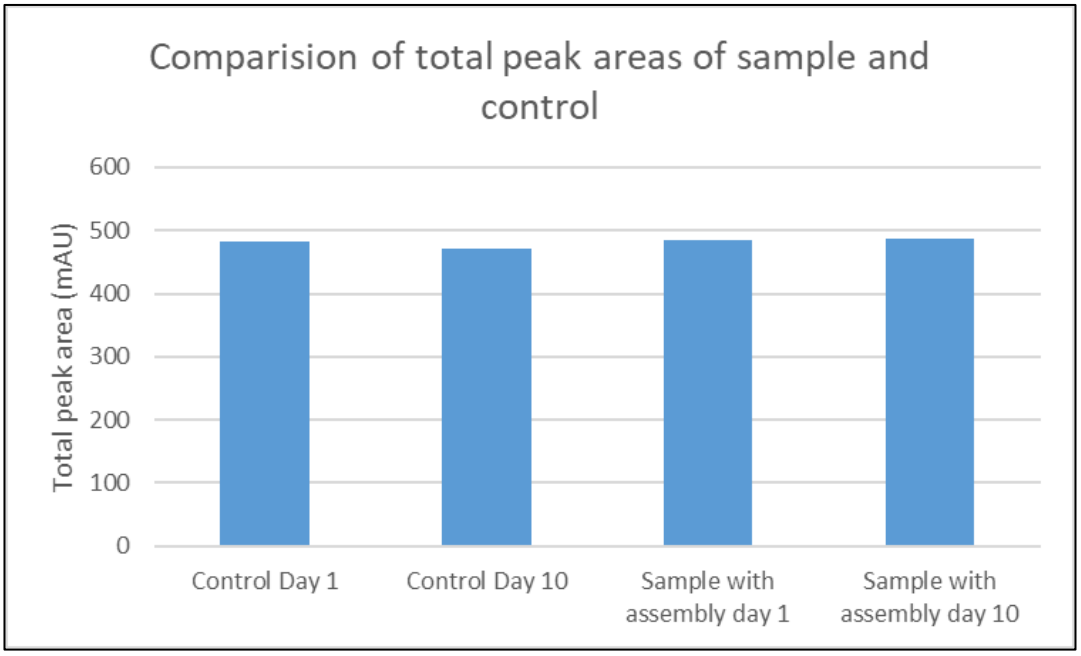


Figure 9-9: Comparison of the total peak areas of paclitaxel by HPLC at day 1 and 10 in the presence and absence of the sample holding device (assembly). This data indicates that the selected device has no significant impact on paclitaxel dissolved (released) in the release media.

Appendix H ToF-SIMS survey spectra of reference materials including PVA, PLGA, Carboplatin and Paclitaxel

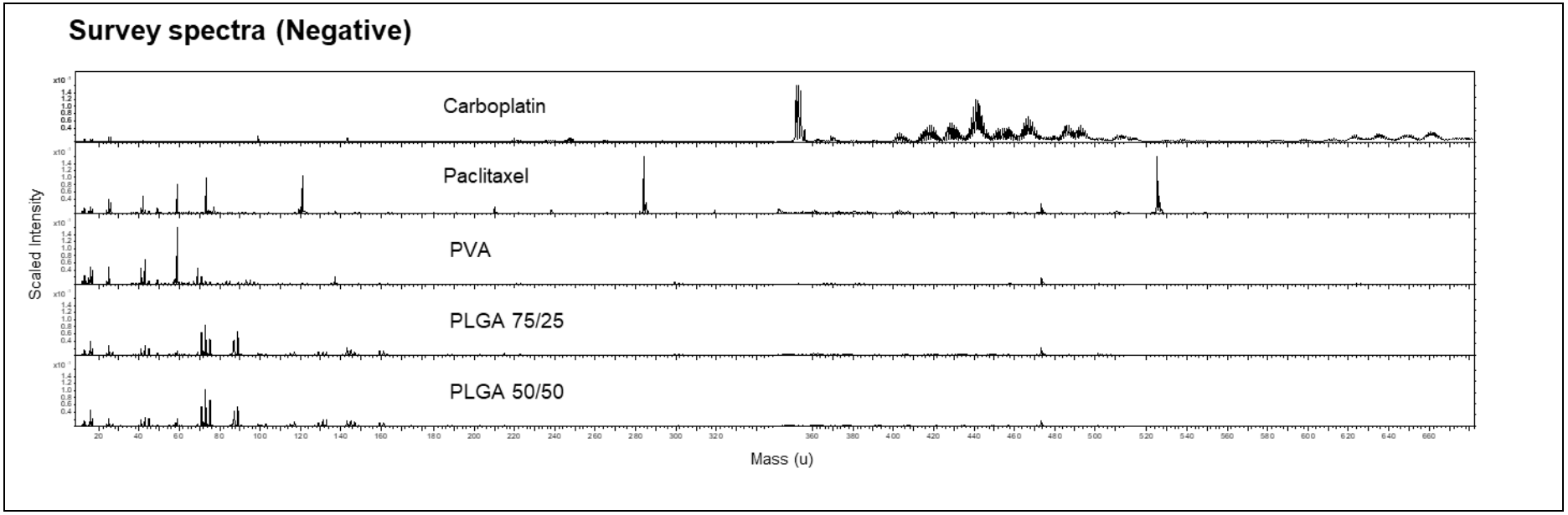


Figure 9-10: ToF-SIMS survey spectra (negative ions) by analysing reference materials for carboplatin, paclitaxel, PVA and two PLGA 50kDa (75/25 and 50/50)

Appendix I Supporting data for the release testing

Paclitaxel solubility determination in different aqueous medias

Release medias tested:

1) 10% HPBCD in pH7.4 PBS + 0.02% Na-azide
2) 1% HPBCD in pH7.4 PBS + 0.02% Na-azide
3) 1% tween 80 in pH7.4 PBS + 0.02% Na-azide

Method:

Paclitaxel is insoluble in water (Drugbank – DB01229). Therefore, prior to in-vitro release testing paclitaxel solubility was determined in three aqueous release medias to select an appropriate release media with highest solubility. This is to ensure a sink conditions of at least three times the solubility of paclitaxel is achieved while using smallest possible volume during release testing. The tested release medias included i) 10% w/v hydroxyl-propyl-beta-cyclodextrin in 10 mM PBS pH 7.4 buffer containing 0.02% w/v sodium azide, ii) 1% w/v hydroxyl-propyl-beta-cyclodextrin in 10 mM PBS pH 7.4 buffer containing 0.02% w/v sodium azide and iii) 1% w/v Tween 80 in pH 7.4 PBS containing 0.02% w/v sodium azide.

Results:

Release media	Concentration (µg/ml)
1	45.7
2	8.6
3	51.1

Solubility samples were prepared by weighing approximately 5 mg of the compound in individual 1.5 ml eppendorf tubes containing 4-5 glass beads and 1 mL release media. All the samples were agitated at 1400 rpm and 37 °C for 2 hr in a thermal orbital shaker (Grant Instruments™ PCMT, Fischer scientific, UK Ltd.). These samples were ultracentrifuged

at 44000 rpm (RCF ~ 119044 g) at 37 °C for 15 min. The supernatant was transferred into new eppendorf tubes and ultracentrifuged again. Finally, the supernatant was analysed by HPLC after 1:10 dilution in DMSO (i.e. 0.1 mL supernatant and 0.9 mL DMSO).

Discussion/Conclusion:

Although release media 3 gave slightly higher solubility but paclitaxel is prone to degradation in aqueous buffers and it has been shown that cyclodextrin can improve the stability of paclitaxel in aqueous buffer ([239]). Therefore, release media 1 was selected for the release testing of paclitaxel.

Effect of microsphere degradation during release testing on the sampling of supernatant, preliminary experimental data.

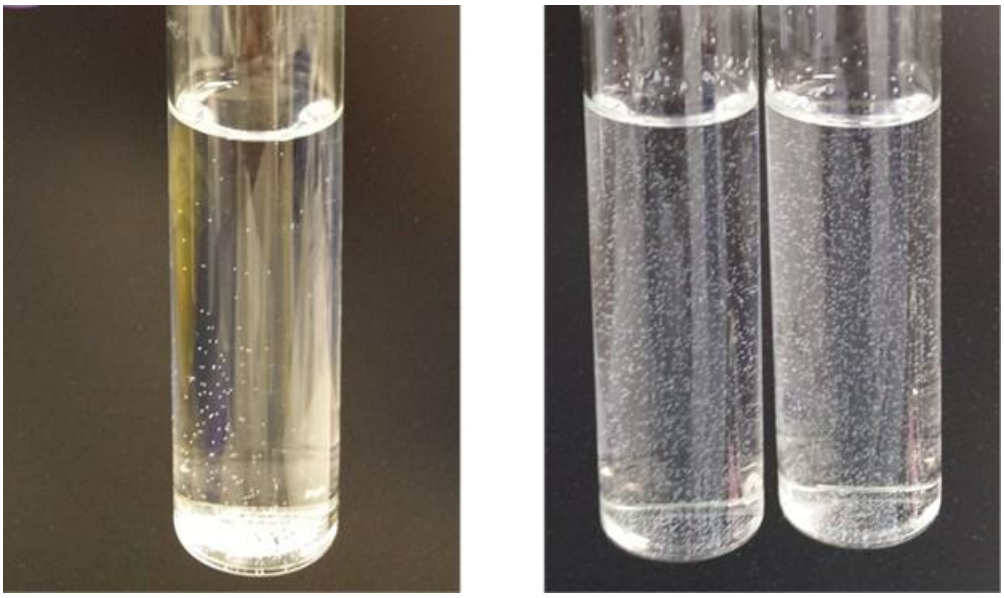


Figure 9-11: Pictures showing the release samples at the start and end of release testing. Left: paclitaxel-PLGA microspheres suspended in release media (replicate 1) at the start of release testing. Right: Paclitaxel-PLGA microspheres suspended in release media (replicate 1 and 2) at the end of release testing.

Figure 9-11 shows data from a preliminary experiment, and as it can be seen that the microspheres at the start of release testing settled down to

the bottom of the vial very quickly due to gravitational force, which allowed to take the supernatant samples without centrifugation. Whereas, as the experiment progressed the particle settling time slowly increased and towards the end of the release testing (~ 60 days) all the microspheres started floating in the release media and it was not possible to isolate these microspheres even after centrifugation or ultracentrifugation (>90K x g RCF).

The SEM pictures of the samples at the end of the release period confirmed the formation of high degree of porosity (Figure 9-12). This phenomenon is widely reported in the literature for PLGA based drug delivery systems and it is attributed to the hydrolytic degradation of PLGA which results in reduction of molecular weight and weight loss of PLGA polymer over time [240]

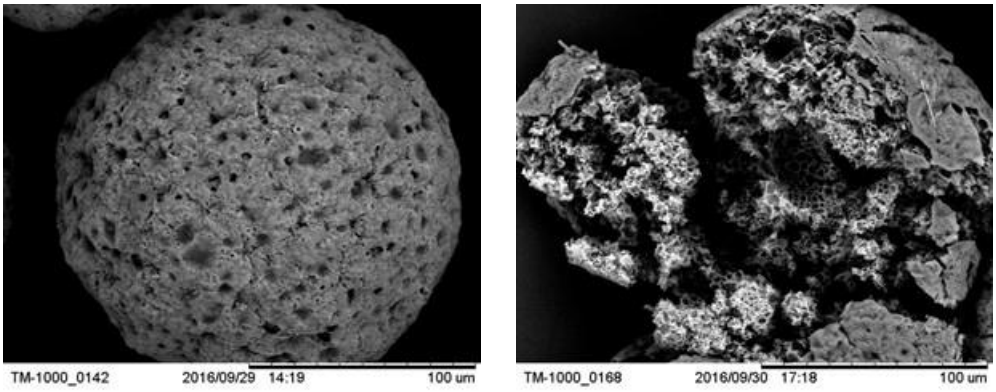
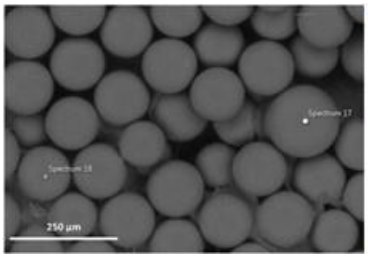
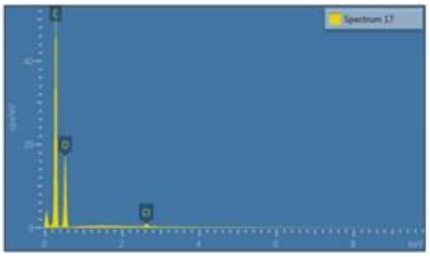
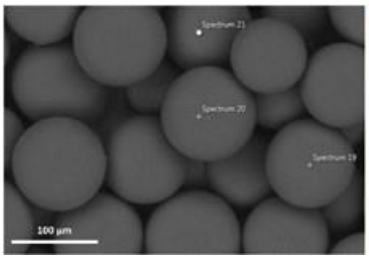
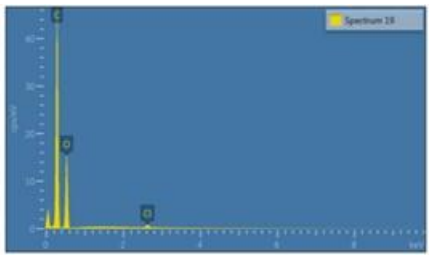
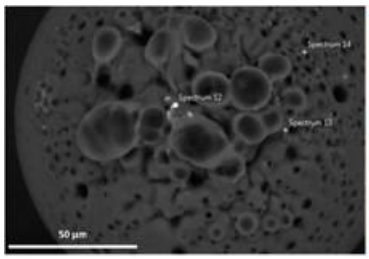
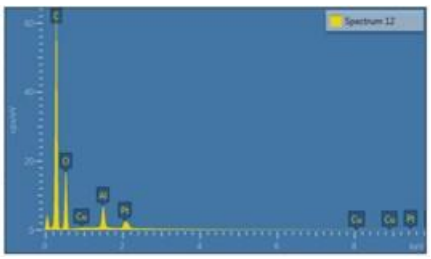


Figure 9-12: SEM images of the microspheres after 60 days of release testing. Sample preparation included the isolation of microspheres by filtration, drying under vacuum at ambient temperature for at least 24 hours and gold sputter coating before SEM analysis.

From this preliminary experimental work, this phenomenon was envisaged as a concern. Therefore, the microsphere samples for release testing were encased in a suitable sample holding device (see Appendix G for device selection details) which may retain the microspheres but allow free movement of released payload in order to conveniently allow the supernatant sampling throughout the release experiment.

Appendix J ESEM and EDX/EDS supplementary data showing the presence of platinum in the carboplatin samples. All samples were made from PLGA 75/25 50 kDa.

Sample ID	ESEM picture	EDX/EDS data
Blank		
Paclitaxel		
Carboplatin		

Appendix K Mathematical IP PK model codes for implementation in Berkeley Madonna

Paclitaxel IP PK Model code (by combining two formulations) implemented in Berkeley Madonna

```
METHOD RK4

STARTTIME = 0.01
STOPTIME = 280
DT = 0.02

{Fraction of each type of particle formulation in dosage form}
{f1 = fraction by mass of API of faster release form}
{f2 = fraction by mass of API of slower release form}
f1 = 0.46
f2 = 1.0 - f1

{Hill function fitted parameters for fast formulation}
{Paclitaxel Fast}
b1 = 2.9684
c1 = 7.6894

{Hill function fitted parameters for slower formulation}
{Paclitaxel Slow}
b2 = 7.3672
c2 = 19.7122

{Interval between dosing in days}
t_dose = 23.0

{Amount of API per dose in mg}
dose = 0.096

{Absorption constant from API cavity - API specific}
k_ip = 3.84

{Fluid volume in IP cavity in litres}
V_ip = 0.01

{Total number of dosing events}
n = 6

{Input rate contribution from each dose of n doses}
R_in[1..n] = IF TIME > t_dose * (i - 1) + 0.01 THEN
                dose * f1 * b1 * c1 ** b1 * (TIME - (i - 1) * t_dose) ** (b1 - 1)
                / ((c1 ** b1 + (TIME - (i - 1) * t_dose) ** b1) ** 2)
                + dose * f2 * b2 * c2 ** b2 * (TIME - (i - 1) * t_dose) ** (b2 - 1)
                / ((c2 ** b2 + (TIME - (i - 1) * t_dose) ** b2) ** 2)
             ELSE
                0.0

{Sum up input rate for all doses to get the net total input}
R_in_total = ARRAYSUM(R_in[*])

{Differential equation for the rate of change of amount of released API in the IP cavity}
{with respect to time}
d/dt(X_ip) = R_in_total - k_ip * X_ip
d/dt(Rel) = R_in_total

{Initial amounts at TIME = 0}
Init X_ip = 0.0
Init Rel = 0.0

{Divide by volume to give concentration in the}
{IP cavity}
c_ip = X_ip / V_ip

{Fraction unbound in IP cavity - assume similar to plasma)}
f_bound = 0.94

{Calculate minimum effective concentration in mg/L}
{(as free unbound drug in the IP cavity) from GI50 in mg/L}
GI50 = 1.45e-3
conc_MEC = GI50 * 3.0

{Target concentration (as total released, i.e., bound and unbound)}
target_conc = (conc_MEC / (1 - f_bound)) * TIME / TIME
```

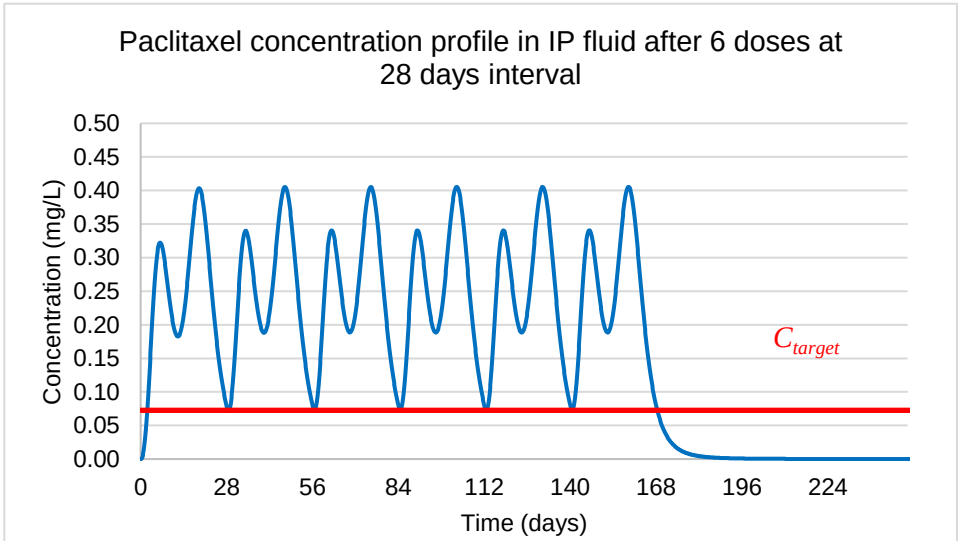
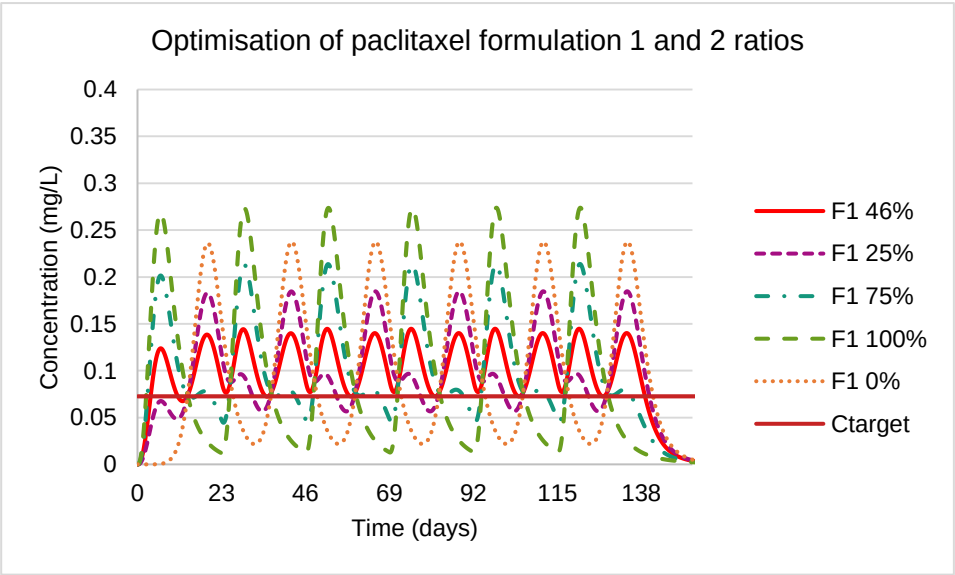


Figure 9-13: A "nonideal" simulated intraperitoneal (IP) steady-state concentration of paclitaxel above the target concentration (0.0726 mg/mL) by using a IP pharmacokinetic model implemented in Berkeley Madonna (software package). These results are after administering total 6 doses of 0.27 mg/dose paclitaxel by using a blend of paclitaxel formulation 1 (43% w/w) and formulation 2 (57% w/w) at a dosing interval of 28 days. The pulsatile periodic variations have different heights i.e. nonideal.



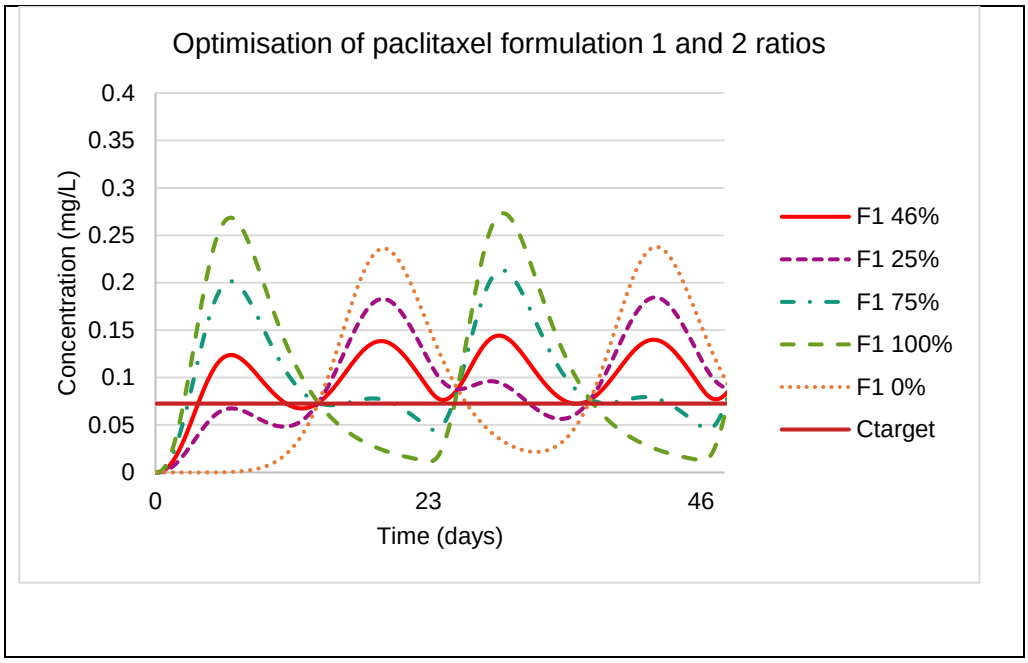


Figure 9-14:Optimisation of paclitaxel formulation 1 and 2 blend ratios to find the steady state at minimum dose required to consistently keep the intraperitoneal concentration of paclitaxel above the target concentration (0.0726 mg/L) after six doses with dosing interval of 23 days. Top: Profile showing all six doses, Bottom: profile showing first two doses.

Carboplatin IP PK model code implemented in Berkeley Madonna

```
METHOD RK4

STARTTIME = 0.01
STOPTIME= 280
DT = 0.02
DTOUT = 0.2
{Note TIME is in days}

{STARTIME is not exactly zero to avoid divided by zero in the differential}
{equations - we start very close to zero time, hence STARTTIME = 0.01}

{Hill function fitted parameters for fast formulation}
{Carboplatin}
b1 = 2.2859
c1 = 17.3619

{Interval between dosing in days}
t_dose = 28.0

{Amount of API per dose in mg}
dose = 14.5

{Absorption constant from API cavity - API specific - units are per day}
k_ip = 4.75

{Fluid volume in IP cavity in litres}
V_ip = 0.01

{Total number of dosing events}
n = 6

{Differential equations}
R_in[1..n-1] = IF TIME > t_dose * (i-1) + 0.01 THEN
                  dose * b1 *c1 ** b1 * (TIME - (i-1) * t_dose) ** (b1-1)
                  / ((c1 ** b1 + (TIME - (i-1) * t_dose) ** b1) ** 2)
                  - k_ip*X[i]
               ELSE
                  0.0

{Initial amounts at TIME = 0}
```

```
Init X[0..(n-1)] = 0

{Sum up amounts from each dose and divide by volume to give concentration in the}
{IP cavity in mg/L}
c_ip = ARRAYSUM(X[*]) / V_ip

{Calculate minimum effective concentration in mg/L}
GI50 = 1.89
conc_MEC = GI50 * 3.0

{Target concentration (as total released, i.e., bound and unbound)}
target_conc = conc_MEC * TIME
```

The effect of intraperitoneal fluid volume on the dose

Following Figure 9-15 shows that the increase in the IP fluid volume will result in the increase of dose by the same amount e.g. a 10 fold increase in IP fluid volume will increase the dose by 10 fold.

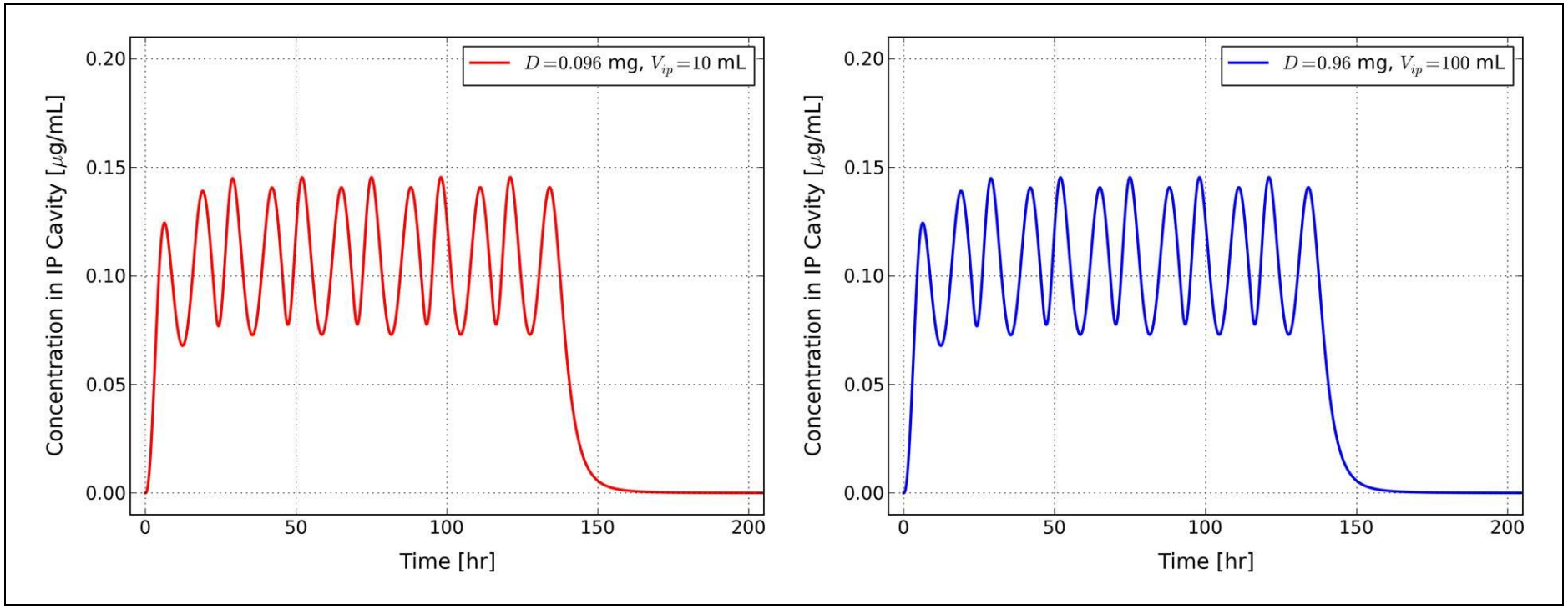


Figure 9-15: A coparison of simulated intraperitoneal (IP) fluid steady-state concentration of paclitaxel at two different IP fluid volumes. The simulation is performed by using a IP pharmacokinetic model implemented in Berkeley Madonna (software package). These results are after administering total 6 doses of paclitaxel-PLGA micropsheres by using a blend of formulation PF2 (54% w/w) and PF3 (46% w/w) at a dosing interval of 28 days.